UNITED KINGDOM · CHINA · MALAYSIA

MODELLING THE AGEING BEHAVIOUR OF SUPERCAPACITORS USING ELECTROCHEMICAL IMPEDANCE SPECTROSCOPY FOR DYNAMIC APPLICATIONS

NUR NAFISAH MOHAMMAD NAIM, BEng

Thesis submitted to the University of Nottingham for the degree of Doctor of Philosophy

JULY 2015

ABSTRACT

Diagnosis of ageing mechanisms in supercapacitors with acetonitrile-based electrolyte is made difficult by the enforcement of various ageing factors in the current ageing tests. This situation complicates the analysis when trying to predict the true cause of failure in supercapacitors. The thesis presents the exact determination of the ageing mechanism by separating impacts of high temperature, current cycling and constant voltage applications in an accelerated ageing test. The state of health of the supercapacitors have been monitored periodically with electrochemical impedance spectroscopy, cyclic voltammetry and constant current tests to observe the evolution of ageing.

The results reveal that each ageing factor has a distinctive ageing signature. The thesis also presents the cause of the increase in ESR and the loss of capacitance in supercapacitors. High temperature application causes the appearance of high frequency semicircle which reflects the loss of contact between the electrode and current collector. A tilt of impedance line at low frequencies reflects changes to the porous electrode in the form of increased heterogeneity and it is most sensitive to current cycling and constant voltage applications. The increase in ESR is observed to be caused by a single ageing mechanism while the capacitance loss is caused by multiple interactions of these ageing mechanisms at the same time. Post-mortem analysis with field emission scanning electron microscopy (FESEM) has revealed a modification to the electrode surface morphology especially at positive electrodes, in addition to the deposition of aluminium on the electrode-current collector interface.

In the second part of the thesis, a supercapacitor model in the form of electrical equivalent circuit is developed using data collected from the accelerated ageing test. The model is divided into two parts to represent the changes at the impedance due to the ageing process in supercapacitors. The first model, the baseline model, represents the initial state of the supercapacitor before ageing occurs. The second, more complex model, is the ageing model which represents the state of the supercapacitor when ageing process occurs. The baseline model and ageing model have been validated to show dynamic interaction between the process of ageing and supercapacitor electrical performance. The models, which are in the form of fractional-order models, reduce the number of circuit components when compared with lumped models. The models also show excellent electrical behaviour particularly at the open circuit voltage decay when the current source is removed with a small root mean square error between 0.03 and 0.05.

Parameterisation of the model parameters that are most affected by ageing using an empirical approach shows that aged supercapacitors experience an increase of distributed resistance in the electrode pores and an increase of diffusion impedance under high temperature stress. The implication of these findings shows that the model can be used to predict future changes in supercapacitors internal and electrical performance.

AFFIRMATION

The work reported in this thesis is solely the work of the author and has not been published elsewhere at the time this thesis is written, except for the following publications:

Published manuscript

Naim, N., Isa, D. and Arelhi, R. (2015) 'Modelling of ultracapacitor using a fractional-order equivalent circuit', International Journal of Renewable Energy Technology, Vol. 6 No.2, pp.142–163., DOI:10.1504/IJRET.2015.068595

Submitted for Publication

Nafisah Naim, WenJinn Chang, Dino Isa, Rajprasad Rajkumar, Michelle T.T. Tan (2015). 'Modelling of ageing and the effects of constant and cyclic voltage in supercapacitors'.

Planned for Publication

Nafisah Naim and Dino Isa (2015). 'Electrical equivalent circuit modelling of supercapacitor ageing under current cycling at elevated temperature using electrochemical impedance spectroscopy.'

To mama,

who made sure I got this done.

&

To W,

who made sure I got this done and did not lose my marbles.

ACKNOWLEDGEMENTS

"And will provide for him from where he does not expect. And whoever relies upon Allah – then He is sufficient for him. Indeed, Allah will accomplish His *purpose. Allah has already set for everything a [decreed] extent."*

—Quran 65:3

All praises and thanks are purely to Allah, alone. He is the Exalted, the All-Knowing, the Lord of the Universe. Thanks to Him for all His amazing grace and blessings that He has bestowed upon me, for granting me the strength and patience during this four years of solitary adventure.

Indeed, He is the best of planners. Without His grace, I would not have crossed path with these amazing people, whom each of them has played a significant role in contributing to the materialisation of this thesis. To the person who I am most indebted to in my academic career, Professor Dino Isa, I could not have wished for a better supervisor than you are. Thank you for giving me freedom to exercise my unusual research style. I am also thankful to you for always believing in me even when I myself was swarmed with self-doubt. You always have the right words to say to pull me back on my feet when I almost drowned in an ocean of facts and figures, especially during my second and third year of study.

My heartfelt thanks go to Dr Roselina Arelhi and Dr Michelle Tan for providing valuable insights and constructive feedbacks on my work while we

worked on producing papers out of this thesis. Your comments have certainly put things into perspective.

Thank you to Dr Chia Yen Yee and Ridhuan Ahmad Samsuri for lending me your helping hands when the environmental oven broke down and helped me fixed the chiller when the sound of the alarm broke the silence of the entire department. Thank you for making me realised I was not alone and that I could always turn to you when I needed an ear and a shoulder to cry on. Thank you to Mr Steven Liew Kah Heng from LLT Engineering Sdn Bhd for coming to the laboratory during weekends to fix the oven to make sure it would be up and running on the next day and Mr K. Parthipann for always be available to help.

Dr Goh Chia Chieh, Dr Muhsin Hassan, Nik Ahmad Akram, thank you for sharing your knowledge in coding and circuitry. Also, thanks to Ms JC Chua from Metrohm and Nicole Ho Mui Yen for the discussion in electrochemistry and supercapacitor. Thank you to Chang Wen Jinn, although I only had a short time working with you, you had made the dull laboratory so much lively and exciting.

Of course, thank you to my loving mother for her undying and selflessness love, for the sacrifices she has made for me. Mama, I know it is not easy to raise us as a single mother. You always put our best interest before you. You show me that the best of things in this world do not come easy and they require hard work and dedication to achieve. Thank you for being infinitely supportive to my dreams and for your countless advices that I should finish school for my tower of dreams will need a strong foundation. Thank you for always believing in your daughter.

Thank you Kak Mus for caring me for the past 20 years. I am sorry that I was not being as helpful as I would have like to with the house chores while I was immersed with writing this thesis. Thank you for picking up after me and your delicious meals are my pick-me-up after a long day's work.

To my cousin, Kak Faiz, thank you for keeping me sane during this challenging years. Thank you for showing me the world has so many things to be explored, we just need the courage to open the door. Your sparkling personality is infectious and your confidence is an envious.

To Redhuan, thank you for putting up with me when I feel jaded and need an escape from the world. From you, I get my daily doses of encouragement and motivation to make it through the years.

Bandar Baru Bangi, Selangor

November 2014

CONTENTS

LIST OF FIGURES

LIST OF TABLES

LIST OF ABBREVIATIONS

Abbreviation	Meaning
AC	activated carbon
Al	aluminium
AN	acetonitrile
CC	constant current
CNLS	complex nonlinear least squares
CNT	carbon nanotube
CPE	constant phase element
CV	cyclic voltammetry
EEC	electrical equivalent circuit
EIS	electrochemical impedance spectroscopy
EOL	end-of-life
ESR	equivalent series resistance
ESS	energy storage system
EUCAR	European Council for Automotive R&D
EV	electric vehicle
F	fluorine
HCV	Hybrid Commercial Vehicle
HEV	hybrid electric vehicle
IEC	International Electrotechnical Commision
IL	ionic liquid
O	oxygen

PC	propylene carbonate
PVDF	polyvinylidene fluoride
SC	supercapacitor
T	bounded diffusion circuit element
USABC	United States Advanced Battery Consortium
W	Warburg circuit element

DEFINITION OF TERMS

Accelerated ageing test – A set of test which is used to expedite ageing process in supercapacitors. It is performed at stressful conditions usually involving temperature and voltage to aggravate chemical reactions in supercapacitors.

Ageing factor – the cause of stress or pressure in a device which eventually causes the device to fail. The ageing factor can be categorised as mechanical stress, environmental stress or operational stress.

Ageing mechanism – a detail description of an ageing process usually ignited by mechanical, electrical or environmental stress on a device which then contributes to a failure event.

Ageing model – an electric equivalent circuit model which is the extended version of the baseline model to include ageing effect. It is built based on the response of aged supercapacitor. The ageing model contains information on the ageing mechanism and the state of health of aged supercapacitor.

Anomalous behaviour – a behaviour which deviates from the common or normal behaviour, usually a sign of changes to the properties of the device.

Ageing rate – ageing rate is related to the chemical reactions in supercapacitor. Chemical reactions in supercapacitors is speeded up usually either by voltage or temperature. When the rate of the chemical reactions are increased, ageing happens quicker.

Baseline model – an electric equivalent circuit model which is built from the response of the initial state of the supercapacitor, before ageing occurs. Baseline

model also acts a reference for any changes to the properties of the supercapacitor.

Cell opening – swelling on the casing of the supercapacitor due to build-up of pressure which leads the cell to open up.

Cycle life – the number of complete charge and discharge cycle in supercapacitors, cycled from the minimum voltage of the supercapacitor to its rated voltage, before the supercapacitor loses 20% of its initial capacitance or its resistance increases by 100%.

Cycling – a repeated charge and discharge cycle between two voltages using a set current on supercapacitor.

End-of-life – refers to the end of the useful life of supercapacitors. The criteria for the end-of-life is usually set by the manufacturers.

Failure mechanism – refer to ageing mechanism.

Failure mode – the manner in which a failure occur in a device either in a total lost in functionality to perform its intended function or unable to meet its requirement.

Open circuit – no current source or voltage source is attached to the supercapacitor, therefore no charge flows between the supercapacitor terminals.

Premature failure – a failure before its specified lifetime.

State of health – the condition of the supercapacitor usually referred to the cell capacitance.

Stress factor – refer to ageing factor.

Voltage hold – the voltage of the supercapacitor is held at a defined value using a constant voltage.

CHAPTER 1

INTRODUCTION

"For the things we have to learn before we can do them, we learn by doing them."

—Aristotle, The Nicomachean Ethics

1 Introduction

This thesis deals with studying the ageing mechanisms related to reliability in supercapacitors and an approach to close the gap among three specific areas that improve the performance of supercapacitors: research on degradation mechanisms on components and materials, degradation mitigation strategies and supercapacitor modelling. The introduction to the thesis begins with a background to the research, the problems that exist with the current state of knowledge and the research issues that were addressed.

1.1 Background to the research

In recent decades, supercapacitors have attracted much attention (Frackowiak et al., 2013; Li and Wei, 2013; Calvo et al., 2013; Fletcher et al., 2014; Jang et al., 2013). Supercapacitors are proposed to be the panacea for the shortcomings in batteries (Uno and Tanaka, 2012). Batteries are bulky, not environmental friendly, have limited cycle life, low power capability and cannot release energy as quickly, particularly for use in power hungry applications (Araujo et al., 2014; Vlad et al., 2014). Today, supercapacitors are still far from being able to replace batteries per se: supercapacitors struggle in meeting the demand for a high energy density; although, there have already been views that supercapacitors can complement batteries to reduce the size of batteries, especially in the hybrid transport and automotive industry (Brown et al., 2010; Carter et al., 2012; Araujo et al., 2014; Farma et al., 2013; Karangia et al., 2013). In such applications, batteries are usually sized to meet the system power requirement and cycle life (Burke, 2010; Omar et al., 2014) which often results in a heavy system. There is also a continuing effort to find ways to blend these two technologies (Choi et al., 2012; Vlad et al., 2014), apart from improving the material aspect of supercapacitors in order to improve their energy density (Li and Wei, 2013; Farma et al., 2013; Jang et al., 2013).

Supercapacitors require low maintenance (Sharma and Bhatti, 2010). They have almost unaffected performances even after a long-term of use, thanks to the non-Faradaic process supercapacitors use to store charge. Their utilisation in a system can potentially eliminate the need for frequent replacement as required by batteries, hence, saving the resources invested in the upkeep of the whole system in the long run. Despite having the characteristics of the ideal

energy storage device, a number of issues with the use of supercapacitors have been reported worldwide. Like many energy storage devices, after a number of years of usage, supercapacitors will demonstrate capacitance fading and an increase in resistance (El Brouji, Briat, Vinassa, Henry, et al., 2009). Moreover, the almost unlimited number of cycle life which has been used to push the adoption of supercapacitors in power hungry applications is only presumably true if all the boundaries are met (usually defined by manufacturers).

Fig. 1.1 shows three major areas of research that are currently pursued to improve the reliability of supercapacitors. While, the long life of supercapacitors can be expected if all the boundaries are met, there is a growing interest on the supercapacitor response outside these boundaries. During the last decade, a large number of investigations within supercapacitors and also automotive industries have been dedicated to test these boundaries to maximise the capability of supercapacitors and also to understand their ageing behaviour under certain conditions. Depending on the conditions under which they are operated, they will be impacted in many ways, thus calling for more studies in degradation mechanisms in supercapacitors (e.g. (Azaïs et al., 2007; Kötz et al., 2010; Briat et al., 2010; Cericola et al., 2011; Bittner et al., 2012; Ayadi et al., 2013; Jänes et al., 2012; Kurzweil and Chwistek, 2006; Nozu et al., 2009; Ruch, Cericola, Foelske-Schmitz, et al., 2010; Zhu et al., 2008)).

Besides that, there are also research on the improvement of product design (Lungoci and Oltean, 2010; Walden et al., 2011; Hijazi et al., 2012; Wang et al., 2013). Management systems and control strategies are also proposed to address the imbalances in terms of voltage and temperature distributions which can lead to different ageing rate, typically encountered in supercapacitor

modules, where many individual cells are connected to produce voltage that meet application requirements (Kötz et al., 2007; Sakka et al., 2009; Gualous et al., 2009).

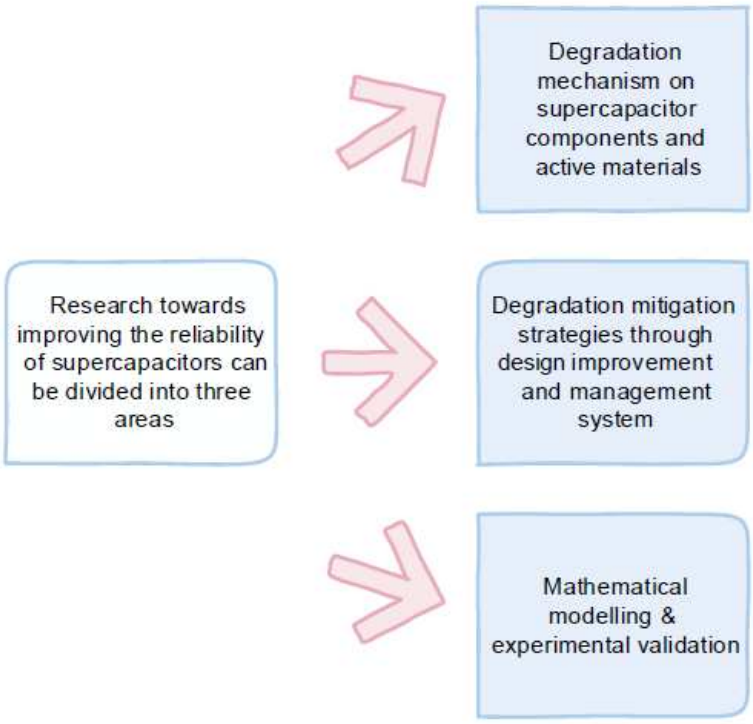

Fig. 1.1 Three major research areas to improve the reliability of supercapacitors.

A number of research has also been directed in the development of supercapacitors model to understand their behaviour and the implication of the product design on the electrical performance (Ban et al., 2013; Fletcher et al., 2014; Ike et al., 2015). The modelling of the device also has the merit in giving a first insight into its response in practical applications. For instance, before supercapacitors are physically integrated into a system, system designers will model the system in simulation software to simulate results of which will form the basis for how the whole system will behave in real situations. The modelling

approach often involves developing a model to match the real outcome from using supercapacitors.

In the supercapacitor modelling field, a large number of the proposed models are in the form of electrical equivalent circuits (EECs) (Ban et al., 2013; Faranda, 2010; Zhang and Yang, 2011; Tironi and Musolino, 2009; Diab et al., 2009). The EECs are usually built to specific applications. The problem lies in the time scale of the EECs operation. First, they are built for short-term operation, thus the response of the EECs covers only the short-term dynamic effects of supercapacitors. Second, they do not take into account the degradation in the state of health of supercapacitors. In reality, supercapacitors will be exposed to prolonged operations, where in due time, ageing will become inevitable. Therefore, efforts have been invested ever since to search for an approach that does not only look at the behaviour of the supercapacitor in a short operation, but is also interested in how supercapacitors will behave if it is used in the entire life of the system. This need has fuelled the emergence of complex models built to resemble the long-term behaviour of supercapacitors (e.g. (Martín et al., 2008a; Bohlen et al., 2007a; Lajnef, Vinassa, Briat, Azzopardi, et al., 2007; N Bertrand et al., 2010; Mitkowski and Skruch, 2013)).

1.2 Research problem, questions and justification for research

1.2.1 Research problem

Growing concern to improve the reliability of supercapacitor, especially in applications involving long operations, has encouraged the study of the ageing behaviour of supercapacitors. Fig. 1.2 illustrates that after years of use, ageing

will take its toll over time and thus leads to device failure. Unfortunately, the mechanisms of ageing in supercapacitors still an enigma to the industry and the understanding in the area is still lacking. This is probably due to the area is still in its infancy compared to its battery counterpart; therefore, the supercapacitors ageing mechanisms in relation to the stress factor is not as well documented. Although supercapacitors have received rapid development especially in terms of materials advancement to improve their performance, Ayadi et al. (2013) still feel that, "… one of the main challenges still remains in the understanding of the ageing mechanisms …".[1]

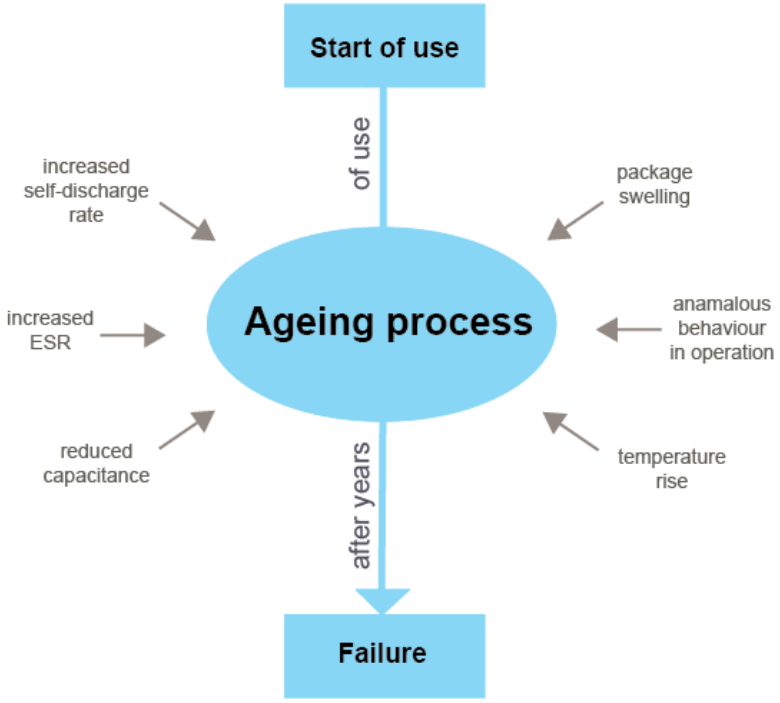

Fig. 1.2 Ageing process causes failure in supercapacitors.

[1] Ayadi, M., Briat, O., Eddahech, A., German, R., Coquery, G. and Vinassa, J.M. (2013) 'Thermal cycling impacts on supercapacitor performances during calendar ageing', Microelectronics Reliability, Vol. 53 No.9-11, pp.1628–1631., DOI:10.1016/j.microrel.2013.07.079

The importance of ageing state detection could not be more stressed than what Oukaour et al. (2013) have written, in which in their own words, state that,"… the improvement of supercapacitor reliability is fundamental and the follow-up and the detection of the ageing state remains a priority in order to avoid breakdowns and thus to intervene at the convenient moment."[2] The detection of the ageing state is important to allow for appropriate actions to be taken. This is only possible if there is a clear distinction between the ageing mechanisms and stress factors. Moreover, the identification of ageing mechanisms in relation to stress factors will allow a more effective and targeted product improvement effort, where supercapacitors can be optimised to meet application needs.

While many studies are dedicated to the effects of ageing on supercapacitors through macroscopic and microscopic evidences (Kurzweil and Chwistek, 2006; Azaïs et al., 2007; Bittner et al., 2012; Jänes et al., 2012) or parametric evidences (Lajnef, Vinassa, Briat, El Brouji, et al., 2007; Chaari et al., 2011; Gualous et al., 2012; Oukaour, Tala-Ighil, et al., 2013), only a few of them have focused on the identification of anomalous behaviour during the operation of the device (Bohlen et al., 2007a; El Brouji, Briat, Vinassa, Bertrand, et al., 2009; Kötz et al., 2010; Iwama et al., 2012). The anomalous behaviour herein refers to the behaviour that falls outside an expected normal behaviour of

[2] Oukaour, A., Tala-Ighil, B., AlSakka, M., Gualous, H., Gallay, R. and Boudart, B. (2013) 'Calendar ageing and health diagnosis of supercapacitor', Electric Power Systems Research, Vol. 95, pp.330–338., DOI:10.1016/j.epsr.2012.09.005

supercapacitor. This behaviour will contribute to the failure of supercapacitors and can be used to investigate the process of degradation and ageing.

In the degradation mechanism study in supercapacitors, the common method to investigate failure is performed backward (Fig. 1.3), that is, the process begins by identifying the supercapacitors failure modes, then the cause of the failure is determined, and the failure process is explained by the identification of the failure mechanism in the post-mortem analysis on the failed supercapacitor. The whole process, thus is carried out only after a supercapacitor has failed.

A better way is to prioritise the detection of the mechanism that leads to this failure. For instance, if early detection of anomalous behaviour or ageing mechanism can be done during system operation, this will allow for an intervention to be performed at the right moment. Therefore, this approach will avert premature failure during operation which will be catastrophic to the whole system. In the event where a failure has already occurred, this approach will also help to uncover the root cause behind any failure and accelerate post-failure analysis. Preventive measures can then be applied in future integration of the system based on the collected data. Furthermore, a ‘maximum operating life’ guarantee can be determined by equipment manufacturers that use these supercapacitors.

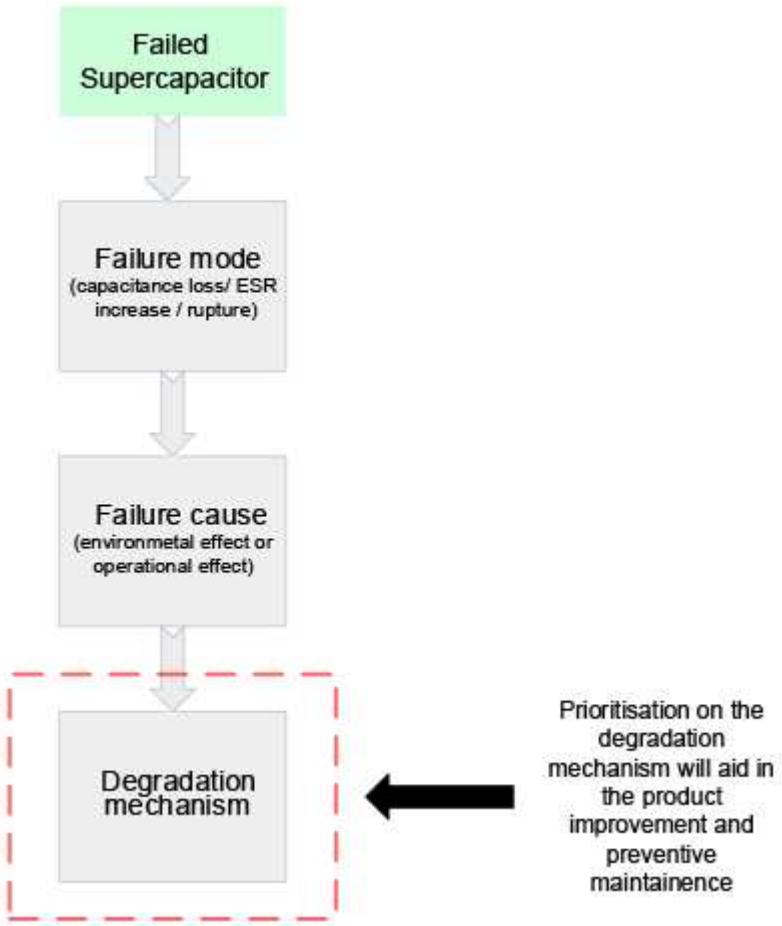

Fig. 1.3 Failure analysis process in supercapacitors.

From the results reported in (Kötz et al., 2010), voltage and temperature have distinctive effects on supercapacitors which can be seen in plotting the supercapacitor impedance data. This generates a presumption that each stress factor may have unique impedance signature. However, a question remains of how this trend or 'ageing signature' is related to the failure of supercapacitors. If the signature of a stress factor is known and its contribution to the decline in electrical performance and the failure in supercapacitors is understood, efforts to improve product design and material can be made accordingly.

The common method for studying the behaviour of supercapacitor is through modelling the current-voltage characteristics of the device using EECs.

However, this method does a little help in uncovering the cause of the deterioration in supercapacitor performance, which requires a deeper investigation at the cell level. The electrochemical processes, from the ageing of supercapacitor, degrade supercapacitor internal components. Either the degradation takes place at physical structural changes or alteration to the chemical characteristic, both of which will affect supercapacitor overall performance.

The EECs, however, are usually made up of components that are chosen based on phenomenological basis (Barsali et al., 2010), in which the components are chosen intuitively to match what is observed during supercapacitor operations. Such EECs may not necessarily related to the physicochemical processes in supercapacitors. Therefore, the lack of meaning of the EECs poses a challenge for the ageing and failure analysis (Nicolas Bertrand et al., 2010). The relationship between the EECs and the contribution of ageing process to the dynamics in supercapacitor electrical performance is not easily interpreted.

Therefore, this thesis aims at finding an approach that could bridge the study of dynamic electrical behaviour and the ageing process in supercapacitors, by means of electrical equivalent circuit modelling, as illustrated in Fig. 1.4. An electrical equivalent model that could expound the ageing mechanism in supercapacitor and the contributions of this mechanism to the decline of supercapacitor dynamic electrical performance is sought in this thesis. This approach is hoped to contribute in the understanding of the underlying physics of supercapacitors and to increase the efficiency of the optimising efforts invested in supercapacitors. In addition, the benefit of this approach can be reaped not only in aiding product engineers in the development of the product

but also will aid system designers to predict the supercapacitor response in real applications, particularly when ageing is involved.

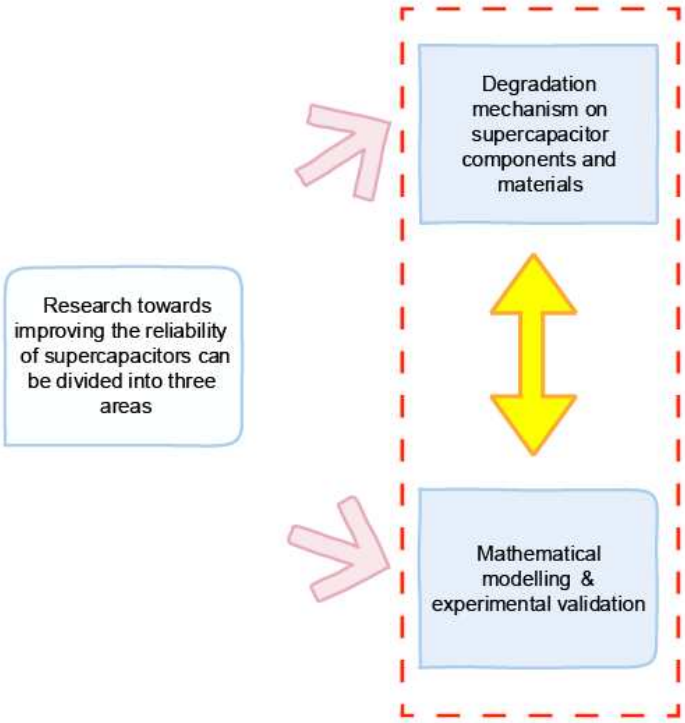

Fig. 1.4 Focus of the research.

1.2.2 Research questions

The research problems presented before have generated a few issues that the thesis seeks to answer. These issues are:

1. **Supercapacitor robustness in electric vehicles (EVs) or hybrid electric vehicles (HEVs) is uncertain.**

   Reliability remains as the central issue in the commercialisation of supercapacitor for hybrid transport and automotive application, although it is known that the integration of supercapacitor with battery will produce a better energy storage system (Burke, 2010). Car makers have

yet to adopt battery-supercapacitor marriage into their systems as there still remains a considerable uncertainty regarding the reliability of the supercapacitor, in particular, in which calls for the device to be studied in a greater detail to ensure the smoothness of operation throughout the lifetime of the vehicle (Umemura et al., 2003; Briat et al., 2010; Burke, 2010). Using a battery-supercapacitor energy storage system (ESS) in a vehicle system would mean that the car makers will have to deal with different degradation properties of each energy storage (Araujo et al., 2014). To complicate matters further, supercapacitor performance in real life and its degradation mechanism is not as deeply studied and understood as its lithium-ion battery counterpart and this has stymied the implementation of this system in automotive applications. The causes of supercapacitors ageing is addressed in Chapter 2, Section 2.3.1, page 62.

2. **The failure of an individual cell leads to failure of the whole supercapacitor module.**

   In automotive applications, particularly electric vehicles, supercapacitors used are in the form of modules (bank). A pack of supercapacitors are connected in series and parallel to form a module in order to meet voltages suitable for the vehicle electrical system, see Fig. 1.5.

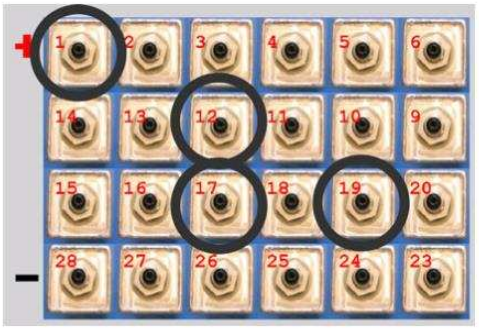

Fig. 1.5 Inside of a supercapacitor module. Multiple supercapacitor cells are connected in series and parallel (Rizoug et al., 2012).

However, the inequalities of capacitance and resistance between individual supercapacitors (from manufacturing dispersion) will result in the total voltage being unevenly distributed throughout the whole module. Therefore, a voltage balancing circuit is required to ensure a balanced voltage during charge and discharge cycle (Kötz et al., 2007). Dispersion of supercapacitor parameters also leads to different ageing rate for each individual supercapacitor. The location of the individual supercapacitor, too, contributes to the different ageing rate, whereby an individual supercapacitor that is closest to the terminal or combustion engine will be exposed to a higher stress and thus experiencing a stronger degradation than the rest of the cells (Bohlen et al., 2007b; Rizoug et al., 2012). Moreover, the temperature uniformity in supercapacitor modules is also a concern where a thermal management of supercapacitor modules is needed for automotive applications to ensure a uniform temperature distribution, hence, an even ageing rate among the individual cells can be expected (Schiffer et al., 2006; Sakka et al., 2009). From the above evidences, the failure of an individual cell will therefore

be detrimental to the entire module (Wei et al., 2009). In this thesis, the effect of ageing factors: temperature, current cycling and constant voltage, on the degradation of supercapacitors performance are addressed in Chapter 2, Section 2.3.2, page 72, and subsequently studied in detail in Chapter 5.

3. **Supercapacitors are sensitive to the ageing process and can only meet the requirements on life expectancy if certain boundary conditions are met. Can this failure be investigated and characterised?**

   The first step is to identify the boundary conditions and then to design a suitable experiment protocol so that any deterioration to supercapacitor performance can be observed within a reasonable time frame. One of the most difficult conundrums, however, is to isolate the cause of ageing. Capacitance loss and power fading do not originate from one single cause, but from a number of various processes and their interactions. This can be a result from electrical, mechanical or environmental stresses and it may also be influenced by the nature of the cell components itself. Most likely, voltage and temperature affect the lifespan of supercapacitors, whereby at these conditions the ageing process is accelerated. The knowledge of the effects of temperature, voltage and also charge-discharge cycle on supercapacitor performance and lifetime are vital for a successful utilisation of this device into the automotive system. Therefore, there is a need to identify and evaluate different ageing processes caused by these ageing factors and their contribution to the performance fading in supercapacitors, in order to establish a solid

basis for further investigations. Chapter 5 evaluates and characterises the ageing processes caused by temperature, voltage and repetitive charge-discharge cycling on supercapacitors.

4. **What type of model is able to capture and replicate this degradation mechanism?**

   To address the questions above, there is a need for a model which could give information not only on the supercapacitor electrical performance, but also contains information on the ageing mechanism in supercapacitors and the contribution of the ageing process to their declining performance after a long-term use. There are several models proposed in this area. Therefore, the next step is to find a suitable model which could meet these requirements (this model appears in Chapter 6):

   a. The model should be in the form of electrical equivalent circuit so that it can be implemented in a system modelling.
   b. The model should be able to represent the physicochemical process in supercapacitors with precision. The model should be able to differentiate this process to help with the optimization of cell design.
   c. The model should be able to cover a wide frequency range. Different physical effects take place at different time constants. Ageing effect, in particular, occurs at a very long time and for supercapacitor, this usually takes months to years.
   d. The model should be able to simulate the current-voltage characteristics for the evaluation of the electrical performance of supercapacitors.

1.3 Research objectives

This research aims to seek an approach through the modelling of supercapacitors which can shed light on the dynamic interactions between ageing process and electrical behaviour of supercapacitors in order to improve product development effort and assist in reliability assessments. Specifically, the research aims:

1. To investigate the principle effect of a single ageing factor and the effect of combining two or more ageing factors on supercapacitor electric performance and degradation, in order to distinguish the ageing mechanism in relation to these ageing factors. The typical failure resulting from the interactions of these factors is also to be investigated in order to understand the risks associated with supercapacitors failures under conditions which they will be operated. This will therefore aid in the design of a reliable supercapacitor and a control system to protect against conditions that can cause supercapacitor to fail.
2. To develop a model of supercapacitor electrical performance in electrical equivalent circuits which covers all the important dynamics in the supercapacitor behaviour, and at the same time is also able to model the degradation process in aged supercapacitors. The model, thus, needs to be related to the physicochemical process in supercapacitor to permit for the identification of the dominant degradation mechanism, which affects the electrical performance of supercapacitor. This is done to understand the process leading to the decline in supercapacitor performance; so, it will help to facilitate a correct design of supercapacitor for the targeted application and the design of supercapacitor management system. This

way, the model can be used as a tool to locate the problem in the supercapacitor design and also tells the effectiveness of the current supercapacitor design for the targeted application.

3. To relate the ageing mechanism and the electrochemical and structural changes in aged supercapacitor to the electrical equivalent circuit in order to understand how the ageing mechanism contributes to the failure in supercapacitors.
4. To identify and evaluate the main changing parameters of the electrical equivalent circuit during the ageing process and the evolution of these parameters as a function of time which will be useful for predicting the current-voltage characteristics after a long operation and also for the state of health monitoring.

1.4 Significance of the study

This research prioritises the ageing mechanism in supercapacitor. The prioritisation of the ageing mechanism is useful for predicting time to failure and to increase the effectiveness of product improvement effort. Usually failure analysis is done backward, that is, the analysis is carried out after the supercapacitor has failed. The step usually begins by identifying the supercapacitor failure modes, then determining the cause of failure, only then the process of failure is explained through an identification of the failure mechanism after a post-mortem analysis is performed to the failed supercapacitor. The hypothesis presented here is that if knowledge of the ageing mechanism is first known, the failure cause can be pinpointed and resources can be freed to mitigate the failure caused by device. In that regards, the thesis seeks

to identify this ageing mechanism during device operation, so that intervention can be done at the right moment. Ageing model, sought in this thesis, will help in the understanding of the ageing process through the evaluation of the precursor parameters which lead to a failure and thus helping in predicting the future behaviour of the supercapacitor especially in applications involving long operations.

1.5 Methodology

In order to achieve the goals set in the thesis, the thesis started with the investigations on the reported ageing phenomenon, the cause of ageing and the type of failure this ageing phenomenon has led to in supercapacitors. This also includes the research on suitable methods and tools to monitor ageing process and to gather the respective information. A correct selection of tool and method is key to the success of the research. The experimental method was chosen based on these requirements: (1) it shall permit the study of the interactions between the causes of ageing to the failure events in supercapacitors, (2) able to accelerate the ageing process to the duration permissible for laboratory testing, and (3) can be reproduced and replicated outside the laboratory.

Literature have shown that accelerated ageing test could compress the long duration required for ageing process to manifest. Therefore, the thesis employed the accelerated ageing test to speed up the ageing. The test bench is shown in Fig. 1.6. The accelerated ageing test requires the test to be done at the maximum capability of the supercapacitor to withstand stress; therefore, a careful selection of the level of stress was done by referring to the manufacturer's specification to establish test boundaries, at the same time taking

into consideration the applications the supercapacitors will be operated in. With the use of accelerated ageing test, the duration of the experiment was shortened from years to months. The observed ageing results were compared with the literature to find any regularity or irregularity in the observed behaviour of aged supercapacitors, in order to confirm that the experimental method did not cause spurious effect on the supercapacitors under investigation.

Fig. 1.6 Test bench of the experiment: RANSCO Environmental Chamber used to perform the accelerated ageing test (left) and inside view of the environmental chamber shows a fibre glass tray with supercapacitors mounted on top. Each supercapacitor is connected to a separate current source (right).

Since many techniques have been used in the literature to measure the health of supercapacitors, a study on the measurement methods were conducted to find the correct measurement settings, befitting the supercapacitors tested in this thesis, and the relations between the values reported from each measurement method. Based on the findings, a periodic measurement protocol was laid out for use during the accelerated ageing test to periodically monitor the state of health of supercapacitor and the ageing process.

The diagnosis of the ageing effect in supercapacitors was mainly done with electrochemical impedance spectroscopy (EIS). EIS plots the impedance data of the supercapacitors at each stage of the supercapacitor life, thus providing the evolution trend of the supercapacitor impedance, also as a useful tool to detect changes in supercapacitor properties caused by ageing process. Given that EIS applies a very small AC signal, in which the supercapacitors were ensured to be in their linear states, no destruction to the cell was made during measuring. This aspect is crucial to ensure that the integrity of the collected data is not compromised by the measurement.

EIS provides detailed electrochemical information in supercapacitor, which is useful for the development of EEC. The development of EEC allows a detailed investigation on how the ageing process affects the electrical performance of supercapacitors. Moreover, the EEC makes it possible to identify and select precursor parameters which cause the failure in supercapacitor. Since each of these parameters is associated to the kinetic information in supercapacitors, the changes of these parameters indicate changes to the supercapacitor health and properties. The evolution of these parameters were plotted to reveal how the ageing process proceeds as a function of time under a given condition.

The EEC not only aids in the understanding of the kinetic information in supercapacitor and how the ageing progresses, it is also used to predict the supercapacitor current-voltage characteristic which is extremely useful in the application. Therefore, a detailed procedure to simulate the EEC were given at the end of the thesis. The key contribution of this thesis, hence, lies in the proposed EEC which model the ageing process in supercapacitor. The EEC is

referred to as the ‘ageing model’. The ageing model contains information on the ageing process and how the supercapacitor state changes due to the ageing process. Furthermore, the ageing model can also be used to simulate the current-voltage characteristic. Therefore, the ageing model is useful to both the materialist and product engineer to improve supercapacitors; investigations can directly be made based upon the ageing model in order to determine which aspect of the supercapacitor contributes to the declined performance in field and needs to be improved. The ageing model is also useful to the system engineer to predict the behaviour of the supercapacitor in long-term operations.

1.6 Scope of the thesis

The study here is limited to single cell symmetric supercapacitors in cylindrical packages, with voltage rated at 2.7V, and capacitance of 25F, made using activated carbon electrodes and acetonitrile electrolyte.

Furthermore, this study only covers the wear out failures and ageing behaviour induced by external factors such as environmental stress and operational stress. This study only covers the ageing behaviour caused by high temperature, constant voltage and cycling.

In case for the ageing behaviour at high temperature, the supercapacitors are aged at 85℃. The choice of the temperature is made based on the maximum operating temperature of the supercapacitor and taking into account the boiling point temperature of the acetonitrile electrolyte. It is believed that sufficient acceleration of the ageing process can be achieved at this temperature that is practical for a laboratory setting.

In case for the supercapacitor ageing behaviour due to cycling, only ageing behaviour in response to a symmetric square cycling profile made up of 0.6A current is studied in this thesis. The choice of the current is anchored on the capability of the supercapacitor, the charge and discharge duration for each cycle and the capability of the hardware.

The ageing behaviour due to constant voltage application with voltage of 2.7V is studied. The 2.7V constant voltage is chosen according to the maximum voltage of the supercapacitors, defined by the manufacturer.

1.7 Outline of the thesis

Chapter 2

Chapter 2 begins with the introduction to the current market situation for supercapacitors: where they currently stand and the market expectation of the device. Then, the chapter proceeds to explain what supercapacitor is, why many research have been invested on the technology and how it is made. The fundamental theory behind supercapacitors is explained next; this includes a description on the different types of supercapacitors available in the market and the materials used. A review on the testing and industry standards on supercapacitors is brought next, touching also the use of independent laboratory test procedures and manufacturers published testing manuals. A review on the supercapacitor models is followed next, beginning with the theory behind the development of the models to the different types of models existing today. Next, a review on the causes of ageing in supercapacitors reported from literatures is presented; in addition to the classification of ageing according to where ageing

occurs inside the supercapacitors. After that, the chapter describes the types of ageing tests that have been conducted worldwide; this includes identification of the ageing factors and the method used by the researchers to conduct the test and analyse ageing. The chapter ends by stating the gap seen from the pool of literature.

Chapter 3

Chapter 3 of this thesis contains the methodology employed in this research work. The chapter starts by stating the need for a prediction of when a failure of a product occurs, in order to better prepare for the risk involved with a failure of a product. The chapter states the step by step process of the development of the methodology from, first, through the determination of the end-of-life criteria, to the types of failures to be investigated in this thesis, the choice of stress level for the accelerated ageing test, characterisation methods of the supercapacitors and the tools used to monitor ageing. This follows with the development process of the electrical equivalent circuit models and finally, the empirical method used to analyse the evolution of model parameters to explain the ageing process is described. The chapter contains information on all the tools and the type of supercapacitors used in this thesis. The chapter ends with an introduction to the experimental techniques used throughout the work.

Chapter 4

Chapter 4 presents the study on measurement methods for supercapacitors which are currently being used in the industry and in laboratories worldwide. The varying results being reported from these measurement methods, pertaining to the value of capacitance and ESR, have sparked the need to investigate how

these methods contribute to the discrepancy in the values. A survey on the methods used by supercapacitor manufacturers is also presented. The results from each measurement method are compared. From the comparison result, the appropriate testing methods and test settings are chosen for use in the experimental work which appears in subsequent chapters.

Chapter 5

This chapter presents the results from accelerated ageing test on supercapacitors. The chapter is interested in studying the effect of environmental and operational stresses on the supercapacitors ageing process. Therefore, the effect caused by high temperature, current cycling and constant voltage are studied individually in order to distinguish the ageing mechanism in relation to these ageing factors. The changes to the state of health and properties of the supercapacitors are monitored periodically in the periodic characterisation test. The results from electrochemical measurements are compared with the supercapacitor electrical performance in order to find a correlation between the ageing processes to the declined performance in supercapacitor. From the isolation of the ageing factors, this chapter identifies the ageing signature of each factor and hence, identifying the primary contributor to the deterioration in performance.

Chapter 6

Chapter 6 presents the development process of the baseline model and the ageing model using the results obtained in Chapter 5. These models expound the kinetic processes which govern the dynamic behaviour in supercapacitors. Ageing models of each ageing factor are proposed based on the observed ageing mechanisms from these factors. The evolution from the baseline model to the

ageing model is illustrated in this chapter, thus representing the changes in the state of health of the supercapacitors due to the ageing process. Since, the baseline model and the ageing models are in the form of electrical equivalent circuit model, this permits the simulation of the current-voltage characteristic of these models. The development of the models in simulation software to simulate the current-voltage characteristics are explained in detail. The chapter also provides an approach which can be used to select parameters which have the most influence on the ageing mechanism. The chapter also monitors the evolution of these parameters during ageing which are useful to predict the supercapacitor state of health, and at the same time to understand how the kinetic processes interact.

Chapter 7

Chapter 7 discusses and concludes the work in this thesis. The contributions of the thesis to the body of knowledge are summarised. This chapter also discusses the areas that the thesis does not address but can be an avenue for future research.

CHAPTER 2

BACKGROUND AND LITERATURE REVIEW

"Wisest is she who knows she does not know"

—Jostein Gaarder, *Sophie's World*

2 Introduction

This chapter begins with a background on supercapacitors, covering its current characteristics and some fundamental aspects. The chapter proceeds with reviewing literature on the following topics: supercapacitor models, causes of ageing in supercapacitors, types of ageing tests and results, including the tools used by these researchers to quantify the ageing process. The final section of the chapter highlights the implications of the literature and identifies the missing element in the existing body of knowledge. The chapter concludes with formulating the research question that this thesis seeks to answer.

2.1 Supercapacitor

2.1.1 Where it stands in the market?

Supercapacitors (SCs) are not new. Its historical precedents reach back to 1957 with the first patent submitted by H. Becker (Conway, 1999; Kötz and Carlen, 2000). However, it was not until recently did we see the growing use of SCs, particularly in the automotive industry and portable electronics. Globally, SCs still remain far behind batteries; until now, batteries dominate the largest market segment for energy storage, mostly due to their superiority in terms of energy density. Nevertheless, SCs have shown a very promising future. Lux Research projects the market for SCs will increase to $836 million in 2018, double the figure in 2013 (Jacques, 2013).

According to the ten year market forecast report published by IDTechEx Ltd. in 2014 (Harrop et al., 2014), 61% of SC manufacturers are in East Asia, 24% are in North America, followed by Europe by only at 6%, see Fig. 2.1. The biggest name in the market is Maxwell Technologies Inc. (USA) and other suppliers include: Cap-XX (Australia), Nesscap Co. Ltd. (Korea), Yunasko (Ukraine), Panasonic Electric Devices Co. Ltd. (Japan), just to name a few (Harrop et al., 2014; Wang et al., 2012). In 2014, SC has the largest market shares in electronics, and followed by hybrid transport and automotive industry; it is projected that in 2020, the automotive segment will increase by twofold (Fig. 2.2) (Gonzalez, 2014).

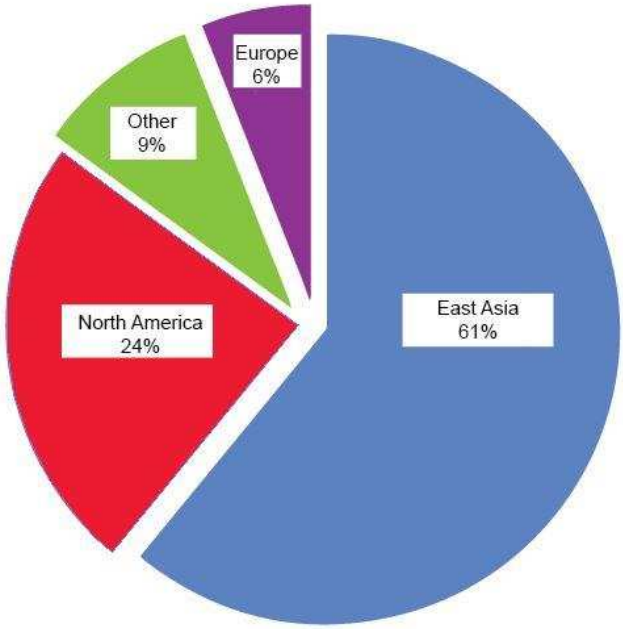

Fig. 2.1 The location of 66 supercapacitor manufacturers by continent. Figure adapted by author from (Harrop et al., 2014).

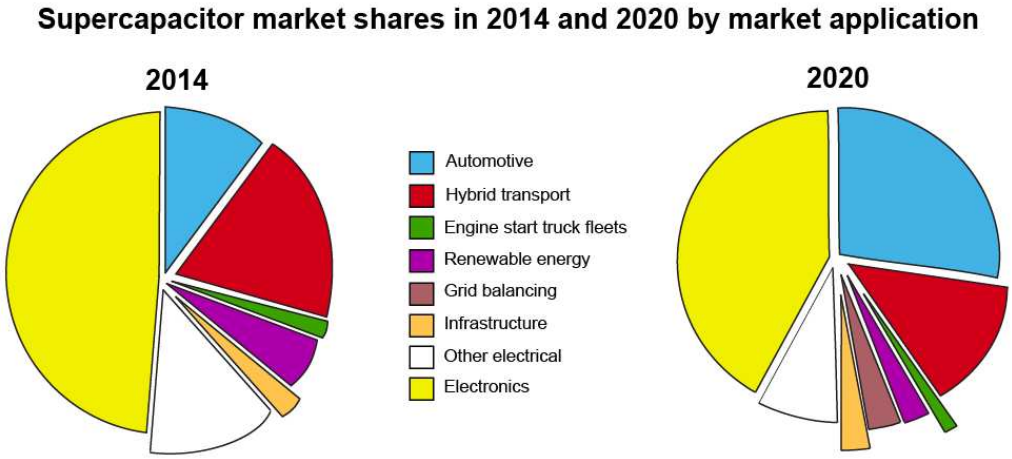

Fig. 2.2 Supercapacitor market shares in 2014 and 2020 by market application. Figure adapted by author from (Gonzalez, 2014).

2.1.2 The What, The Why and The How

There are not many textbooks on SCs on the shelves. The first monograph on SCs was written by B.E. Conway in 1999 (Conway, 1999) and just quite recently a text edited by Béguin and Frąckowiak (Béguin and Frąckowiak, 2013) has been published. When we talk about SCs, it is ineluctable to compare them with batteries. Batteries long-standing record as the energy storage of choice in many sectors, including but not limited to, consumer electronics, portable electronic, automotive, and industrial electronics, are attributed to their large energy reservoir, for example, lithium-ion (Li-ion) battery has an energy density in the range between 120 to 200 Wh/Kg (Li and Wei, 2013). The lower cost of batteries also contributes to their deeper penetration into the market; and also partly due to their long-understood technology.

The energy in the battery is generated by reduction-oxidation (redox) reactions at the anode and cathode (Winter and Brodd, 2004). The process is faradaic, which means, the high energy generated through this reaction is at the expense of the active materials of the battery, which will be irreversibly consumed over the operation time. Therefore, this limits the lifetime of battery, for instance, Li-ion batteries can only last for 1,000 to 10,000 cycles or between 5 to 10 years (Wang et al., 2012).

Today, batteries are facing challenges. The first is pertaining to their limited life cycle—a frequent replacement of batteries are always required and this induces substantially high maintenance cost. Secondly, their low power density cannot meet the increasing demand of power hungry applications, such as in multifunctional portable devices (Gonzalez and Harrop, 2014). The world

has realised that SCs can potentially replace batteries or can be used as a complement to batteries; the efforts have been directed to improve this energy storage. As depicted in the Ragone plot in Fig. 2.3, SC lies somewhere between a capacitor, it can store up to 100x the specific energy (Wh/Kg) of conventional capacitors, and a battery, with up to 10 times more specific power (W/kg) (Béguin and Frąckowiak, 2013). It takes the advantage of capacitor's rapid delivery and has the energy density almost like a battery.

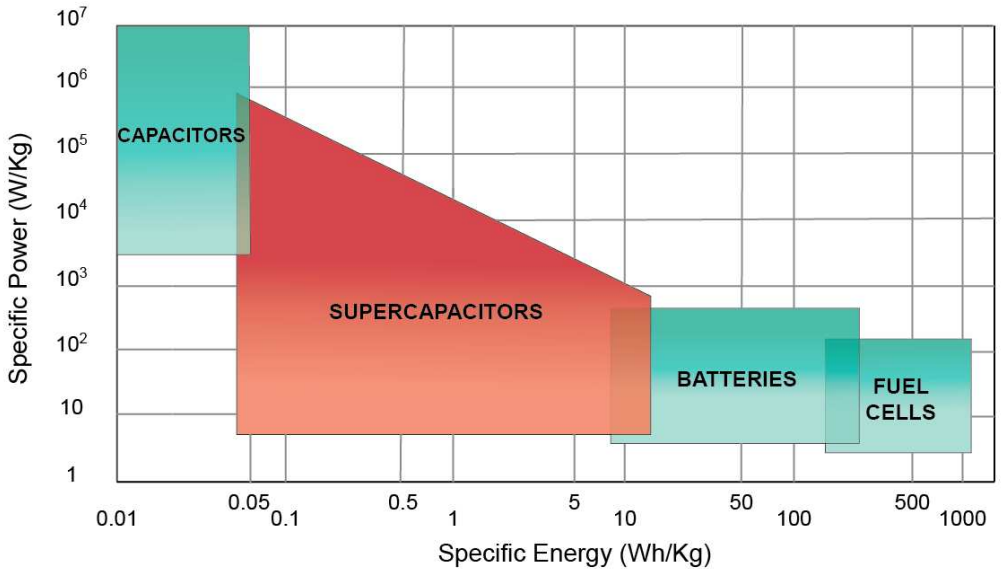

Fig. 2.3 Ragone plot of different electrochemical energy storage. Figure adapted by author from (Kulsangcharoen et al., 2010).

In SCs, the charge storage process is non-Faradaic, that is, the charge is stored electrostatically and no electron transfer takes place at the electrode/electrolyte interface. The energy is stored by charge accumulation at the electrode/electrolyte interface through ion adsorption. SCs consist of two electrodes, electrolyte and separator. The charge storage mechanism is illustrated in Fig. 2.4. The charge accumulation forms a double layer (DL) at each electrode: the first layer is comprised of an adsorbed fixed layer and the

second layer is a diffuse layer. The DL at the electrode/electrolyte interface behaves like a parallel plate capacitor, and since the SC has two electrodes, the complete cell can be described as two capacitors connected in series. When a potential is applied to charge SCs, the charges travel from one electrode to the other electrode and during discharging, the charge movement is reversed. The charging/discharging process is rapid. Since there is no electron transfer involved across the electrode/electrolyte interface, SCs have a long life cycle, almost unlimited. SCs can last for up to 1,000,000 charge/discharge cycle (Wang et al., 2012).

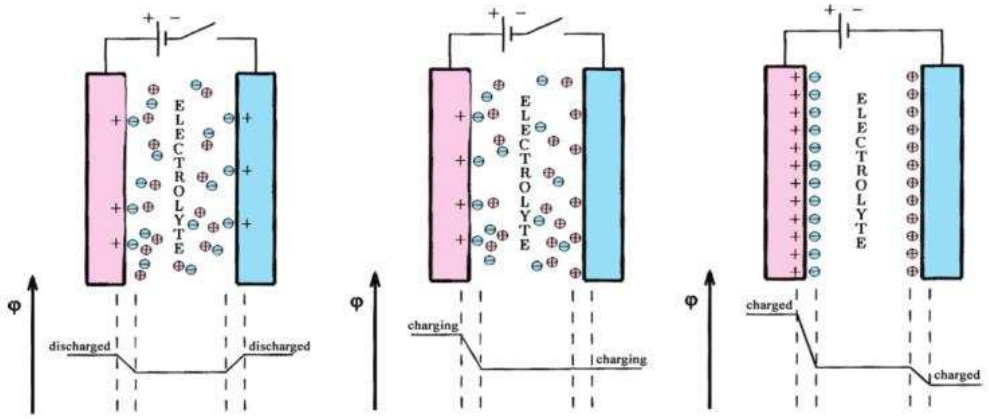

Fig. 2.4 Charge storage mechanism in supercapacitor illustrated in (Winter and Brodd, 2004).

2.1.3 Supercapacitor principles

Supercapacitors (SCs) are sometimes called Electrochemical Double Layer Capacitors (EDLCs), because of the DL formed at the electrode/electrolyte interface. In the United States, the term ultracapacitors are more popular. Regardless which name is used, they all refer to capacitors with very high surface area electrodes.

A capacitor is, in fact, two parallel electrodes separated by a dielectric, hence it is also known as a parallel plate capacitor. Fig. 2.5 shows a simplified parallel plate capacitor. The dielectric is usually a non-conducting material (Sharma and Bhatti, 2010). When a potential is applied to the capacitor, positive charge Q^+ will migrate toward the surface of an electrode plate and negative charge Q^- to collect on the surface of the other electrode plate. This charge separation develops an electric field, E between the plates.

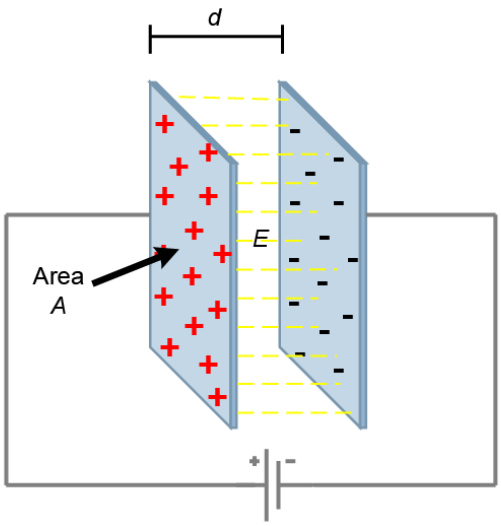

Fig. 2.5 A simplified parallel plate capacitor.

Capacitance (C), has a unit in Farad (F), is the ratio of the electric charge (Q) on each plate to the potential difference (V) between them.

$$C = \frac{Q}{V} \tag{2.1}$$

The derivatives of $Q = CV$ in Eq. (2.1), gives the voltage/current relationship in a capacitor as,

$$i(t) = \frac{dQ}{dt} = C\,\frac{dV}{dt} \tag{2.2}$$

In a parallel plate capacitor, capacitance (C) is also proportional to the area (A) of each electrode plate and the permittivity (ε) and inversely proportional to the distance between plates (d).

$$C = \frac{\varepsilon A}{d} \tag{2.3}$$

From Eq. (2.1) and Eq. (2.3), the potential difference (V) of a capacitor can be calculated as,

$$V = \frac{\varepsilon A}{Qd} \tag{2.4}$$

and a charged capacitor has the energy (E), measured in joules (J), is described as,

$$E = \frac{1}{2}QV = \frac{1}{2}CV^2 \tag{2.5}$$

SCs share the same basic principles as capacitors. As previously mentioned in the subsection 2.1.2, SC consists of two electrodes immersed in an electrolyte, as shown in Fig. 2.4. Each electrode behaves like a parallel plate capacitor and therefore a complete SC cell, having identical electrodes, is essentially behaving like a parallel plate capacitor. If the capacitance of the positive and negative electrodes are C_+ and C_-, respectively, the capacitance (C) of a SC is therefore,

$$\frac{1}{C} = \frac{1}{C_+} + \frac{1}{C_-} \tag{2.6}$$

Note from the Eq. (2.3), the capacitance can be increased by: (1) increasing the surface area of the electrode plate, A, or (2) decreasing the distance between the plates, d, or (3) using a dielectric material with higher permittivity, ε. While capacitors typically can be found in the range between

thousands of picofarad (pF) to tens of thousands of microfarad (μF), SCs can have capacitance up to thousands of farads. In SC, the high capacitance is achieved by using electrode material with a very high surface area (1000-2000 m^2/cm^3) and the distance between the electronic and ionic charge at the interface (Sharma and Bhatti, 2010), that is, the thickness of the DL, is so small (Fig. 2.6). The DL thickness depends on the concentration of the electrolyte (Zhang et al., 2009). For instance, the thickness of the DL in liquid electrolytes is in the range of nanometer (nm) (Burke, 2000).

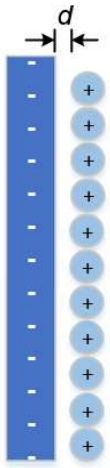

Fig. 2.6 Schematic representation of the double layer. ***d*** is the thickness of the double layer.

In terms of performance characteristics, capacitor and SC show a very distinctive impedance response, as exemplified in Fig. 2.7. In the Nyquist plot, a capacitor will exhibit a 90° straight line. Meanwhile, SC impedance exhibits a line with 45° angle to the real axis at high frequency and the line continues to extend to an almost vertical line at low frequency. The impedance line is shifted by an amount of equivalent series resistance (ESR).

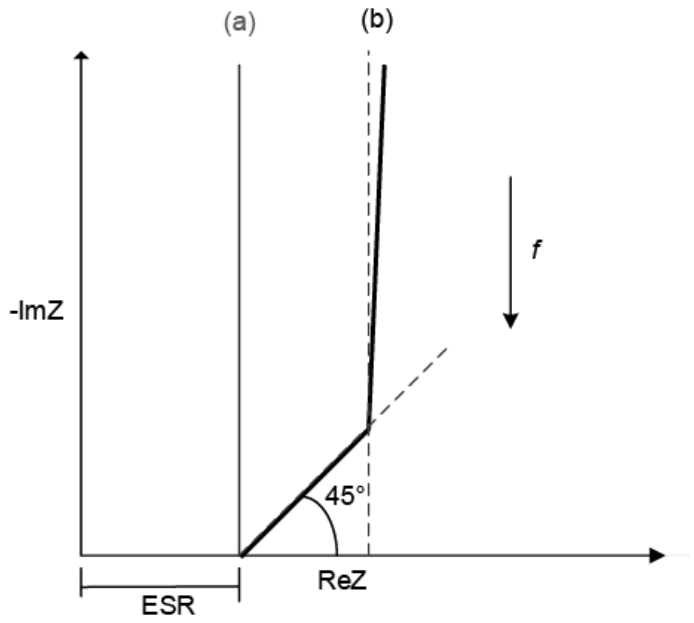

Fig. 2.7 Nyquist plot of an ideal capacitor (a) and a supercapacitor (b). ESR is the equivalent series resistance from the components inside the cell. Figure adapted by author from (Kötz and Carlen, 2000).

2.1.4 Taxonomy of supercapacitors

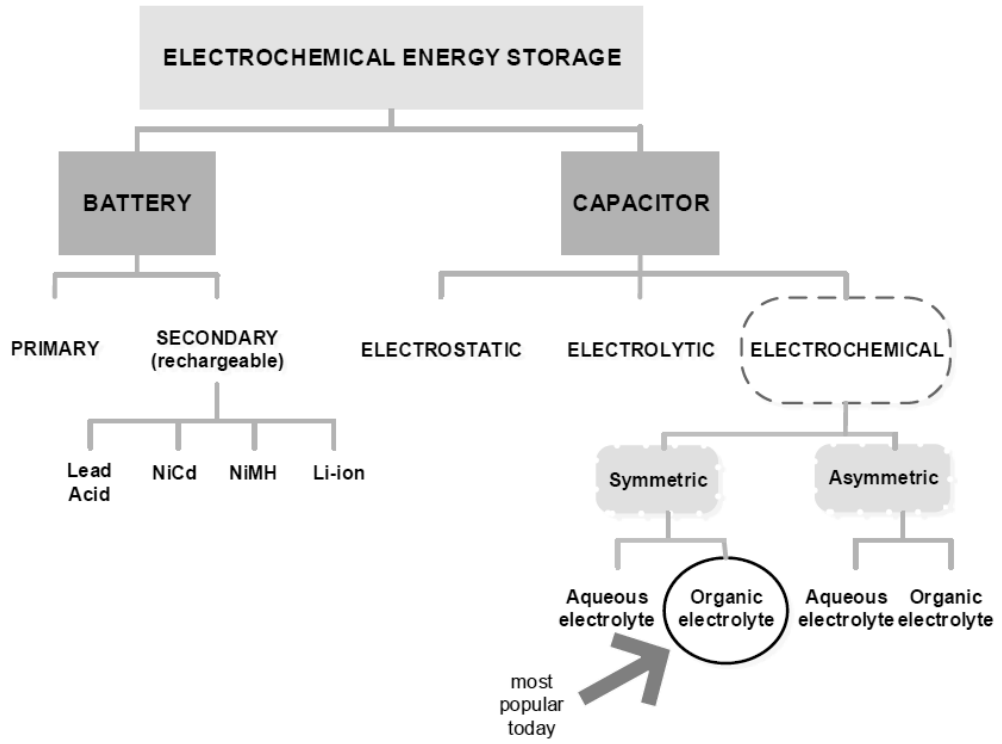

Fig. 2.8 Taxonomy of electrochemical energy storage. Figure adapted by author from (Miller, 2011).

Currently, many different types of SCs are available, categorised based on the cell design and types of dielectric used, as indicated in Fig. 2.8. Fig. 2.9 illustrates the inside of a SC cell. The construction of SCs are similar to batteries, in which they are constructed by two electrodes immersed in an electrolyte solution. The two electrodes in SCs are separated with a separator in order to prevent electrical contact between them. In symmetric SCs, both electrodes are identical and use the same electrode material. Meanwhile, in asymmetric SCs, two different materials are used for the positive and negative electrodes (Sharma and Bhatti, 2010), usually one electrode is made of carbon and the other

electrode utilises pseudo-capacitance[3] material or battery electrode (Burke, 2010). The discussion in this thesis is only limited to symmetric types.

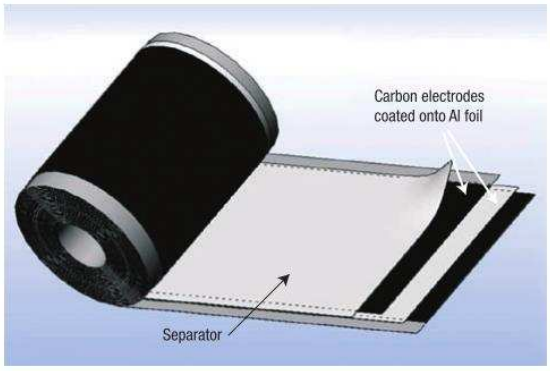

Fig. 2.9 Inside a cylinder-type supercapacitor (Simon and Gogotsi, 2008).

2.1.4.1 Electrode materials

SCs achieve a high surface area due to the highly porous electrode materials. The most popular electrode material to date is carbon, owing to its low cost, high surface area and easy production (Ruiz, Blanco, Granda, Menéndez, et al., 2008). Other materials are also being used, typically in asymmetric SCs, for example, conducting polymer and metal oxides (Simon and Gogotsi, 2008). Carbon materials are produced through carbonization and activation procedure (Pandolfo and Hollenkamp, 2006) and they exist in a variety of forms which include the most widely used activated carbon (AC), template carbons, carbon fibres, carbon nanotubes (CNTs) (Li and Wei, 2013) and graphene (Volfkovich et al., 2013). Activated carbons are derived from carbon-rich natural precursors,

[3] Pseudo-capacitance electrode involves faradaic process when a potential is applied. The most common materials to construct pseudo-capacitance electrode are conducting polymers and metal oxides like ruthenium oxide RuO_2 and manganese dioxide MnO_2. (Wang et al., 2012)

for example, coconut shells, wood or coal, or synthetic materials like polymers (Simon and Gogotsi, 2008).

The specific capacitance of SCs depends on the surface area of the carbon-based materials. The larger the surface area, the higher the specific capacitance is. The surface area of a carbon electrode consists of pores of various sizes. Fig. 2.10 illustrates the pore of activated carbon. The largest pore are macro- (greater than 50nm diameter), followed by meso- (2-50nm diameter) and micro-pores (less than 2nm diameter) are the smallest pores (Wang et al., 2013). The macro-pores are usually located at the mouth of the pores and meso- and micro-pores are located deeper inside. In electrodes immersed with electrolyte, cations and anions will first fill the macro-pores and then moving towards the interior in order to fill the other smaller pores, as illustrated in Fig. 2.11.

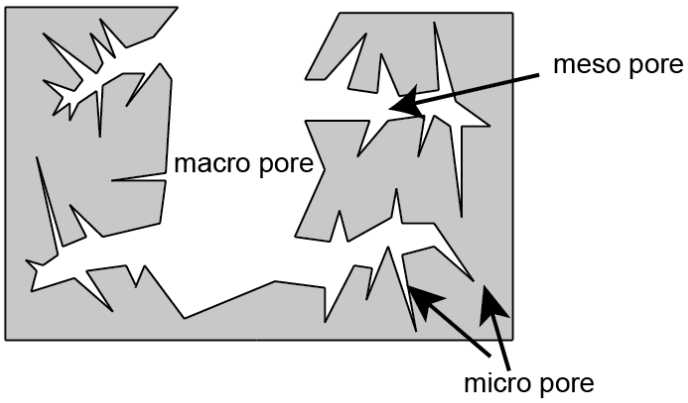

Fig. 2.10 Conceptual scheme of pore of activated carbon. Figure adapted by author from (Itagaki et al., 2007).

Aside from the surface area, capacitance is also influenced by the pore size distribution. Pandolfo and Hollenkamp (2006) stated that not all pores are electrochemically accessible (Pandolfo and Hollenkamp, 2006). Pores that are too small will obstruct electrolyte ions from penetrating inside the pore (Li and

Wei, 2013) and consequently, the formation of DL will be hampered. There is now several research, such as those listed in (Sun et al., 2013; Morita et al., 2014), have already been underway to increase the pore size distribution and thus increasing the electrolyte accessibility. Besides that, the compatibility of electrolyte and the carbon material need to be considered (Zhou et al., 2007).

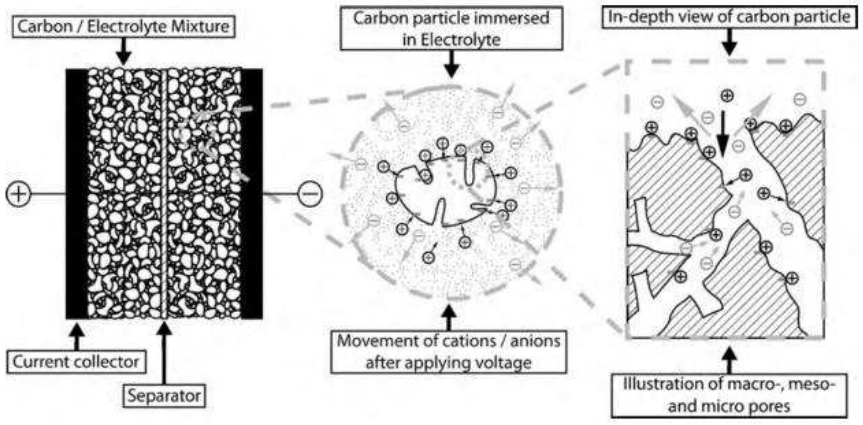

Fig. 2.11 Illustration of the movement of cations and anions inside the pore of activated carbon electrode (Kaus et al., 2010).

The SC electrode is typically composed of activated carbon, as the main element, carbon black, as the conductive agent, and polymeric binder. All the components are mixed together to form a slurry, which will be used to coat both sides of an aluminium foil which acts as the current collector. The carbon black is essentially used to improve the conductivity and the polymeric binder (usually polyvinylidene fluoride (PVDF)) is used to hold the carbon-mixture together and to promote adhesion of the carbon-mixture to the aluminium foil. To improve the adhesion of carbon to the aluminium foil, the aluminium foil is made porous through etching and so increasing the contact surface-area (Pandolfo and Hollenkamp, 2006).

2.1.4.2 Electrolyte

The SC operating voltage window is limited by the type of electrolyte used. There are two most widely used electrolytes in SCs: aqueous and organic electrolytes. The third type of electrolyte is the ionic liquid (IL), however, it will not be discussed in this thesis. The pie chart below (Fig. 2.12) shows the percentage of manufacturers using organic, aqueous and IL in their SCs.

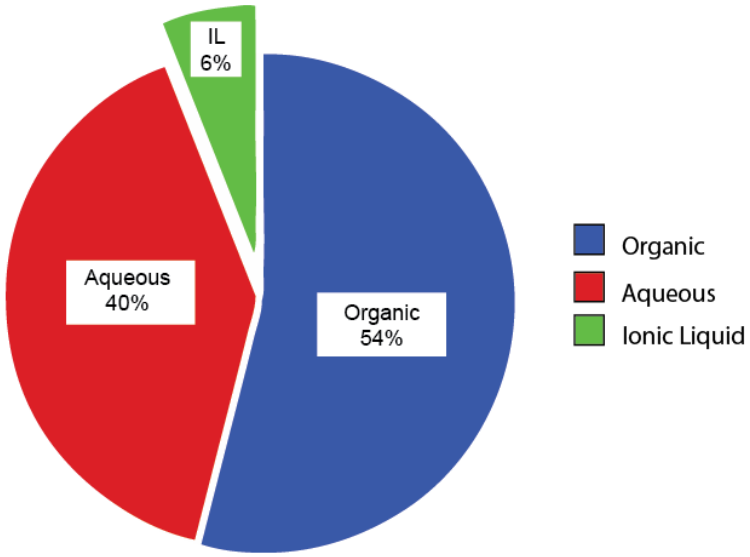

Fig. 2.12 The percentage of supercapacitor manufacturer using organic, aqueous and ionic liquid electrolytes. Figure adapted by author from (Harrop et al., 2013).

Listed under the aqueous group electrolyte are H_2SO_4, KOH, Na_2SO_4 and NH_4Cl. Aqueous electrolyte has high ionic concentration and low resistance. SCs utilising this type of electrolyte have higher specific capacitance and higher specific power than SCs utilising non-aqueous electrolytes. Moreover, aqueous electrolyte is low in cost (Béguin and Frąckowiak, 2013). However, aqueous electrolyte has a small voltage window due to its low decomposition voltage. Its

decomposition voltage can be as low as 1.2V. Recently, Ratajczak et al. (2014) have demonstrated that SC using Li_2SO_4 aqueous electrolyte can operate until 1.5V, higher than 1V, that is typically attained by KOH and H_2SO_4 aqueous electrolyte (Ratajczak et al., 2014).

Organic electrolyte, on the other hand, has higher decomposition voltage, as high as 3.5V (Wang et al., 2012). Aqueous low decomposition voltage makes it harder to improve SC energy and power densities. Furthermore, a high operational voltage wold mean that the supercapacitor will generate a greater specific energy. This is why organic electrolyte is always preferred than aqueous electrolyte in commercial SCs and in high-energy applications. The only drawback is the organic electrolyte has higher resistance than the aqueous electrolyte. Under the organic electrolyte group, there are propylene carbonate (PC) and acetonitrile (AN) solvents. PC-based electrolytes are environmental friendly, but suffer at low temperature. Whereas, AN-based electrolytes can dissolve larger amount of salt (Wang et al., 2012), but are toxic to the environment. Nevertheless, AN-based electrolytes have excellent low temperature performance than PC-based electrolytes (Liu et al., 2006).

In organic electrolytes, salts will be dissolved in PC or AN solvents. The most common salts are tetraethylammonium tetrafluoroborate ($TEABF_4$) and triethylemethylammonium tetrafluoroborate ($TEMABF_4$). Nevertheless, Ionica-Bousquet et al. (2010) have demonstrated that polyfluorododecarborate-based salts, usually used for Li-ion batteries, can be used in SC to reduce solvent degradation under harsh condition and thus, extending cell life (Ionica-Bousquet et al., 2010).

2.1.4.3 Separator

A separator is used in the fabrication of SCs to prevent electrical contact between the two electrodes. Separators are porous membrane that is ion-permeable to allow ionic flow across the separator and into the electrode (Kötz and Carlen, 2000). Separators for SCs utilising organic electrolytes are usually cellulosic papers. Glass fibre separators are also used, often with aqueous electrolytes (Sharma and Bhatti, 2010).

The separator does not participate in the cell reactions, but its properties can affect SC performance. Presently, there is not much discussion on SC separators can be found in the literature. Nevertheless, the effect of separator thickness to SC resistance has been studied by Stoller and Ruoff (2010) (Stoller and Ruoff, 2010). A thicker separator yields higher resistance because it increases electrode spacing. Therefore, a thinner separator is preferred; however, it must have adequate strength to withstand the pressure of being wound up, in particular, during the construction of cylinder-typed SCs.

2.1.4.4 Fabrication and supercapacitor form factors

SCs are available in varieties of form factors, but they can be categorised into three types: (1) cylindrical packages, (2) prismatic packages, and (3) coin-cell packages. SCs in cylindrical packages are visually similar to electrolytic capacitors but with a much higher capacitance. Fig. 2.13 below shows aluminium electrolytic capacitors manufactured by Vishay Roederstein and cylindrical SCs manufactured by Maxwell Technologies. Maxwell Technologies also manufactures high capacitance SCs (thousands of farads) for

transportation segment (Fig. 2.14a) and high voltage SCs modules for hybrid vehicles (Fig. 2.14b).

In cylindrical SCs (refer to Fig. 2.9), the dried carbon-coated electrodes are cut into long strips. A separator layer is interposed between a pair of electrodes to prevent the electrodes from touching each other. Two leads, one positive and the other one is negative, which will be the SCs legs, are attached between the electrodes. In a coiling process, the electrode-separator-electrode-separator layer is wound up as tightly as possible into the desired shape and then it is impregnated with an electrolyte in a wetting process. A rubber seal is placed on the leads and the soaked electrode is inserted into an aluminium cylindrical case. Finally, the bottom of the case is crimped and curled to seal the formation.

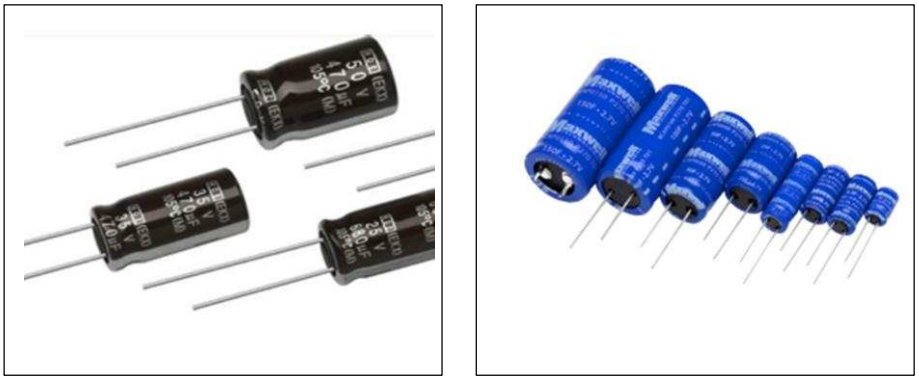

(a) **(b)**

Fig. 2.13 Capacitors and supercapacitors: (a) Aluminum electrolytic capacitors with rated capacitance of 0.22 to 15,000 μF manufactured by Vishay Roederstein (Vishay, 2012) and (b) Maxwell's board mounted cells for consumer electronics, 2.7V, 1F-150F (Maxwell, 2014b).

(a) **(b)**

Fig. 2.14 Supercapacitors manufactured by Maxwell Technologies Inc.: (a) Maxwell 2.85V/3400F for transportation (Maxwell, 2014c), and (b) 48V modules for Hybrid vehicles. Each module consists of series connection of supercapacitor cells (Maxwell, 2014a).

SCs also available in thin, flat prismatic form (Fig. 2.15a) and coin-type cell (Fig. 2.15b). Currently, prismatic SCs in the market are mostly manufactured by CAP-XX Limited, based in Sydney, Australia. CAP-XX has been dominating small SCs market and recently, CAP-XX announced it is looking to produce large prismatic SCs and modules for automotive applications (CAP-XX, 2013). Prismatic SCs are usually used in space-constrained application and small electronic devices. It is lighter, smaller and thinner than cylindrical SCs. Coin-type cell SCs are more compact than cylindrical SCs. The size is similar to button cell battery and it fits into small electronic devices.

(a) **(b)**

Fig. 2.15 Prismatic and coin-type supercapacitors: (a) Cap-XX prismatic supercapacitors, 5.5V/0.60F (Cap-XX, 2008), and (b) Cooper Bussmann PowerStor coin cell supercapacitors, 5.5V/0.1F-1.5F (EATON, 2013).

Coin-type cell is fabricated by mixing active materials (activated carbon, carbon and polymeric binder) to form a paste with almost dough-like consistency. Then the paste is flattened and rolled to form an electrode sheet. A disc cutter is used to cut the electrode sheet into disc shapes. Two disc electrodes are stacked with a separator slightly bigger than the disc is inserted in between. The electrode-separator-electrode layer is placed inside a coin cell case and the electrolyte is filled into the case. The coin cell is then sealed by crimping the case.

2.1.5 Testing and industry standards

There are only a handful of testing and industry standards available on SCs than there were on batteries. For that reason, Wang et al. (2012) have voiced out the need for industry standards for SCs performance and constructions (Wang et al., 2012). The available standards for SCs are published by several independent testing organisations, consortiums and groups. There are some similarities in the

test procedures for SCs and batteries, particularly the constant current and constant power tests which are seen performed for both types of devices (A. Burke, 2007; Sharma and Bhatti, 2010).

The most well-known standard is IEC 62391 published by International Electrotechnical Commission (IEC). IEC 62391 defines a procedure for determining the capacitance and resistance of fixed electric double-layer capacitors for use in electronic equipment (IEC, 2006a; IEC, 2006b). There is another standard published by the same organisation, which is IEC 62576, for testing SCs to be used for peak power assistance in hybrid electric vehicles (HEVs). It is identical to BS EN 62576 that is published by the British Standards Institution (BSI) for the UK implementation (BSI, 2010). Underwriters Laboratories (UL) issued a standard for electrochemical capacitors, UL 810A, for use in electronic devices, uninterruptible power supplies (UPS) and power equipment. There is also another standard targeted for HEV applications, which is JIS D 1401, published by Japanese Industrial Standards (JIS).

Consortiums like the United States Council for Automotive Research (USCAR) founded by Ford, Chrysler and General Motor, has also published its own manual under a team called FreedomCAR in 2004 (FreedomCAR, 2004). The manual describes procedures for characterisation test and life testing. The procedures are tailored to evaluate SC performance against the FreedomCAR SC goals for HEV applications. In Europe, a SC testing manual for electric vehicle application has been published by the European Council for Automotive R&D (EUCAR), a consortium which is formed by the European vehicle manufacturers (Burke and Miller, 2010).

Also available, is a test manual published by university laboratories, for example, the University of California, Davis (UC Davis) (Miller and Burke, 1994). Although it is intended for electric vehicle applications, the test procedures can also be used in SC general applications. In addition to those presented, manufacturer like Maxwell Technologies also has its own test procedures for characterising capacitance, ESR, leakage current and self-discharge (Maxwell, 2009a). Maxwell Technologies has named it as 'Maxwell 6 Step Process'. The test procedure is developed to fit a production line environment which requires for faster test time yet still provide reliable data. Testing methods like IEC 62391 and EUCAR take longer time to test, thus inefficient in a fast-paced production line environment.

All of the test manuals presented here are done in DC, but some of the test manuals like the one in (IEC, 2006a) and (Miller and Burke, 1994) also list out a procedure for AC impedance test. Test manuals which are developed for electric and hybrid electric vehicles, usually specify a series of pulse test cycles. The pulse test cycles are made up of a short current pulse with various duration. The pulse test cycles are used to determine the power and energy capability and the efficiency of SC when it is subjected to a test profile that incorporates discharge/charge pulses similar to HEV operation.

2.2 Supercapacitor models

The SC is a complex system. The interaction of different parts in the system produces such a dynamic behaviour that intuition alone is insufficient to fully understand them. Much work have been done during the last century on

modelling the system in an effort to understand the fundamental processes underlying this complex system and what the interactions entail. Not only that, the scientific community has exploited this mode of research to predict the performance characteristic of SCs. This has entirely reduce the time and costs for fabrication and physical experimentation.

One of the early work that contributes to the expansion of knowledge in this area is a model developed by von Helmholtz in 1853 (Sharma and Bhatti, 2010; Simon and Gogotsi, 2008). The model is later known as the Helmholtz model (Fig. 2.16). The Helmholtz model has been widely used to describe SC. This model describes the charge separation occurs on polarization at the electrode-electrolyte interface and brings to light the double-layer concept (Simon and Gogotsi, 2008). He describes the electrode/electrolyte interface behaves as a parallel plate capacitor. The Helmholtz model, however, is not able to take into account voltage dependence of the capacitance (Belhachemi et al., 2000).

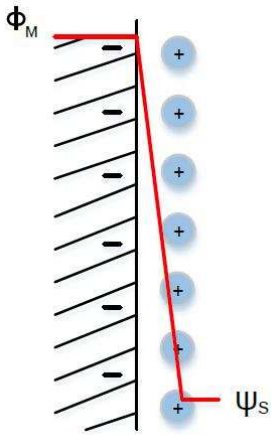

Fig. 2.16 The Helmholtz model. A double layer forms at the electrode-electrolyte interface with one layer at the surface inside the conductor and the other layer in the electrolyte. Figure adapted by author from (Conway, 1999).

Other models that describe the double-layer characteristic in greater detail, are soon, follow. These models are Gouy-Chapman model (Fig. 2.17) and Stern and Geary model. Gouy recognised the shortcoming of the Helmholtz model. In 1910, Gouy introduced the diffuse layer after considering space distribution of the ionic charge in the electrolyte (Belhachemi et al., 2000). Chapman, later, established the mathematical formulation based on the combination of the Poisson equation and the non-linear Boltzmann distribution function. Although the Gouy-Chapman model made significant improvement to the Helmholtz model, it has one major weakness—it tends to overestimate the double-layer capacitance. Therefore, it is only valid for dilute electrolytes and low surface potential (Hossain and Adamiak, 2013).

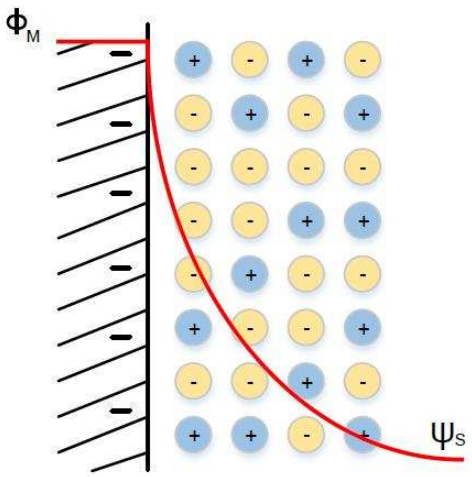

Fig. 2.17 The Gouy-Chapman model. Figure adapted by author from (Conway, 1999).

In 1924 Stern identified that there are two layers of ion distribution exist at the electrode-electrolyte interface: an inner region called the compact layer (or Stern layer) and a diffuse layer (see Fig. 2.18) (Hossain and Adamiak, 2013). He combined Helmholtz model with Gouy-Chapman model where some ions

adhere to the electrode as suggested by Helmholtz, giving an internal Stern layer, while some form a Gouy-Chapman diffuse layer. The compact layer is constituted of adsorbed ions at the electrode surface. The ions have a finite size, hence, they cannot approach the electrode surface closer than the ionic radius (Conway, 1999). In Stern model, the Helmholtz and Gouy-Chapman models are connected in series. The electrode-electrolyte interface double-layer (C_{dl}) is made up of two components: the compact double-layer capacitance (C_H) and the diffuse layer capacitance (C_{diff}), and are mathematically described in Eq. (2.7).

$$\frac{1}{C_{dl}} = \frac{1}{C_H} + \frac{1}{C_{diff}} \tag{2.7}$$

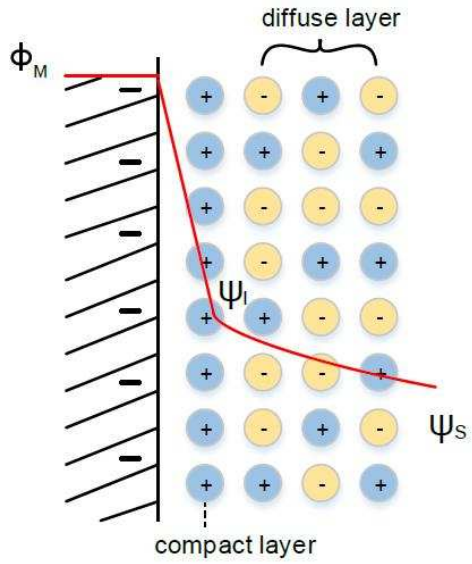

Fig. 2.18 The Stern model. Figure adapted by author from (Conway, 1999).

In 1947, Grahame updated Stern model and included the effect of adsorbed ions (Fig. 2.19). He took into account the different sizes of the ions and their reactivity with the surface. He proposed the existence of three different layers in the electrolyte: inner Helmholtz layer (IHP), outer Helmholtz layer (OHP) and a diffuse layer, which is a region beyond the OHP (Hossain and

Adamiak, 2013). As Winter and Brodd (2004) have described, the first region, the IHP, refers "to the distance of closest approach of specifically adsorbed ions (generally anions) and/or adsorbed solvent molecules to the electrode surface"[4], and the second region OHP, denotes, "the distance closest of non-specifically adsorbed ions (generally cations) in solution. Cations that populate the OHP are usually solvated and thus are generally larger than the less solvated anions "[5].

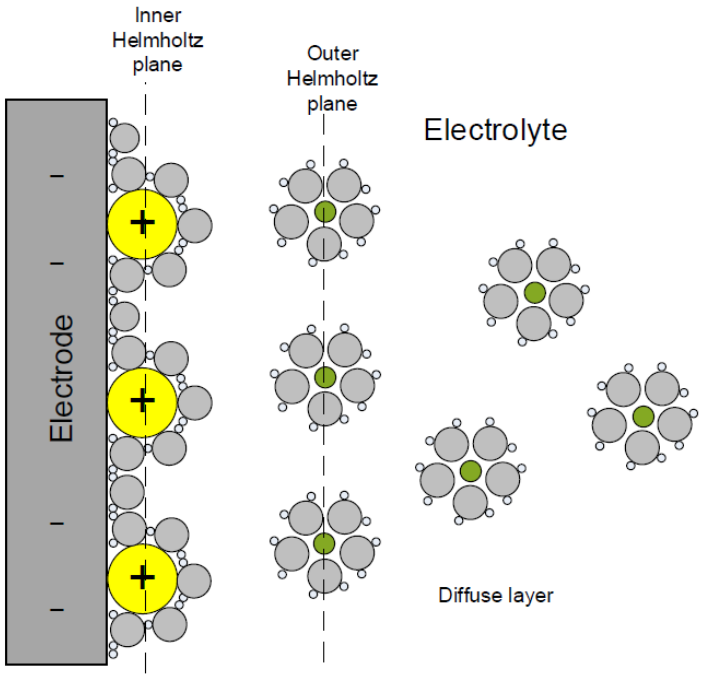

Fig. 2.19 Grahame model.

These early works have contributed to the emergence of models built either analytically, experimentally or numerically. These models can be further grouped into: electrical model (Ban et al., 2013), thermal model (Gualous et al., 2009; Sakka et al., 2009), electrochemical model (Martín et al., 2008b), black

[4] Winter, M. and Brodd, R.J. (2004) 'What are batteries, fuel cells, and supercapacitors?', Chemical reviews, Vol. 104 No.10, pp.4245–69., DOI:10.1021/cr020730k

[5] Ibid., p.4267

box model (Eddahech et al., 2013) and mathematical model (Srinivasan and Weidner, 1999; Lin et al., 1999). Nonetheless, modelling the SC by means of deriving its equivalent circuit is still a preferable choice, not only that it represents SC conceptually through the arrangement of circuit elements, it can also be implemented in hardware and would replicate the actual behaviour and produce the same impedance response as the system under study.

Before that, it is important to mention the work by De Levie (1963), in which his seminal work on the electrical behaviour of a porous electrode has influenced later developments in equivalent circuit modelling (de Levie, 1963). In 1963, De Levie came out with the Porous Electrode Theory and demonstrated that the distribution of capacitance in porous electrodes is a result of each pore being modelled as a transmission line. The theory assumes that the pores in the electrodes are cylindrical and are filled with homogeneous electrolyte solution. Each single cylindrical pore are modelled by a uniformly distributed electrolyte solution resistance, R, and double-layer capacitance, C. The distribution of Rs and Cs highlights the increasing resistance of capacitive networks with increasing pore depth. This description is summarised schematically in Fig. 2.20.

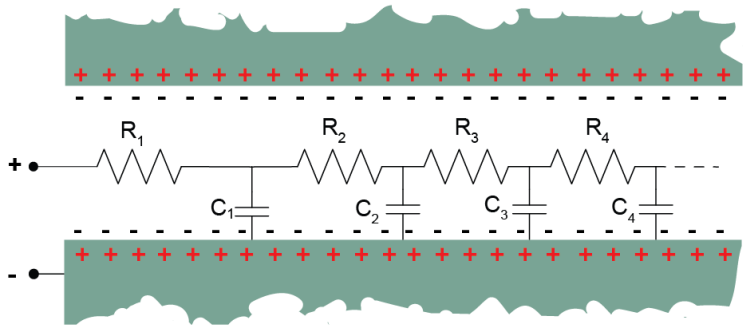

Fig. 2.20 Illustration of the distributed resistance and capacitance inside an electrolyte-filled cylindrical nanopore in a carbon electrode. Figure adapted by author from (Miller and Simon, 2008).

The behaviour of a SC is, electrically, dissimilar to that of a simple capacitor. While RC circuit has been used to model the electrical response of the device, the model has been proven as being too simplified. Nevertheless, it is still useful for modelling at a system level, though, it comes with a limited accuracy at very low frequencies. Therefore, it is insufficient for modelling that is interested in the long-term behaviour. This, again, is attributable to the nature of the porous electrode itself. As the surface area of the porous electrodes consists of pores of various sizes, it is only rational that the SC is modelled by a complex network of non-linear capacitors and resistors (Fig. 2.21) (Belhachemi et al., 2000). These resistances depend on various parameters like electrode materials resistivity, electrolyte resistivity, pores sizes, membrane porosity and packaging technology. This, however, produces a model that is very complex and impractical for computer simulations. More simplified models are, later, introduced. This include lumped models (Fig. 2.22) that are represented in either two- (Faranda, 2010), three- (Zubieta and Bonert, 2000) or four-branch (Lajnef et al., 2004) equivalent circuit model. These models represent the SCs short-, medium- and long-term behaviour.

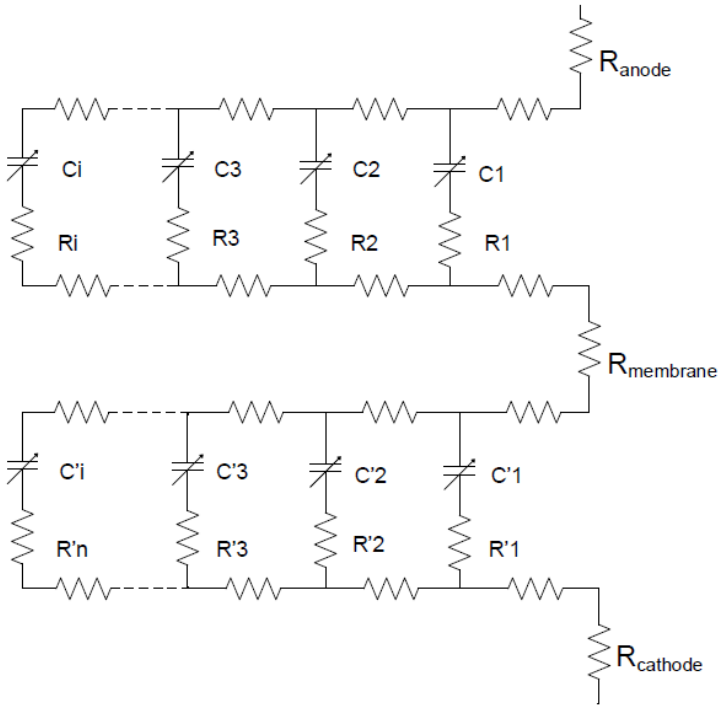

Fig. 2.21 Supercapacitor theoretical model which comprises of many non-linear capacitors and resistors. Figure adapted from (Belhachemi et al., 2000).

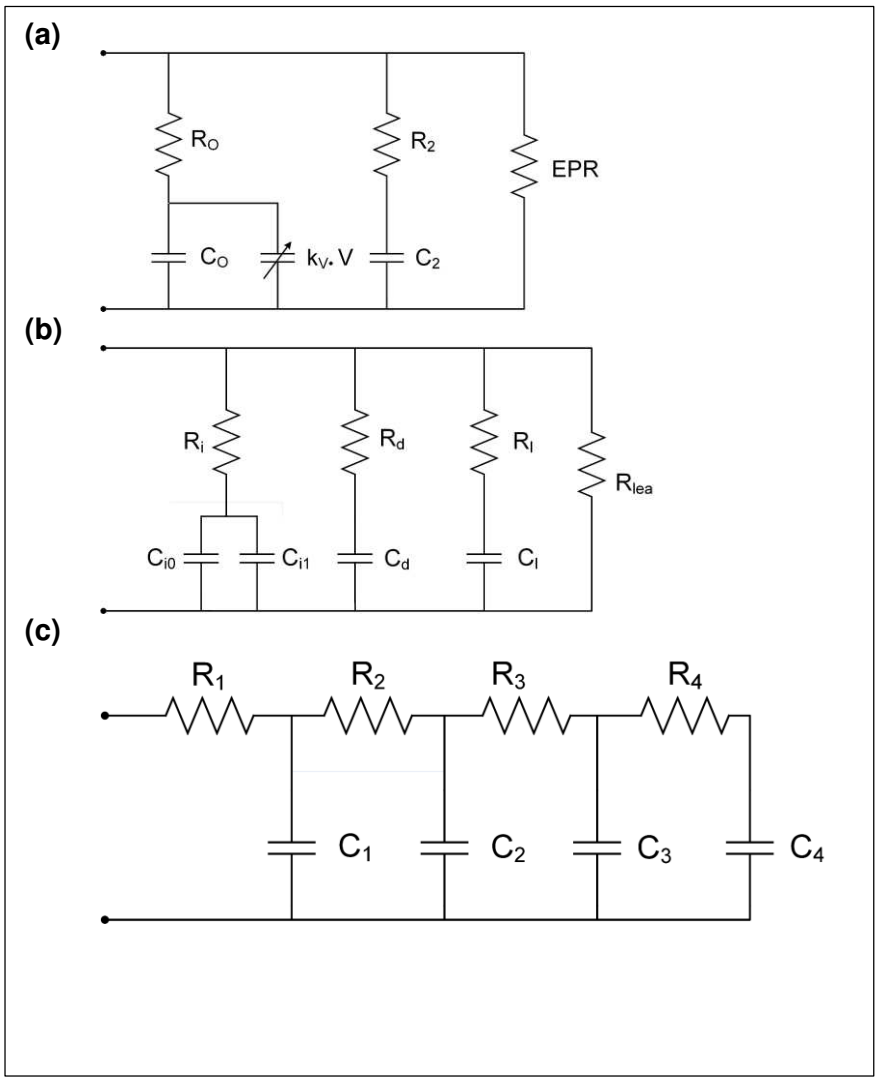

Fig. 2.22 Electrical models taken from literatures: (a) two-branch model (Faranda et al., 2007), (b) three-branch model (Zubieta and Bonert, 2000), and (c) four-branch model (Lajnef et al., 2004).

There is also transmission line model (Fig. 2.23a) that comes forth based on De Levie's porous theory. The identification of the parameters for this type of model is usually based on a temporal approach (Belhachemi et al., 2000; Wang et al., 2008) or on a frequency approach (Itagaki et al., 2007; Du, 2009) or a combination of both temporal and frequency approach like in (Lajnef, Vinassa, Briat, Azzopardi, et al., 2007; Rizoug et al., 2010; Devillers et al., 2014). Temporal approach uses charge test using a constant current for the parameter

identification method. Whereas, frequency approach uses electrochemical impedance spectroscopy (EIS) for the parameter identification. Again, this type of model is found to be rather taxing as it is often required between 4 to 20 orders to achieve a satisfactory accuracy (Lajnef, Vinassa, Briat, Azzopardi, et al., 2007). Although this equivalent-circuit model is developed based on the assumptions that the pores are cylindrical, it is still commonly used to describe SC distributed characteristic and charge propagation along the electrode surface and its complex internal geometries (Song et al., 1999). Fletcher et al. (2013), however, argued that the transmission line model should not be used to model SCs because the pores are neither identical nor uniform (Fletcher et al., 2014).

Another type of model, which is a ladder network model, has also appeared in papers written by (Nelms et al., 2003), (Dougal et al., 2004), (Li and Crow, 2009) and most recently (Fletcher et al., 2014), to mimic the distributed nature of the resistance and capacitance in a porous electrode. Ladder network models are formed by resistances and capacitances that are connected in series and parallel, they can take either a horizontal form (Fig. 2.23b) or a vertical form (Fig. 2.23c). A higher order circuit, between 3 to 4 orders (Nelms et al., 2003), fits SC transient behaviour better. In addition to that, five-stage ladder model has been recommended by (Dougal et al., 2004) for most applications which often require frequency range up to 10kHz.

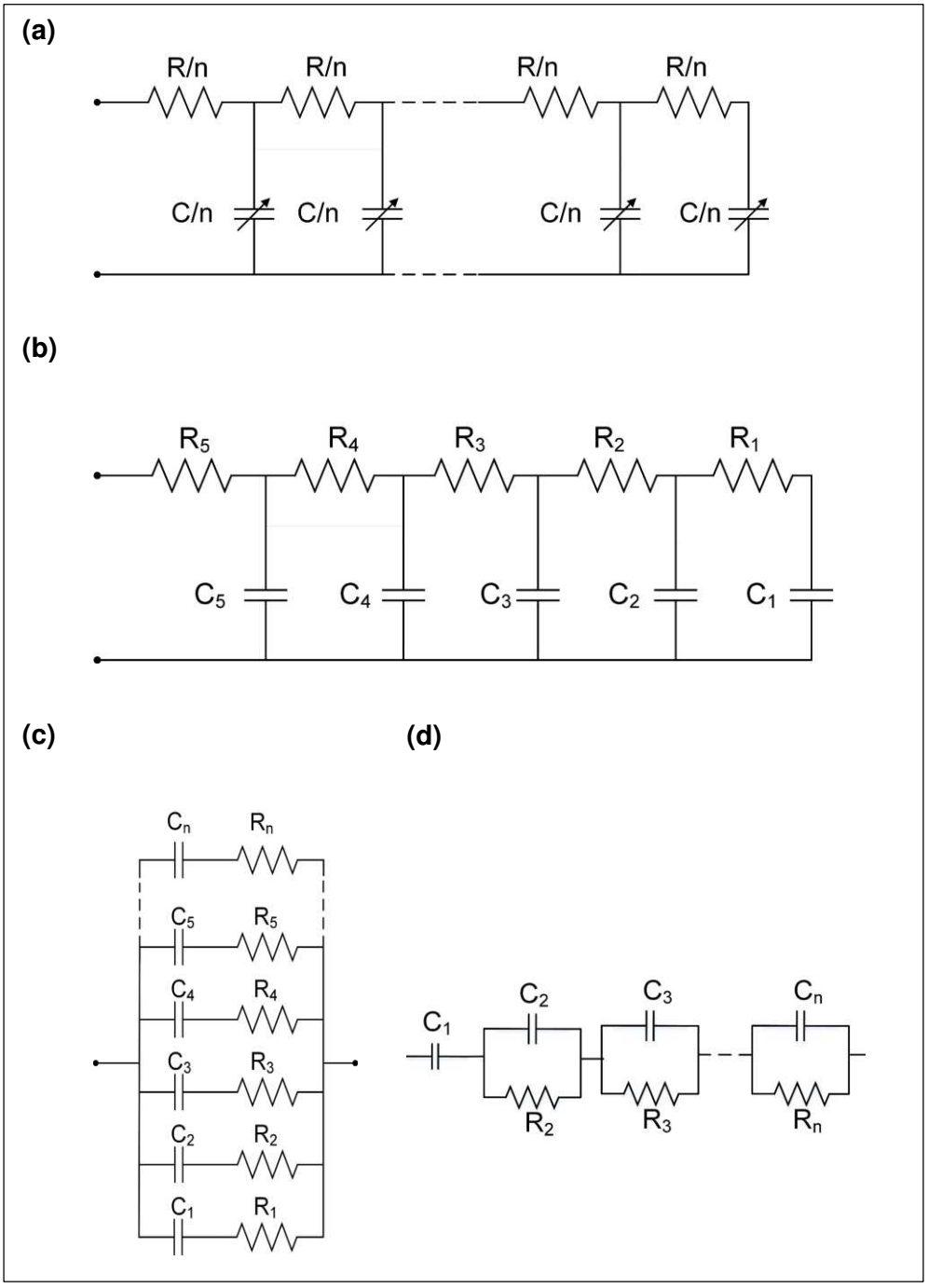

Fig. 2.23 Types of supercapacitor models appeared in literature: (a) A transmission line model as appeared in (Rizoug et al., 2012); (b) a horizontal ladder network model as appeared in (Dougal et al., 2004); (c) a vertical ladder network as appeared in (Fletcher et al., 2014); and (d) a multi R-C branch model in Voigt topology (Buller et al., 2002).

The basis of the idea behind ladder network models still lies on the different time constant of SCs dynamic behaviour. Some researchers have shown that the frequency model of the transmission line can be simplified by a multi R-C branch (Fig. 2.23d). This method was explored by (Buller et al., 2002; Moss et al., 2007; Riu et al., 2004). The time domain representation of this circuit can be obtained by taking the inverse transformation of the impedance spectra in frequency domain. The transformation of this model to the time domain model is shown extensively in (Buller et al., 2002). Recently, (Musolino et al., 2013) integrated the model proposed by (Buller et al., 2002) with the model proposed by (Zubieta and Bonert, 2000) to represent SC behaviours at both low and high frequencies, but still, the model requires many number of branches for good accuracy. Building a model that is able to simulate SC behaviour at wide frequencies often requires the extension of circuit branches until a good accuracy is achieved, thus, leading to many parameters to be identified. Some researchers have explored a method based on separating the model according to the frequency range or the time constant at interest, for instance, (Du, 2009) and (El Brouji, Briat, Vinassa, Henry, et al., 2009).

SC nonlinear response due to an applied voltage has led the emergence of nonlinear models. The nonlinearity of SCs behaviour to the applied voltage is addressed by introducing a nonlinear component, often a capacitor, which varies with voltage (observed in time domain when the charging process is stopped). This method is used in (Niu and Yang, 2011; Zhu et al., 2007; Zubieta and Bonert, 2000; Funaki, 2010; Zhang and Yang, 2011). In 2007, Lajnef et al. proposed an equivalent circuit made of a nonlinear transmission line with voltage dependent capacitors for a peak-powered SC where they investigated the

relationships among OCV, temperature and charging frequency (Lajnef, Vinassa, Briat, Azzopardi, et al., 2007). Rafik et al., also in 2007, proposed a 14 RLC equivalent circuit to describe the influences of operating frequency, voltage, and thermal effects on SCs (Rafik et al., 2007).

Besides that, nonlinear models have been built by following the evolution of the model parameters as a function of voltage to obtain polynomial expressions that contained the voltage dependency terms of these parameters as demonstrated in (Nicolas Bertrand et al., 2010). Recently, (Torregrossa et al., 2013) attempted to model the long-term redistribution phenomenon in SC by the inclusion of two 'virtual' current sources and nonlinear capacitors, to take into account the short and long duration of SC redistribution phenomenon. Wu et al. (2012) used artificial neural networks (ANNs) to determine the parameters of their nonlinear circuit model (Wu et al., 2012).

Most of the circuits presented previously fall into macroscopic modelling and are usually built for a specific application. While they all serve their purpose well within a set of boundary conditions (these boundary conditions could vary greatly for different disciplines), a dynamic model is preferred in a long term studies. This type of circuit, also known as dynamic model, is aimed at modelling at a microscopic scale. Unlike those equivalent circuit models, which does not necessarily represent the physical phenomena in the SC, the dynamic model is built in a way that it can represent the internal phenomena with precision. The dynamic behaviour of SCs takes place in a wide frequency range, starting at frequencies of some μHz towards frequencies of some kHz and it is influenced both by internal and external parameters. This wide range is caused by different electrochemical effects, such as mass transport, the electrochemical

double layer and simple electrical effects. Microscopic scale modelling focuses on the electrochemical process at this range in detail. The duration for this dynamic behaviour according to (Lajnef, Vinassa, Briat, Azzopardi, et al., 2007) is given in Fig. 2.24 .

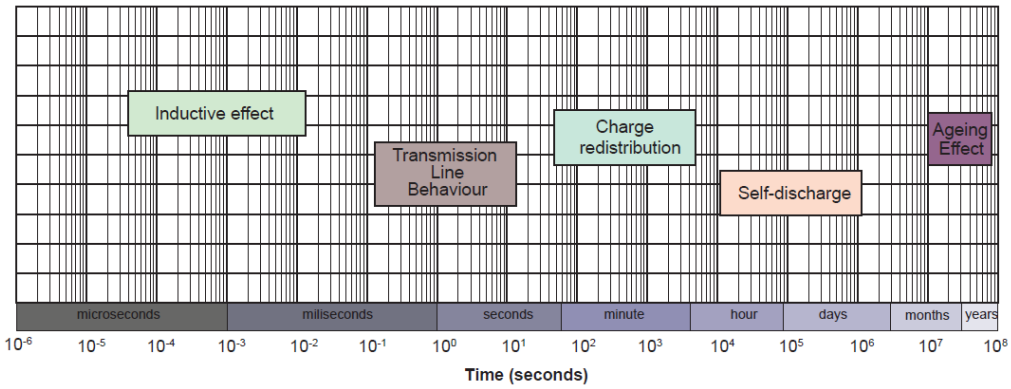

Fig. 2.24 The time range of dynamic effects in supercapacitors.

The crux of the dynamic behaviour is the properties of the electrolyte (Musolino et al., 2013). It is also strongly related to the effects of the porous electrodes. The charging process of SCs shows some non-linearity to the capacitance and voltage relationship, as mentioned in (Zubieta and Bonert, 2000). The charging/discharging processes do not occur with the same time constant throughout the electrode material, as has also been mentioned by De Levie in (de Levie, 1963). A cessation of the charging process leads to a drop in voltage. This is due to the finite conductance of the electrolyte (Kaus et al., 2010). Double-layer charge distribution that extends throughout the pore takes place following removal of the current source. The charge will first allocate at macro-pores (which are at the mouth of the pore) and then distributes to the meso- and micro-pores which are situated further deep inside the pore. A more detail illustration can be found in (Kaus et al., 2010).

The dynamic characteristic of SC is observable in the frequency domain. While an impedance spectra of an ideal capacitor exhibits a vertical line, the SC begins with a 45° impedance and it continues to extend into an almost vertical line at low frequencies (see Fig. 2.7). According to Kötz and Carlen (2000), the 45° region, known as the Warburg region, is an indicial of the distributed resistance/capacitance in a porous electrode (Kötz and Carlen, 2000). The diffusion phenomena causes a 'fractional behaviour' and that middle and low frequencies area can be mathematically described by fractional differential equations (García et al., 2010; Dzieliński et al., 2010; Martín et al., 2008b). It has been shown in (Dzieliński et al., 2011) that this type of modelling gave accurate results over a wider range of frequencies. In the time domain, (El Brouji, Vinassa, et al., 2009) have shown that the fractional term was able to simulate satisfactorily the voltage evolution upon the cessation of the charging process. In 2013, Mitkowski and Skruch (2013) proposed fractional-order models in the form of RC ladder networks (Mitkowski and Skruch, 2013). Nevertheless, fractional models have been proved able to minimise the number of parameters in the development of SC equivalent circuit models (Martín et al., 2008a).

Apart from the traditional equivalent circuits, SCs 'fractionality' has been modelled by electrochemical equivalent circuit. In 2000, Kötz and Carlen proposed that the non-vertical line at the low frequency can be modelled by replacing the capacitance expression with a constant phase element (CPE) expression (Kötz and Carlen, 2000). CPE is a unique circuit component in Electrochemistry that is used to represent the frequency dispersion of capacitance—one of SC dynamic characteristics caused by surface roughness or nonuniformly distributed properties of an inhomogenous electrode surface

(Martín et al., 2008b). Similarly, the use of CPE in SC equivalent circuit modelling can also be found in (García et al., 2010; Dzieliński et al., 2011; Quintana et al., 2006; Mahon et al., 2000; Nicolas Bertrand et al., 2010; El Brouji, Briat, Vinassa, Bertrand, et al., 2009). The CPE can be discretized into a finite ladder network as shown in (Fletcher et al., 2014). Biswas et al. (2006) have attempted to realise CPE to a form that can be used as a circuit device (Biswas et al., 2006).

2.3 Ageing and life cycle issues in supercapacitors

2.3.1 Causes of supercapacitors ageing

Despite SCs have been around for nearly 60 years—the first patents can be traced back to 1957 and SCs are commercially available since 1978 (Kötz and Carlen, 2000)—only a handful of studies in regards to SCs reliability can be found, as opposed to their lithium-ion battery counterparts, in which the investigations in their region are more mature. The scarcity of study in SC reliability is probably due to the fact that the electrical energy generated in SCs is not by redox reaction, thus, SCs can loosely be regarded as a 'safe' energy storage than batteries and fuel cells (Winter and Brodd, 2004).

SC has always found its position in niche markets for low power applications such as memory back-up in RAM and in an application that requires instantaneous power (A. Burke, 2007; Kötz and Carlen, 2000). There is a rising interest in using SCs in EVs and HEVs. In view of several claims (Burke, 2010; Hu et al., 2011; Embrandiri et al., 2011) that SC can alleviate the stress on the battery, this certainly has become a promising prospect of a wider market for

SCs. The upsurge attention received by SCs as the next energy storage for EVs and HEVs has driven more assessment on the ageing of SCs to better understand the outcome that can be expected after a long-term use of SC in that particular application, as well as to fulfil the risk mitigation strategies. The need for such studies has become stronger after lithium-ion batteries have been reported to hold several shortcomings—one of them is in regards to the limited shelf and cycle life (Burke, 2000) owing to the irreversible chemical processes in battery. SCs are seen as the panacea for all the weak points in batteries (low power capability and limited cycle life) (A.F. Burke, 2007; Wang et al., 2012)).

Contrary to popular belief that SCs have almost unlimited cyclability, since they experience close to no chemical reactions during charging and discharging (Wang et al., 2012), SC is not perfect; several reports have appeared to contradict the claim. Hahn and Barbieri et al. (2006) observed a reversible expansion of the electrode material in activated carbon SCs utilising organic electrolyte $TEABF_4$ in AN during charge/discharge cycle that is due to intercalation/insertion processes. This dimensional change that is often observed in batteries is believed to contribute to degradation and cycle life limitation in batteries. Therefore, considering that the similar observation is also observed in SCs, this suggests that the process might, too, be a possible cause of limited cycle life in SCs (Hahn, Barbieri, et al., 2006).

SCs have high power density, but suffer low energy density. This characteristic is generally ascribed to their small voltage window. Therefore, it was thought that increasing the voltage window will improve the energy density and power density. However, such move has the potential danger of causing faradaic reactions, ion insertion and gassing caused by electrolyte

decomposition, which could affect the lifetime of SCs as demonstrated in (Hahn et al., 2005). Hahn and Kötz et al. (2006) found a significant pressure increase in SCs based on $TEABF_4$ in PC aqueous electrolyte when cycling between 0 and 2.5V, as well as when constant voltages up to 3V are applied to the cell (Hahn, Kötz, et al., 2006). The decomposition products found from PC electrolyte are CO_2, propene and H_2 (Hahn et al., 2005).

Two years later, Kötz et al. (2008) wrote a paper on the pressure evolution in cylindrical-type SC based on three different solvents: PC, AN and γ -butyrolactone (GBL) (Kötz et al., 2008). 1 mol/l solutions of tetraethylammonium tetrafluoroborate ($TEABF_4$) was used in all three solvents. At 3V constant voltage, GBL has the highest leakage current, followed by AN, while PC shows the lowest leakage current (half as much as the leakage current in AN). Despite the twofold higher leakage in AN, PC is found to produce a higher gas evolution rate, by a factor of 5, than in AN, while GBL marks the highest number both in terms of leakage current and gas evolution rate.

While (Kötz et al., 2008) have highlighted the relevance of pressure evolution, which depends significantly on the type of electrolyte used in SC, Ruch et al. (2010) attempted to draw distinctions between the ageing of electrode from two different types of solvent; they are AN and PC (Ruch, Cericola, Foelske, et al., 2010). Even though, the ageing of SC at a constant elevated voltage (3.5V in this case) for both types of electrolytes, can be conclusively said to be dominated by the ageing of a single electrode, Ruch et al. (2010) identified that in AN, the ageing is more profound at the positive electrode, while in PC, ageing is dominated at the negative electrode. The degree of ageing is reflected in the increase of resistance and the loss in capacitance in both types

of electrolytes. It was concluded by the authors that different faradaic processes occur in the negative and positive electrodes and it is directly dependent on the type of electrolyte used. The surface deposits by electrolyte degradation in AN have caused partial blockage of porosity of the positive electrode, whereas in PC, the solid degradation products found on the negative electrode are in the form of thin film formation as well as the formation of carbonates and local passivation of the electrode surface. This finding suggests that SC construction need to be optimised according to the type of electrolyte used.

To address the above findings, the concept of different electrode mass of the positive and negative electrode has been suggested previously in the literatures, in order to obtain full utilization of cell capacitance of SC electrodes; however, the reported effect of ageing on the 'asymmetric construction' is lacking. Therefore, this has drawn Cericola et al. (2011) to study the effect of the electrode mass ratio for SC based on AN electrolyte and PC electrolyte on the stability during constant voltage of 3.5V (Cericola et al., 2011). When the mass ratio of the positive electrode mass to the total electrode mass, r is increased to 0.65 (the total electrode mass is retained at 35 ± 5 mg cm^{-2}) in AN, the degradation process at the positive electrode reduces and both electrodes achieve a similar ageing rate. Whereas in PC, r above 0.5 produces smaller degradation rate. The different ageing rate on positive and negative electrodes are due to the different potentials experience by the electrodes. Moreover, the 'asymmetric construction' has been recommended to increase the life of SC.

In 2007, Azaïs et al. showed that after a long-term operation of 2.5V constant voltage, SCs based on AC and organic electrolytes AN experience a capacitance loss and a resistance increase that could be further enhanced by

microscopic phenomenon. These microscopic phenomenon are gas evolution, raising electrode mass and local separation of the coating layer from the metallic collector (Azaïs et al., 2007). The main gases identified are methane, ethane, di-oxygen, carbon monoxide and carbon dioxide. The gaseous products from the decomposition of electrolyte blocks electrodes pores, by which the aged positive electrode shows a substantial reduction in its specific surface area than that of the aged negative electrode, which in turn, resulting in the loss of capacitance. These findings show that SCs undergo redox processes, most probably due to the traces of water in the organic electrolyte, which are accountable for SCs ageing. Similarly, this finding is also backed up in (Zhu et al., 2008) where it was found that anodes suffer conspicuous ageing in terms of specific area and pore volume as compared with cathodes after the samples were subjected to prolonged polarization at 2.9V. They suggested that thicker anodes should be utilised to compensate for capacitance loss.

Two years after (Kurzweil and Chwistek, 2006) found a brownish salt residue on a burst SC which has been long-term exposed to 90℃ and 2.3V constant voltage, they updated their findings by reproducing the brownish salt residue by electrolysis in order to identify the components of the salt residue (Kurzweil and Chwistek, 2008). They detected that the AN electrolyte decomposes to form acetamide, acetic and fluoroacetic acid. They also found that after a thermal ageing experiment at 70℃ for 550h, white spots appear on the aluminium foil which is immersed in AN, whereas, the aluminium which is in contact with air shows a greyish colour. This white spots are detected to contain Al, F and O clusters, thus showing that this decomposition may be due

to the dissolving Al_2O_3 layer on the etched aluminium foil caused by fluorination.

The role of water in SC ageing was pointed out in (Kurzweil et al., 2005). In 2008, (Kurzweil and Chwistek, 2008) wrote that the possibility of water in the electroactive materials to have an effect on ageing and it should not be taken lightly; for every ten parts per million (0.001%) water dissolved in the electrolyte, the voltage window is reduced by circa 10mV compared with when using dry electrolyte. Commercial electrolytes usually contain <10ppm of water. During fabrication, carbon electrodes will absorb the water in the electrolyte and in order to entirely remove the water absorbed, the drying temperature needs to be more than 150℃. However, drying at such high temperature will destroy the organic binder between carbon particles and aluminium support (Kurzweil and Chwistek, 2008). Moreover, the separator, of which contains polyolefine, cannot endure such high temperatures. Meanwhile, Zhu et al. (2008) stressed that incomplete drying can increase the oxygen contents in real devices (Zhu et al., 2008).

Aside from the electrolyte-based ageing, the ageing phenomenon in SCs is also caused by the carbon materials used in the electrodes. The carbon electrodes should be inert and can guarantee the reversibility of charge transfer reactions. However, this is not the case; the presence of heteroatoms identified in carbon materials causes pseudocapacitance and faradaic reactions in SCs (Ruiz, Blanco, Granda and Santamaría, 2008). Zhu et al. (2008) studied the chemical and electrochemical ageing of carbon materials in SC electrodes (Zhu et al., 2008). To make the case simpler to analyse, the role of binder was not taken into account.

In (Zhu et al., 2008), the activated carbon powder samples were assembled in a flowbox in steel electrode cells and paper was used as a separator. After polarizing the activated carbon power electrodes at 2.9V $\pm$ 0.1V for 45 days, the authors observed microstructural changes in activated carbon; asymmetric pore structure changes at the aged anode powders. Moreover, the pore size distribution is also affected, particularly in the aged anodes, whereby the amount of micropores in aged anodes drops which it can be linked to the loss in capacitance. Ageing is also more pronounced in electrodes from natural precursors than that from synthetic resin which means that the impurity and heterogeneity in natural-based electrodes affect ageing considerably. Aged anodes contain a higher nitrogen content than cathodes, in addition to fluorine, oxygen and carbon, which are detected on both anode and cathode electrodes—these compounds are produced from trace of water and also from the electrolyte—similar observation is also reported in (Bittner et al., 2012). It was reported that the polymerization of AN causes the appearance of nitrogen in the aged anode, whereas the fluorine is due to fluorination of the activated carbon. Zhu et al. (2008) also suggested that the alteration on the electrode microstructure is largely due to the polymerization of AN at anodes and cathodes; put simply, chemical and electrochemical reactions at the electrolyte adversely affect the electrode through structural change, leading to carbon degradation and thereby causing ageing. While Zhu et al. (2008) took a simplified approach—the interactions from the binder and aluminium foil to ageing were not studied—a more complete study can be found in (Bittner et al., 2012).

In a float charge test at constant voltage 3.0V and 70℃ carried by Nozu et al. (2009), they found out that side reactions occurred during the float charge of the SCs (Nozu et al., 2009). The electroxidation on the positive electrode and the electroreduction on the negative electrode cause the degradation in the performance of the electrode. The product of electroxidation, namely oxygen, carbon and also the elements in the anions of the electrolyte, blocks the positive materials and therefore obstructing desorption and diffusion of ions on the positive electrode.

Drawing on an extensive range of sources, Gualous et al. (2010) were able to identified three SC failure modes: (1) cell container opening caused by pressure build up in the cell, (2) more than 20% capacitance loss due to the reduced accessibility for the ions following electrochemical cycling, and (3) more than 100% increase of ESR from the weakening adhesion between electrode and collector with time and temperature (Gualous et al., 2010). Based on the findings reported above, Fig. 2.25 summarises the effect of ageing on SCs and Fig. 2.26 illustrates the process in the electrolyte- and electrode-based ageing.

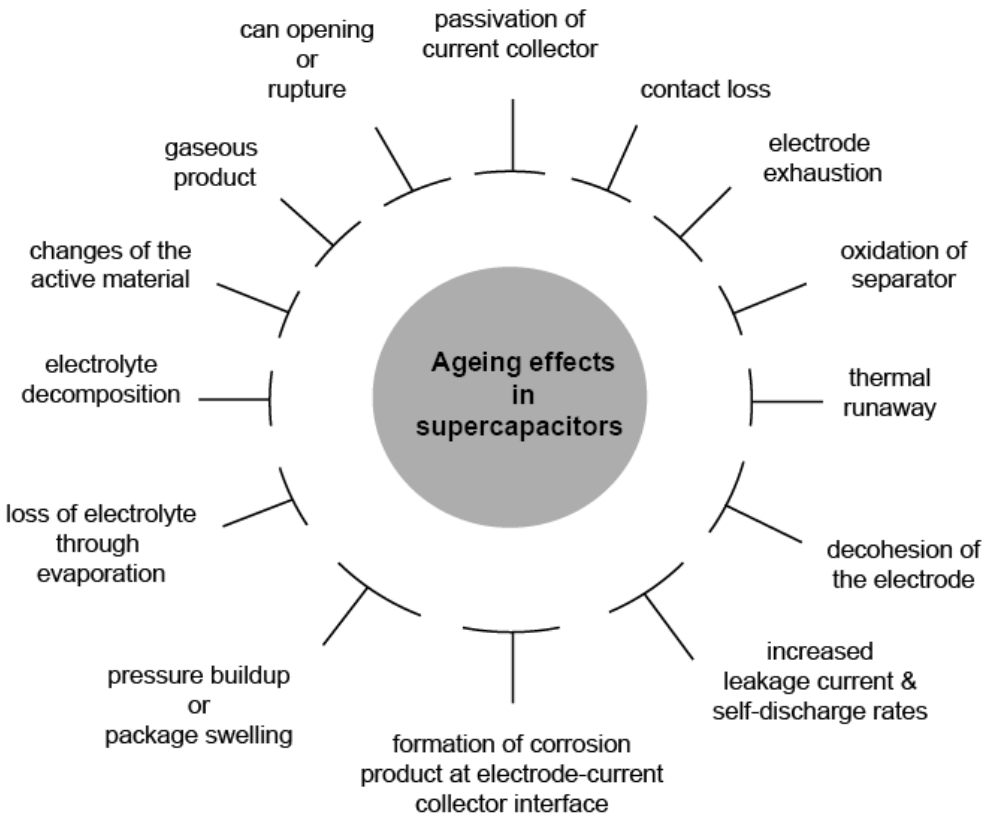

Fig. 2.25 Effects of ageing on supercapacitor as reported in literature.

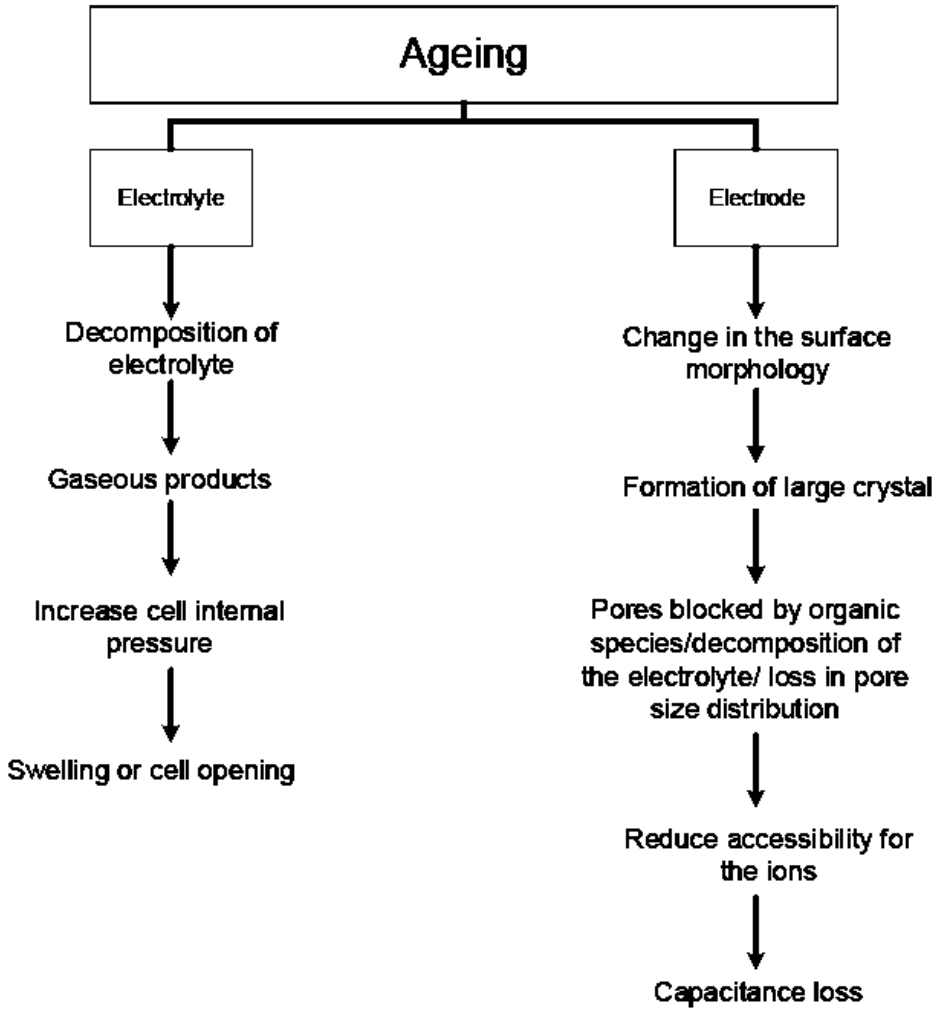

Fig. 2.26 Electrolyte- and electrode-based ageing in supercapacitor.

2.3.2 Ageing tests

Based on the data reported in the previous subsection, SCs, too, suffer from performance degradation, conflicting to what was initially believed; more and more studies are now focusing on unravelling what causes the deterioration to the seemingly potential energy storage, which could one day be equally important as batteries. One of the ways to gather this data is to age SCs at different stress levels and then measuring their responses to that particular stress for the whole experimental duration.

The most common ageing stimuli are high temperature and high voltage (Bohlen et al., 2007a). Besides temperature and voltage as the ageing stimuli, SCs are also aged by applying constant current charge/discharge cycle. Like many electrochemical devices, the chemical reactions in SCs follow the Arrhenius law which states that higher temperature causes in more rapid chemical reactions—for every 10℃ increase or for each 100mV, the chemical reaction rates double and the life is halved (Uno and Tanaka, 2012; Schiffer et al., 2006; Bohlen et al., 2007a). Hinged on the Arrhenius law, researchers have found ways to speed up ageing to a more realistic duration in laboratories that, if tested in a normal condition, would take longer than 10 years (Uno and Tanaka, 2011).

The accelerated ageing test has been practised widely. It is a test which is able to hasten failure in a short amount of time. The accelerated ageing tests are carried out by applying stress levels that are near the maximum tolerated limit or, beyond the conditions that the SC would be exposed to in its normal service. The manufacturers typically set the operation temperature for SCs either

based on AN or PC, at -40℃ to +70℃ (Kötz et al., 2006); despite the fact that SC based on PC suffers performance reduction at temperatures below 0℃ (Liu et al., 2006).

2.3.2.1 Temperature and voltage as ageing stimuli

The influence of temperature on SC performance is highlighted next. In 2003, Gualous et al., stated that temperature influences the lifetime and performance of SCs (Gualous et al., 2003). The authors studied the ESR variation with temperature on commercial SCs based on organic electrolyte and they found out that the ESR decreases as the temperature increases (Fig. 2.27). They also noticed that at a positive temperature of 25℃, it takes longer to charge the SC, whereas at a negative temperature of -25℃, the charging time is 9 seconds shorter. This is due to the ESR increases as the temperature is decreased, consequently causing a reduction of the voltage. Additionally, the observation is also impacted by the decreased of the total capacitance with temperature. This examination is in line with (Michel, 2006) who observed that, "…the conductivity of the electrolytes decreases at falling temperatures due to an increase of the viscosity of the solvent and a decrease of the solubility of the conducting salt [and cause] dramatic changes of capacitance and ESR in particular at temperatures below freezing point"[6]. In addition to that, Gualous et al. (2003) observed that the charging and discharging process raises the SC surface temperature by about 2℃ when 140A current is applied to the device.

[6] Michel, H. (2006) 'Temperature and dynamics problems of ultracapacitors in stationary and mobile applications', Journal of Power Sources, Vol. 154 No.2, pp.556–560., DOI:10.1016/j.jpowsour.2005.10.084

Therefore, they recommended that the thermal behaviour of SC to be characterised, especially in the case of SC module in transportation applications.

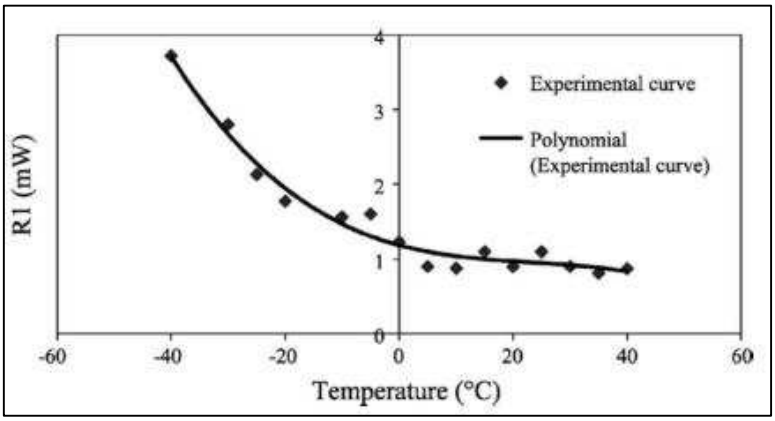

Fig. 2.27 Evolution of 2700F serial resistance R1 as a function of temperature (Gualous et al., 2003)

Often, the effect of temperature is studied by storing the SCs at a constant temperature and a fixed voltage is applied to the SCs at the same time—usually at the maximum potential according to the decomposition point of the electrolyte system. This mode of testing is often mentioned in literatures as calendar life testing. Bohlen et al. (2007) in the Part I of their work, increased the ageing rate by a factor of 64 so that the end of life criteria can be achieved in 3 months (Bohlen et al., 2007a); this factor is attained by either increasing the temperature by 40K above the nominal temperature 25 ℃ —which resulted in test temperature of 64.85℃ —or by increasing the voltage by 200mV above the rated voltage (or increment of 20K and 400mV).

The negative impact of elevated temperature on SC ageing, results in the increase of resistance and the decrease of capacitance; therefore, these two values are usually monitored to quantify ageing. The escalating ESR and capacitance fall can be attributed to two phenomena (Alcicek et al., 2007): (1)

degradation of the electrolyte; (2) degradation of the activated carbon. At high temperature, the electrolyte decomposes and leaving by-products that block the pores of the electrode, which in turn reduces the surface area and restrict the accessibility of ions in the activated carbon pores. The reaction of the chemical components is accelerated at higher temperature, whereas the high voltage speeds up the decomposition of the electrolyte and the impurities cause redox reaction in SCs. In the AFM surface observation by Umemura et al. (2003), a degraded activated carbon has a surface of, "an orange-skin structure with many bumps of about 10-50nm size, which might be degradation by-products accumulated on the activated-carbon surface."[7] They also noted that the change in capacitance is different in the positive electrode and the negative electrode, after 1,000 hours of ageing under floating voltage 2.5V at 70℃.

In a test done by Kurzweil et al. (2005) on commercial SC based on organic electrolyte, they found that the increase of resistance after 1000 hours of constant voltage test at 2.5V and at 70℃ is more pronounced than the capacitance loss (Kurzweil et al., 2005). The change of resistance is apparent in the impedance spectra which is taken before and after the test. The shape of the impedance spectra, however, unaltered—they are consistent with the shape of the spectrum taken at the beginning of the test. The leakage current also increases significantly by a factor of 8 after the test has stopped.

[7] Umemura, T., Mizutani, Y., Okamoto, T., Taguchi, T., Nkajima, K. and Tanaka, K. (2003) 'Life Expectancy and Degradation behavior of Electric double layer Capacitor Part I', in Proceedings of the 7th International Conference on Properties and Applications of Dielectric Materials, 2003. (Volume 3). IEEE, pp.944–948., DOI:10.1109/ICPADM.2003.1218577

Kötz et al. (2006) used a procedure that is based on aluminium electrolytic capacitors to monitor SC ageing (Kötz et al., 2006). The procedure involved in measuring the leakage current under various temperature and voltage conditions and then deriving the activation energy. The activation energy is higher for temperature range of 0℃ to 60 ℃ than the activation energy for temperature range of -40℃ to 0℃. The authors, however, were unsure if the SC measurement history affects the results. Also referring to Fig. 2.28, the decreased temperature increases the ESR and reduces the capacitance, consistent to the report in (Gualous et al., 2003).

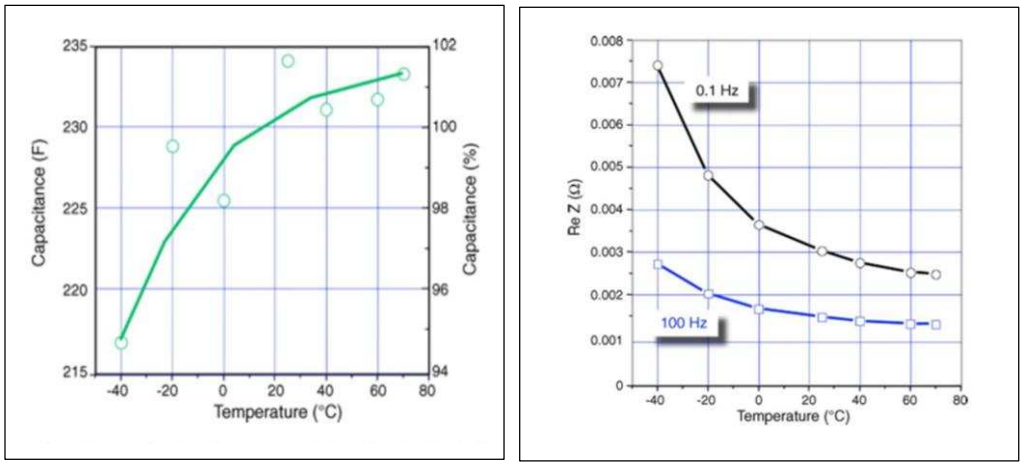

Fig. 2.28 Capacitance as a function of temperature (left) and ESR as a function of temperature (right) (Kötz et al., 2006).

In a test done by Bittner et al. (2012), SCs based on $TEABF_4$ in AN organic electrolyte were aged at various voltages (between 2.3V to 2.5V) and temperatures (50℃ to 80℃) (Bittner et al., 2012). It was found that the effect of voltage increase is more significant than the effect of temperature increase; for instance, SCs which were stressed with 2.5V, 70℃ age faster than the SCs at 2.3V, 80℃. Also found was, a high pore volume loss and a high surface area

loss at aged anodes than that at aged cathodes. In the pore size distribution test, ageing seems to affect pores with size in the range of 1.26-3.2nm in anodes and 0.5-0.79nm in cathodes; larger pores than those show almost no change—these losses can be linked to pore blockage by the precipitation of TEA^+ and TFB^- salt. The structural change in anodes is caused by oxidation of the carbon. In addition to that, the separator of aged SCs, particularly on the side exposed to anode, also changes colour from white to yellow/brownish with a dark residue—potentially came from carbon. Aluminium and oxygen that are caused by partial destruction of the passive layer are detected on the aluminium foils; the findings are in concordance to the results in (Kurzweil and Chwistek, 2008).

While power cycling has been reported to cause obstruction to the pore size and geometry in (El Brouji, Briat, Vinassa, Bertrand, et al., 2009), the same authors found the observation is absent from the calendar life tests; the ion mobility in the porous structure remains unaltered and the electrolyte resistance R_{el} and the γ parameter are quasi-constant. Therefore, calendar life test has a uniform effect on SC when the same parameters are compared with that of the power cycling test.

The evolution of the SC declining performance under several voltages and temperature conditions are studied in (El Brouji, Briat, Vinassa, Henry, et al., 2009). The temperatures were varied in the range of 55℃ to 65℃ and the voltages were varied between 2.5V to 2.9V. This ageing evolution is observed by monitoring the shape of the Nyquist plots. Although, no visible change in the Nyquist shape, the effect of voltage and temperature is translated to the shifts of the Nyquist along the real axis, corresponds to the increasing ESR. The higher the voltage, the ageing is more significant. From the voltammograms, a clear

distortion to the wave shape is observed on the aged SCs and it becomes more prominent with increasing voltage. The authors suggested that these distortions can be attributed to a reduction of the pseudo-capacitive charge storage mechanism.

A similar observation regarding the ageing process which causes changes to SC impedance was also reported by Kötz, Ruch and Cericola (2010). In constant load tests done by Kötz, Ruch and Cericola (2010), commercial SCs based on AN electrolytes were exposed to: (i) nominal voltage and elevated temperatures up to 85℃, (ii) room temperature (30℃) and elevated voltages up to 3.5V and (iii) both elevated temperature and voltage up to 3.0V and 70℃ (Kötz et al., 2010). The authors showed the effect of voltage and temperature on SC ageing are distinct, as noted by the shape of the impedance spectrum from EIS measurements. The effect of ageing at increasing voltage is depicted by the shift of the impedance spectrum along the real axis and the low frequency parts are tilted with a clear decrease in slope. Whereas, most of the effect of temperature on ageing is visible from the movement of the real part of impedance spectrum towards higher values; a tilt to the low frequencies part is also observed but hardly distinguished—it was almost negligible. However, when temperature and voltage are applied at the same time to increase the level of stress, a semi-circle appears at higher frequencies on a destroyed SC through can opening. The semi-circle is reported to be caused by an increase in contact resistance between the electrodes and the current collector.

Gualous et al. (2010) were interested in questions concerning the effect of thermal shock on SC (Gualous et al., 2010). Although their findings are preliminary, they are worth considering, in particular, for the case where SC will

be exposed to a rapid change of temperature. The thermal shock test was performed on a stack of SCs (no voltage was applied to the module) with the cycle of the process as presented in Fig 2.29. Two climatic chambers were used to realise the process; the stack was first placed in the climatic chamber 1 at 80℃ for 2 hours and then it was transferred to climatic chamber 2 at a regulated temperature of -20℃. After 20 temperature shock cycles, an increase in the ESR value is detected at about +12% by EIS measurement, whereas the capacitance variation is around 3%. Three years later, (Gualous et al., 2013) updated their findings to include the effect of vibration on SC ageing. While Gualous et al. (2010) were more interested in the effect of extreme change of temperature (+80℃ to -20℃), Ayadi et al. (2013) did in a narrower window of between 40℃ and 50℃ temperature change (Ayadi et al., 2013). The results from the thermal cycling are compared with the results from calendar test held at fixed temperature of 50℃. They found out that changing temperature has certainly caused SCs to age more than that exposed to calendar test (Fig. 2.30).

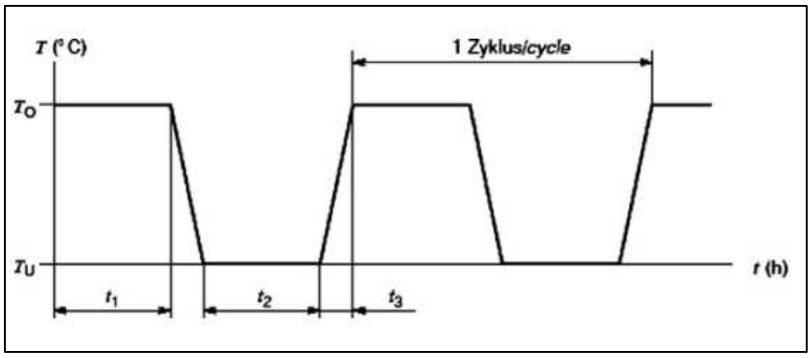

Fig. 2.29 Thermal shock test in (Gualous et al., 2010).

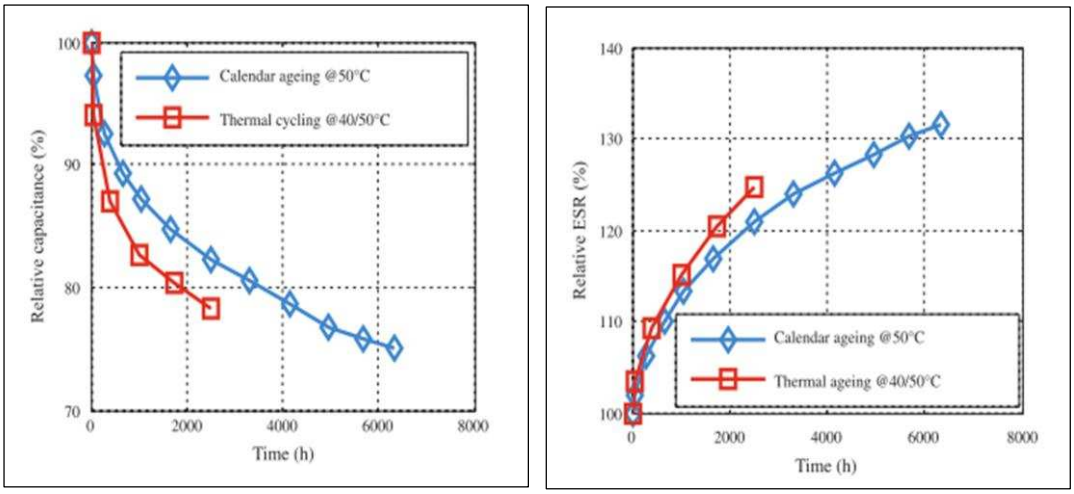

Fig. 2.30 The effect from thermal cycling on capacitance (left) and resistance (right) were more pronounced than calendar ageing test (Ayadi et al., 2013).

Generally, ageing tests that are based on temperature and voltage as the ageing stimuli, do not exceed the maximum voltage (determined by the decomposition voltage of the electrolyte system), and the maximum temperature (determined by the electrolyte boiling point). We have seen a growing interest in understanding SC behaviour beyond this range. This type of test is usually destructive and is meant to study the robustness of SC and its response to undesirable conditions. An example of an 'abusive' testing was done by Kurzweil et al. (2006) in (Kurzweil and Chwistek, 2006). Constant voltages up to 6V and temperatures up to 90℃ were used in their experimentations. They found out that, although the SCs are tested well beyond their tolerated limits, they can still be operated for several months. For instance, a 50F SC can operate for approximately 4.6 months at 2.5V, 7.7 months at 2.3V and 12.5 months at 2.1V, all at 90℃ temperature condition, before the ESR quadrupled. It is noteworthy that lowering the voltage by 0.4V will prolong the lifetime of SC by

a factor of 3. Brownish salt residues are identified at burst SCs, which contain acetamide, aromatic and unsaturated organic acids. However, the authors did not rule out the possibility of the various compounds found in the crystalline mass are due to the exposure of the burst SC to air, thus, the crystalline mass are reproduced by electrolysis of the electrolyte at 4V. The detail results can be found in (Kurzweil and Chwistek, 2006).

Another abusive study is the work done by Ruch et al. (2010) in (Ruch, Cericola, Foelske-Schmitz, et al., 2010), although it is not as destructive as the test done by Kurzweil et al. (2006). The SCs based on activated carbon and AN electrolyte were aged at constant voltage between 2.75V and 4.0V. Three galvanostatic charge/discharge cycles between 0 and 2.5V were performed for every 10 hours of constant voltage application. The domination of ageing at positive electrode is more pronounced at cell voltage 3.5V and above. The observation translates into the loss of capacitance and the increase of resistance, although capacitance loss was already observed at 2.75V and 3.0V. This finding indicates that both the capacitance loss and the increased resistance are electrode polarity dependent and shall not be associated with the change in electrolyte conductivity during ageing; instead, the ageing is attributed to either an increase in contact resistances between interfaces or to an increase distributed resistance in the electrode. Furthermore, the appearance of semicircle after 100 hours at 4.0V backs up the former theory. The decomposition of poly(tetrafluoroethylene) (PTFE) binder at 3.5V and above after 500 hours leads to the embrittlement of the negative electrode, in particular. Although, the embrittlement of the negative electrode does not affect the capacitance and resistance in any notable way, it has indirectly affected the way positive

electrode degrades. Consistently to (Azaïs et al., 2007), (Zhu et al., 2008), (El Brouji, Briat, Vinassa, Bertrand, et al., 2009) and (Bittner et al., 2012) in regards to the effect of ageing on the pore size distribution, the ageing effect is striking on the positive electrode, possibly via electrolyte degradation products, and it is stronger at 3.25V and above, as evidenced by the dramatic drop of the surface area (Fig. 2.31).

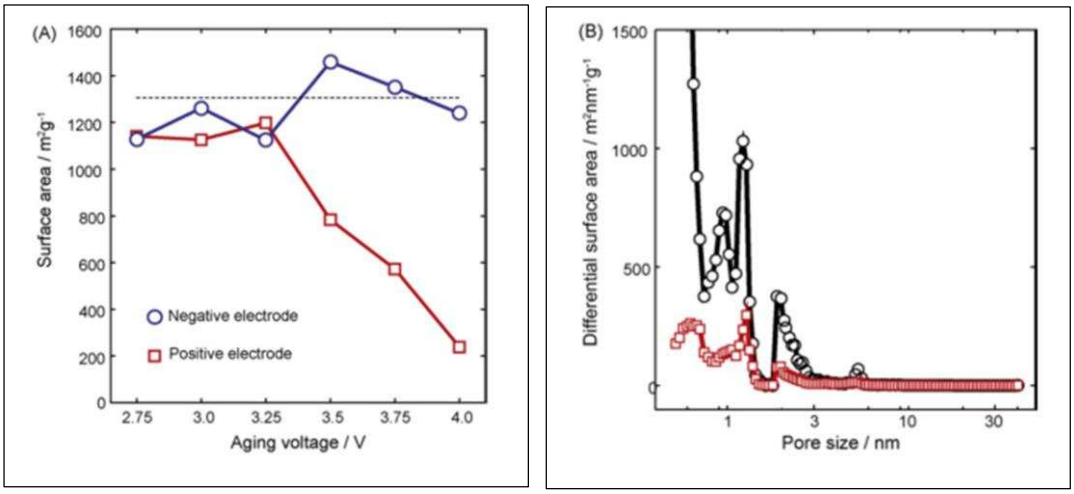

Fig. 2.31 The surface area of positive and negative electrode after ageing for 100H at different voltages (Ruch, Cericola, Foelske-Schmitz, et al., 2010).

2.3.2.2 Charge/discharge cycling on ageing

As has been noticed in the work of Gualous et al. (2003) in (Gualous et al., 2003), mentioned earlier, charging and discharging cycle induces heat generation in SC through joule heating, consequently SC efficiency is reduced. The effect of charging was also investigated in (Schiffer et al., 2006). The authors used a symmetric square wave profile to charge and discharge SCs. The current profile used raised the SC surface temperature to about 6.5K. The temperature rise is due to the effect of irreversible Joule heating. Further to that,

the authors also investigated the impact of current rate on SC surface temperature. 100A current profile generates two times the temperature generated from 50A current profile and 6 times the temperature produced by 25A current profile. In regards to the surface temperature generated from cycling, Omar et al. (2014) detected that the surface temperature of 1600F SCs increases by 4℃ with 70A current, meanwhile 90A current increases the surface temperature to 8℃, after both were cycled for 110,000 cycles (Omar et al., 2014).

Pascot et al. (2010) developed a calorimetric technique to measure the heat generated from cycling in SC based on PC electrolyte from the transient temperature change (Pascot et al., 2010). During charge/discharge cycling, a fraction of the energy within the SC cell is dissipated into heat through Joule losses. The SCs were subjected to galvanostatic cycling with current range between 0.1 and 1A. After 200s and about 30 current cycles at 0.4A, the temperature of the SC has increased exponentially but not exceeding 2.5℃. The thermogram of the SC, calculated by Finite Elements Method, displays the heat dissipation during cycling whereby the hottest area is at the surface of the SC and the temperature gradually drops further away from the cell as the heat is dissipated to the ambient.

Time-dependent heat profiles as SCs went through charge-discharge cycling were also studied by Dandeville et al. (2011) in (Dandeville et al., 2011). The profiles were gathered from the change of temperature as SCs were cycled in a customised calorimeter. It was found that two types of heat is generated: a reversible heat and an irreversible heat. They found that irreversible heat is caused by the Joule loss from the porous structure, whereas the reversible heat is produced by the ion adsorption on the carbon surface. Apart from SC of the

type of double layer, heat generated by a hybrid SC based on carbon-manganese dioxide MnO_2 was also studied.

As it has been pointed out by many authors, charge and discharge cycling induces heat generation in SC. In order to accelerate ageing, (Gualous et al., 2012) has demonstrated the use of 62A constant current on 350F SCs, to achieve component temperature of 65℃. The SCs were cycled continuously without any rest time in between charging and discharging, from voltage between 1.25V and 2.5V. After 1,000 hours, the ESR increases to 20% above the initial value and the capacitance drops 15% from the initial value.

Constant current cycling has been demonstrated by Omar et al. (2014) to have a significant effect on SCs impedance (Omar et al., 2014). The authors observed a shift of the impedance spectra along the real axis at different temperature and current. Consistent to what have been reported by other researchers, higher current contributes to the higher increase in resistance. Despite the findings, there is no clear trend that can explain the increasing resistance with respect to the number of cycles—except for that the ageing of the SC is nonlinear, and the nonlinearity is observed in all test temperatures. Apart from that, at low frequency, the imaginary part increases during cycling, thus, showing that the capacitance has decreased.

2.3.2.3 Power cycling on ageing

SCs are also tested using charge/discharge pulses (Fig. 2.32) where the pulsed current profiles are defined according to the typical profile of HEVs, as in reference (Briat et al., 2006). This type of test is known as the power cycling test. A current profile with a period of 1 min used in this type of test is based on

the acceleration/braking or start/stop operations in HEV. The pulse width depends on the vehicle type: 0.5 to 2s for micro-hybrids and 2 to 10s for mild-hybrids (Briat et al., 2006). The purpose of this test is to generate self-heating in SC, so that it acts as an accelerating factor to SC deterioration. The test is carried out under safe operating conditions, with the aim of reaching the same degradation mechanisms as it is in normal use, but at a quicker pace. The RMS value of the current profiles is chosen based on the RMS current value that will lead to a rise of 60℃ at the beginning of the power cycling test. The 60℃ is normally the maximum temperature limit for SC based on organic electrolyte. This test is usually done in a climatic chamber which is set at 40℃ temperature, therefore, 20℃ self-heating is required to reach the 60℃ target temperature.

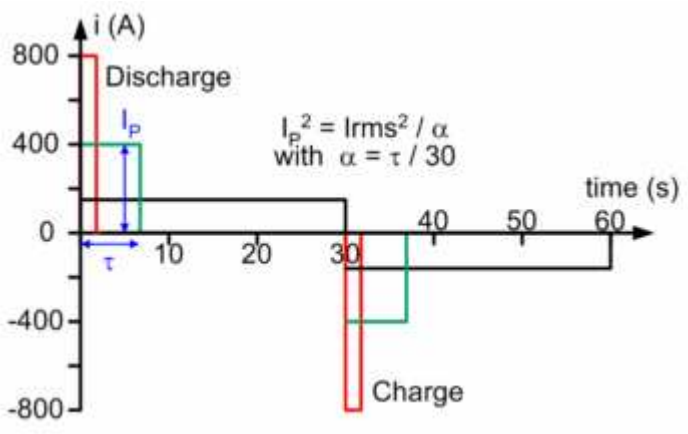

Fig. 2.32 Current profile used in power cycling test (Briat et al., 2006).

The discontinuity in the pulsed current profile of the power cycling test has proven to have an effect on SC ageing by Briat et al (2006) in (Briat et al., 2006). Two pulsed current profiles were used, 200A and 400A current profiles, but both having the same 200A RMS value. Although the RMS value is the same by which it is supposed to result in the same heating, the results prove the otherwise. After 25,000 cycles, the 400A current profile leads to higher

temperature rise, higher resistance increase and a bigger capacitance loss than those of the 200A current profile. This data proves that the current shape can impact the way SCs age. Likewise, this method was employed in (Lajnef, Vinassa, Briat, El Brouji, et al., 2007), but this time the target temperature is lowered to 55℃ in response to the 300A and 400A current profiles used.

Lajnef et al. (2007) studied the effect of power cycling on SCs from two different manufacturers (Lajnef, Vinassa, Briat, El Brouji, et al., 2007). They found out that ageing rate depends on the cell design. Also studied was, the effect of relaxation time on the SCs characteristics. A performance recovery phenomenon is observed when the SCs are in resting periods. The results showed that the impedance real part, which corresponds to the ESR, is higher after 24 hours of rest and it gradually decreases with resting time, and whereas, the capacitance increases. In 2009, Brouji et al. reported that the recovery phenomenon was only observed in power cycling experiments and not in calendar life tests which suggests that the ageing effect from calendar life is irreversible (El Brouji, Vinassa, et al., 2009). This finding was also reported in (Briat et al., 2010).

Brouji et al. (2009) reported that the effect of power cycling is more pronounced at low frequencies of the impedance results, in addition to the distortion observed in the impedance real parts (El Brouji, Briat, Vinassa, Bertrand, et al., 2009). Power cycling affects the SCs by increasing the slope of the Nyquist plot and this process continues for the whole test duration. This rising slope has been linked to the modification of the electrode structure, particularly related to a change in pore sizes and distribution. In comparison to the calendar life tests, the authors noticed a pronounced capacitance loss from

power cycling test couples with an increasing electrolyte resistance R_{el}, which again can be related to the change in pore geometry, by which this reduces the mobility of the ions. This observation is formulated based on a parameter γ which is a representation of the pore size dispersion and it is linked to the slope of the Nyquist plot at low frequencies. These findings show that power cycling causes mechanical stress on the SCs since it modifies the electrode structure.

Chaari et al. (2011) used a current profile based on repetitive start-stop, boost and regenerative braking phases, typical in micro-hybrid electric vehicle (Fig. 2.33) (Chaari et al., 2011). The method is somewhat similar to (Lajnef, Vinassa, Briat, El Brouji, et al., 2007). They highlighted that the end-of-life criteria for SC in terms of capacitance and ESR are not reached at the same time; as a matter of fact, 20% loss of capacitance is met before the 100% increase of the ESR. The authors explained that the recovery phenomenon observed in earlier research, are due to the charges trying to redistribute themselves within the porous electrode in order to reach a thermodynamic steady-state of the cell. The self-discharge and the charge redistribution mechanisms under various conditions: temperature, initial voltage, charge duration, state of charge and short-term history, have been studied in (Kaus et al., 2010) and (Kowal et al., 2011).

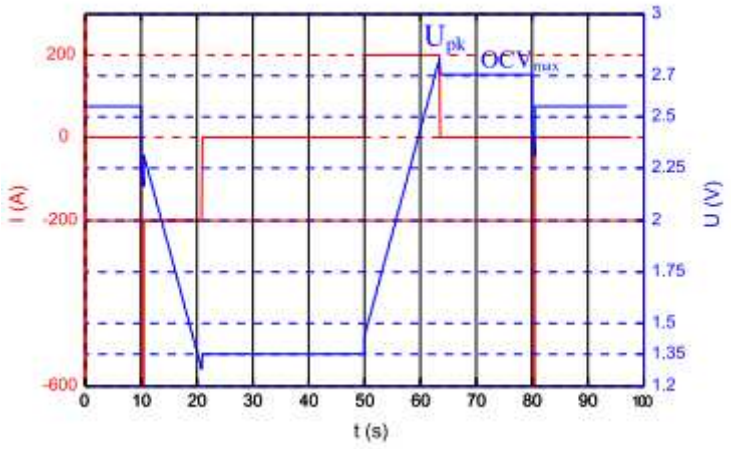

Fig. 2.33 Current profile used in (Chaari et al., 2011) and its voltage response.

While many efforts concentrated on the issue of ageing in SC cells, Rizoug et al. (2012) found the need to study the ageing process of SC modules (Rizoug et al., 2012). In their experimentation a SC module was exposed to power cycling. An important finding from the test is, although all cells in the module are subjected to the same power cycling profile, the authors noted that ageing is more egregious at the cells situated inside than the SC cells located at the edges of the module. This observation is probably caused by the fan placed at the edges of the module. Therefore, the temperature around the edges is lower than other areas in the module. This finding has pointed out the need for a careful planning for the thermal management system to make sure an equal temperature distribution inside the module so that ageing rate between each cell does not differ much. Moreover, Michel (2006) has urged the need for a proper way of attaching the cooling elements with high electrical insulating and high thermal conductivity (Michel, 2006).

2.3.3 Quantification of ageing

SCs ageing are monitored periodically to follow the course of ageing. Electrochemical impedance spectroscopy (EIS) has been shown to be a pertinent tool to study the ageing phenomenon. EIS is usually applied on fresh SC and at every stage of the SC lifetime, in order to track the ageing course. Another method is the time domain characterisation, sometimes applied together with EIS.

In (Alcicek et al., 2007), the characterisation was performed every week after an eight hours rest at ambient temperature of 20 ℃. The ageing test increases the imaginary axis –ImZ of the impedance spectra, thus indicating that the capacitance value decreases as SC ages. A clear right shift along the ReZ axis signifies that the ESR has increased with the ageing duration.

Bohlen et al. (2007) showed that the EIS was able to track the gradual change in the SCs electrical behaviour while they went through an ageing process (Bohlen et al., 2007a). Contrary to the method used in (Alcicek et al., 2007), the SCs were not allowed to rest prior to characterisation test. Nevertheless, a shift of the impedance spectra along the real axis is observed, identical to the observation in (Bohlen et al., 2007a). The real axis shift continues and then accelerates when the end of the test is almost reached. A circuit model was fitted to the impedance spectra to aid in the analysis of the ageing behaviour.

Both methods above required the SCs to be disconnected from the test for regular check-ups and they are reconnected afterwards to resume testing. Lajnef et al. (2007) devised a method which permits the characterisation to be

performed online while SCs are in test in order to minimise the effect of rest time on the test results (Lajnef, Vinassa, Briat, El Brouji, et al., 2007). The online method is based on the determination of charge resistance R_{cyc} and the capacitance C_{cyc}, unfortunately, a detail description of how the method was conducted is nebulous and is not provided by the authors. Chaari et al. (2011) also employed an online characterisation method (Chaari et al., 2011). The method is based on the determination of the capacitance and ESR based on the voltage response to the current profile.

Perhaps, the use of EIS for ageing monitoring was best demonstrated by Brouji et al. (2008) in (El Brouji et al., 2008). To appreciate the significance of the data, they proposed a generic model that was built on the initial state of the SC. The model is based on the main physical description of the porous electrode and the electrode-electrolyte interface. The model parameters are identified using EIS. While the SC is going through ageing, these parameters also change. The authors found that these parameters change differently and are very much dependent on the type of ageing tests. Therefore, they compare the evolution of these parameters between two ageing tests: calendar life test and power cycling test, in order to identify the ageing mechanisms.

Outside the SC ageing research sphere, EIS as a diagnostic tool has been practised widely in the study of battery ageing. Hafsaoui and Sellier (2010), for instance, have employed a method whereby an initial model is built, which then is used as the reference model (Hafsaoui and Sellier, 2010). Then, the corresponding model parameters are periodically monitored throughout the different stages of battery life in order to follow the evolution of the battery behaviour, which in turn, produced a numerical model of battery ageing that is

able to simulate the dynamical voltage response of the battery as a function of current and temperature. The model, based on an electrochemical model, simulates various physical phenomena observed, like diffusion, charge transfer, just to name a few, as battery experiences ageing.

In the same vein, Ran et al. (2010) used the method of EIS to predict lithium-ion battery state of charge (SOC) (Ran et al., 2010). Similar to (Hafsaoui and Sellier, 2010), the authors first established an initial model which is built based on the impedance data, and then it is used as reference for later measurements. After that, the impedance data of the battery at various SOC in the range of 0 to 0.70 is recorded which corresponds to the battery voltage between 3.0V to 4.0V. The trends and behaviour of the component parameters of the initial model at these SOC, are monitored and their relations with the battery SOC are formulated to assist in predicting the SOC.

EIS has also been promoted in (Xing et al., 2011) as "…a significant technology in the construction of 'PoF [physic-of-failure] mechanism'…"[8]. EIS has also been used in (Eddahech et al., 2011) to identify the main parameters impacted by power cycling tests, thus aiding in the determination of the most prominent ageing mechanism in lithium-ion cell battery. The lifetime prediction model for lithium-ion battery proposed by Ecker et al. (2012) is based on the parameterisation of ageing model by experimental data from accelerated ageing tests and it was shown that this method is able to simulate the real ageing behaviour (Ecker et al., 2012). A few years before that, (Vetter et al., 2005)

[8] Xing, Y., Miao, Q., Tsui, K.-L. and Pecht, M. (2011) 'Prognostics and health monitoring for lithium-ion battery', in *Proceedings of 2011 IEEE International Conference on Intelligence and Security Informatics*. Ieee, Beijing, China, pp.242–247, ISBN:978-1-4577-0082-8., DOI:10.1109/ISI.2011.5984090

recommend that EIS can be employed to identify ageing process and for analysis of ageing mechanisms in battery.

2.3.4 Ageing models

The lifetime of SCs can be quantified, for example, by plotting capacitance against time and deriving its mathematical relationship. In (Alcicek et al., 2007), the SC lifetime is calculated based on the law of Arrhenius, which is written as,

$$v = A \cdot e^{-\frac{E_A}{kT}} \tag{2.8}$$

where,

v: Reaction velocity

E_A: Energy activation in eV

k: Boltzmann constant

A: Factor of Arrhenius

T: Absolute temperature in K

A similar approach has been adopted in (Gualous et al., 2010) to determine SC lifetime. The lifetime model is formulated by taking the inverse reaction rate of the Arrhenius law,

$$t_i = Be^{\frac{E_A}{kT_i}} \tag{2.9}$$

where,

t_i: The reaction time for T_i in hour

T_i: Absolute temperature i in K

B: Parameter to be determined

Eq. (2.9) allowed the calculation for the energy of activation that will give the variation of the lifetime as a function of temperature at a fixed voltage of 2.7V.

Uno and Tanaka (2012) proposed a cycle life prediction model that makes use of the acceleration factor and activation energy determined from the Arrhenius equation (Uno and Tanaka, 2012). The work can be traced back to (Umemura et al., 2003) where they found that the degradation mechanism in SC is governed by the Arrhenius law, therefore, enabling the determination of the activation energy of a particular degradation process. Kötz et al. (2006) used the activation energy to determine the leakage current for temperature range between 0℃ to 60℃ (Kötz et al., 2006). Kötz et al. (2006) reported that the acceleration factors of 2 can be expected for every 10℃ increase in temperature. Uno and Tanaka (2012) reported an acceleration factor of 1.2 for the temperature range of 0℃ to 40℃, which signifies that the degradation occurs at a rate of 1.2 times faster for every 10℃ increase.

Besides those mentioned, another method is based on the quantification of ageing through EIS measurements. This technique allows for a mathematical relationship of impedance parameters with stress level to be derived. Ageing directly affects the impedance spectra; thus, fitting a circuit model to the spectra and obtaining circuit parameters at various ageing states was done in (Bohlen et al., 2007a) to obtain an ageing trend. Therefore, the circuit model allows for the extrapolation of the ageing test results as a function of voltage and temperature. In the Part II of their work (Bohlen et al., 2007b), the ageing model is improved to provide electrical and thermal simulation for a more holistic ageing model.

The thermal simulation of their model shows the temperature distribution in the module after 7 years simulated service time; the SC cells are hotter as they are placed closer to the hot wall. If the differences of temperatures between SC cells in the module are not addressed, this situation can lead to different ageing rate between cells. Moreover, the internal heat generation during operation will cause self-accelerated ageing processes. The holistic model will therefore be beneficial in the stack design and the cooling system design.

Omar et al. (2014) argued that to model SC long-term performance, the model should not be based on fixed parameters (Omar et al., 2014). Therefore, they proposed a model based on 3 levels: (1) electrical model, (2) thermal model, and (3) lifetime model. The third level, the lifetime model, is based on following the evolutions of the calendar and the cycling tests at different conditions and formulating the relationships between the results. The authors, however, do not explain in detail how the process is conducted.

Concerning the heat generation during operation, particularly in HEV application, where the very large current rate to charge and discharge the SCs produces a considerable amount of heat, Gualous et al. (2007) proposed a thermal model based on the finite-differential method (Gualous et al., 2007). The proposed model takes into account the material, structure and packaging properties. As the SCs go through a charging/discharging regime, the temperature increases exponentially with time as a result of accumulated heat. The heat transfer in SCs can be attributed to (1) conduction, (2) convection, and (3) radiation. A temporal evolution of the SC temperature for different charge and discharge current values was proposed. An update of their work can be found in (Gualous et al., 2009). D'Entremont and Pilon (2014) proposed a

spatiotemporal physical model which took into account the irreversible Joule heat generation and the reversible heat generation due to diffusion, steric effects and entropy changes (d'Entremont and Pilon, 2014).

The evolution of ESR and capacitance as ageing proceeds have been used as ageing indicators and parameters to predict and calculate the lifetime of SCs in SC health diagnosis. (Soualhi et al., 2013) predicted the ageing of SCs by monitoring the ESR and the capacitance and these information are used to train neo-fuzzy neuron (NFN). In (Oukaour, Pouliquen, et al., 2013), the evolution of ESR and capacitance from the beginning of ageing are realised by using least squares algorithm. The SC diagnosis method proposed in (Oukaour, Tala-Ighil, et al., 2013) calculates the correlation between capacitance loss as a function of ageing time by measuring two different points, M_1 and M_2 on the voltage-time charging curve. Similar approach of using an experimental dataset to establish the ageing model was also proposed in (Ayadi et al., 2013). The ageing model consists of two parts, to take into account the two stages of SC ageing: the first stage involves a rapid chemical break-down in the SC structure, represented by the sum of an exponential part, and the second stage involves a slower process and it is related to the diffusion phenomenon, represented by a square root of the time function.

2.4 Summary

Manufacturers continually seeking to increase SC energy density. Although substantial progress has been made in SC technology with many efforts to find better materials and better cell design are being invested, ageing of SCs is yet to

be fully understood. There are many studies reported in literatures, investigating the effect of voltage, temperature and cycling on SCs. While these studies successfully describe the ageing characteristics of SCs and add to the general understanding about the system, this knowledge has not been fully utilised to develop an ageing model that is not only able to elucidate failure mechanisms seen during degradation processes, but will also shed light on the dynamic interactions between ageing and electrical behaviour of the SC, also at the same time is able to predict the lifetime of SC.

One of the problem is because of the ageing tests are usually conducted by imposing many ageing factors at a time. Therefore, the interpretation of the ageing process is not always clear cut, especially if the present situation is different from the one tested in lab.

Furthermore, it has been demonstrated in (Omar et al., 2014; Kötz et al., 2010; El Brouji, Briat, Vinassa, Henry, et al., 2009; El Brouji et al., 2008; Bohlen et al., 2007a) that the changes in SC impedance bespeaks ageing. Therefore, an impedance-based ageing model can be built to take account for the impact of ageing on the dynamic behaviour of the SC through the variations of the circuit parameters during the course of ageing.

Ageing in SCs is a long-term effect and a complex process; it takes between months to years to observe ageing. Researchers like (Dzieliński et al., 2011), (García et al., 2010) and (Quintana et al., 2006) have demonstrated that fractional-order model can cover over a wide frequency range related to SC dynamic behaviour. As ageing effects usually involve long time constant, the fractional-order model is found suits to achieve the objective of this thesis. To

realise this, a suitable tool is needed. EIS has been used by (Ecker et al., 2012), (Eddahech et al., 2011), (Ran et al., 2010) and (Vetter et al., 2005) to study battery ageing. Therefore, it is assured that EIS is the most fitting tool in the diagnostic studies of SC ageing.

CHAPTER 3

METHODOLOGY

"Sometimes the questions are complicated and the answers are simple."

—Dr. Seuss

3 Introduction

In this chapter, the research approach taken is discussed. Having understood the need for a robust product and the exigency for a way to predict SC long-term performance, various aspects on devising a strategic plan to gather relevant information that will enable prediction of failure, are discussed. This too includes the challenges faced to collect the data, the suitability of the method used and the rationale behind the decision. Also in this chapter, the equipment and tools used are introduced along with descriptions on the scientific methods employed.

3.1 Research Methodology

In this time of rapid technology advancement, forecasting how a product behaves over its life to eventually no longer perform its intended function, has become even more important; this has directed many efforts in the area of prediction (e.g (Uno and Tanaka, 2012; Soualhi et al., 2013)). The ability to predict what may happen in real situations allows for strategic preparations and sound decisions to be made. This includes crucial information such as on how long the product will serve its intended function and if failures happen, what types of failure can be expected, so that remedial actions can be directed and also to mitigate the product risks. Any unexpected failure or premature failure creates consternation and can result in revisions of planning and expectations—this can be costly to both the manufacturer and customers.

However, the task has become elusive with continuing advances and rising complexity in product technologies. The steps to predict potential failures so that they can be eliminated early in the development cycle often requires a deep understanding of the failure mechanisms and the physical processes contributing to the appearance of these failures. By understanding the cause and the mechanism of which a failure occurs, preventive measures can be taken.

Therefore, the following strategy (Fig. 3.1) is devised in order to gather this information. The plan begins with the determination of the end-of-life (EOL) criteria of the SCs. Various sources are referred to which include: testing procedures by several independent testing organisations such as IEC (International Electrochemical Commission) (IEC, 2006a), USABC (United States Advanced Battery Consortium) (FreedomCAR, 2004), EUCAR

(European Council for Automotive R&D) (EUCAR Traction Battery Working Group, 2003), UC Davis (University of California Davis) (Miller and Burke, 1994) and HCV (Hybrid Commercial Vehicle) (Conte, 2010); manufacturer documents and datasheets (Maxwell, 2009b); and journal papers like (Kötz et al., 2010; Gualous et al., 2010). Although there is a variation on the EOL criteria, depending on the applications, the general consensus for the EOL criteria are 20% loss of capacitance and/or more than 100% increase of the ESR.

Having understood the criteria and requirements for a good SC, the next step is to list out all possible failure causes and mode of failure from the literature. Failures can be divided into two groups: early failures and wear out failures (Gualous et al., 2012). Early failures are usually endogenous in which they take place during the production stage. For instance, they can be caused by variations in the materials or components used in production of the cells, contamination of the active materials or they can be due to design faults. Wear out failures are failures that occur during operation and consequently, causing the SC ceases to function. This type of failure can be aggravated by a number of causes which include stress from the operating conditions—environmental based or usage based. Hence, failure cause is an activity that leads to failure; it can be from an internal cause, external cause, or it can happen naturally. The area of investigation of this thesis is, however, limited to wear out failures that are caused by external factors. Therefore, the steps followed are formulated around this regard.

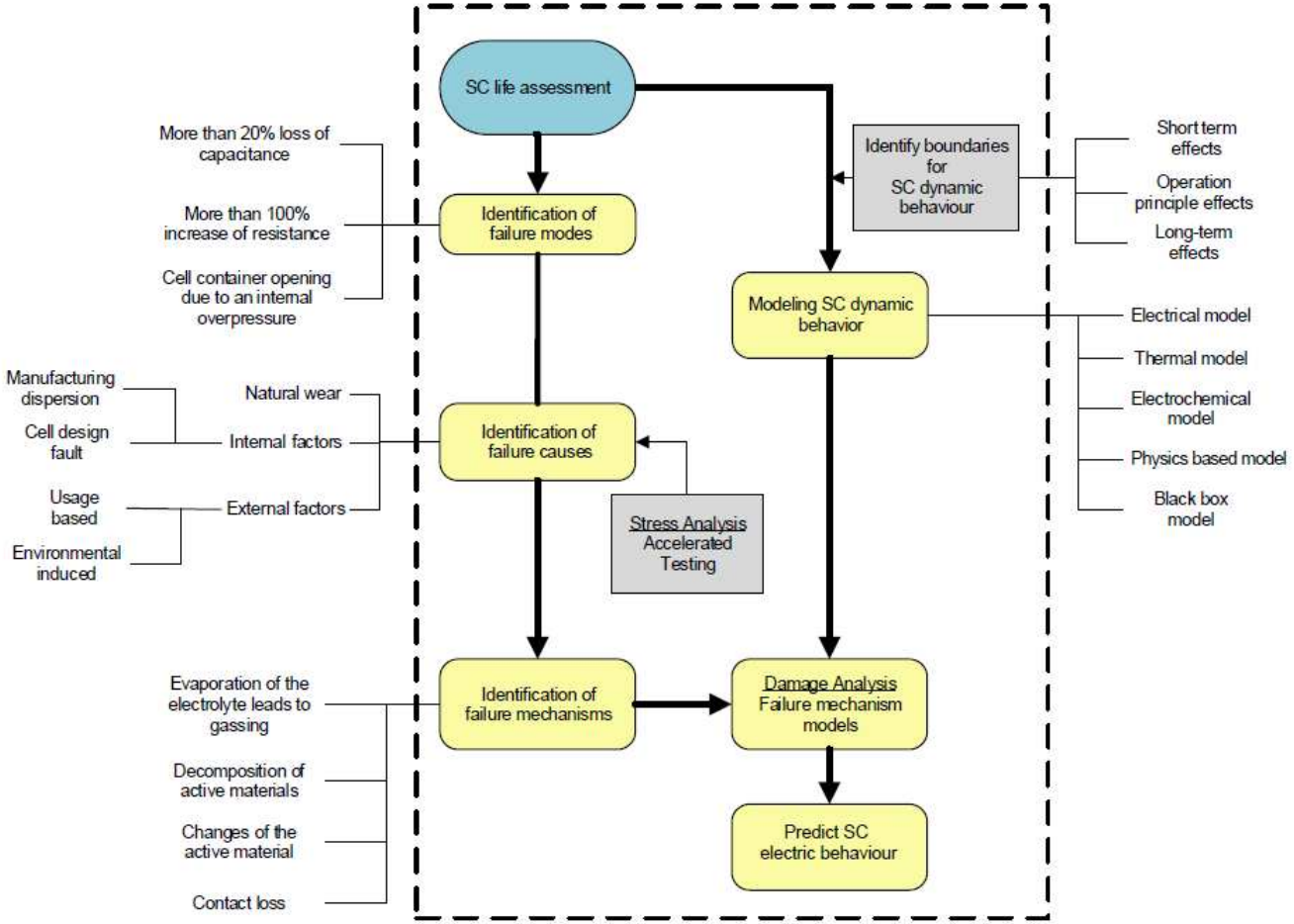

Fig. 3.1 Research methodology.

Oftentimes, failure does not happen immediately. Nevertheless, the rate and severity of a failure depend on the stress applied to the device (device herein is referred to SC) (Mathew et al., 2008). Naturally, a failure is preceded by a decline in performance. The state of failure (failure mode) can be observed in the following ways: (1) parametric; an increase in the resistance and loss in capacitance, (2) functional; short circuit and open circuit, or (3) through physical evidence like package swelling.

The process that leads to these modes of failure in SCs are known as failure mechanisms. They can be of physical degradation of components or change in chemical properties. Ageing mechanism and failure mechanism are used interchangeably in this thesis to refer to the symptoms to a failure. The identification of the ageing mechanism enables determination of the root cause of the failure, if the relation between ageing mechanism and failure cause is established, so that preventive measure can be taken to improve the reliability of the device. The next step is therefore to list out the potential ageing mechanisms. Fig. 2.25 in Chapter 2 presents the impact of ageing on SCs.

SCs have a long-life performance up to more than 10 years (Wang et al., 2012), which make it unfeasible for many laboratory scale tests. Accelerated ageing tests have been used by many researchers to expedite degradation so that information can be gathered in a compressed time. From this pile of information, the dominant failure mechanism can be identified. Accelerated ageing tests in this work are conducted by, first determining the ageing factors or stimuli. Typically, temperature is used as the ageing stimuli. By applying a high level stimulus to the device but still confining it to the maximum capability of the device to endure stress, the degradation process can be hastened. However, there

is a potential danger to this method; the chosen method could precipitate spurious failure mechanism (Kurzweil and Chwistek, 2006). Therefore, a careful selection of the appropriate method is key to success.

Three factors that need to be considered when choosing the appropriate level of stimuli are: (1) the capability of the device to withstand stress, (2) the time frame of the experiment and (3) the rate at which ageing proceeds according to the stress applied. Manufacturer's specifications are referred to establish test boundary, also taking into consideration the device applications. This boundary includes the setting of the maximum and minimum test temperature and the applied voltage limit. Typically, these conditions are limited by the type of electrolyte used in the SC.

As SCs can take months to several years to degrade (Uno and Tanaka, 2011; Bittner et al., 2012), it is of the utmost importance that all possible degradation can be observed within a realistic duration for a laboratory scale testing. In electrochemical devices like SCs, the unwanted chemical reaction is the classic cause of reduced cycle life (Hahn et al., 2005; Azaïs et al., 2007; Zhu et al., 2008; Ruch, Cericola, Foelske-Schmitz, et al., 2010); the rate at which this reaction occurs at high level stress needs to be known to make it possible to correlate this data with how it will age at normal conditions. The most common model that is used to describe the relationship between temperature and the chemical-reaction rate is the Arrhenius model; the rate doubles or the lifetime is halved for every 10℃ increase in temperature and for each 100mV above the nominal voltage (Schiffer et al., 2006).

Testing procedures like (IEC, 2006a), (FreedomCAR, 2004), (Miller and Burke, 1994), and (BSI, 2010) are again referred to identify common tests used for SCs. Many of these tests are application-driven; they are different from one another and are applied in different ways depending on the applications and needs. Some of the testing are modelled on the tests used in battery testing, for example, calendar life testing and cycle life testing. Calendar life testing is similar to storage experiment at different temperatures but a constant voltage is applied to the device, while cycle life testing uses current profile that emulates, for instance, the HEV operation. Thereupon, a way to tailor these tests with the accelerated ageing test to meet the research objectives is sought after. Again, one of the objectives of the research is to study the principle effect of a single ageing factor, so that the respective mechanism which leads to the failure in SCs can be identified. This requires the isolation of the ageing factor to determine the individual contribution of each factor to the ageing in SCs.

Once the failure site and the dominant failure mechanism are found, the next step is to perform failure analysis of the identified dominant failure mechanism. Development of mathematical models for the failure mechanisms are employed at this stage to aid in the interpretation of the results. The selection of an appropriate model is paramount—the model needs to cover all the salient points of the SC dynamic behaviour. The SC dynamics take place in a very wide range of time constant, from microseconds up to several years. This range can be divided into four: fast effect, short-term effect, mid-term effect and long-term effect. The fast effect, usually between 1 and 10kHz in frequency domain, is due to the connecting cable. Short-term effect (10Hz to 1kHz) is pertaining to the operation effect and cell design. Mid-term effect (10mHz to 10Hz) is in regards

to the charge redistribution phenomenon and double layer effect and finally, the long-term effect (1 to 10mHz) is caused by operation regimes and ageing (Rafik et al., 2007).

For the reason that complex SC operating mechanisms happen at different time scales and ageing only occurs after a very long time, it is necessary for the chosen model to be able to cover time scales relevant to ageing. On top of that, the model also needs to be able to model at a microscopic scale to include all the electrochemical processes in SCs. Types of mathematical models available are then explored. Based on the method they are constructed, they can be divided into: (1) empirical models (e.g. (Merrett et al., 2008; Martín et al., 2008b; Uno and Tanaka, 2011; Hijazi et al., 2012)), (2) semi-empirical models (Bohlen et al., 2007a; Nicolas Bertrand et al., 2010) and (3) physics based models (Wang and Pilon, 2013). A dynamic modelling by means of equivalent circuit is preferred as this approach shows explicit physical meaning and able to replicate the electrical terminal characteristics. This thought leads to electrical equivalent circuit (EEC) based on electrochemical model built using empirical approach.

The development of an electrochemical model requires a specific measurement method called the electrochemical impedance spectroscopy (EIS). In that regard, the accelerated ageing test needs to include the EIS measurement during the periodic check-up of the SCs to obtain data related to the ageing process in SCs. Furthermore, it is important to bear in mind that the accelerated ageing test itself is destructive to the SCs. From this point, it is critical that a non-destructive measurement is used during periodic observation and data recording to avoid erroneous data and potential loss of important information.

EIS measurement fills this need. For diagnostic purposes, EIS is applied at each defined stages during the SC lifetime to monitor any electrochemical changes to the SC properties. For application purposes, EIS is used to obtain the parameters for the EEC through a fitting process which will be useful for simulating the SC electrical behaviour. Therefore, the EEC aids in the result interpretation and the assessment of the relationship between failure and stress as each component of the circuit can be related to the kinetic process that occurs during ageing.

Unfortunately, this approach has a drawback; the developed EEC will be based on fixed parameters. Consequently, the model is only good for the state at which the model is developed. In order to use the model for assessing the impact of stress on the lifetime of SCs and how the ageing process affects the electrical performance of SCs, additional approach has to be taken. The important criteria is that the model cannot be static. Therefore, this requires that the modelling approach to follow closely what the SC is experiencing. For this reason, an empirical approach is explored by means of parameterising the EEC parameters.

The development of the EEC based upon the ageing test results makes it possible to identify and select precursor parameters which caused failure in SCs. Therefore, by plotting the evolution of these parameters during ageing duration, it gives an insight on how the ageing process proceeds as a function of time under a given condition. Through the parameterisation of the developed EEC, the most affected parameters by ageing are selected and the evolutions of these parameters are empirically explained to represent the main degradation mechanism, thus, will be useful for predicting what changes the SC will experience in the future.

The use of EEC is not only for getting an insight of the kinetic information in SCs and how ageing progresses. Since the EEC is essentially an equivalent circuit, this makes it possible to obtain the current-voltage characteristic for the electrical assessment of SCs. The parameterisation of the EEC parameters not only will help in anticipating the changes in SCs with time in term of the SC properties, but also allows to obtain the impedance of the SC for simulating the current-voltage characteristics in any stage of SC life.

The experimental and modelling works above are premised on the framework set out in Fig 3.2. In Phase 1 of the research, experimental works are performed to investigate the effect of ageing factors to the decline performance and to monitor the ageing process in SCs. In Phase 2 of the research, the SCs are modelled using EEC to study the dynamic behaviour and how it is affected by ageing process. The approach employed in this research permits the understanding of ageing as an ongoing process, from the beginning of the lifetime to the point where failure occurs. Hence, the model describes changes in the SC properties and also changes to the part structures. Knowledge gained from the assessment and quantification of the degradation, thus, allowing for the identification of the main ageing mechanism which contributes to the failure in SCs. This information is useful for SC improvement effort and also aids in predicting failure before it manifests.

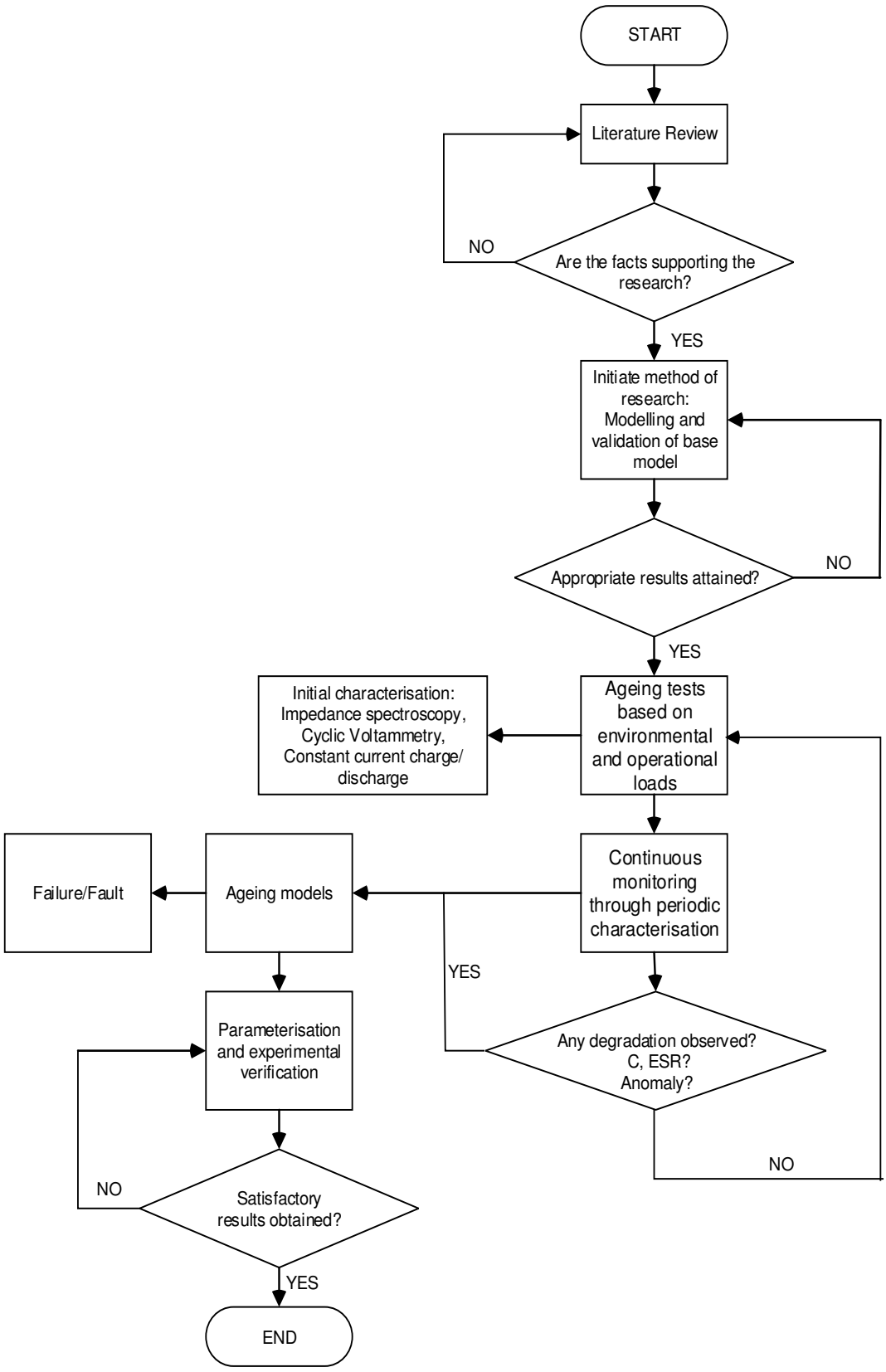

Fig. 3.2 Testing framework.

3.2 Equipment and Instrument

The lists of equipment, instrument and software used in this thesis are shown in Table 3.1-3.3. Fig. 3.3 shows the experimental setup.

Table 3.1. List of equipment used in this thesis.

Equipment	Supplier	Description
Environmental Chamber Model 7102-1	RANSCO	Environmental chamber. Temperature range: -70℃ to +200℃
Fibre glass product tray	TwoYSP Marketing & Trading	A customised product tray to hold SC under test
Power Supply GPS-3303	GW Instek	3-Channel Power Supply
Iteaduino Leonardo	Iteadstudio.com	Microcontroller board based on ATmega32u4
MotoMama	Iteadstudio.com	Arduino shield based on L298N H-bridge driver chip

Table 3.2. List of instrument used in this thesis.

Instrument	Supplier	Description
NI USB-6212	National Instruments	16 analogue input data acquisition device for voltage measurement
NI USB-9211	National Instruments	4-Channel thermocouple input module for use with NI CDAQ-9171 for temperature measurement
NI CDAQ-9171	National Instruments	1-slot NI CompactDAQ USB chasis used with NI USB-9211
PGSTAT302N with FRA2 module	Metrohm Autolab B.V.	Potentiostat/galvanostat
FEI Quanta 400F FESEM	FEI	Scanning electron microscopy (SEM)
EDX with 20mm^2 X-Max Detector	Oxford-Instruments	Energy Dispersive X-ray Spectroscopy (EDX)

Table 3.3. List of software used in this thesis.

Software	Developer	Description
MATLAB v.7.10 (R2010a)/SIMULINK	MathWorks	A program for numerical computing and simulation
NOVA 1.10.3	Metrohm Autolab B.V.	A software to control Autolab instruments and for data analysis
NI LabVIEW 8.6	National Instruments	Software development environment for creating custom application to interact with data acquisition device.
Arduino 1.0.5 IDE	Arduino Software	Arduino development environment for writing code and communicating with Arduino board

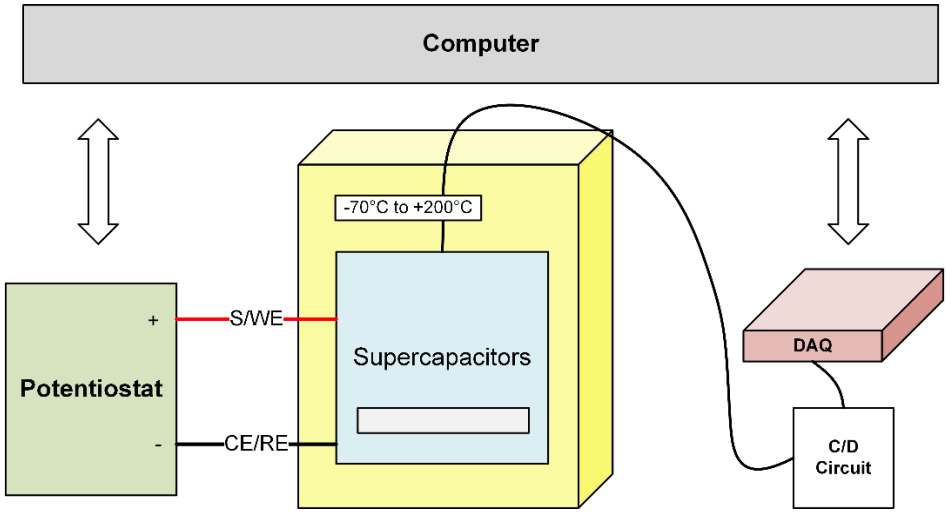

Fig. 3.3 Experimental Setup.

3.2.1 Supercapacitors

The size and type of SCs used in this thesis are chosen based on several requirements and one of them is that the SC has to be in the form of individual cells. Considering that SCs used in automotive applications are typically based

on organic electrolyte, owing to its high voltage limit, hence, SC with the same electrolyte technology need to be used so that the results obtained can be correlated with data from automotive application. Whereas, the size of the SC is limited to the testing facilities.

SCs (Fig. 3.4) used are from Maxwell Technologies, USA. They are from HC series (BCAP0025) – board mounted cells range in radial cylinders form factor. The cell is rated at upper voltage 2.7V and capacitance of 25F. The casing is made of aluminium. The electrodes are made of activated carbon. The SCs use organic electrolyte tetraethylammonium tetraflouroborate ($TEABF_4$) in acetonitrile (AN). The cell information is listed in Table 3.4.

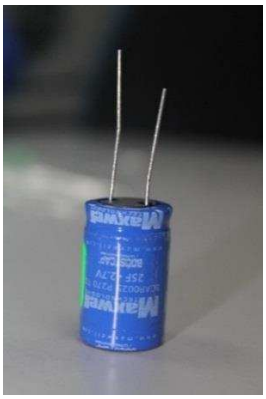

Fig. 3.4 BCAP0025 supercapacitor used in this research.

Table 3.4 Supercapacitor information.

Part Number	**BCAP0025 (HC series)**
Maker	Maxwell Technologies Inc.
Case Type	Radial cylinder
Rated Capacitance	25F
Rated Voltage (65℃/85℃)	2.7V / 2.30V
Maximum ESR_{DC} initial	42mΩ
Operating Temperature	-40˚C to +65˚C / +85˚C

3.2.2 PGSTAT302N with FRA2 Potentiostat/Galvanostat

A potentiostat/galvanostat (PGSTAT302N) is used to carry out electrochemical testing on SCs. PGSTAT302N (Fig. 3.5) is a high performance modular potentiostat/galvanostat from Metrohm Autolab B.V. It consists of a data-acquisition system for data sampling and recording and FRA2 module for electrochemical impedance spectroscopy. The functions of PGSTAT302N are controlled by a control software NOVA 1.10.3 (Fig. 3.6), also developed by Metrohm Autolab B.V. PGSTAT302N provides four electrode connections: counter electrode (CE) and working electrode (WE), for current measurement; reference electrode (RE) and sense electrode (S), for voltage measurement. 2-electrode connection is used in this thesis as shown in Fig. 3.7. This connection measures the potential across the whole electrochemical cell, including contributions from working electrode and electrolyte. The impedance measurement, therefore, is given by;

$$Z_{cell} = \frac{V_{WE} - V_{CE}}{I} \tag{3.1}$$

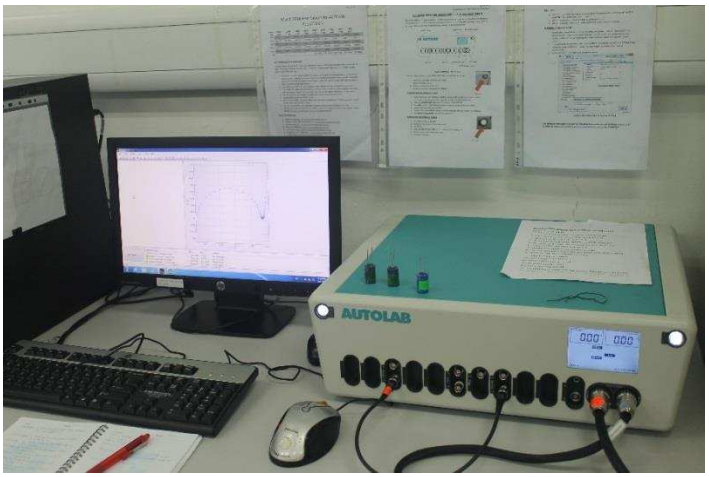

Fig. 3.5 PGSTAT302N and Nova 1.10.3 loaded on computer.

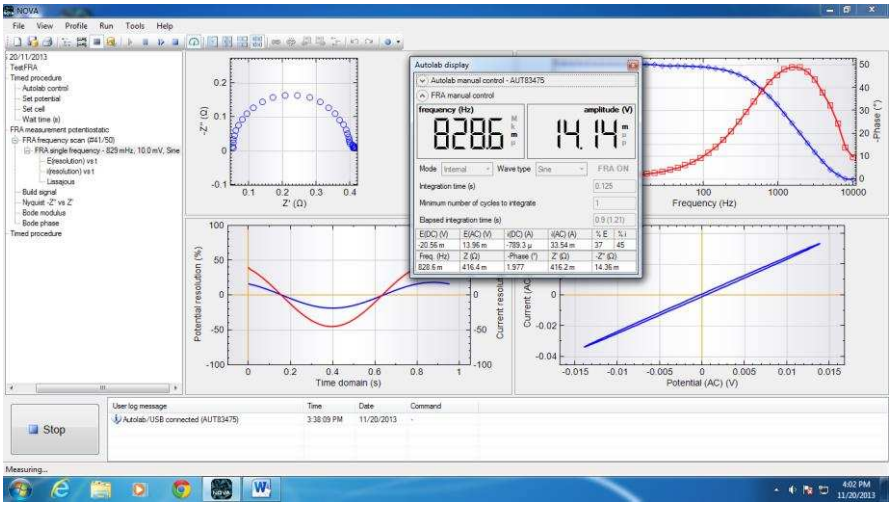

Fig. 3.6 The measurement view of Nova 1.10.3.

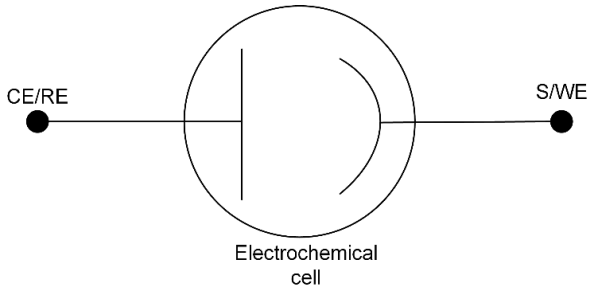

Fig. 3.7 2-electrodes connection.

3.2.3 Data Acquisition System

Data acquisition system is set up with two data acquisition devices connected to a computer and a data source (Fig. 3.8). NI USB-6212 from National Instruments is used to record voltage from SC terminals during cycling. As cycling generates heat, the heat generation is measured by attaching K-type thermocouples on SC surface (Fig 3.9) with Kapton tape. K-type thermocouple can measure temperature range of -200℃ to +1250℃. NI USB-9211 is used to measure and record the thermocouple signals. The operation of the DAQ devices are controlled by a programmable software, LABVIEW. Graphical programs are

written to display and analyse the data (Fig 3.10). The setup of the DAQ system is illustrated in Fig 3.11.

Fig. 3.8 NI USB-9211 with NI CDAQ-9171 (left) and NI USB-62121 (right).

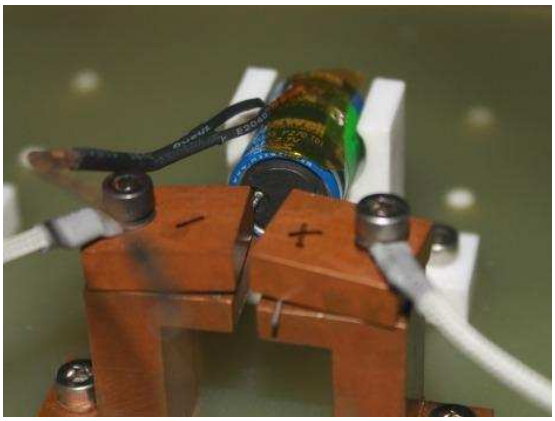

Fig. 3.9 K-type thermocouple attached on supercapacitor surface for temperature measurement.

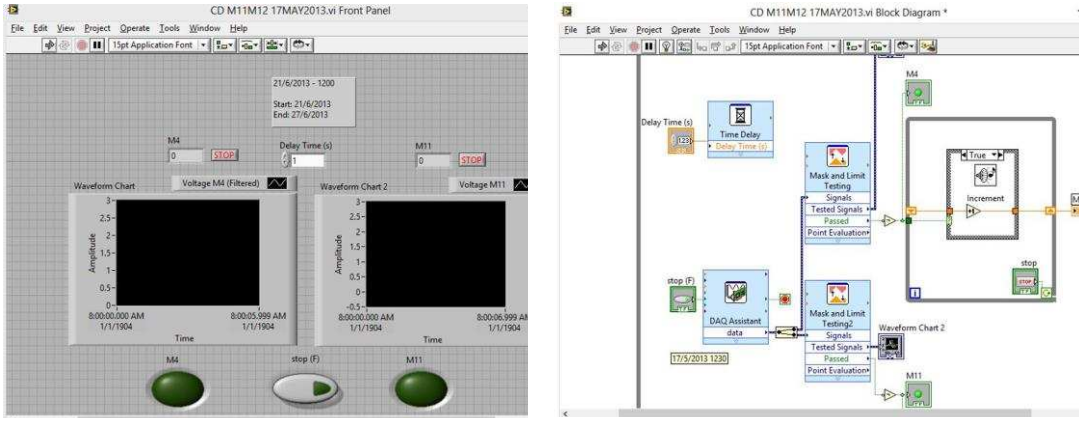

(a)

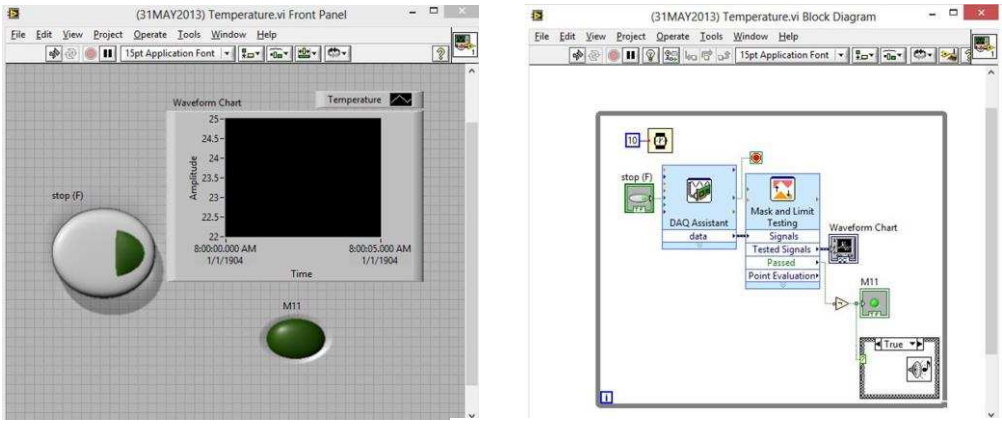

(b)

Fig. 3.10 Screenshot of the programs written in LabView: (a) the program to control the operation of NI USB-6212. The front panel (left) and the block diagram (right); (b) the program to control the operation of NI USB-9211. The front panel (left) and the block diagram (right).

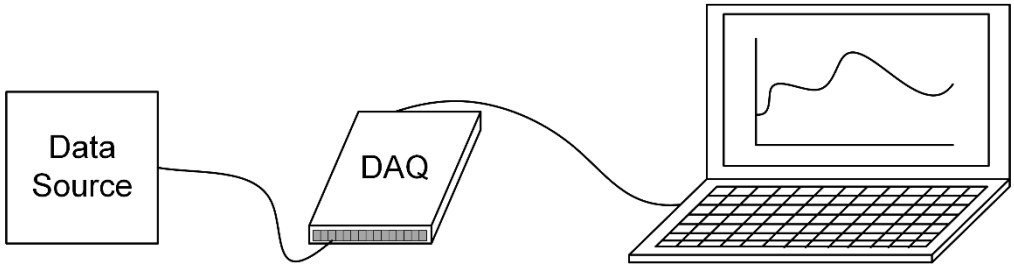

Fig. 3.11 DAQ System Setup.

3.2.4 Charge-discharge circuit

Charge-discharge circuit is built using Iteaduino Leonardo and Arduino Shield, MotoMama, both manufactured by Iteadstudio.com (Fig. 3.12).

Iteaduino Leonardo is a microcontroller board based on ATmega32U4. A dual full-bridge L298N based motor driver, MotoMama is used to control current flow. It has two output channels which can connect two SCs at the same time. The motor driver can supply 2A per channel, making it a total of up to 4A dc current. The motor driver is mounted on the Leonardo and it is powered separately by an external power supply. The external power is connected by plugging the wires from the power supply to the Vsupply and GND screw terminal. Whereas, the Leonardo is powered by AC-to-DC adapter by plugging a mini USB cable to the USB connector. A program is written in Arduino IDE (refer to Appendix A) and loaded to the Iteaduino Leonardo.

The whole circuit acts as a switch, changing the direction of dc current when the voltage at SC terminal reaches a predefined limit, to charge or discharge the SC. The analogue input pins read the voltage at SC terminal. If the terminal voltage reads less than 2.7V, the current moves forward, thus charging the SC. When the voltage reaches 2.7V, the current direction is reversed to discharge the SC to 0V. The whole operation is illustrated in Fig. 3.13. The charge-discharge cycle continues until the operation is manually stopped. The schematics of both circuits are attached in Appendix B and Appendix C.

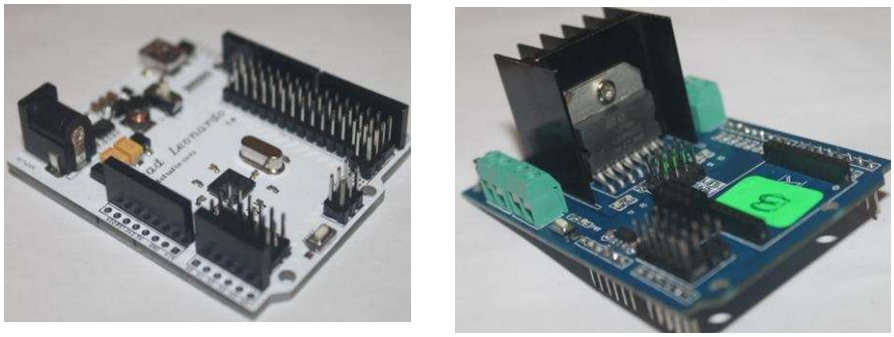

(a) **(b)**

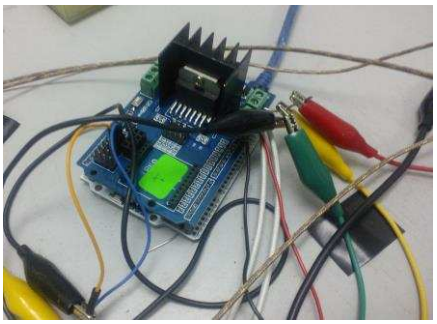

(c)

Fig. 3.12 The circuits used in this work: (a) Iteaduino Leonardo; (b) MotoMama; (c) the complete circuit.

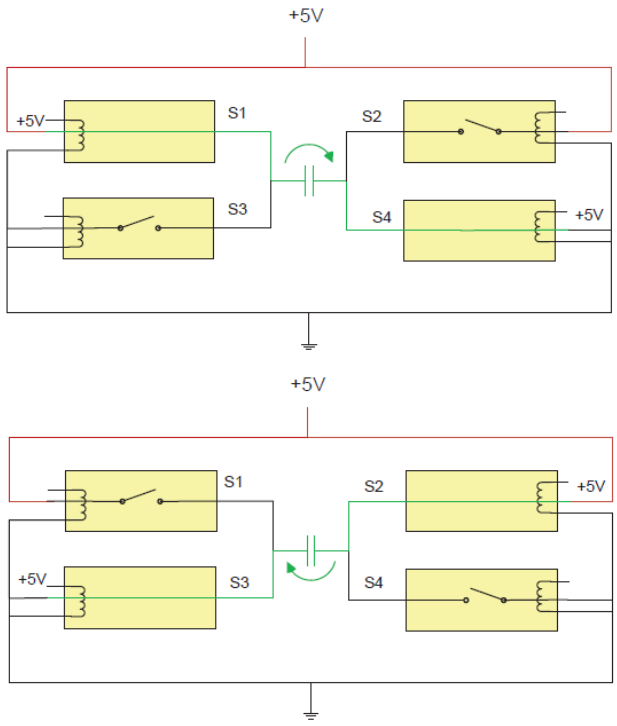

Fig. 3.13 Charging (top) and discharging (bottom) supercapacitor.

3.2.5 FOMCON toolbox for MATLAB

FOMCON toolbox for MATLAB is used in this thesis during the development of SC equivalent circuit model, in Chapter 6. FOMCON (Tepljakov, 2013) is a fractional-order modelling and control toolbox for MATLAB developed by Aleksei Tepljakov. The toolbox is built from an existing mini toolbox FOTF introduced in (Xue et al., 2007; Chen et al., 2009; Monje et al., 2010).

3.3 Experimental Techniques - Electrochemical characterisation and DC test procedure

It is critical to select suitable methods to study and analyse the performance losses in SC under different experimental conditions. The difficulty to analyse the degradation mechanism with naked eyes requires a sophisticated method that can penetrate deep into the cell to gather the data. Analysing the data also poses a challenge—the electrochemical processes often overlap due to contribution of different changes in an electrochemical cell, therefore it is often inextricable if they were to be analysed with standard methods. Therefore, a method that can, as precisely as possible, distinguish between the influence of different processes is needed. With that in mind, data collection in this work follows a measurement protocol comprises electrochemical characterisations and a DC test procedure. The measurement protocol is carried out to track changes in SC performance during the ageing test. The data collection is done in a systematic manner: electrochemical impedance spectroscopy is done first, followed by cyclic voltammetry and constant current test.

3.3.1 Electrochemical impedance spectroscopy (EIS)

3.3.1.1 Introduction

Electrochemical impedance spectroscopy (EIS) is gaining popularity for characterisation of electrochemical systems. It is one of the many methods out there that can provide information about electrochemical reactions that occur in cell without altering or destroying the cell, thus ensuring the integrity of the data. This is particularly useful when studying SC decay and ageing where it requires observation on tiny details.

In EIS, a small amplitude sinusoidal signal is applied to the cell. The signal is sufficiently small (1 to 10mV) that the nonlinearity behaviour of most electrochemical cells, including SC (Zubieta and Bonert, 2000), is not observed (Dominguez-Benetton et al., 2012) . The resulting response should at least approaching quasi-linear behaviour, if not linear, for the data to be valid. This is one of the unique advantages of EIS by which it ensures the truthfulness of the data. Other criteria for a valid data are stability, causality and finiteness (Lasia, 1999).

EIS is done at a very broad frequency range. The wide frequency allows isolation of electrochemical processes (Itagaki et al., 2007) which have different time constants. This permits for a thorough understanding and immediate identification of what is going on inside the cell. The process to identify the provenance of failure can be a mare's nest. With the capability to separate different processes, EIS can be a good diagnostic tool.

In this thesis, EIS is performed in the frequency range of 10kHz to 100mHz with 10 points/decade. The applied AC amplitude used is 10mV rms, single sine wave. The measurements are carried out in potentiostatic mode, which allows control of the applied voltage. No bias voltage is applied to the cell. EIS is applied to gain insight of the electrochemical processes at the electrode/electrolyte interface and also to substantiate results from other measurement techniques.

The application of EIS in this work is therefore to achieve the following aims:

1. To provide insight, at a microscopic level, of the fundamental aspects of the processes involved in a SC overall response.
2. To identify and differentiate the individual contributions of each electrochemical process to the total impedance and to allow investigation of how these processes interact and affect SC overall performance.
3. To allow modelling of the system with an appropriate equivalent circuit so as to describe the electrochemical reaction that takes place at the electrode/electrolyte interfaces; consequently, obtaining the electrochemical parameters of the system that will later assist in identifying the largest hindrance to SC high power performance.
4. To identify possible degradation mechanism.
5. To obtain current/voltage/time behaviour of the equivalent circuit that can be used to predict system behaviour in real condition.

3.3.1.2 The working principle of EIS

A sinusoidal signal perturbation signal is applied to the system. If the system is linear, the current response will also be a sinusoid and has the same frequency as the applied voltage signal but shifted in phase, by the angle φ (Gamry, 2010), refer to Fig. 3.14.

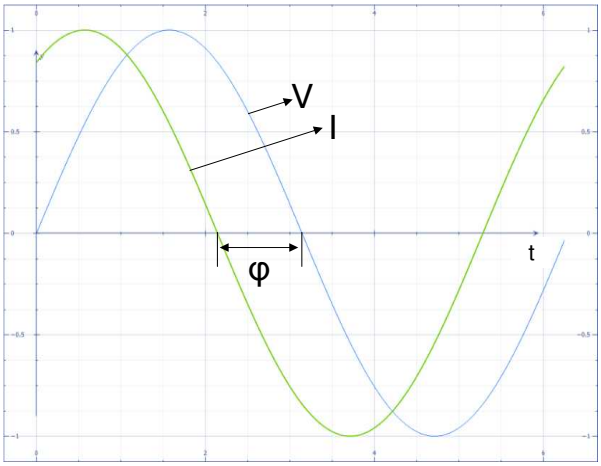

Fig. 3.14 Sinusoidal voltage perturbation and current response in a linear system.

The sinusoidal voltage is given by,

$$V_t = V_0 \sin(\omega t) \tag{3.2}$$

where V_t is the voltage at time t, V_0 is the signal amplitude, $\omega = 2\pi f$ is the angular frequency.

The responding current signal is,

$$I_t = I_0 \sin(\omega t + \varphi) \tag{3.3}$$

Therefore, the impedance of the system, by Ohm's law, can be calculated as,

$$Z = \frac{V_t}{I_t} = \frac{V_0 \sin(\omega t)}{I_0 \sin(\omega t + \varphi)} = Z_0 \frac{\sin(\omega t)}{\sin(\omega t + \varphi)} \tag{3.4}$$

The impedance of the system is displayed in a bode plot and is expressed in terms of a magnitude Z_0, and a phase shift φ.

Nova 1.10.3 allows for assessment of linearity on the system under study. Plotting the applied sinusoidal signal V_t and the sinusoidal current response I_t on a graph produces an oval shaped response, known as the Lissajous representation of the signals (Fig. 3.15). Lissajous plot provides information on the impedance magnitude and the phase angle between input and output signals. The shape of the Lissajous plot changes depending on the phase shift. When the linearity condition is satisfied, the shape of the Lissajous plot is symmetrical and any distortion to the Lissajous shape reveals that the system is nonlinear, as shown in Fig. 3.16.

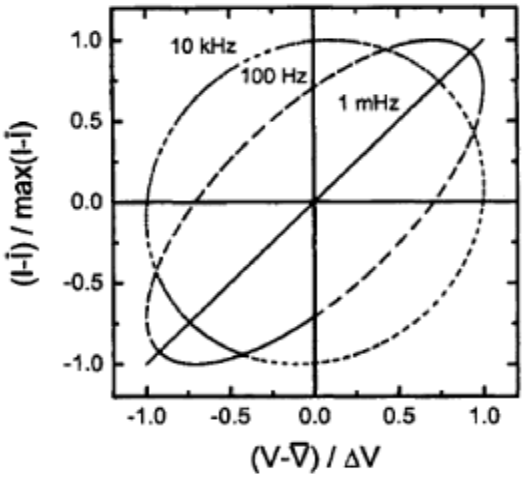

Fig. 3.15 Lissajous plots at 10kHz, 100Hz and 1mHz (Orazem and Tribollet, 2008).

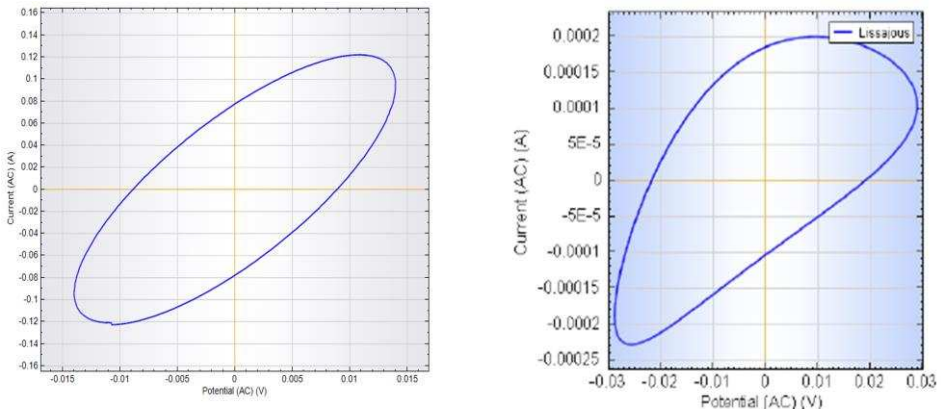

(a) **(b)**

Fig. 3.16 Lissajous plots: (a) Lissajous plot of a linear system is symmetrical, whereas for a nonlinear system (b), Lissajous plot shows distortions that are associated with an input perturbation that is too large (Metrohm, 2012).

3.3.1.3 Experimental consideration

The experimental design depends upon the system under investigation. A careful selection of the parameters is important to minimise the risk of error of judgement and to ensure the information obtained is adequate for identifying all possible processes involved in the overall response.

3.3.1.3.1 Frequency range and number of frequencies

The frequency range applied, for which data to be collected, should be sufficiently wide to observe the dynamic response of the system under study. Depending on the system's time constants, typically the range starts from 10kHz down to 10mHz. Above 10kHz, inductance effect usually dominates, which most of the times the response does not belong to the system, but is contributed

by measurement artefacts like the connecting cables. The measurement always starts from high frequencies to low frequencies. High frequency takes shorter time to complete, while longer time usually required for measurement at low frequency. By beginning from high frequency, more data are collected within a shorter period. In fact, the duration of a complete measurement is largely influenced by the low frequency. Generally, the lower the frequency, the longer the time it takes to complete test (ref. to Table 3.5). In addition, a careful selection in the number of frequencies is also necessary to avoid erratic and futile data. The frequencies should be equally distributed and that all responses are captured. Typically, 10 data points per decade of frequency, in a logarithmic distribution, is used.

Table 3.5 The estimated duration of the frequency scan computed by commercial software, NOVA 1.10.3.

Frequency range	No of frequencies (10 points/decade)	Estimated duration	Integration time[9]
10,000Hz to 1Hz	40	3m	1.25s
10,000Hz to 0.1Hz	50	6m	1.25s
10,000Hz to 0.01Hz	60	19m	1.25s
10,000Hz to 0.001Hz	70	2h44m	1.25s
10,000Hz to 0.0001Hz	80	26h47m	1.25s
10,000Hz to 0.00001Hz	90	267h32m	1.25s

3.3.1.3.2 Signal perturbation amplitude

The linearity of an electrochemical system is very much dependent on the applied potential. In order to fulfil the linearity requirement for a valid EIS data, the applied ac perturbation signal has to be small enough not to disturb the system from its steady state. This amplitude depends upon the system under investigation. Usually there is a need for a compromise between minimising nonlinearity, which exists in most electrochemical systems, with the level of noise that accompanies such a low signal amplitude. Although the amplitude

[9] The integration time is the time during which the impedance response of the cell is recorded for data analysis. The duration of the test increases when the integration time increases, but signal to noise ratio is improved (Autolab, n.d.). The 1.25s integration time used in this thesis is a compromise between the test duration and the signal to noise ratio.

should be small to ensure, at least, a quasi-linearity, it needs to be adequately large to have a measurable response. The typical signal amplitude in SC testing is between 5 to 10mV.

3.3.1.4 Data presentation and modeling

The data obtained from EIS measurements are represented in Bode plot and Nyquist plot; the latter is the most widely used, although the Bode plot contains explicit frequency information. In Bode plot, two plots can be obtained—the modulus $|Z(j\omega)|$ and the phase are plotted versus the frequency in logarithmic scale. Nyquist plot is represented by negative imaginary part of the impedance, $-ImZ(j\omega)$ vs. real part of the impedance, $ReZ(j\omega)$. The beginning of the impedance measurements are made in the high frequency range and then towards the low frequency range; this is why the sign convention of the imaginary part axis is in the negative for an ease of plotting the impedance response on the first quadrant.

The interpretation of the impedance measurements is aided by fitting discrete electrical components, like resistors and capacitors, to the impedance spectrum. The Nyquist plot is in fact has very characteristic shapes for some processes, for instance, diffusion process to the $\pi/4$ slope of impedance line. The direct relation of the impedance spectrum to the electrical component has certainly made this method a preference in many fields for, but certainly not limited to, studying new material. Caution should be exercised when assigning electrical component to the impedance spectrum. It is always appealing to select and fit a component in an ad hoc way, especially for a system that has yet to establish in-depth knowledge. The fact that EIS is generally a transfer function

method, meaning that there exists countless circuit combinations that can represent any given impedance. Therefore, knowledge of the system under study is the first step to minimise ambiguity in the fitting process. The most common impedance responses to electrical components are compiled in the following sub-subsection.

3.3.1.4.1 The impedance response of some common circuit component

3.3.1.4.1.1 Resistor

The relationship between current $I(t)$ and voltage $V(t)$ for a resistor is

$$V(t) = RI(t) \tag{3.5}$$

where R is the resistance.

Frequency domain of Eq. (3.5) for a sinusoidal voltage is

$$V(j\omega) = RI(j\omega) \tag{3.6}$$

Therefore, the impedance of a resistor is given by

$$Z = \frac{V(j\omega)}{I(j\omega)} = R \tag{3.7}$$

Nyquist plot for the resistor is illustrated in Fig. 3.17.

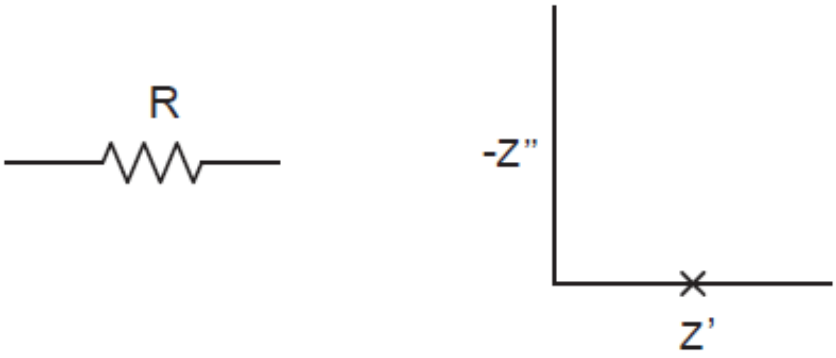

Fig. 3.17 Nyquist plot of a resistor.

3.3.1.4.1.2 Capacitor

The current flowing through a capacitor, C is given by

$$I(t) = C\frac{dV(t)}{dt} \tag{3.8}$$

The frequency domain of Eq. (3.8) to a sinusoidal voltage for a capacitor is

$$I(j\omega) = j\omega CV(j\omega) \tag{3.9}$$

The impedance for the capacitor is therefore

$$Z = \frac{V(j\omega)}{I(j\omega)} = \frac{1}{j\omega C} \tag{3.10}$$

And is illustrated in Nyquist plot in Fig. 3.18.

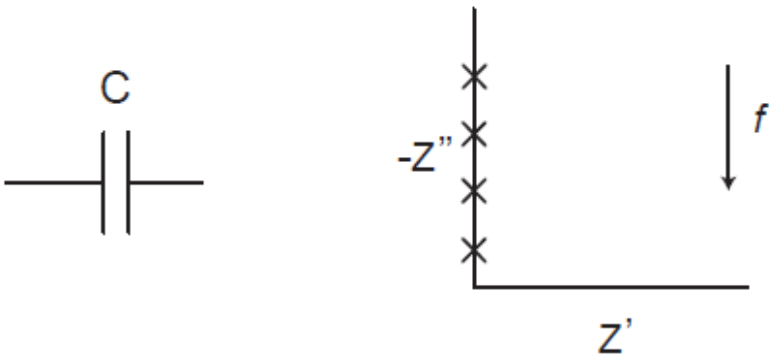

Fig. 3.18 Nyquist plot of a capacitor.

3.3.1.4.1.3 Inductor

The voltage across an inductor, L is

$$V(t) = L\,\frac{dI(t)}{dt} \tag{3.11}$$

In frequency domain,

$$V(j\omega) = j\omega LI \tag{3.12}$$

The impedance for the inductor is

$$Z = \frac{V(j\omega)}{I(j\omega)} = j\omega L \tag{3.13}$$

Nyquist plot for the inductor is illustrated in Fig. 3.19.

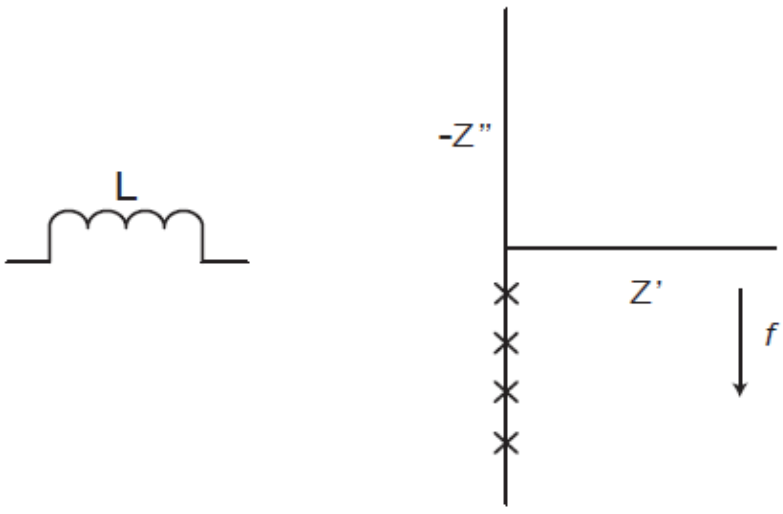

Fig. 3.19 Nyquist plot of an inductor.

3.3.1.4.1.4 Resistor and capacitor in series

The total impedance of a resistor and capacitor in series is

$$Z = R + \frac{1}{j\omega C} \tag{3.14}$$

And in Nyquist plot (Fig. 3.20),

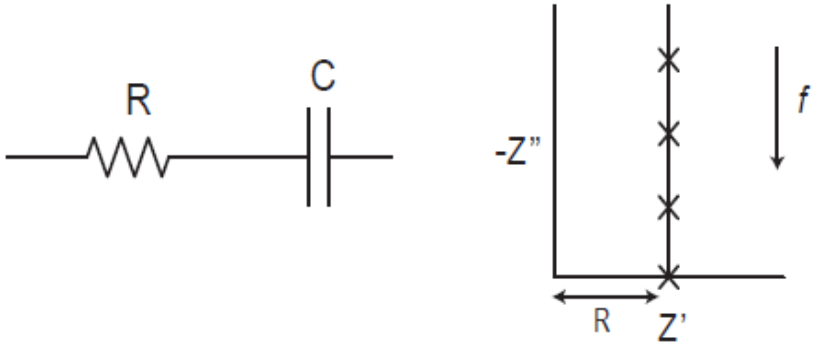

Fig. 3.20 Nyquist plot of a resistor and a capacitor in series. The impedance line is shifted by the amount of R.

3.3.1.4.1.5 Inductor, resistor and capacitor in series

The total impedance of an inductor, resistor and capacitor in series is

$$Z = j\omega L + R + \frac{1}{j\omega C} \tag{3.15}$$

and the Nyquist plot of the circuit is illustrated in Fig. 3.21.

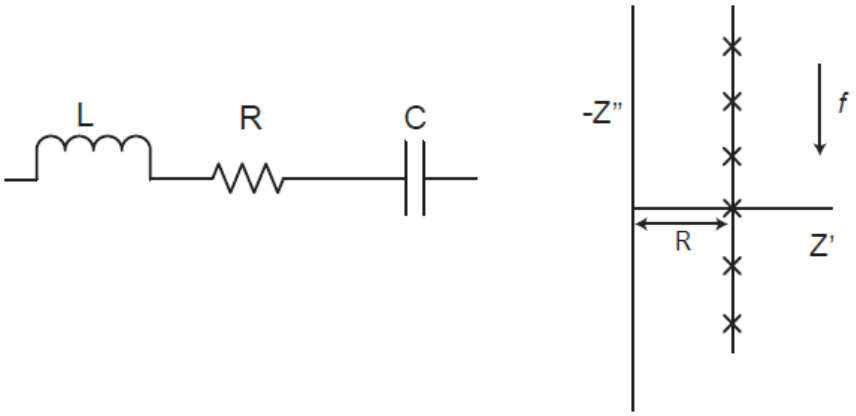

Fig. 3.21 Nyquist plot of an inductor, a resistor and a capacitor in series.

3.3.1.4.1.6 Capacitor and resistor in parallel

The total impedance of a parallel arrangement of capacitor and resistor is

$$Z = \frac{R}{1+j\omega RC} \tag{3.16}$$

and the Nyquist plot of the arrangement is illustrated in Fig. 3.22.

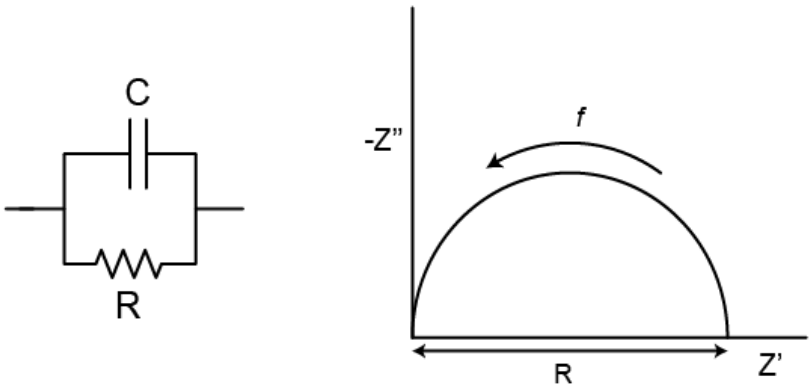

Fig. 3.22 Nyquist plot of a parallel arrangement of resistor and capacitor.

3.3.1.4.1.7 Resistor in series with a parallel combination of capacitor (or constant phase element) and resistor

When a series resistor is added to the arrangement, the impedance response in the Nyquist plot is shifted by the amount of series *R* (Fig. 3.23).

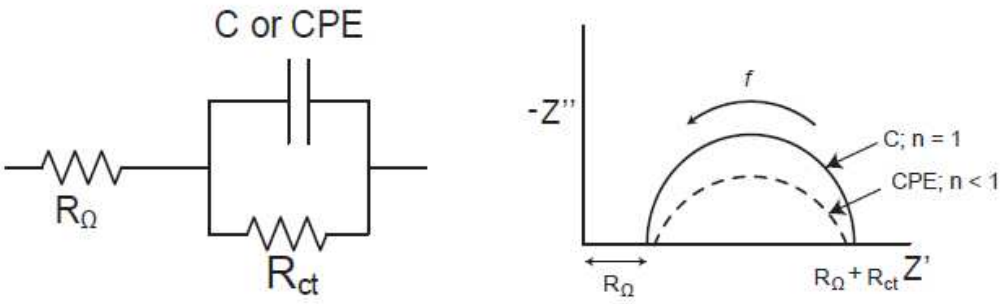

Fig. 3.23 Nyquist plot of resistor in series with a parallel arrangement of resistor and capacitor. The semicircle is depressed if the capacitor is replaced with CPE.

3.3.1.4.1.8 Resistor in series with parallel combinations of capacitors and resistors

When two parallel connections of resistor and capacitor are connected to a series resistor, the circuit arrangement produces two semicircles in the Nyquist plot (Fig. 3.24).

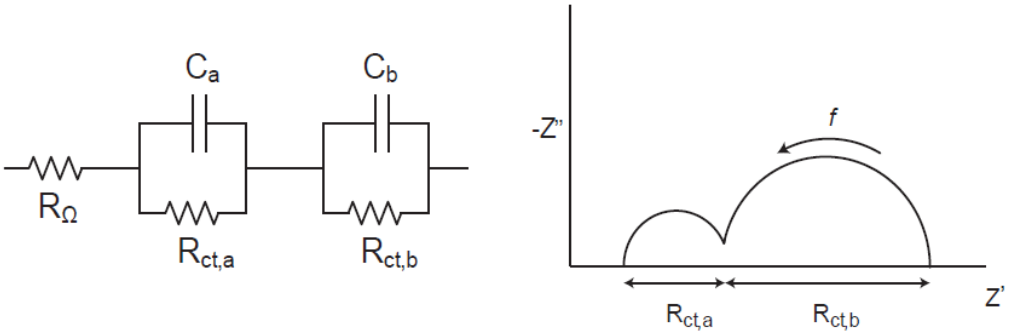

Fig. 3.24 Nyquist plot of two parallel arrangement of resistor and capacitor shows two semicircles.

3.3.1.4.2 Electrochemical components

Although it has become customary to use passive electrical components to interpret impedance data, many electrochemical systems in reality are more complex. The interpretation of the impedance data requires for an enhanced model to better accord for the complex behaviour that cannot be accurately modelled by ordinary circuit elements which generally involve ideal properties. Electrochemical systems often exhibit distributed response that calls for distributed elements to better fit the impedance data (Raistrick et al., 2005). These distributed elements are explained next.

3.3.1.4.2.1 Constant Phase Element (CPE)

Constant Phase Element (CPE) is an element that is used to model the inhomogeneity that cannot be accounted by an ideal capacitor. Sometimes, the conventional double layer capacitor is replaced by a CPE in a porous electrode system. The imperfections on the electrode causes the double layer capacitance to be distributed along the length of the pores in the porous electrode (Yuan et al., 2007; Fletcher et al., 2014). CPE impedance is given by,

$$Z_{CPE} = \frac{1}{Y_0(j\omega)^n};\ 0 < n < 1 \tag{3.17}$$

where Y_0 is the CPE magnitude and n is the fractional exponent. The unit for Y_0 is $S \cdot s^n$ or $Farad\ (s^{1-n})^{-1}$ where n is the exponent in Eq. (3.17).

When $n = 1$, Eq. (3.17) is equal to the equation for the impedance of a capacitor,

$$Z_{CPE} = \frac{1}{Y_0(j\omega)^1} = \frac{1}{j\omega C} = Z_C \tag{3.18}$$

From the equations above, CPE magnitude corresponds to its effective capacitance at $n = 1$. Therefore, when n is close to 1, the CPE resembles a capacitor, but the phase angle is not 90°.

Correspondingly, Eq. (3.17) can be reduced to represent pure resistance for $n = 0$ and pure inductance for $n = -1$. For when $n = 0.5$, Eq. (3.17) represents an infinite Warburg impedance, which is discussed next. The impedance of a CPE is almost a straight line when plotted in the Nyquist plot (see Fig. 3.25).

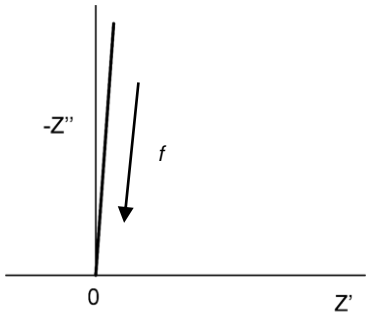

Fig. 3.25 Nyquist plot of constant phase element. The line is almost vertical.

3.3.1.4.2.2 Semi-infinite Warburg diffusion

Diffusion at the electrode/electrolyte interface leads to a distributed circuit element. Several expressions exist to describe diffusion impedance which are based on whether the system exhibits infinite diffusion layer, semi-infinite diffusion or finite length diffusion (Bisquert et al., 1999; Raistrick et al., 2005). Warburg element is used to model semi-infinite diffusion in electrochemical system.

For a semi-infinite diffusion layer, the impedance of the Warburg element is (Bisquert, 2002),

$$Z_W = \frac{1}{Y_0\sqrt{j\omega}} \tag{3.19}$$

When plotted in the Nyquist plot, Z_W shows a straight line with a slope of $-\pi/4$ (Fig. 3.26a).

3.3.1.4.2.3 Bounded diffusion (finite-length diffusion with reflective boundary)

Another type of diffusion is the bounded diffusion that is represented by T. This type of diffusion is typical for thin samples with reflective boundary conditions (Bisquert et al., 1999). At low frequencies, the impedance of a bounded diffusion in the Nyquist plot terminates in a vertical line (Fig. 3.26b). This type of diffusion is normally observed, for example, in battery materials, where the active material or electrolyte layer has a limited thickness (Barsoukov, 2005).

The impedance of T is given by,

$$Z_T = \frac{1}{Y_0\sqrt{j\omega}}\coth\left(B\sqrt{j\omega}\right) \tag{3.20}$$

$$B = \frac{\delta}{\sqrt{D}} \tag{3.21}$$

B is the time ($s^{1/2}$) it takes for a reactant to diffuse from one side of the layer to the other, D is diffusion coefficient and δ is the thickness of the thin layer.

3.3.1.4.2.4 Finite-length diffusion layer (transmissive boundary)

For diffusion related to the transmissive boundary, often observed in rotating disk electrodes (Lasia, 1999; Jossen, 2006), the diffusion impedance is described by

$$Z_O = \frac{1}{Y_0\sqrt{j\omega}}\tanh(B\sqrt{j\omega}) \tag{3.22}$$

The impedance of Z_O in the Nyquist plot (Fig. 3.26c) has a straight line at high frequencies with a slope of $-\frac{\pi}{4}$, characteristic of a Warburg, but decreases and approaching resistive behaviour at low frequencies due to the limited diffusion length and transmissive boundary. At low frequencies, the impedance response is equivalent to a resistor and a capacitor in parallel.

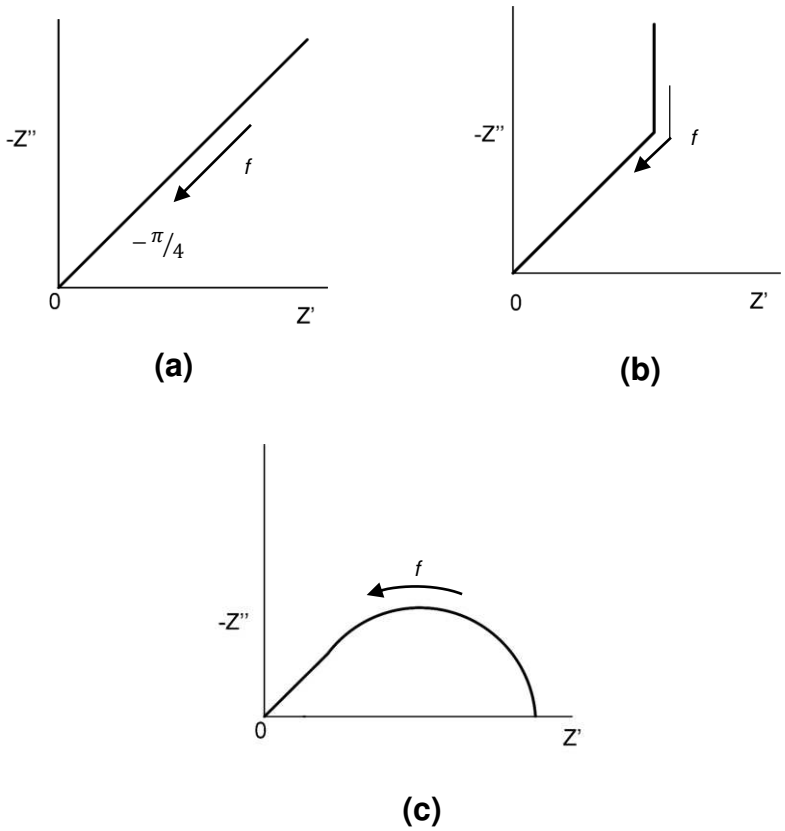

Fig. 3.26 Nyquist plot of diffusion elements: (a) semi-infinite diffusion, (b) bounded diffusion with reflective boundary conditions, (c) finite-length diffusion with transmissive boundary.

3.3.2 Cyclic voltammetry (CV)

3.3.2.1 Introduction

While EIS is a powerful diagnostic testing method for studying ongoing electrochemical processes in SC, a full quantitative analysis with EIS can be difficult. It is compelling to use EIS as a stand-alone method, considering the long list of advantages it has to offer. This is concerning to its complex data analysis. Because of the inherent ambiguity in the process of fitting equivalent circuit to interpret impedance response, the process can be demanding and technically exacting. For example, when studying new area or material, the

investigator has to rely on his scientific judgement and countless resources before coming to a conclusive decision. Therefore, supporting EIS measurement with other electrochemical technique is recommended and often times, is required.

Cyclic voltammetry (CV) can play a complementary role to EIS in the analysis of electrochemical mechanisms. For instance, if a phenomenon appears in the impedance response of a cell that previously does not exist, then CV can be used to further confirm the observation. CV curve provides information related to electron transfer kinetics and transport phenomena at electrode/electrolyte interface (Wang and Pilon, 2012). An examination of the voltammetric response can elucidate whether the changes in EIS shape is an epitome of an electron transfer phenomena.

3.3.2.2 The working principle of CV

Cyclic voltammetry measurement is carried out by sweeping linearly a potential at a working electrode. The voltage is swept repetitively between two potential values at a fixed scan rate. The two potentials are given as (Wang and Pilon, 2012),

$$\psi_s(t) = \begin{cases} \psi_{min} + vt & \text{for} \quad 2(n-1)t_0 \le t < (2n-1)t_0 \quad \text{(a)} \\ \psi_{max} - v[t-(2n-1)t_0] & \text{for} \quad 2(n-1)t_0 \le t < 2nt_0 \quad \text{(b)} \end{cases} \tag{3.23}$$

where v is the scan rate in V/s, n=(1,2,3,…) is the cycle number, and $t_0 = (\psi_{max} - \psi_{min})/v$ is half the cycle period.

These two potential values are usually restricted by the minimum and maximum potential limits of the solvent and the electrolyte; therefore, CV is also used to determine the voltage limits (Ratajczak et al., 2014; Mahon et al., 2000). When the working electrode potential reaches the maximum limit, the scan is reversed and run in the opposite direction, until it reaches the minimum set potential. Hence, calculating $\Delta\psi = \psi_{max} - \psi_{min}$ gives the 'potential window' of an electrode, which should not include any irreversible faradic reaction.

The resulting current from the applied potential is plotted in a current-potential curve. Analysis of the current response can give information about the kinetics of electron transfer at the electrode-electrolyte interface, redox peak (Wang et al., 2012), as well as other electrochemical reactions. A standard practice in cyclic voltammetry measurement is to perform several scans until the system reaches equilibrium; thus, the measurement technique is also useful to evaluate the cyclability of an electrochemical system, particularly SCs. The charge (Q) can be calculated by integrating the current response of the CV waveshape with time,

$$Q = \int i \, dt \tag{3.24}$$

3.3.2.3 The influence of scan rate

Scan rate is the rate at which the potential is ramped linearly versus time. In cyclic voltammetry, the potential ramp is inverted at a chosen potential. The resulting current-potential response generally has a waveshape as illustrated in Fig. 3.27 (right). The selection of scan rate has an effect on the current-potential waveshape. A slow scan rate allows slow processes to occur. As the scan rates

increase, the waveshape becomes more and more of a leaf-shaped (Fletcher et al., 2014), as shown in Fig. 3.28. This happens when the scan rate is faster than the electrochemical reactions; the slow reactions on the electrode surface cannot keep up with the applied voltage. Therefore, a correct scan rate is important especially for electrochemical cells where the chemical reactions are voltage-driven.

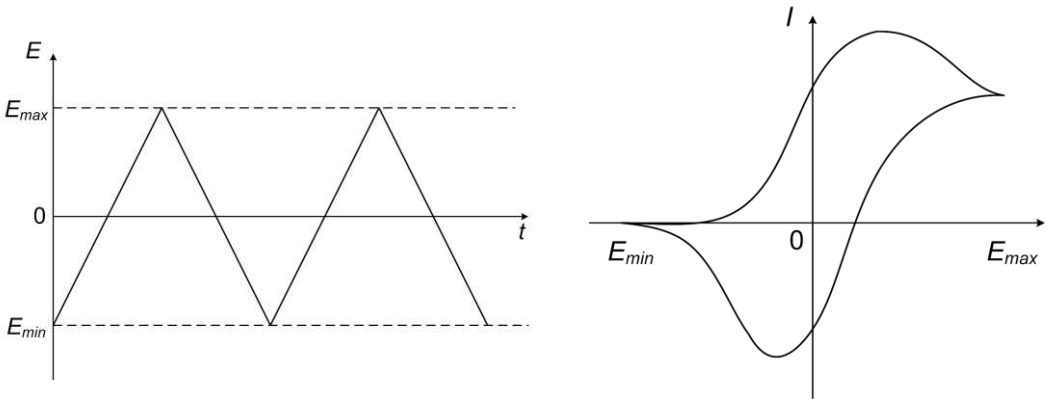

Fig. 3.27 Cyclic voltammetry waveform, from a lower potential E_{min} to an upper potential E_{max}, then finally back to E_{min} (left) and the resulting current-potential waveshape (right).

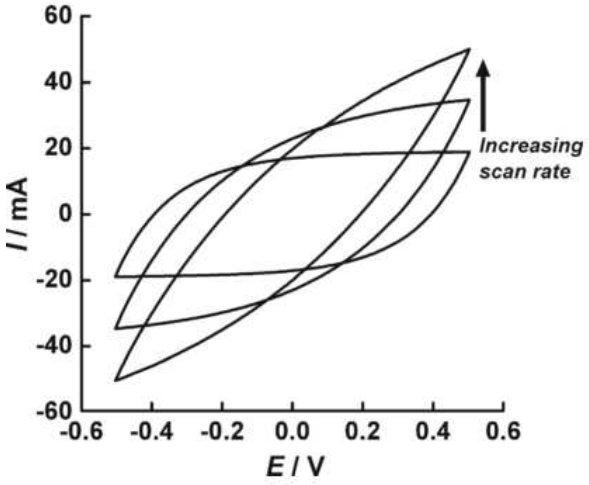

Fig. 3.28 Increasing scan rate shows the cyclic voltammograms become increasingly leaf-shape (Fletcher et al., 2014).

3.3.3 Constant current test

Perhaps, the most widely used technique in the industry, is the constant current (CC) test. One of the reasons that contributes to the popularity of this technique is that, it can be applied in most laboratories and it can be extended to be suited for industrial scale. Constant current test has its origin in battery testing (Miller and Burke, 1994).

While there are many variations on how this test is conducted, refer to (IEC, 2006a; Maxwell, 2009a; FreedomCAR, 2004; Miller and Burke, 1994), depending on the applications and requirements, this test in general is carried out by applying a constant current to charge or discharge the cell and then measuring the resulting voltage. CC test allows the determination of the rated capacitance and the ESR. Results of this test are also used for modelling the terminal behaviour at various charge discharge conditions; these models are listed in reference (Devillers et al., 2014; Tironi and Musolino, 2009; Faranda, 2010; Zhu et al., 2007; Zubieta and Bonert, 2000; Islam et al., 2010; Ban et al., 2013; Lajnef, Vinassa, Briat, Azzopardi, et al., 2007; Belhachemi et al., 2000; Zhang and Yang, 2011).

The currents used in this testing are selected based on the device capability and also based on the applications. For example, in (Miller and Burke, 1994), the current is selected in the order that enable charge and discharge times between 2 to 100 seconds. In (FreedomCAR, 2004) a 5C constant-current rate which corresponds to discharging the device from V_{max} to V_{min} within 12 minutes is used. The 5C rate established is suitable for HEV applications. Additionally, the discharge current set in (IEC, 2006a) is in accordance with 30

minutes charge time. Manufacturers of SCs, however, have a different notion on the amount of current used—this is discussed in detail in Chapter 4.

Despite the differences above, the calculation for capacitance and resistance are pretty standard. The capacitance is measured by the slope of the discharge curve and the resistance is measured by the voltage drop, from the device terminal voltage during open circuit to the beginning of discharge, commonly known as the 'iR drop'.

The capacitance to the constant discharge current equals to,

$$C = \frac{I_{discharge}}{slope\ of\ discharge\ V(t) curve} \tag{3.25}$$

The ESR is given by,

$$R = \frac{\Delta U}{I} \tag{3.26}$$

Where ΔU is the drop voltage (V) and I is the discharge current (A).

3.4 Summary

Having understood that ageing and performance deterioration in SCs certainly is a long-term process, the methodology was developed in regards to the research objectives which were:

1. To investigate the principle effect of single environmental parameters and the effect of combing these parameters on SC electric performance.
2. To model SC electrical performance in electrical equivalent circuits which covers all the important dynamics in the SC behavior, and at the same time is also able to model the degradation process in aged SCs.

3. To relate the ageing mechanism and the changes in SC due to ageing to the equivalent circuit in order to understand how the ageing mechanism contributes to the failure in SCs.
4. To identify and evaluate the main changing parameters of the electrical equivalent circuit during the ageing process for predicting the current-voltage characteristics after a long operation and also for the state of health monitoring.

Given the many phases of the research, the first step was to establish the requirement and criteria that makes for a good SC from available testing standards and procedures and literatures. Then, test boundary was drawn to only include environmental-caused and operational-caused failures.

SC ageing was understood to be caused by many factors and analysing the failure mechanisms can be tricky. This calls for a search on which testing method most suitable to identify and distinguish these mechanisms which often overlaps with one another. It was later understood the need for a model that not only able to emulate the terminal response, but, it had to have the ability to adapt with the changing conditions in SCs as they went through ageing.

This research was primarily based on performance changing analysis methodology and monitoring framework. The changes in SC performance were tracked and recorded periodically to identify the main changing parameters, hence the ageing mechanism that contributes to this change. The collected data were useful for the development of an ageing model for the state of health monitoring and prediction.

CHAPTER 4

A REVIEW OF COMMON MEASUREMENT USED TO DETERMINE SUPERCAPACITOR CHARACTERISTICS

"You think because you understand 'one' you must also understand 'two', because one and one make two. But you must also understand 'and'."

—Jalal ad-Din Muhammad Rumi

4 Introduction

While measurement methods for packaged SCs are well developed, different methods are currently being used in the industry and in laboratories worldwide which result in widely varying results being reported on papers. This also raises uncertainties in interpreting the data on literature and on manufacturer's datasheet for the devices (Burke and Miller, 2010).

Electrochemical methods like electrochemical impedance spectroscopy (EIS) and cyclic voltammetry (CV) are the two most often used in research laboratories, whereas transient technique like constant current test is more popular in the industry. The results of measured capacitance, in particular, is dependent on the method. Rafik et al. (2007) has demonstrated the dependency of capacitance on voltage (Rafik et al., 2007). The test done in the Sahz-Nottingham NANO Super-capacitor Pilot Plant further confirmed their finding, in which Fig. 4.1 shows that the capacitance of BCAP0025 supercapacitor from Maxwell Technologies varies with the state of charge of the supercapacitor.

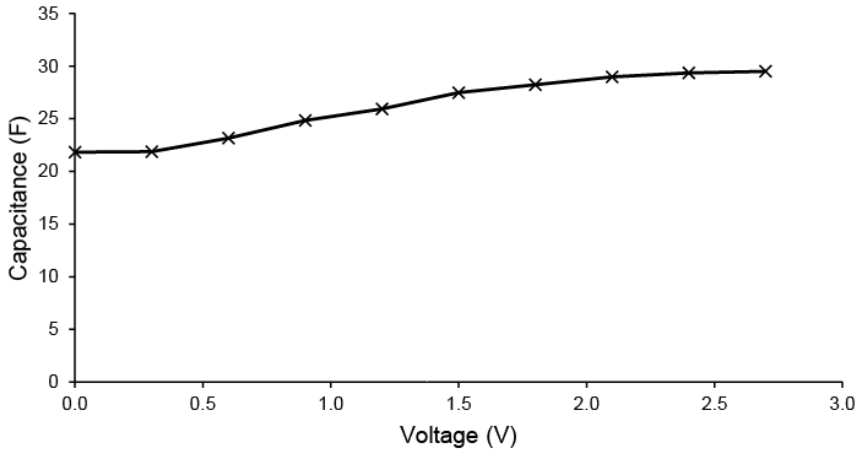

Fig. 4.1 Capacitance of BCAP0025 at various state of charge of the supercapacitor measured with EIS at 20℃, 10mHz.

Moreover, Kurzweil et al. (2006) has written that, "capacitance determined by [constant current test] strongly depends on the discharge current and the voltage (state of charge) of the capacitor"[10]. The scan rate used in CV

[10] Kurzweil, P. and Chwistek, M. (2006) 'Electrochemical and Spectroscopic Studies on Rated Capacitance and Aging Mechanisms of Supercapacitors', in 2nd European Symposium on Super Capacitors & Applications (ESSCAP). Lausanne, pp.1–23.

measurement, which is essentially the rate at which the voltage change in 1 second, can affect the measured capacitance (is discussed in Section 4.3.2). Likewise, the current used in the constant current test can affect the duration of charging of the SC to the rated voltage, hence influencing the measured capacitance as the charge Q is related to current by $Q = it$, where i is the current (A) and t is time in seconds, and the capacitance is related to Q by $C = Q/V$, where V is the voltage (V). This is study in detail in Section 4.3.1.

As has been pointed out by Burke and Miller (2010), the uncertainties in the interpretation of the reported data arises due to the disparity of charging algorithm and also on the voltage used in measurements. Therefore, the intention for this chapter is not to seek which method gives the accurate values, but rather to study the effect of each measurement method (constant current test, CV and EIS) on the two most quoted values for SCs, i.e. capacitance and ESR, so that the findings from this study will aid in determining the most suitable measurement methods and settings used in subsequent chapters.

4.1 Standard Measurement Methods for SC Electrical Characteristics

The most referred test standard for testing SCs is the IEC 62391. IEC 62391 describes two methods to measure capacitance: (1) constant current discharge method and (2) constant resistance charging method. In addition, for measuring resistance IEC 62391 recommends the following: (1) AC resistance method and (2) DC resistance method.

In the constant current discharge method, the SC is charged and discharged with a constant current. The charging and discharging cycle is separated by a voltage holding period for 30 minutes. Then, the capacitance is measured during the discharging cycle. The discharge current has to meet the conditions set by IEC 62391 based on the SC application. The discharge conditions are given in Table 4.1.

Meanwhile in the constant resistance charging method, the capacitance is calculated by measuring the time constant for the SC to reach its rated voltage in which the capacitance $C = \tau/R$, where τ is the charging time to reach 63.2% of the rated voltage and R is the series resistance connected to the SC. The constant resistance charging method is not as widely used as the constant current discharge method. Perhaps this is due to the measurement setup requires finding the correct load to be connected to the SC so that the time constant is within 60s to 120s. In this case, the constant current discharge method is more practical than the constant resistance charging method especially when the measurement involves many SC samples of various capacitances and voltages. Therefore, the constant resistance charging method is not discussed in this chapter.

Table 4.1 IEC 62391 discharge conditions for supercapacitors (IEC, 2006a)**.**

Classification	**Class 1**	**Class 2**	**Class 3**	**Class 4**
Application	Memory backup	Energy storage	Power	Instantaneous power
Charge time	30 min	30 min	30 min	30 min
I (mA)	$1 \times C$	$0.4 \times CU_R$	$4 \times CU_R$	$40 \times CU_R$
$\boldsymbol{U_1}$	The value to be 80% of the charging voltage $0.8 \times U_R$			
$\boldsymbol{U_2}$	The value to be 40% of the charging voltage $0.4 \times U_R$			

Note: C is the rated capacitance in F (Farad) and $U_R$is the rated voltage in V (Volt).

To measure resistance, that is the ESR of the SC, the AC resistance method recommends the frequency of the measuring voltage to be 1kHz and the ac current should be from 1mA to 10mA. The ESR is then calculated by the following equation (IEC, 2006a):

$$R_a = \frac{U}{I} \tag{4.1}$$

where R_a is the ac internal resistance (Ω), U is the effective value of ac voltage (V_{rms}), I is the effective value of ac current (I_{rms}).

In the DC resistance method, the method used is similar to the constant current discharge method for measuring capacitance, but with a different discharge current, depending on the class of the SCs. The discharge current is specified in Table 4.2. The ESR is measured from the voltage drop upon the start of the discharging procedure according to Eq. (3.26).

Table 4.2 Discharge current in the DC resistance method (IEC, 2006a)

Classification	Class 1	Class 2	Class 3	Class 4
I (mA)	$10 \times C$	$4 \times CU_R$	$40 \times CU_R$	$400 \times CU_R$

Note: C is the rated capacitance in F (Farad) and $U_R$is the rated voltage in V (Volt).

Although IEC 62391 provides guidelines on how the measurement should be conducted and also the amount of current that should be used to discharge SCs, SCs manufacturers have their own discharge current condition. Moreover, manufacturer like Maxwell Technologies has published its own test procedure to suit its production line environment (Maxwell, 2009a). In fact, a survey on 15 SC manufacturers all over the world shows that the discharge current used by these manufacturers varies from 1mA/F to 75mA/F (see Table 4.3). Despite the variation, the discharge current is chosen not to affect the lifetime of SCs.

Table 4.3 Discharge current used by supercapacitor manufacturers.

Manufacturer (Origin)	**Commercial Name**	**V** (V)	**C** (F)	**T** (℃)	**Type**	**Parts/ Test Current**
NEC TOKIN (Japan)	Super capacitor	2.7 to 12V	0.01 – 200F	-2.5 to 70℃	Bulk, taping, winded	HV series/ 1mA/F
Panasonic (Japan)	Gold capacitor	2.3 to 5.5V	0.022 to 70F	-10 to 70℃	Coin type, Cylin-drical	HW series/1 mA/F
ELNA (Japan)	DYNACAP, POWERCAP	2.5 to 6.3V	0.047 to 1500F	-25 to 85℃	Cylin-drical cell	DZ series/ 1mA/F
MAXWELL (USA)	BOOSTCAP Ultracapacitor	2.7-160 V	1 to 3400F	-40 to 85℃	Cylin-drical cell, module	HC series/ 75mA/F
VINATech (South Korea)	Hy-Cap	2.5-6V	0.5 to 500F	-40 to 70℃	Cylin-drical cell, module	Single cell series/ 1mA/F

Note: **V** is the rated voltage, **C** is the rated capacitance and **T** is the operating temperature. All data are obtained from manufacturers' product datasheets and technical documents, available on their respective websites.

Table 4.3 Discharge current used by supercapacitor manufacturers. (continued)

Manufacturer (Origin)	**Commercial Name**	**V** (V)	**C** (F)	**T** (℃)	**Type**	**Parts/ Test Current**
NICHICON (Japan)	EVerCAP	2.5-2.7V	0.47 to 6000F	-40 to 70℃	Cylin-drical cell, stacked	UK series/ 0.01A
NESSCAP (South Korea)	NESSCAP EDLC	2.3 to 2.7V	3 to 3000F	-25 to 65℃	Cylin-drical cell, primatic	10mA/F
Illinois capacitor (USA)	Super capacitor	2.3 to 5.5V	1 to 3800F	-25 to 70℃	Cylin-drical cell	DCN series/ 10mA/F
Korchip (South Korea)	STARCAP	2.3 to 7.5V	0.047 to 120F	-40 to 70℃	Coin type, cylin-drical, stacked	DR series/ N/A

Note: **V** is the rated voltage, **C** is the rated capacitance and **T** is the operating temperature. All data are obtained from manufacturers' product datasheets and technical documents, available on their respective websites.

Table 4.3 Discharge current used by supercapacitor manufacturers. (continued)

Manufacturer (Origin)	**Commercial Name**	**V** (V)	**C** (F)	**T** (℃)	**Type**	**Parts/ Test Current**
Vishay (USA)	196 DLC	5.5 to 6.3V	0.047 to 1F	-25 to 85℃	Cylin-drical	(0.047 to 0.33F)/ 0.1mA (0.47 to 1F)/ 1mA
Taiyo Yuden (Japan)	PAS capacitor	2.3 to 3V	0.011 to 50F	-25 to 70℃	Cylin-drical	(1 – 22F)/ 1A 56F/ 5A 4F/0.5A (9 & 20F)/ 1A 50F/ 2A

Note: **V** is the rated voltage, **C** is the rated capacitance and **T** is the operating temperature. All data are obtained from manufacturers' product datasheets and technical documents, available on their respective websites.

Table 4.3 Discharge current used by supercapacitor manufacturers. (continued)

Manufacturer (Origin)	**Commercial Name**	**V** (V)	**C** (F)	**T** (℃)	**Type**	**Parts/ Test Current**
Cooper Bussman (USA)	PowerStor	2.5-16V	0.1-600F	-40 to 70℃	Coin, cylin-drical, module	N/A
AVX (USA)	BESTCAP	3.6V to 15V	6.8mF to 1F	-20 to 70℃	Planar	BZ series/4 mA
Tecate (USA)	Powerburst	2.3 to 2.7V	0.33 to 400F	-40 to 85℃	Cylin-drical	TPL series/ N/A
CAP-XX (Australia)	CAP-XX Supercapa-citor	2.3 to 5.5V	80mF to 2400mF	-40 to 85℃	Pris-matic	100mA

Note: **V** is the rated voltage, **C** is the rated capacitance and **T** is the operating temperature. All data are obtained from manufacturers' product datasheets and technical documents, available on their respective websites.

Besides the variation of the discharge current, another interesting finding is on the differences in the voltage holding period between charging and discharging cycle. IEC 62391 recommends 30 minutes voltage holding, however, a much shorter duration is used in the industry; manufacturers like NESSCAP (South Korea) and Illinois capacitor (USA) hold the voltage for 5 minutes before applying discharge current on their SCs during characterisation tests (NESSCAP, 2014; Ilinois capacitor, 2012). Meanwhile, the laboratory at UC Davis practices 60s voltage hold before the initiation of the discharge condition (Burke and Miller, 2010). In contrast, Maxwell (USA), in its 6 step process for measuring capacitance and ESR, advocates the use of a resting period between charge and discharge, that is, the SC is let open circuit for a predefined time (Maxwell, 2009a). At the same time, a direct charge and discharge cycle is also practised in laboratories, as it can be found in reference (Ban et al., 2013; Cazorla-Amorós et al., 2010; Dandeville et al., 2011; Masarapu et al., 2009). Perhaps, it is more appropriate to call this method the galvanostatic cycling.

While the use of constant current test is popular in industry, EIS and CV are often used in laboratories to calculate capacitance and ESR. However, there is no standard procedure available for both methods. Capacitance, in particular, depends on scan rate and voltage range in CV measurements (Stoller and Ruoff, 2010). Likewise, capacitance also depends on the applied frequency in EIS measurement. In IEC 62391, EIS measurement method is given less emphasis, although it is recommended as an alternative to dc measurement methods particularly in a time-constrained situation.

With the number of uncertainties in SCs measurement methods, the following experimental procedure is designed to seek the appropriate test settings for the SC tested in this thesis and thus finding how results from these methods differ from one another.

4.2 Experimental

SC from Maxwell Technologies with rated voltage of 2.7V and rated capacitance of 25F were used. The SC was tested with constant current test, electrochemical impedance spectroscopy and cyclic voltammetry. The measurements were performed using AUTOLAB PGSTAT302N potentionstat/galvanostat, equipped with FRA2 module from Metrohm Autolab B.V. The SC was connected using a two-electrode connection.

4.2.1 Constant Current Test

Two methods of constant current (CC) test were compared: IEC 62391 and Maxwell 6 Step Process.

Fig. 4.2 shows the resulting voltage characteristic between SC terminals using the IEC 62391 constant current discharge method. The SC was charged to its rated voltage 2.7V using the constant current for Class 1 in Table 4.1, which gave the current value of 0.025A. When the rated voltage was reached, the SC charge was held at constant voltage of 2.7V for 30 minutes and then, a discharge current of 0.025A was applied to discharge the SC to 0V. To measure the ESR,

the same process was applied to the SC, but the discharge current was now increased to 0.25A, based on Class 1 in Table 4.2.

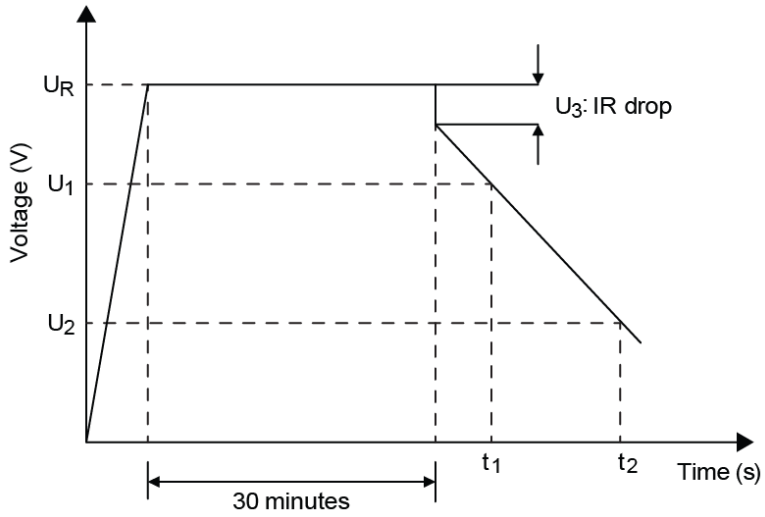

Fig. 4.2 Voltage characteristic between supercapacitor terminals in IEC 62391 constant current discharge method. Adapted from (IEC, 2006a).

Fig. 4.3 shows the current profile used in Maxwell 6 Step Process and the resulting voltage. Maxwell 6 Step Process specified that the value for the charge and discharge current has to meet the current rate of 75mA/F; this gave the test current of 2A. The process began with a rest period of 10s. Then using the specified test current, the SC was charged to 2.7V. After that, the SC was left at open circuit for 15s. Next, the SC was discharged to one-half its rated voltage (1.35V). The process was repeated twice. After the second cycle, the SC was left to rest again for 5s before being completely discharged to 0V.

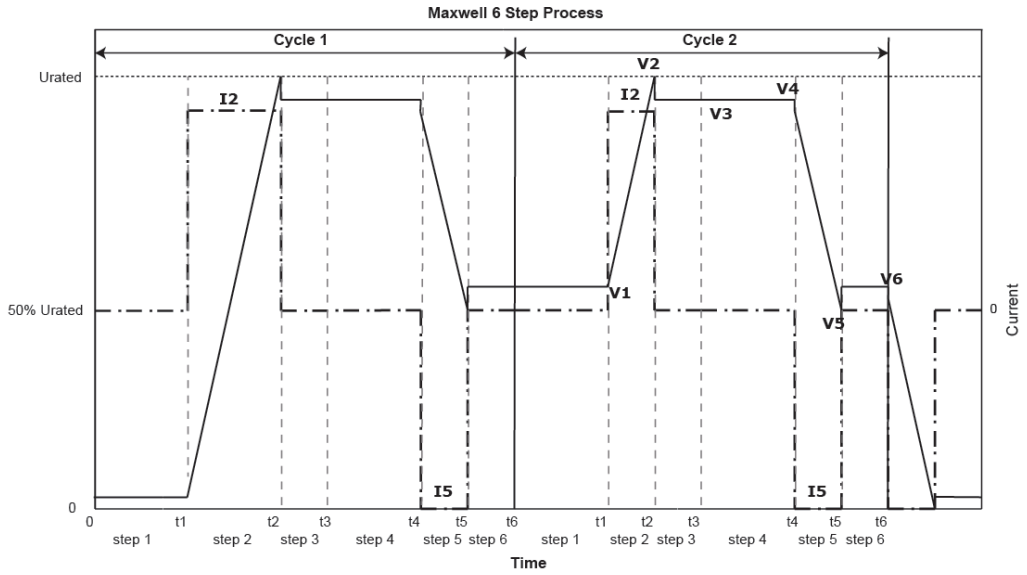

Fig. 4.3 The current profile used in Maxwell 6 Step Process and the voltage response at supercapacitor terminals. Figure adapted by author from (Maxwell, 2009a).

The effect of holding the voltage between charge and discharge on the capacitance and the ESR was also studied. Two voltage holding/SC open circuit periods were used: 30 minutes and 3 minutes. To ensure test repeatability and accurate comparison between the effect of holding the voltage and leaving the SC at open circuit between charge and discharge, the current was set to 2A (75mA/F). For the purpose of investigating the effect of different current level on capacitance and ESR, the experiment was repeated with 0.025A (1mA/F) discharge current, to calculate the capacitance, and 0.25A (10mA/F), to calculate the ESR. For reference, the direct charge and discharge method was also conducted on the SC. The result of this comparison is presented in Section 4.3.1.

4.2.2 Cyclic voltammetry

In cyclic voltammetry (CV) test, a linear voltage ramp was applied to the SC between 0V to 2.7V. The scan rate for the CV test was varied to study the influence of scan rate on the capacitance. The scan rates were increased by 5mV/s for each test, starting from 5mV/s until 50mV/s, and finally end at 100mV/s. For each test, the CV was repeated twice. The resulting current was measured and recorded on a current-potential curve. The result of the effect of scan rate on the measured capacitance is presented in Section 4.3.2.

4.2.3 Electrochemical impedance spectroscopy

IEC 62391 recommends EIS as a short cut method to reduce measuring time for capacitors with low internal resistance.

To investigate the influence of frequency on capacitance, an experiment to measure capacitance with two frequency ranges were carried out. The measurement was done in potentiostatic mode by sweeping frequencies over the range of 1kHz to 100mHz with 10 points per decade. The applied AC amplitude used was 10mV rms on a single sine wave. No bias voltage was applied. The current through the SC was measured and the impedance data was recorded. The experiment was then repeated for frequency range of 1kHz to 10mHz. Section 4.3.3 presents the result of varying the range of the applied frequency on the measured capacitance and ESR.

4.3 Results and Discussion

4.3.1 Constant Current Test

4.3.1.1 IEC 62391 and Maxwell 6 Step Process

The capacitance and ESR in IEC62391 can be determined from the voltage characteristic in Fig 4.2

From the constant current discharge curve, the capacitance (C) is

$$C = \frac{I \times (t_2 - t_1)}{U_1 - U_2} \tag{4.2}$$

With I is the discharge current (A) and $\frac{(t_2 - t_1)}{U_1 - U_2}$ is calculated from the slope of the discharge curve. U_1 is 80% of the charging voltage and U_2 is 40% of the charging voltage.

The ESR is determined from the voltage drop at the discharge curve based on the following expression:

$$R_d = \frac{\Delta U_3}{I} \tag{4.3}$$

Where ΔU_3 is the voltage drop obtained from the intersection of the auxiliary line extended from the straight part and the time base when the discharge starts. I is the constant discharging current.

On the other hand, Maxwell 6 Step Process used the discharge curve of the second cycle to calculate the capacitance and the ESR. The first cycle was not used because during this time, the SC was not fully activated, hence, the capacitance and the ESR values will be different from the second cycle.

Referring to Fig. 4.3, the capacitance and the ESR, according to Maxwell 6 Step Process, are:

$$C_{dch} = \frac{I_5 \times (t_5 - t_4)}{(V_5 - V_4)} \tag{4.4}$$

$$R_{dch} = \frac{(V_5 - V_6)}{I_5} \tag{4.5}$$

where I_5 is the discharge current (A) at the second cycle, V_4 is the discharge starting voltage (V), V_5 is the discharge end voltage (V), t_4 is the time from discharge at V_4 , t_5 is the time from discharge to reach V_5 and V_6 is the voltage (V) after a 5s open circuit.

Table 4.4 gives the results from both methods. IEC 62391 reports a higher capacitance and ESR than the results from Maxwell 6 Step Process. The higher capacitance from IEC 62391 may be due to the small discharge current used in IEC 62391. IEC 62391 used 0.025A discharge current whereas Maxwell 6 Step Process used 2A discharge current. Furthermore, IEC 62391 involved holding the voltage at constant for 30 minutes, while Maxwell 6 Step Process introduced open circuit period between charging and discharging the SC; the different treatment used by these two methods at the period between charge and discharge, may also contribute to the discrepancy in the results.

Table 4.4 Capacitance and ESR calculated using IEC 62391 and Maxwell 6 Step Process.

Method	Capacitance (F)	ESR (Ω)
IEC 62391	29.08188	0.0516
Maxwell 6 Step Process	28.39581	0.01145

4.3.1.2 The effect of voltage hold and open circuit and the duration of charging on supercapacitor

Table 4.5 shows the influence of voltage hold and open circuit duration on the capacitance. The result from voltage hold always gives a higher capacitance than the open circuit method, regardless the holding or the open circuit duration. In ascending order, the open circuit method gives the smallest capacitance, followed by the direct charge and discharge and the highest capacitance is obtained from the voltage hold method.

Table 4.5 The effects of voltage hold and open circuit rest duration on the capacitance.

	Capacitance (F)				
Duration	**30 mins**		**3 mins**		**Direct charge-discharge**
	Voltage hold	**Open circuit**	**Voltage hold**	**Open circuit**	
2A	27.8760	27.0073	28.2035	27.5429	27.3067
0.025A	29.0819	28.5815	-	-	28.6155

However, when the voltage holding and the open circuit period were reduced from 30 minutes to 3 minutes, the open circuit method produced a higher capacitance than the direct charge-discharge method. Moreover, it is also noted the effect of discharge current on the measured capacitance, whereby the 0.025A discharge current gave a higher capacitance than the 2A discharge current, both in the voltage hold method and the open circuit method.

The effect from voltage hold and open circuit rest duration on the resistance can be seen from the results tabulated in Table 4.6. The treatment performed between charge and discharge cycles did indeed show a significant effect on the ESR. The direct charge-discharge produced the highest ESR, followed by the result from the open circuit method and the voltage hold method, where both methods were conducted in 30 minutes duration, with 2A discharge current. When the discharge current was reduced to 0.25A, the trend no longer held; the open circuit method produced the highest ESR, followed by the voltage hold method and then the direct charge-discharge method.

Table 4.6 The effects of voltage hold and open circuit rest duration on the resistance.

	ESR (Ω)				
Duration	**30 mins**		**3 mins**		**Direct charge-discharge**
	Voltage hold	**Open circuit**	**Voltage hold**	**Open circuit**	
2A	0.04315	0.07383	0.042875	0.042575	0.15368
0.25A	0.0516	0.0536	0.044	0.044	0.0416

In the 3 minutes duration and with 2A as the discharge current, voltage hold method gave a higher ESR compared with the open circuit method, although the difference was minuscule. This observation contradicts the one in the 30 minutes test, in which the open circuit method produced a higher ESR. When the discharge current was reduced to 0.25A in the 3 minutes test, both the voltage hold and the open circuit methods gave the same ESR, and surprisingly, these values were higher than the direct charge-discharge method.

Comparing the results in both durations, the results are conflicting and tricky to conclude. This is because, it was initially thought that the direct charge-discharge method, regardless the level of discharge current, will produce the highest ESR. In spite of that, we can see there is a consistency in the results from the 30 minutes test, whereby whether it is a 2A discharge current or a 0.25A discharge current, the open circuit method will give a higher ESR than that of the voltage hold method.

The purpose of voltage hold is to compensate for the voltage drop due to charge redistribution effect. During the voltage hold period, charges will have more time to penetrate deeper inside the pore, thus will charge the entire surface (Kaus et al., 2010) (a detailed analysis of the charge redistribution in SCs can be found in (Kowal et al., 2011)). It is noteworthy that the difference in the results from the 30 minutes voltage hold and the 3 minutes voltage hold, where both tests used 2A discharge current, is so small that it is almost negligible. Furthermore, the 3 minutes voltage hold also yields nearly the same ESR with that of the 3 minutes open circuit method. This shows that 3 minutes is actually enough to let the charge to redistribute inside the pore and becomes uniformly distributed. Therefore, the continuous charging in the 3 minutes duration is just to stabilise the voltage.

Reducing the current to 0.25A, also increases the charging time which then gives an ample time for the charge to travel deep inside the porous electrodes and sufficiently charge the entire surface area. In the 3 minutes duration, the charge had already become uniformly distributed; this is the reason why the ESR values from the open circuit method is equal to the ESR from the

voltage hold method. Similarly, the ESR after 30 minutes of open circuit was almost the same as the ESR measured after 30 minutes of voltage hold. This shows that, the long time constant from the small current, did indeed give a sufficient time for the charge to penetrate inside the electrode and form a DL on the electrode surface, that even after letting the SC at open circuit for 30 minutes, no real voltage drop was observed. This shows that the long charging time from the small current used, has indeed stabilised the voltage in the SCs. Based on these findings, it shows that the 3 minutes open circuit duration is sufficient for the charges to rearrange themselves and charge the electrode surface. Similarly, if voltage hold method is employed to minimise the effect from voltage drop due to charge distribution, this duration is enough to hold the charge.

Interestingly, the ESR from the direct charge-discharge method (Table 4.6) showed almost a triple value when the discharge current was increased to 2A from 0.25A. Under this very short-period charging regime, the SC was more incompletely charged. During the charging stage, the charges will fill the pores located near the outer surface, that is the meso-pore, and then progressively charge the inner pores. When the charging is stopped, the charges begin to distribute themselves to fill the pores located deeper in, until a uniform voltage distribution is achieved (Kowal et al., 2011). But when the charging time is cut, the charges do not have sufficient time to charge the inner pores, which consists of a much smaller pore size. In the direct charge-discharge method, the measurement was taken immediately after discharge. This means that the charge had yet to redistribute to sufficiently charge the electrode surface and achieve a uniform voltage, thus voltage drop was higher. In contrast, the charge was given some time to penetrate and charge the electrode surface in open circuit method,

thus gives smaller ESR than that from the direct charge-discharge method. The redistribution of charges inside the porous electrode of the SC can be observed visually when the SC is left open circuit i.e. by monitoring the voltage decay. Therefore, voltage loss was high in the direct charge-discharge method and the open circuit method than that in the voltage hold method.

The high voltage loss not only gives a raise to ESR, it also affects the capacitance of the SC as it has been observed in the results earlier. It has been previously mentioned that the charging time affects the amount of voltage loss in SC. The charging time can be increased so as to increase the charge penetration, by introducing a voltage hold period between charge and discharge cycle, or by using a smaller current. This can be explained by the following analogy—SC can be thought of having many small capacitors with various values of resistance in a form of a ladder network, as described by (Kowal et al., 2011). With a long charging time, the first capacitor which is located near the voltage terminal, will be charged, so do the other capacitors. Therefore, when the charging stops, the first capacitor does not have to distribute much of its charge to balance the total charge of the network, hence, the capacitance is higher. Whereas, in a short charging time, much of the charge is accumulated in the first capacitor, therefore, it has to divide its charge to the other capacitors, thus, resulting in a larger voltage drop, hence, smaller capacitance. This is because the voltage measured at the terminal is essentially the voltage of the capacitor located near the terminal, i.e. the first capacitor.

4.3.2 Cyclic voltammetry

In case for an ideal SC, the CV plot will be a rectangle. Therefore, the capacitance can easily be calculated by using the following equation,

$$C = I/\frac{dv}{dt} \tag{4.6}$$

where I is the average current during discharge and $\frac{dv}{dt}$ is the scan rate.

However for a real SC, this is not the case. The CV waveshape of a real SC is leaf-like, yet almost rectangular, due to the non-ideality in real devices and also due to the porous electrodes used in SCs that leads to diffusion and charge redistribution phenomena (Kötz and Carlen, 2000; Pajkossy, 2005; El Brouji, Briat, Vinassa, Henry, et al., 2009; Wang et al., 2013). Therefore, Eq. (4.6) cannot be used to calculate capacitance. Instead, the charge was calculated by integrating the current-potential curve, as per Eq. (3.24). The relation between charge (Q) and the scan rate can be written as follows,

$$Q = \int_0^{\Delta t} I(t)dt = \frac{1}{v}\int_0^{\Delta U} I(U)dU \text{ and } v = \frac{dU}{dt} \tag{4.7}$$

where v is the scan rate.

Then, the capacitance can be computed using the following equation,

$$C = \frac{Q}{V_{max} - V_{min}} \tag{4.8}$$

Fig. 4.4 and Fig. 4.5 show the SC cyclic voltammograms at scan rate 5mV/s to 100mV/s. It can be seen that the selection of scan rate influences the current-potential waveshape. The width of the waveshape increases with faster scan rate. As the scan rate was increased to 100mV/s the waveshape became

distorted, particularly at the beginning of the reversal of the scan. 100mV/s scan may be too fast for the electrochemical reactions to occur, thus, the CV waveshape drifts from the usual rectangular waveshape.

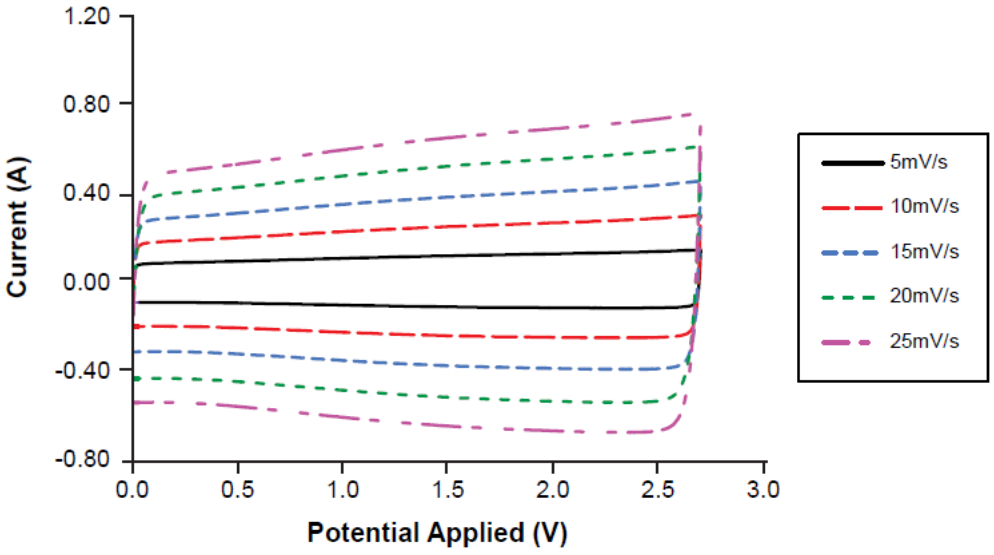

Fig. 4.4 The supercapacitor cyclic voltammograms at scan rates of 5mV/s to 25mV/s.

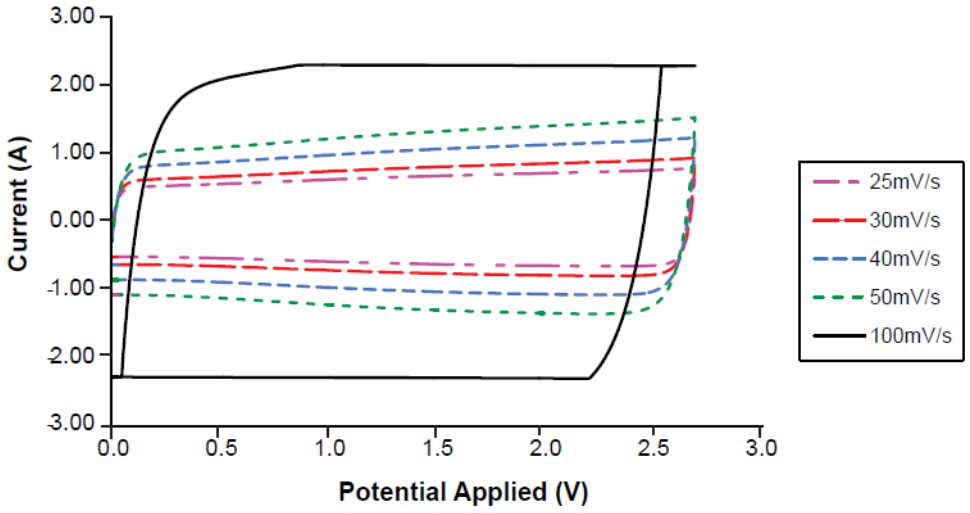

Fig. 4.5 The supercapacitor cyclic voltammograms at scan rates of 25mV/s, 30mV/s, 40mV/s, 50mV/s and 100mV/s.

The capacitance at each scan rate is given in Fig. 4.6. While the capacitance was initially expected to increase with slower scan rate, as it has been observed in (Kurzweil et al., 2005) and (Masarapu et al., 2009), the measured capacitances show opposite trends to decreasing scan rate. From 5mV/s to 30mV/s, the capacitance climbed gradually; however, when the scan rate was increased further, the capacitance started to drop, with a noticeable plunge at 100mV/s. It is also noted that the capacitance at 30mV/s is the closest to the capacitance from the constant current test.

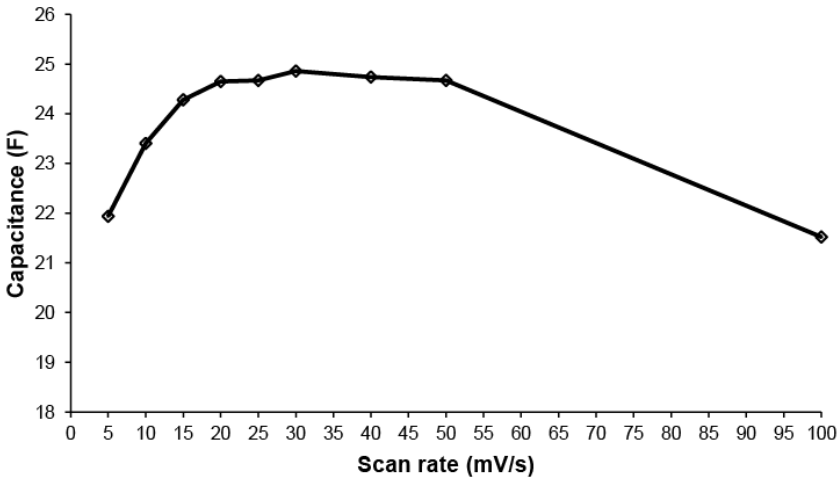

Fig. 4.6 Measured capacitance at various scan rates.

The fluctuation in the measured capacitance at different scan rates is also seen in the work of (Stoller and Ruoff, 2010) and (Zhang, 2010). This observation shows that it is important to find the most suitable scan rate to the material tested. The assumption in which slow scan rate produces higher capacitance, may not hold true in all materials. Nevertheless, an interesting assumption has been given by (Zhang, 2010) to explain this observation. Zhang (2010) relates this observation to the CV step potential applied between two successive current measurements. He stated that an incorrect value of the step

potential can cause low capacitance at low scan rates; the step potential may be too large to obtain an accurate value of the current response at low scan rates, in particular, hence affecting the measured capacitance. It should be noted that 0.002V step potential was applied in all measurements. In spite of that, we did not run additional tests at various step potential to justify this. Therefore, it is recommended for researchers to run test at several scan rates to determine the most suitable scan rate for the sample.

Besides that, in reality real applications have a 'scan rate ceiling', as been observed by (Zhang, 2010). Often, the upper limit of a scan rate for a material can be observed at the CV waveshape—the voltammogram becomes leaf-shaped or olive-shaped. A change in the CV waveshape is a sign that the electrochemical reactions have some trouble to proceed properly (Zhang, 2010; Sun et al., 2010). The upper limit of scan rate is contributed by many factors like ion accessibility and bulk conductivity in electrodes. For the case tested in this thesis, the upper limit for the SC is 100mV/s, in which the waveshape has become more of a leaf-shaped. From the CV results, 30mV/s is the most suitable scan rate for the SC since it gives the highest and the closest measured capacitance to that in constant current test.

4.3.3 Electrochemical impedance spectroscopy

In the time domain, the current through the SC is given by,

$$i(t) = C\frac{dV}{dt} \tag{4.9}$$

The time derivative of voltage $\frac{dV}{dt}$ can be written as $j\omega V$ in phasor form, thus gives

$$I = j\omega CV \tag{4.10}$$

where I and V are the phasor representations of current and voltage.

According to Ohm's law, the impedance of the capacitor Z_C is the ratio of the voltage to the current in phasor, which equals to,

$$Z_C = \frac{V}{I} = \frac{1}{j\omega C} \tag{4.11}$$

Since the impedance of capacitance has only the imaginary component, the capacitance can be calculated from the imaginary part of the complex impedance as,

$$C = -\frac{1}{\omega ImZ} \tag{4.12}$$

Fig. 4.7 displays Nyquist plot of the two frequency ranges tested in this study: 1kHz to 100mHz and 1kHz to 10mHz. The capacitances of these two frequency ranges are plotted in Fig. 4.8. Notice that the capacitance varies with frequencies. Above 308Hz is the effect from inductance, marked by the data below the positive vertical axis. The frequency range 1kHz to 10mHz showed the highest measured capacitance with 21.4787F at 10mHz, where the frequency range 1kHz to 100mHz gave 20.9463F at 100mHz. This result is expected as according to Eq. (4.12), capacitance increases with decreasing frequencies. Moreover, the graph shows a rising trend at low frequencies, in which it can be assumed that the capacitance will continue to increase if the frequency is lowered even more.

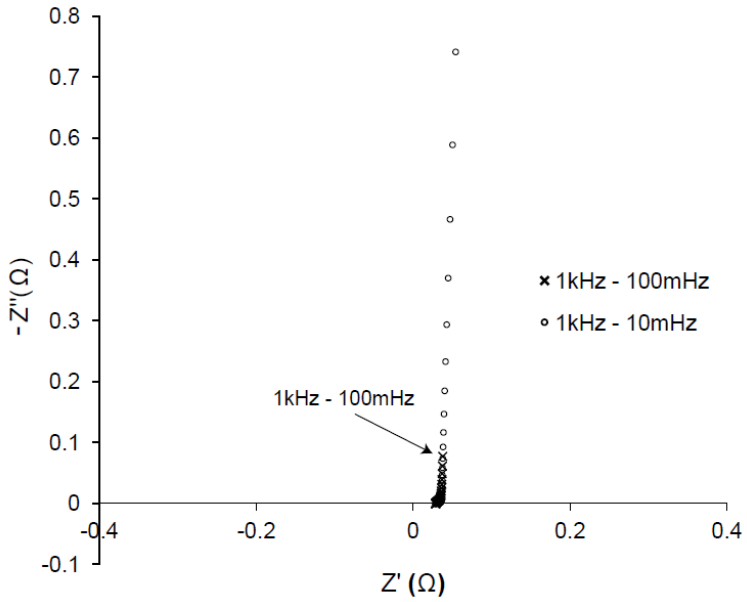

Fig. 4.7 Nyquist plot of the supercapacitor at two different frequency ranges. The unfilled circle is data from 1kHz to 100mHz frequency range and the cross is data from 1kHz to 10mHz.

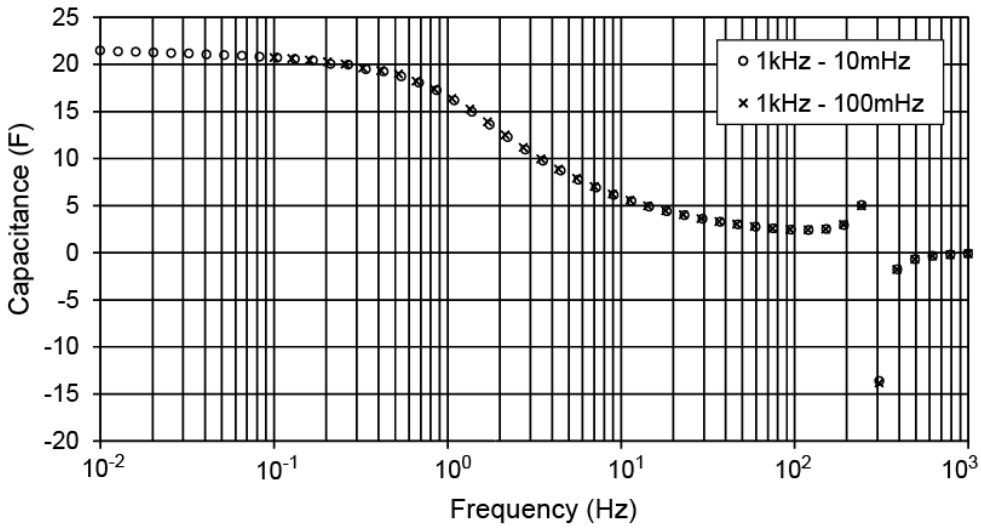

Fig. 4.8 Capacitance vs frequency. The unfilled circle is data from 1kHz to 100mHz frequency range and the cross is data from 1kHz to 10mHz.

To obtain capacitance value close to the one obtained in the constant current test, the frequency needs to be lowered even more, but this will affect

the duration of the test tremendously. This is because, the lower the frequency, the longer the test duration (refer to Table 3.5). Therefore, the practicality and the duration of the test have to be carefully weighed, particularly, in an environment where there is a time constraint.

According to IEC 62391, the ESR should be obtained at 1kHz for the ac method (IEC, 2006a). The 1kHz measurement frequency has become a standard when reporting the ac ESR. Many SC manufacturers like NEC Tokin, Panasonic, and Vishay, just to list a few, report ac ESR at this frequency in their product datasheets instead of the dc ESR (NEC Tokin, 2013; Panasonic, 2014; Vishay, 2014). Whereas, NESSCAP and Maxwell only report the dc ESR; while Tecate and Vinatech include both the dc ESR and the ac ESR in their product datasheets (NESSCAP, 2014; Maxwell, 2014d; Tecate, 2011; Vinatech, 2014).

Accordingly, the ac ESR from the two frequency ranges tested in this study is given in Table 4.7. There is only a slight difference in the ESR values obtained from the two frequency ranges. Since the difference is so small, the frequency ranges tested here do not affect the ESR.

Table 4.7 ESR_{ac} at 1kHz of two frequency ranges: 1kHz to 100mHz, 1kHz to 10mHz, 10 points per decade and AC amplitude of 10mV rms.

Method	ESR_{ac} (Ω) @ 1kHz
1kHz to 100mHz	0.028411
1kHz to 10mHz	0.028437

4.3.4 Comparison of all methods

Fig. 4.9 shows the measured capacitance according to measurement methods. Constant current method, despite how the method is carried out, yields the highest capacitance and followed by the cyclic voltammetry method; while the EIS gives the lowest capacitance among all. This trend is in concordance to the findings made by (Kurzweil et al., 2005). Fig 4.10 shows the ESR from dc measurements and ESR from ac measurements. Despite the various methods used in the dc measurements, dc measurement always gives a higher ESR than that in the ac measurement. ESR_{ac} is 1.5 to 2 times smaller than the ESR in dc measurements.

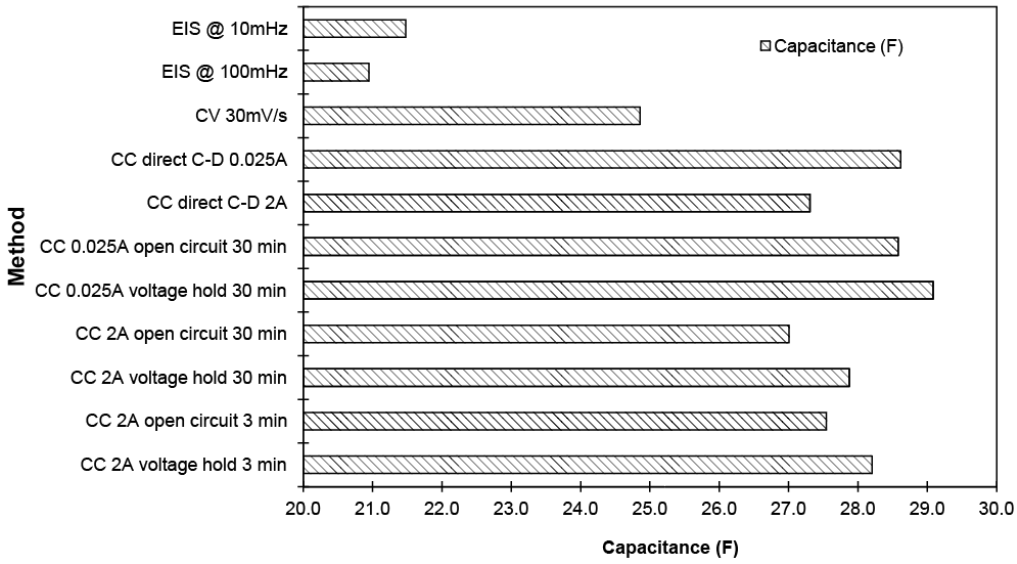

Fig. 4.9 Capacitance by method.

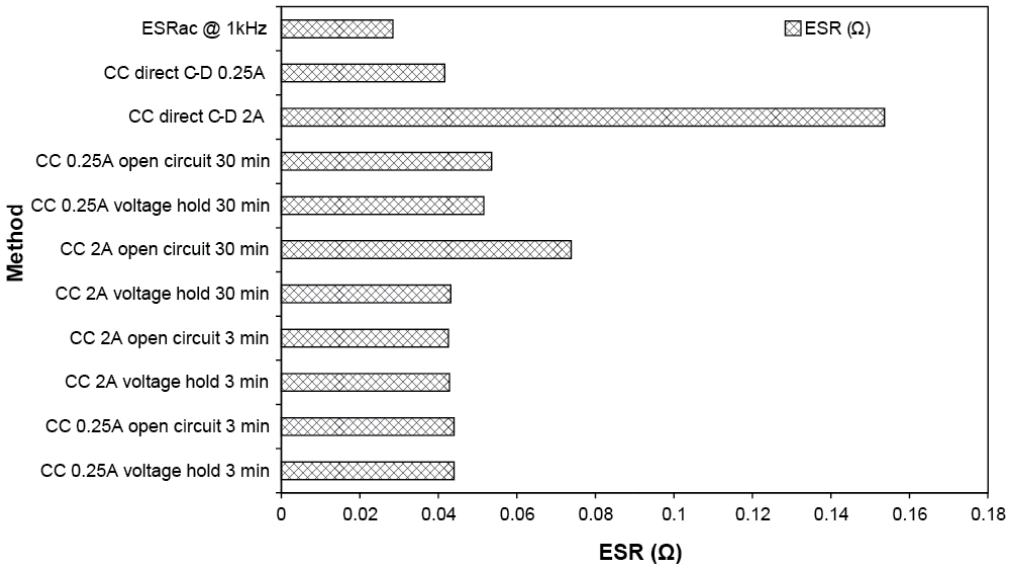

Fig. 4.10 ESR by method.

Fig. 4.11 shows the measured capacitance and ESR from each method. In dc measurements, the direct charge-discharge produces a fairly high capacitance, but in an expense of having a high ESR; the ESR in direct charge-discharge is the highest among all methods. In the voltage hold method, regardless how long the charge is sustained at the maximum voltage, produces the highest capacitance and a small ESR. However, this plus point is only convincing if the application is interested in the duration longer than 30 minutes. Otherwise, the voltage hold method is as good as the open circuit method for the duration of 3 minutes. Also note that, results in dc measurements are larger than the 25F specified by the manufacturer; even with the same measurement procedure used by the manufacturer, the result is still higher (refer to Table 4.4). This could be due to variations in fabricating the SCs (could be due to material variation or process variation). Meanwhile, the EIS method produces the lowest capacitance and the lowest ESR in this study.

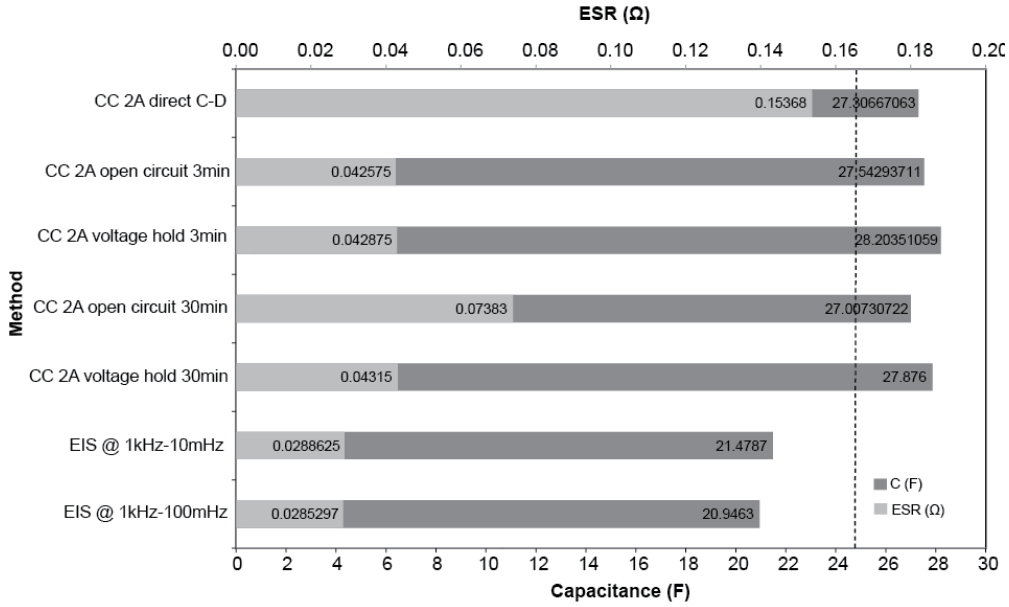

Fig. 4.11 Capacitance and ESR by method. The dash line is the capacitance value specified by the manufacturer.

4.4 Summary

Various measurement methods have been studied, they are: constant current test, cyclic voltammetry test and electrochemical impedance spectroscopy test. While the constant current test is more popular in the industry, the test is conducted in many ways—although there is already a standard published in the area. These differences are in terms of the amount of the discharge current and treatment used between charge and discharge cycle.

The amount of the discharge current influences the reported data, whereby a small discharge current will produce a higher capacitance and a smaller ESR than a larger discharge current does. Additionally, the effect of different treatments on SC in between charge and discharge cycle is also studied,

in which, it is found the voltage hold period produces a higher capacitance and a smaller ESR than that when the SC is left at open circuit or than that when a direct charge-discharge method is used. The voltage hold period reduces the amount of voltage loss and increases the penetration time of the charges to the SC porous electrodes. However, it is also found that the 30 minutes voltage hold period recommended by the IEC 62391 may be too long for the SCs tested in this thesis if the voltage hold method is only to offset the impact of the voltage drop in SCs due to charge redistribution. Even with 3 minutes, the voltage hold period already gives satisfactory results since there was not much difference between the results obtained in the 3 minutes duration and those in the 30 minutes duration.

Moreover, for environments that need results faster than 30 minutes, it would require a method that not only is able to give a reasonably good result in a shorter time but is also easy to set up. In these cases, the open circuit method is worth considering. The open circuit method should be done in 3 minutes, much longer and the results will be affected by leakage current.

Meanwhile, the effect from various scan rates used in the cyclic voltammetry test on the measured capacitance is also studied. The result shows that the capacitance does not necessarily increase with decreasing scan rate. In fact, an opposite trend is observed, in which it is found that the most suitable scan rate for the SC tested in this study is 30mV/s with the upper limit being at 100mV/s. These values are, however, case dependent and therefore various scan rates should be tested to find the most suitable scan rate for the material under test. Moreover, the measured capacitance from CV measurement is lower than

that from the constant current test. According to Eq. (4.4) and (4.8), the capacitance in the CV measurement and constant current test depends on the current. However, the resulting current from CV measurement at 30mV/s scan rate is smaller than the current used in the constant current test, thus resulting in a lower capacitance.

In EIS measurement, the measured capacitance depends on the low frequency, in which capacitance will increase with decreasing frequency. However, at low frequency, the measurement will be longer. Furthermore, EIS produces the lowest capacitance among all methods. Similarly for the ESR, EIS reports a lower ESR value than the dc ESR by 1.5 to 2 times.

With the different values being reported by these measurement methods, it is shown that there is a need for transparency when reporting these values in the literatures and product datasheets so that they can be replicated by others and also to alleviate uncertainties when interpreting these results.

CHAPTER 5

AGEING DIAGNOSIS USING ACCELERATED AGEING TEST

"Intuition is really a sudden immersion of the soul into the universal current of life."

—Paulo Coelho, The Alchemist

5 Introduction

This chapter studies the effect of environmental and operational stress factors on the ageing of SCs by means of accelerated ageing tests. The state of health (SOH) of the SCs are monitored periodically to observe the ageing process. The aim of this study is therefore to understand the ageing process and the ageing mechanism that contribute to the failure in SCs. The data gathered in this study is key to the development of the SC ageing model, which is found in Chapter 6.

Prior studies have noted the effect of voltage and temperature on SCs lifetime (Azaïs et al., 2007; El Brouji, Briat, Vinassa, Henry, et al., 2009; Hammar et al., 2010). Voltage and temperature reduce the lifespan of SCs in which at these conditions ageing processes are accelerated. These two stress factors cause changes to the chemical properties of SCs as it has been reported in many literatures like the one found in (Bittner et al., 2012).

However, one of the most difficult conundrums is to isolate the cause of ageing, since in practice, two or more stress factors are applied together on SCs. Therefore, it is often difficult to associate the observed ageing process with a particular type of stress factor since the resulting ageing process is a product of the sum contribution of many factors at a time. Moreover, by being able to identify the ageing process specific to the stress factor, SCs can be built specifically to the targeted application and solutions can be targeted individually.

In (Kötz et al., 2010), it is shown that voltage and temperature have a distinctive impedance signature on SCs, and thus has become the motivation for this work. Their finding has brought up the idea that each stress factor could possibly has its own signature and it could be identified by monitoring the evolution of SC impedance spectrum. The term ageing factor and stress factor are hence used interchangeably in this thesis.

Therefore, this work is aimed at studying the impact of temperature, current cycling and constant voltage, individually and the part played by temperature during current cycling and constant voltage tests in SC ageing, by means of accelerated ageing test. Thereupon, the main ageing mechanism according to the ageing factor can be isolated and identified accordingly.

5.1 Accelerated Ageing Tests

The duration of an ageing test is long; this is in view of the extremely long life of SCs (more than 10 years or 1,000,000 charge/discharge cycle can be expected at normal condition) (Wang et al., 2012). Therefore to shorten the test duration and accelerate ageing, ageing tests were performed in high temperature and high voltage conditions, but still abiding to the maximum capability of the device to endure stress. Hence, the end of life (EOL) criteria can be met within a few months.

Fig. 5.1 is the test methodology employed in this work. Accelerated ageing tests had been performed for several months on Maxwell SCs rated at 2.7V/25F, based on activated carbon and tetraethylammonium tetraflouroborate ($TEABF_4$) in acetonitrile (AN). Three types of accelerated ageing tests were conducted: (i) storage test at high temperature, (ii) constant voltage test and (iii) cycling test. The constant voltage test and cycling tests were both performed at two test temperatures to study the temperature contribution on each test. The test conditions were as the following:

i. **Storage test:** at high temperature of 85°C.
ii. **Cycling test:** (0.6A, 20°C) and (0.6A, 85°C).
iii. **Constant voltage test:** (2.7V, 20°C) and (2.7V, 85°C).

The tests conditions were selected according to the manufacturer's specification and the equipment capability in the Sahz-Nottingham NANO Super-capacitor Pilot Plant. At this test condition, the SC core temperature will rise, therefore, an open circuit rest period of 24 hour was introduced after each complete test before proceeding with further testing to return the cell within the

normal range and also to ensure that the SC has reached a stable voltage and temperature condition. All tests began with a discharge SC to ensure test repeatability.

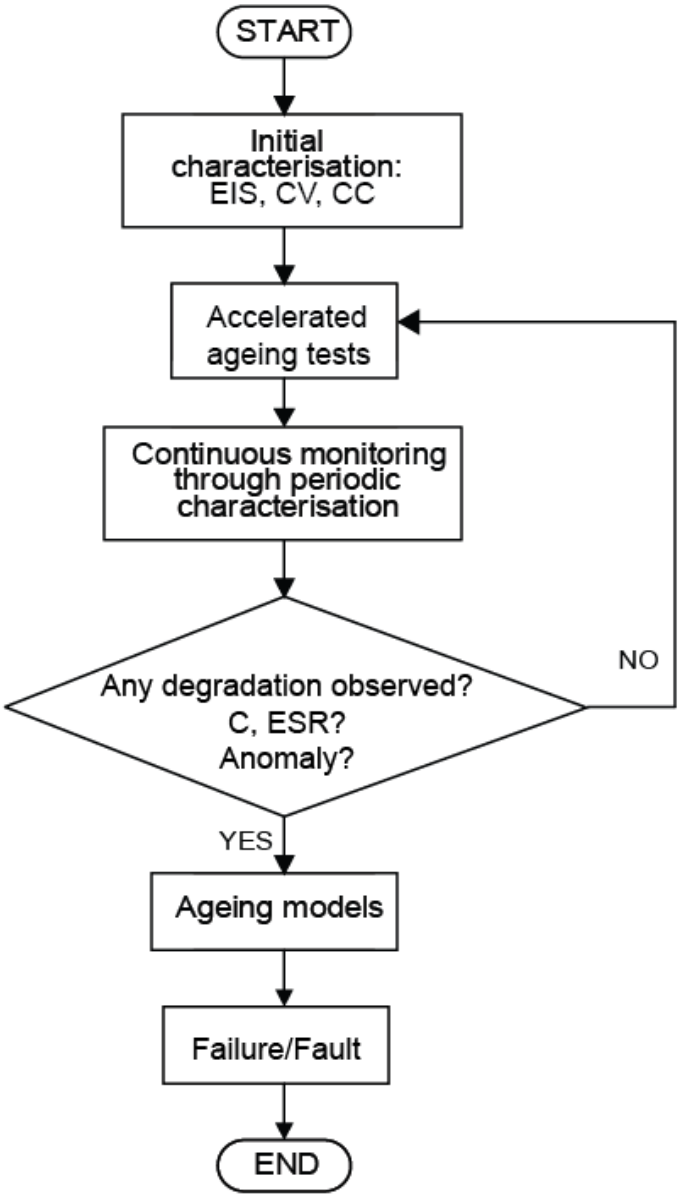

Fig. 5.1 Test methodology.

The SOH of the SCs can be measured by comparing characteristic data at the beginning of the test with the one obtained by measurement at different stages of SC lifetime. This will give a measure of the age of the SC cell and cell functionalities with respect to the SC initial state. In this work, the SOH of the SCs were monitored periodically with characterisation tests for every 1 week which is equivalent to 168H test duration or 2,400 cycles for the case in cycling test. The tests were only stopped when either one of the following end-of-life (EOL) criteria was met:

- 20% loss from the initial capacitance
- 100% increase in ESR
- Cell opening due to the build-up of pressure in the cell

It should be noted that these tests were abusive to SCs. The test temperature used in this study was over the boiling point of AN (81.6℃) (Gualous et al., 2012; Alcicek et al., 2007), although it was within the maximum operating temperature of the SCs. The cycling test was based on a consecutive charge/discharge current cycle. Fig. 5.2 shows the current profile used in this test. The SCs were cycled between 0V and 2.7V with 0.6A current. This current profile took about 113 seconds to charge/discharge the SCs. No rest time in between charging and discharging was introduced so that it gave the electrolyte no time to settle between charging and discharging in order to represent a stressful condition in terms of electrolyte ageing.

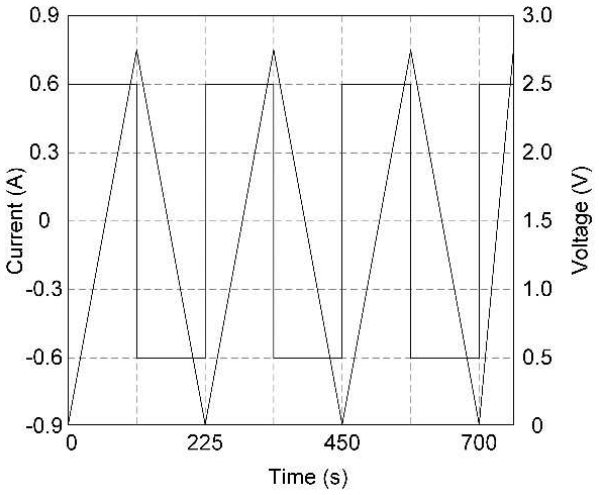

Fig. 5.2 Illustration of the current profile used in this test. SCs are cycled between 0V and 2.7V using 0.6A current with no rest time in between charge and discharge cycle. The triangle wave is the voltage response to the current profile (square wave).

5.2 Periodic Characterisation Tests

The accelerated ageing tests were followed by a periodic measurement protocol to characterise SCs and to monitor degradation in their SOH. Three characterisation tests were performed in a systematic manner based on the following order: (i) electrochemical impedance spectroscopy test, (ii) cyclic voltammetry test and (iii) constant current test. These tests were performed at room temperature and each SC was discharged to 0V prior to testing.

5.2.1 Electrochemical impedance spectroscopy test

Electrochemical impedance spectroscopy (EIS) test was performed on discharged SCs before and after each accelerated ageing test using a potentiostat

(PGSTAT302N) equipped with a frequency response analyser (FRA) module from Metrohm Autolab B.V. The EIS test was done in potentiostatic mode by sweeping frequencies over the range of 10kHz to 100mHz with 10 points/decade. The AC signal applied was a single sine wave of 10mV rms. No bias voltage was applied.

EIS was applied to track the ageing course and to identify any anomaly in the impedance data. EIS, therefore, serves the following purposes: First, to gain insight of the electrochemical processes at the electrode/electrolyte interface and secondly, to identify possible ageing mechanism. The interpretation of the impedance measurements was aided by fitting an electrical equivalent circuit (EEC) to the impedance spectrum as appears in Chapter 6. The capacitance can be deduced from the SC impedance response by the following relation (Paul et al., 2009):

$$C_{spectra} = \frac{-1}{2\pi f \times Im(Z)} \text{ [F]} \tag{5.1}$$

The equivalent series resistance (ESR) can be obtained at the intersection of the Nyquist plot at the real axis Z' at high frequencies. The resistance is thus given by the relation:

$$ESR_{ac} = Re(Z) \text{ [}\Omega\text{]} \tag{5.2}$$

Where Z is the impedance of the SC at the frequency (f).

5.2.2 Cyclic voltammetry test

In this work, cyclic voltammetry (CV) test was performed by applying a linear voltage ramp to the SC between 0V to 2.7V, according to the voltage limit

specified by the manufacturer. The CV was performed at a scan rate of 30mV/s based on the findings in Chapter 4, which it was found to be the most suitable scan rate for the SCs tested in this thesis. The resulting current was measured and recorded on a current-potential curve. As part of the electrode condition process, CV test was performed in many cycles until there was very little change in the data between cycles. This process also allowed for the evaluation of the cyclability of the SC.

5.2.3 Constant current test

Constant current (CC) test was performed to measure the capacitance and the ESR of the SC in order to quantify ageing. The SC was charged at constant current with a current rate of 75mA/F. The SCs were left open circuit (rest) for 15s between charge and discharge cycle as shown in Fig. 5.3. Selection of current rate and open circuit period was set according to Maxwell 6 Step Process as it was suited to the conditions of the experiment and test time was shorter than IEC 62391. This decision was supported by the results obtained in Chapter 4.

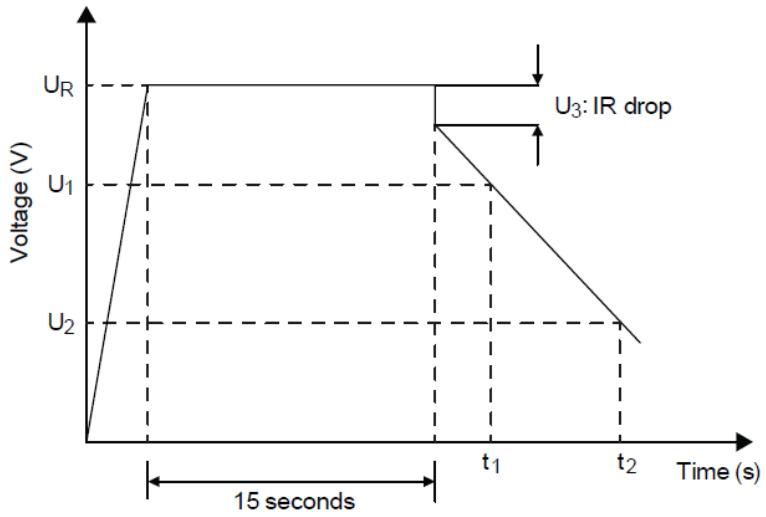

Fig. 5.3 The characterisation method for SCs. U_R is the rated voltage, U_1 is 80% of U_R and U_2 is 40% of U_R. A 15s open circuit period is applied between charge and discharge.

5.3 Post-mortem Analysis of Aged Cells

After the accelerated ageing tests, the aged SCs were disassembled in air. The aged positive and negative electrodes were washed with distilled water to remove the electrolyte. After washing, the electrodes were dried at 40℃ for 4H under vacuum. Fresh electrodes were also washed and dried under the same condition for comparison purposes. The structure of the fresh and aged electrodes were evaluated by field emission scanning electron microscopy (FESEM) with energy dispersive X-ray (EDX) analysis at high vacuum with magnification range of 10,000x and accelerating voltage of 20kV.

5.4 Ageing Tests Results

A Electrochemical impedance spectroscopy results

The effects of each stress factor were investigated by observing the evolution of the impedance spectra. Fig. 5.4 depicts an impedance spectrum of a fresh SC plotted from 100mHz to 10kHz frequency range, in a Nyquist plane. The intersection of the impedance spectrum at high frequency shows a line with 45° slope and it continues to extend almost vertically towards low frequencies. At frequency higher than 472Hz, there is an inductive behaviour related to the geometry of the cell and external artefacts such as external wiring and measurement system.

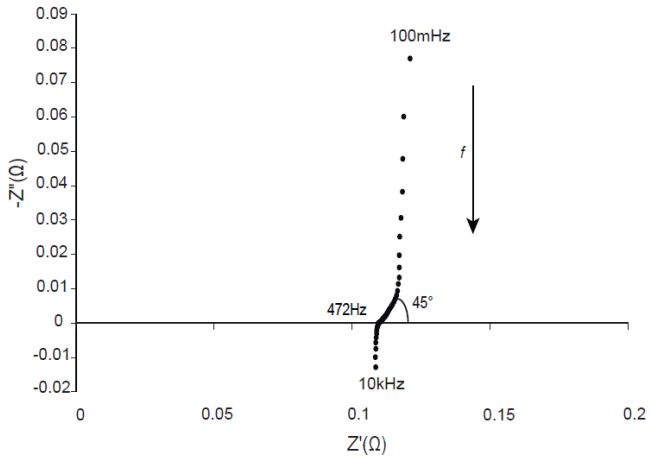

Fig. 5.4 Typical impedance spectrum of a fresh SC. A fresh SC has an almost vertical impedance line which starts with a 45° line from the intersection of the line with the real axis at high frequencies.

Deviations from the initial impedance spectrum were assumed as a presage of a new reaction occurring in the cell or that there are some changes at

the electrode/electrolyte interface or the active material. Accordingly, the initial impedance spectrum was juxtaposed with the measurements obtained at different stages in SC life to monitor these changes.

Storage Test at 85℃ as reference (see page 189)

Fig. 5.5 presents the impedance evolution during storage test at 85℃ at various stages of SC life. Due to limited space in the graph and for the sake of visibility, only impedance spectra that show a significant change are displayed. From the Nyquist plot (top-left corner) in Fig. 5.5, the most direct evidence that ageing process had taken place can be observed in a continual series of change of the impedance spectra from the start until the end of the test. At each stage of SC life, it was observed that the change in impedance occurs by either the addition of a new process or a specific part of the impedance spectrum become more accentuated over time.

The effect of ageing at high temperature was most prominent at high frequency 45° slope line. As ageing time proceeds, the 45° line is replaced by a semicircle; it was first seen at 672H and became clearer at 720H. The semicircle continued to grow and at 1,728H, its size constituted a great portion of the impedance spectrum. The semicircle can be reproduced by a parallel connection of R-C or R-CPE, depending on where the centre of the semicircle is on the real axis.

A shift of the impedance spectra along the real axis was also observed, indicating that the real impedance is increasing with ageing. This is more clearly seen in the Z' vs frequency plot (Fig. 5.5c), whereby at 1,728H, the Z' has increased to 0.325466Ω, almost three times the Z' at 0H (0.12108Ω). However,

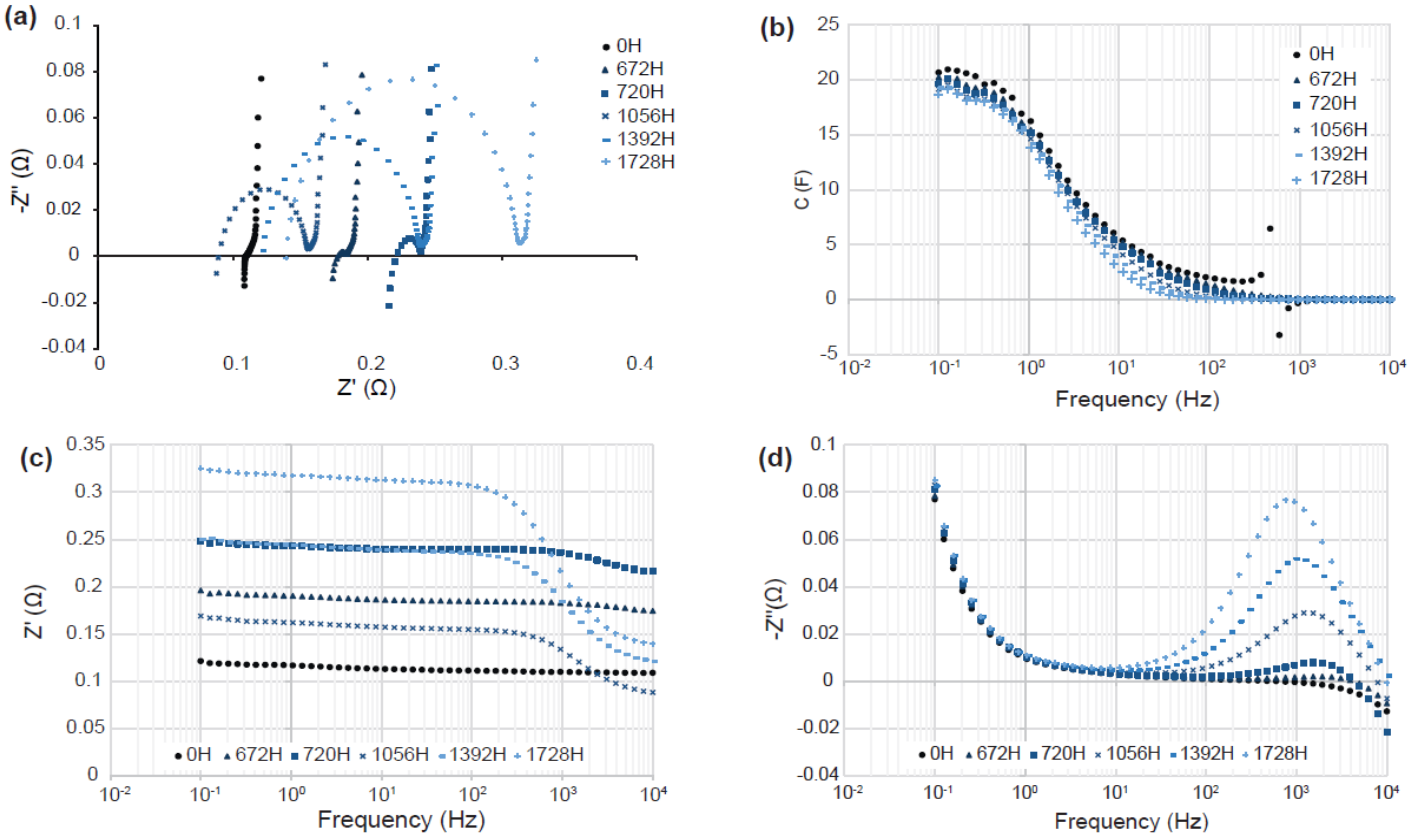

Fig. 5.5 The effect of storage test at 85℃ on SC impedance. The graphs display the results at different stages of SC life. Only impedance spectra that show a significant change are displayed.

the Z' vs frequency plot shows a non-uniform change. Initially, the real part of the impedance was not frequency-dependent; however, as ageing progressed, the real part became distorted and showed a dependency of frequency, particularly at higher frequencies as evident at 1,392H and 1,728H. At 1,728H, the Z' decreased moderately between 100mHz and 145Hz. Then, a curvature distortion took place where Z' plummeted between 145Hz and 10kHz. The start and the end of the distortion were in accordance with the start and the end of the semicircle formation in the Nyquist plot.

Similarly, the $-Z''$ vs frequency graph (Fig. 5.5d) shows a distortion as evidenced by the appearance of a hump at high frequencies. The hump increased in magnitude over time. The remaining part of the imaginary impedance, however, were unaffected. Meanwhile, the cell capacitance (Fig. 5.5b), calculated based on Eq. (5.1), was faintly affected by ageing.

Effect of temperature during cycling tests

0.6A, 20℃ Test: In this test, a cycling test was performed at 20℃. The primary purpose is to study the effect of cycling regime and any possible ageing caused by it in the absence of the stress from temperature. The results from this test are displayed in Fig. 5.6.

From the Nyquist plot (top-left corner of Fig. 5.6), the cycling test at 20℃ showed no significant change to the shape of the impedance spectra after 36,000 cycles. However, a change in the slope of the imaginary part of the impedance spectra at low frequencies was observed. The impedance spectra of aged SCs exhibited tilting of the low frequency part. In order to see the tilting clearly, the initial impedance spectrum (0 cycle) was placed on the impedance

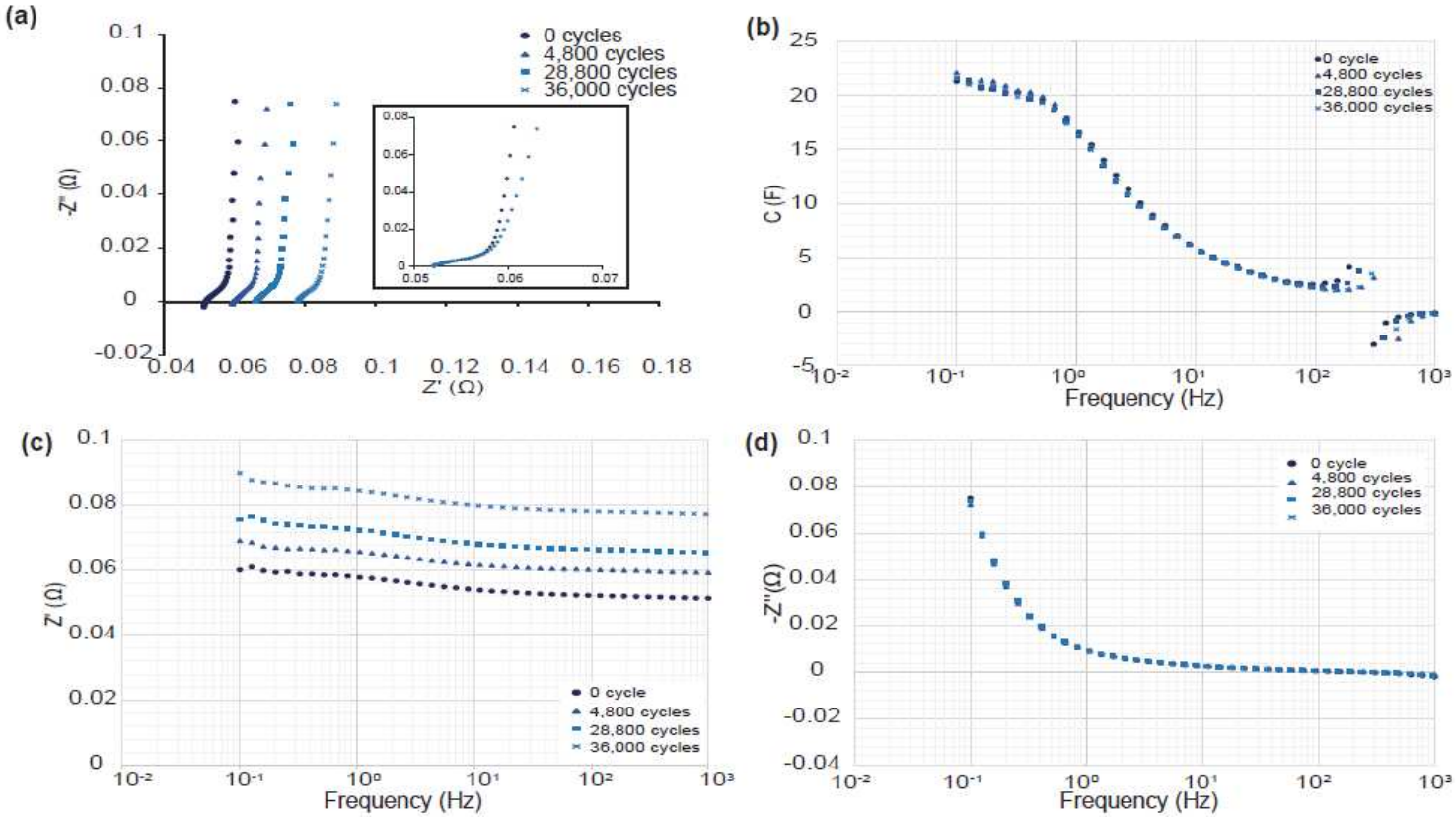

Fig. 5.6 The effect of cycling test at 0.6A, 20℃ on SC impedance. The graphs display the results at different stages of SC life. Only impedance spectra that show a significant change are displayed.

spectrum at 36,000 cycles as shown in the inset. From a linear regression analysis in Nova 1.10.3, the low frequency line at 0 cycle had a slope of 19.788. After 36,000 cycles, the slope of the low frequency line had decreased to 12.972. This result shows that after the SC was charged and discharged for 36,000 cycles, the low frequency line had tilted for 1.5° from the initial impedance spectrum.

Besides the decrease of the slope of the low frequency line, a movement of impedance real part along the real axis pertaining to an increase of the Z' component over the ageing time was also observed; this behaviour is evident in the Z' vs frequency graph (see Fig. 5.6c). From the graph, it can be seen that Z' is frequency-dependent; its value decreases with increasing frequency. The graph was almost linear with no distortion was monitored. In spite of that, the value of Z' had clearly increased with the number of cycling. At 0 cycle, the Z' was 0.0601053Ω at 100mHz and after 36,000 cycles, the Z' increased to 0.0900054Ω, that is a 49.75% increase from the initial value. Meanwhile, the capacitance (Fig. 5.6b) and the imaginary part Z'' of the impedance (Fig. 5.6d), showed neither any degradation nor change for the entire course of ageing duration.

0.6A, 85℃ Test: While the previous test was to study solely the effect of cycling regime on SCs ageing, this test focuses on investigating the contribution of temperature in SC degradation during cycling.

Fig. 5.7 shows the changes of the impedance during cycling test aged at 0.6A, 85℃ at different stages of SC life. Similar to the storage test, the figure displays only important changes to the shape of the impedance spectra as ageing

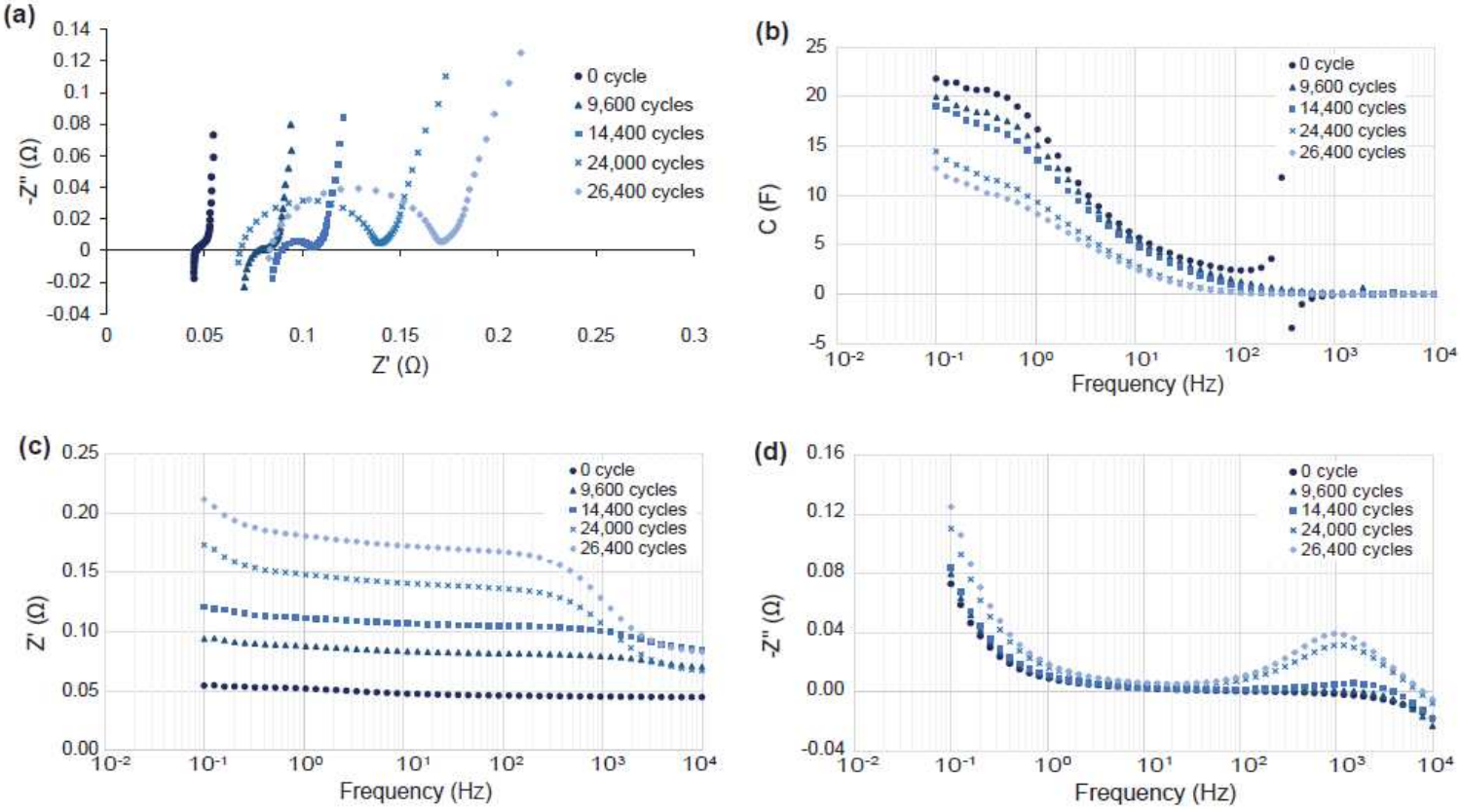

Fig. 5.7 The effect of cycling test at 0.6A, 85℃ on SC impedance. The graphs display the results at different stages of SC life. Only impedance spectra that show a significant change are displayed.

proceeds. Referring to the Nyquist plot (top-left corner), the effect of this test took three forms: (1) a movement of the impedance spectrum along the real axis that presages ageing, (2) an emergence of a semicircle replacing the 45° slope line and a continual expansion of its size and diameter as ageing progresses, and (3) a prominent inclination of low frequency part to the right.

In regards to the emergence of a semicircle, the formation was first detected after 9,600 cycles and became more protuberant at 26,400 cycles. In addition to the appearance of semicircle, the impedance real part increased with ageing, evident in Z' vs frequency graph (Fig. 5.7c). The Z' initially stood at 0.0545226Ω at 100mHz. After 26,400 cycles, the Z' had become 0.211584Ω, which marked a 288.1% increment from the initial Z'. The Z' was also frequency-dependent that it increased as frequency decreased. Similar to the storage test, a curvature distortion was also observed, particularly at 24,000 cycles and 26,400 cycles. At 26,400 cycles, the distortion started at 184Hz following a gradual decrease of Z' and quickly plunged between 184Hz and 10kHz. These two frequencies, 184Hz and 10kHz, were where the semicircle appeared in the Nyquist plot, respectively.

Consistent to the observation in the storage test, the semicircle caused distortion not only to the impedance real part, but also to the impedance imaginary part. The distortion at the Z'' vs frequency plot was described as a hump, appeared at 24,000 cycles and 26,400 cycles (refer to Fig. 5.7d). Apart from the hump, a noticeable increment of Z'' was observed after 26,400 cycles in comparison to the measurement at 0 cycle.

Moreover, the low frequency tail was observed to have declined from having a slope of 22.573 at 0 cycle to a slope of 4.1708 after 24,000 cycles under cycling test. The increase in *Z''* and the decreasing slope of the low frequency tail of the impedance spectrum were directly translated in the drop of capacitance after 26,400 cycles, as visible in the capacitance vs frequency plot (Fig. 5.7b). The capacitance initially stood at 21.7859F, but after 26,400 cycles at 85℃, the capacitance had dropped by 41.63% to only 12.7168F.

Effect of temperature during constant voltage test

2.7V, 20℃ Test: In order to investigate the principle effect of constant voltage test on the SC ageing, the SC was tested at its nominal voltage of 2.7V at temperature of 20℃**.** Fig. 5.8 presents the test results.

The Nyquist plot (top-upper left corner) of Fig. 5.8 shows no changes to the impedance spectrum of the SC. Even after 2,372H, the impedance spectrum still preserved its initial shape (0H). What noticeable was a shift of the impedance spectrum towards higher values of *Z'* axis over the ageing time. However, when the impedance spectrum at 2,372H was placed over the impedance spectrum at 0H (see inset), the impedance spectrum had deviated from the initial response. The low frequency part of the spectrum at 2,372H had a slope of 13.41; the slope of the line was initially at 26.185. Therefore, the impedance spectrum had certainly tilted for 2.078 ° from the impedance spectrum at 0H.

Fig. 5.8c is the *Z'* vs frequency graph. The graph showed a slight frequency-dependent behaviour of the impedance real part. The *Z'* values increased with decreasing frequency. Nevertheless, the whole response was

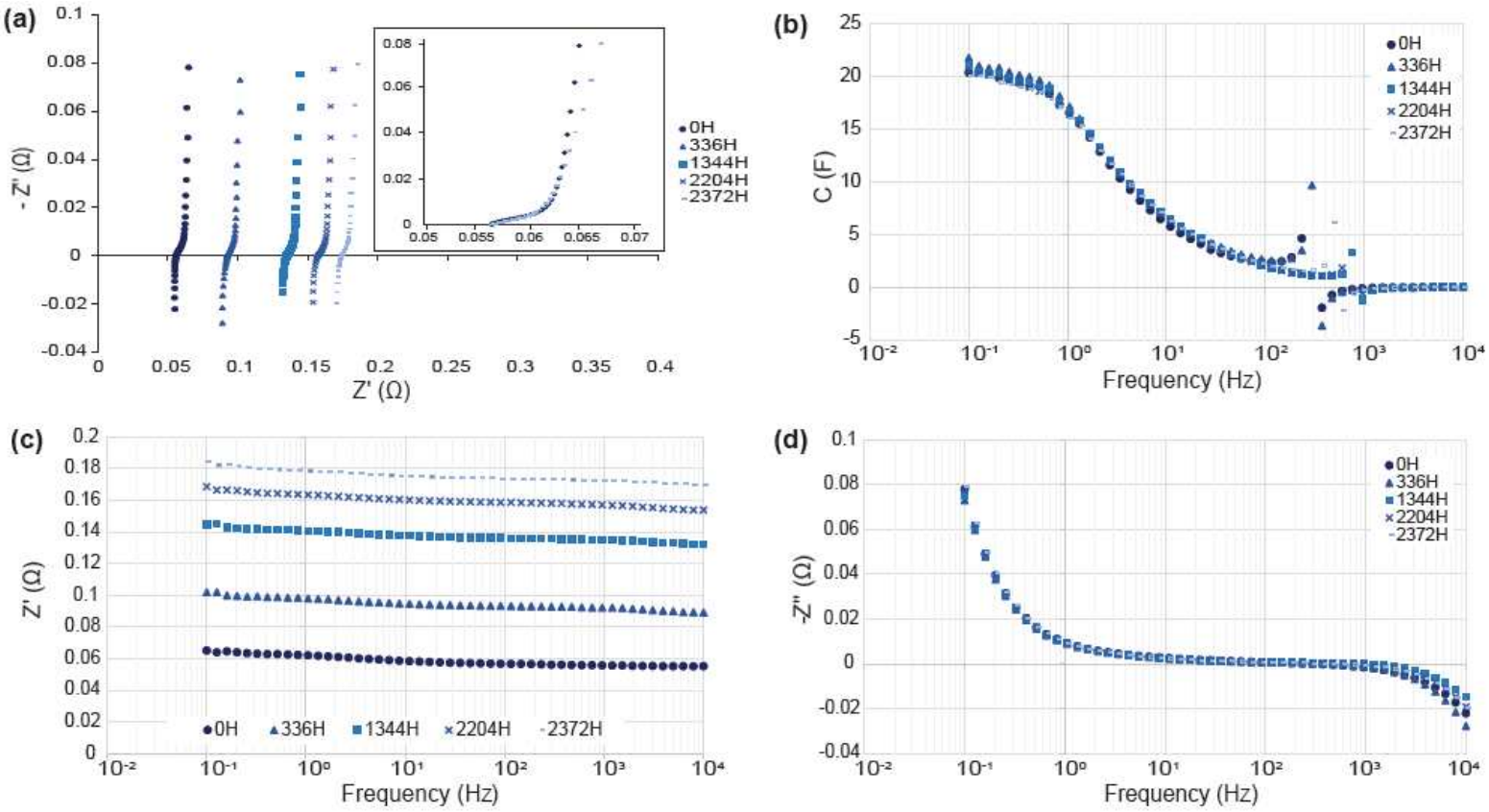

Fig. 5.8 The effect of constant voltage test at 2.7V, 20℃ on SC impedance. The graphs display the results at different stages of SC life. Only impedance spectra that show a significant change are displayed.

nearly linear with no sudden increase nor fall. The Z' vs frequency graph confirmed the earlier observation pertaining to the movement of the Nyquist plot along the real axis. At 0H, the Z' value was recorded at 0.065029Ω at 100mHz. After 2,372H being tested at 2.7V, 20℃, the real part of the impedance had become 0.1820805Ω at 100mHz, which marked a 180% increase. In spite of that, the test did not affect the capacitance and impedance imaginary part Z'' even after 2,372H in test as evidence from capacitance vs frequency graph and Z'' vs frequency graph, Fig. 5.8b and Fig. 5.8d, respectively.

2.7V, 85℃ Test: This test was to investigate the influence of high temperature during constant voltage test on SC performance. The SC was tested by applying a constant voltage of 2.7V while at the same time was exposed to high temperature at 85℃. Fig. 5.9 presents the results from this test.

The Nyquist plot at the top-upper left corner of Fig. 5.9 shows the evolution of the impedance spectrum from 0H to 648H in test. Besides a clear shift of the impedance real part along the Z' axis, the shape of the impedance spectra had certainly deviated from its initial response at 0H. Not only the spectrum at 658H had tilted by a high degree and decreased in slope, there were also two semicircles in the spectrum which replaced the 45° line of the 0H spectrum. The emergence of the two semicircles can be detected in the spectrum at 480H, but only at 648H the second semicircle became more evident. This behaviour was rather peculiar. Unlike previous tests which only showed the appearance of one semicircle, this test condition had raised two semicircles in which both of them differed in sizes and magnitudes. The difference in size signifies that they both have different time constants.

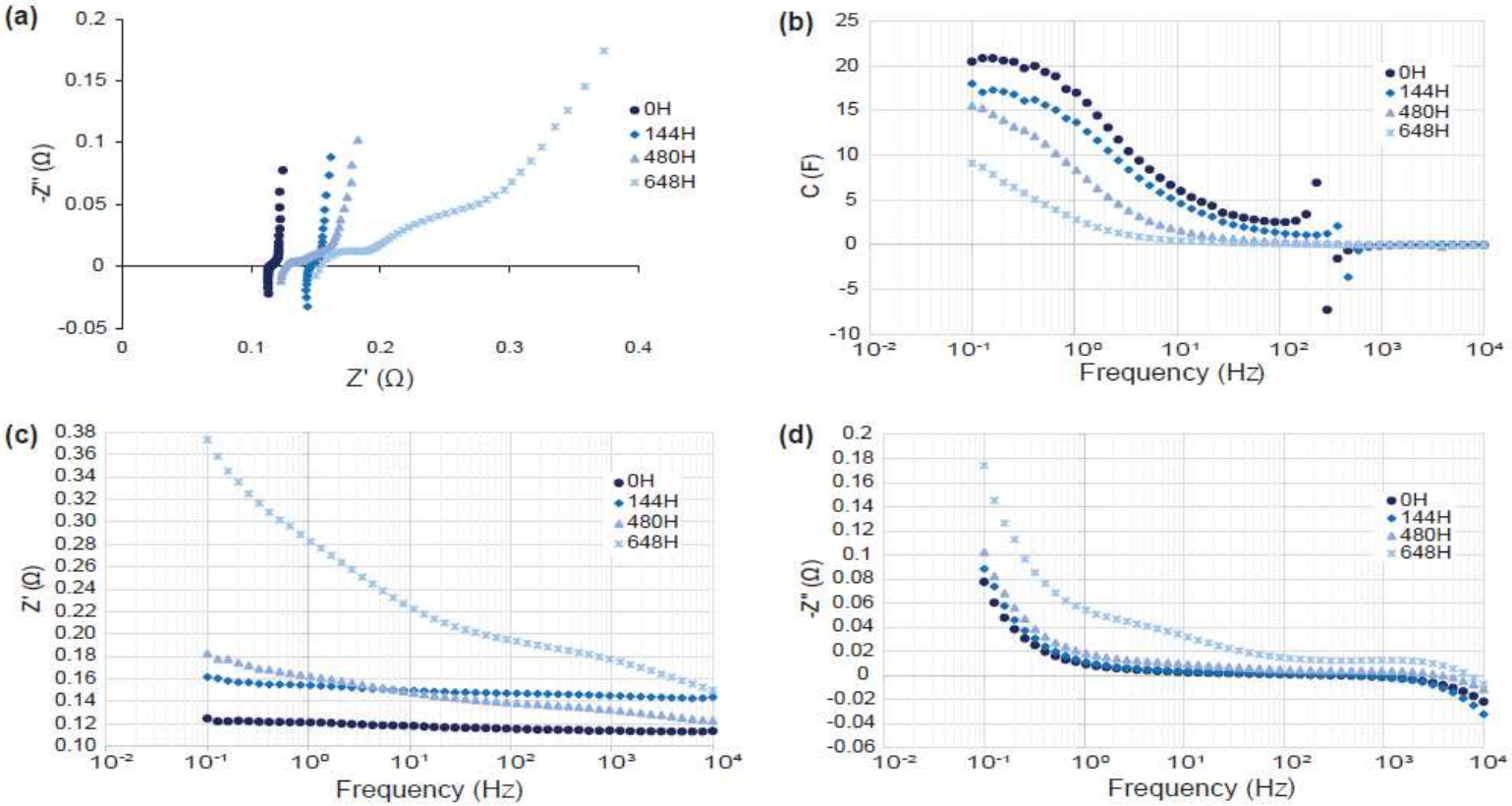

Fig. 5.9 The effect of constant voltage test at 2.7V, 85℃ on SC impedance. The graphs display the results at different stages of SC life where the most significant change is observed.

In the Z' vs frequency graph (Fig. 5.9c), the Z' response after 648H escalated with decreasing frequency. The increase was significant compared with the responses in earlier hours. Similarly, Z'' vs frequency response at 648H also deviated from the rest. The Z'' values increased rapidly with a small bump in between, from 91Hz to 100mHz. The start of the rapid increased was consistent to the beginning of the second semicircle in the impedance spectrum and the end of the bump was in line with the ending of the second semicircle. In addition, the SC capacitance appeared to be greatly affected at this test condition (Fig. 5.9b). At the 648H, the capacitance dropped from 20.5085F to 9.13176F, which was 55.47% loss in capacitance.

B Cyclic voltammetry test results

Fig. 5.10 to Fig. 5.12 show cyclic voltammograms at different stages of SCs life in all test conditions. The shape of CV curves of all fresh cells were almost rectangular. The current slowly rises when charging the SCs from 0V and decreases when the scan is reversed. No 'hump' pertaining to redox reactions at the electrode surface was observed during measurement. This observation is an indication that the cells are in a good condition prior to the start of the accelerated ageing test.

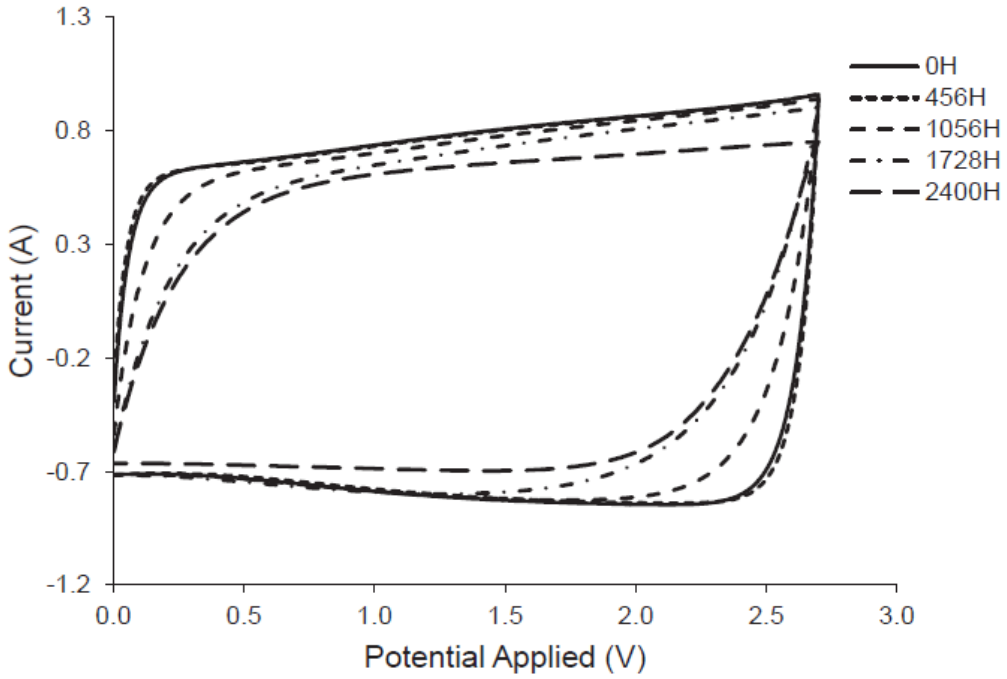

Fig. 5.10 Cyclic voltammograms at different stages of SC life during storage test. The measurement is performed at 30 mV/s scan rate.

After ageing tests were stopped, there was a notable change in the CV shape which showed that the SCs had aged. The recorded cyclic voltammograms after ageing tests showed distortions particularly in those that were exposed to high temperature, such as in storage test (Fig. 5.10), cycling (0.6A, 85℃) test (Fig. 5.11b), and constant voltage (2.7V, 85℃) test (Fig. 5.12b). While the cyclic voltammogram from a fresh SC was almost rectangular, as SC aged the CV waveshape became more of a leaf-shaped. In the constant voltage test at high temperature (2.7V, 85℃), this distortion in the CV waveshape was more pronounced, whereby after 1,152H, the CV waveshape had changed considerably. This could be due to that the 30mV/s scan rate was no longer suitable at this stage; the electrochemical reactions in aged SC had slowed down and the 30mV/s scan rate was too fast to allow the electrochemical reactions to occur.

Furthermore, the observed distortions were more conspicuous than the test conditions in which the stress from high temperature was absent like the cycling (Fig. 5.11a) and constant voltage (Fig. 5.12a) tests done at 20℃. This finding shows that if more than one ageing factor is present, the ageing effect is greater. In fact, SC in the constant voltage (2.7V, 85℃) test showed the most diminution in the CV waveshape after being stressed for 1,488H followed by cycling test at high temperature (0.6A, 85℃) and storage test. The distortion was accompanied with a narrowing of the CV waveshape, indicating that the cell capacitance had decreased. Since the charge Q according to Eq. (3.24) is simply the area between the CV curves; therefore from Fig. 5.12b, SC in the constant voltage (2.7V, 85℃) test had the lowest remaining capacitance as Q is related to capacitance by Eq. (2.1).

Meanwhile, in a test in which the contribution of high temperature was not taken into account, such as cycling (0.6A, 20℃) and constant voltage (2.7V, 20℃) tests, the results show minimal effects on the CV waveshape after 36,000 cycles and 2,372H, respectively. These observations indicate that both test conditions show no significant impact on the capacitance. Nevertheless, no redox behaviour was observed in all test conditions, suggesting that Faradaic reaction did not occur in the SCs during accelerated ageing tests.

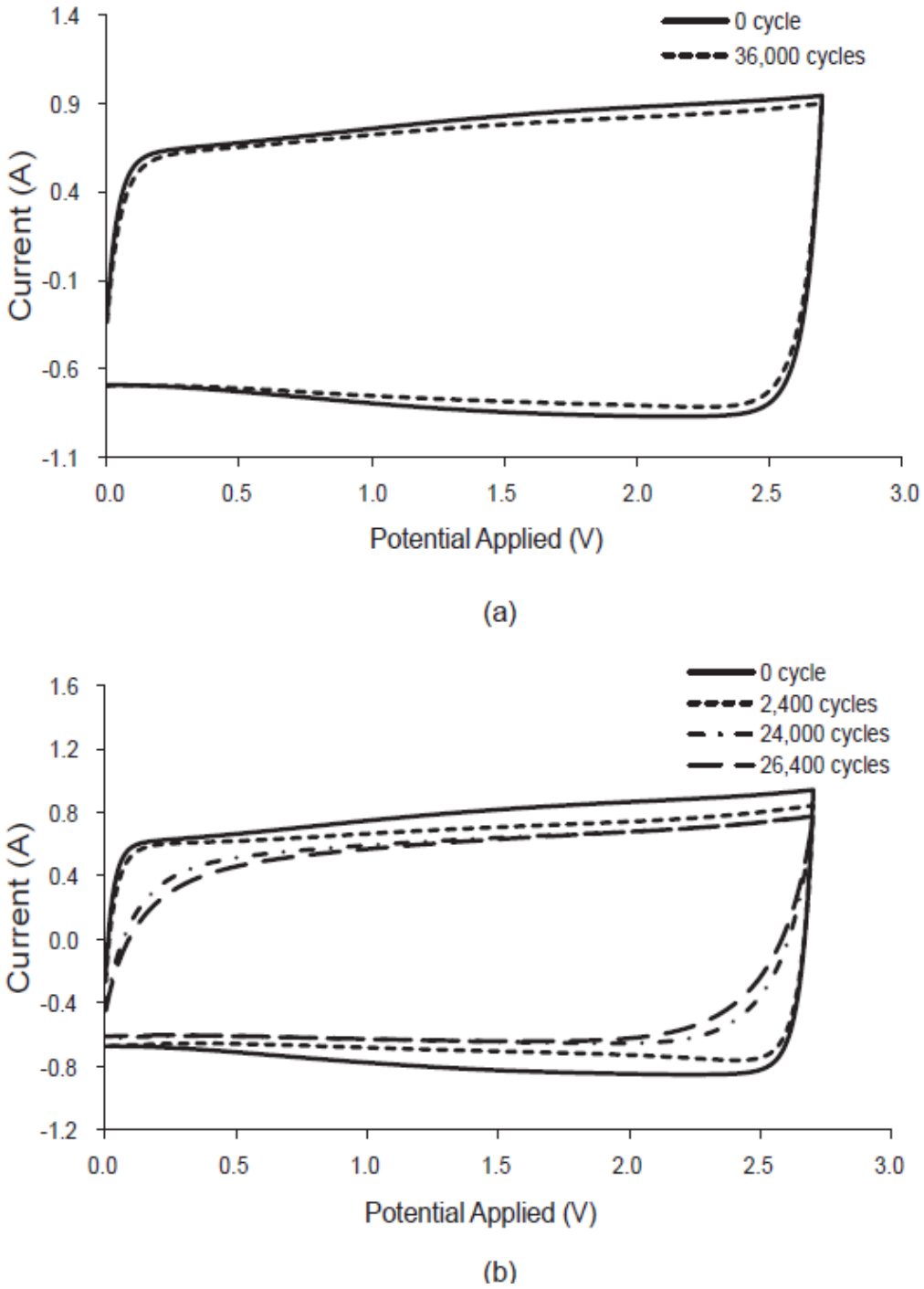

Fig. 5.11 Cyclic voltammograms at different stages of SC life during cycling test. The measurement was performed at 30 mV/s scan rate. (a) 0.6A, 20℃, and (b) 0.6A, 85℃.

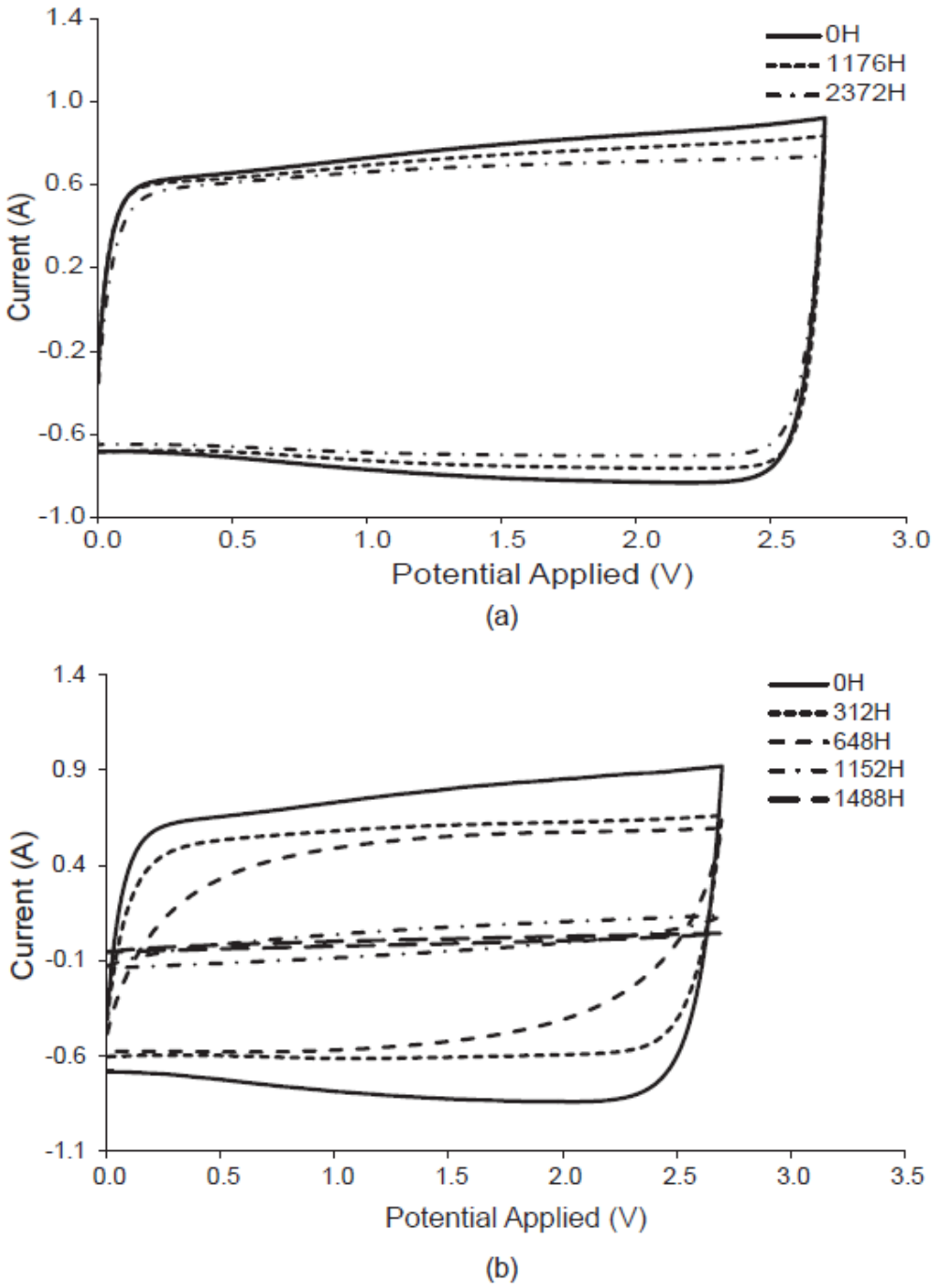

Fig. 5.12 Cyclic voltammograms at different stages of SC life during constant voltage test. The measurement was performed at scan rate 30 mV/s. (a) 2.7V, 20℃, and (b) 2.7V, 85℃.

C Constant current test results

To correlate the results from EIS measurements and CV tests with SCs electrical performances, it is appropriate to plot the charge and discharge characteristics. Fig. 5.13 to Fig. 5.15 show the voltage responses of the SCs to a 2A quasi-square charge/discharge current profile separated by rest period of 15s between charge and discharge before and after each accelerated ageing test.

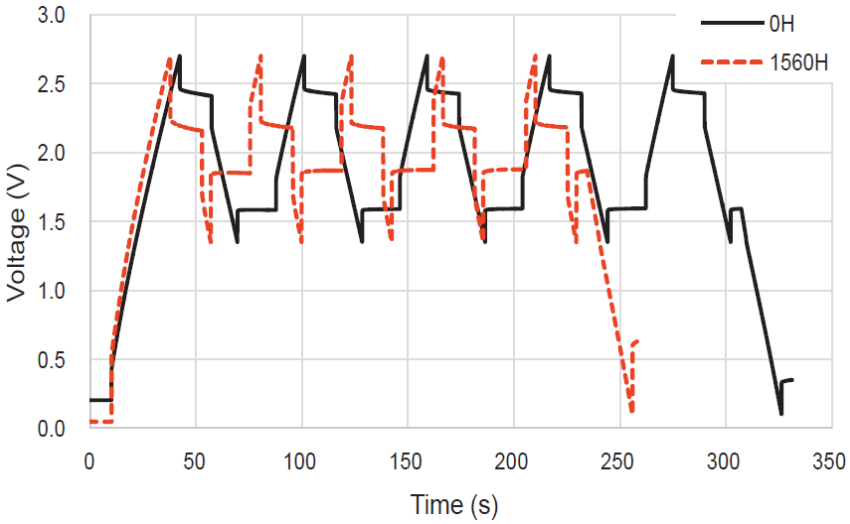

Fig. 5.13 SC voltage response to a 2A charge/discharge current profile after storage test at 85℃ (dashed line). Solid line is the initial response.

In all test conditions, the duration to charge and discharge decreased on aged SCs after ageing tests. The most affected were the SCs which were put under high temperature stress, such as in the storage test (Fig. 5.13), cycling (0.6A, 85℃) test in Fig. 5.14b and constant voltage (2.7V, 85℃) test in Fig. 5.15b.

Moreover, in conditions where two ageing factors were present, the ageing effect on SCs was egregious, evident in Fig. 5.14b and Fig. 5.15b. This finding was consistent to the CV test results presented earlier. The shorter

duration to charge and discharge the aged SCs suggested that the capacitance had decreased. Additionally, the shorter duration can also be contributed by the increase in ESR; it was observed that the voltage drop, pertaining to the ESR, increased in aged SCs. The voltage drop, i.e. the ESR, was the highest in SC from constant voltage (2.7V, 85℃) test (Fig. 5.15b) in comparison to SCs in other test conditions. It seems that whenever temperature and voltage are present, they exacerbate degradation in SCs.

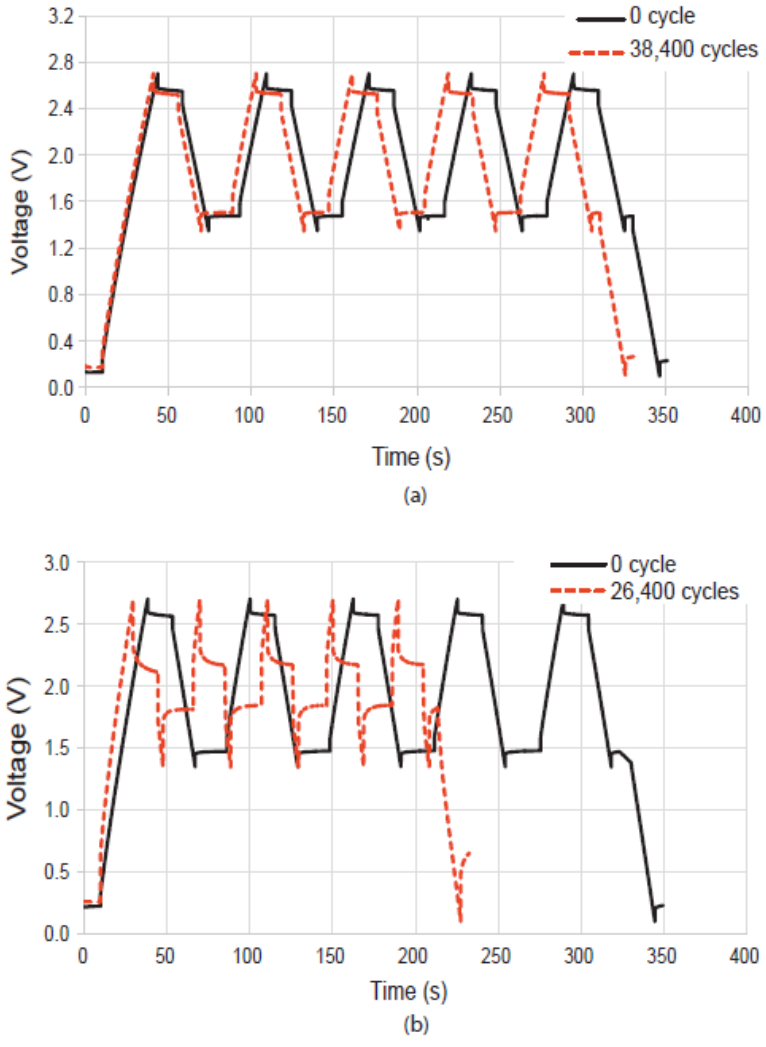

Fig. 5.14 SC voltage response to a 2A charge/discharge current profile after cycling test (dashed line): (a) 0.6A, 20℃, and (b) 0.6A, 85℃. Solid line is the initial response.

On the other hand, a minimal to no change in the amount of voltage drop was observed when there was an absence from temperature stress, as seen in Fig. 5.14a and Fig. 5.15a. In cycling test performed at 20℃, the voltage drop was faint, although charging and discharging duration became shorter after 38,400 cycles.

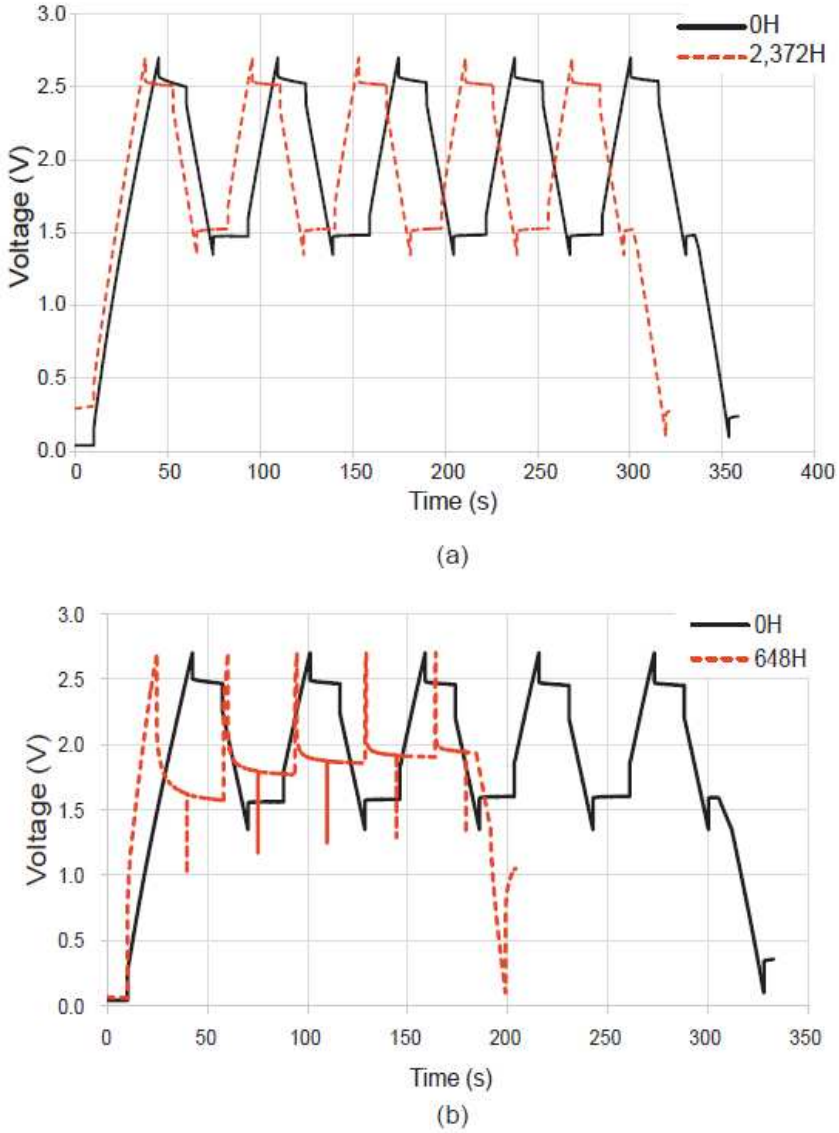

Fig. 5.15 SC voltage response to a 2A charge/discharge current profile after constant voltage test (dashed line): (a) 2.7V, 20℃, and (b) 2.7V, 85℃. Solid line is the initial response.

5.5 Visual Inspection and Post-mortem Analysis of Aged SCs

None of the test conditions had caused SCs to explode or fail abruptly. However, the SC in constant voltage (2.7V, 85℃) test experienced ‘can opening’ together with a bulge at the top of the casing after 648H in test. On the contrary, the SC in storage test showed no ‘can opening’ although the top of the casing also swelled.

Fig. 5.16 displays the damaged SC from constant voltage (2.7V, 85℃) test. The swelling at the top part of the cell, where an X-groove was located (Fig. 5.16a), was typically a result of an accumulation of gas inside the cell. The amount of gas led to the build-up of pressure in the cell, causing the expansion of the active chemicals. A close inspection of the cell showed a white residue on the groove, which can be attributed to a leakage of electrolyte. This observation showed that the casing did not only expand but also open up when the internal of the cell experienced increasing overpressure with time. The electrolyte then leaked out from the cell and evaporated through the groove. The whitish salt residue was a result from the reaction of the leaked electrolyte with air. The X-groove acted as a safety mechanism and a release vent to allow the escape of the gas, thus preventing an abrupt rupture to the cell.

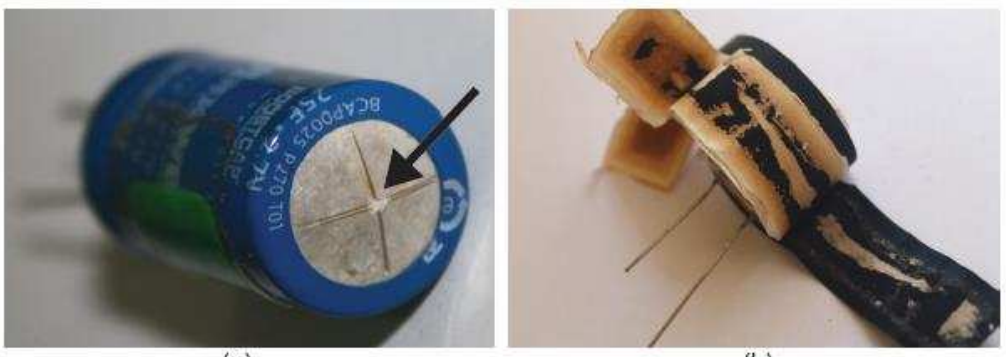

Fig. 5.16 Damaged SC after a long-term stress under 2.7V, 85℃: (a) white residue from electrolyte decomposition seen at the groove of the casing (arrow), and (b) a brown colouration on the separator was found when the cell was opened.

Fig. 5.16b shows the aged SC from (2.7V, 85 ℃) that had been dissembled. The aged SC was cut opened to reveal a separator that had been oxidised due to the accelerated ageing test. The oxidation of the separator appeared as a brown colouration, particularly at the side exposed to the positive electrode. Following disassembly of the cell, an embrittlement of the electrode was also detected, apart from the reduced adhesion of the electrode from the current collector to the separator. The SCs in other test conditions, however, did not show any oxidation on the separator when they were dissembled.

Kötz et al. (2010) showed that the amount of electrolyte loss can be calculated by the weight loss of the SC. Therefore, the SCs were weighed before and after each test and the result revealed that aged SCs experienced loss of electrolyte. The amount of loss was the highest in SC from constant voltage (2.7V, 85℃) which marked 1.45% loss, probably through the can opening. The amount of electrolyte loss in all SCs are presented in Table 5.1.

Table 5.1 The amount of electrolyte loss in percentage according to test conditions by weighing the SCs before and after tests.

Test Conditions	Loss Of Electrolyte (%)
2.7V,85℃	1.45
0.6A, 85℃	1.28
Storage Test at 85℃	1.14
2.7V,20℃	0.3608
0.6A, 20℃	0.3601

Fig. 5.17 displays the results from FESEM with energy dispersive X-ray (EDX) analysis on aged SCs after the ageing tests had stopped. The accelerated ageing tests caused a notable modification to the electrodes surface morphology, particularly on positive charged electrodes. The most striking modification was seen in SC from constant voltage (2.7V, 85℃) test. The aged positive electrode showed changes to the crystalline structure where larger crystals were formed. The surface of the electrode also has become less rough. It was also noticeable that the porosity of the positive electrode had reduced, most likely by the clogging of electrolyte degradation products at the pores. On the other hand, the size and shape of the particles of the negative electrode seems to hardly change. In other test conditions, such as the cycling (0.6A, 85℃) test and the storage test, ageing was also more pronounced in the positive electrodes than in the negative electrodes. The results of this analysis, therefore, show that ageing adversely affects the positive electrode than the negative electrode.

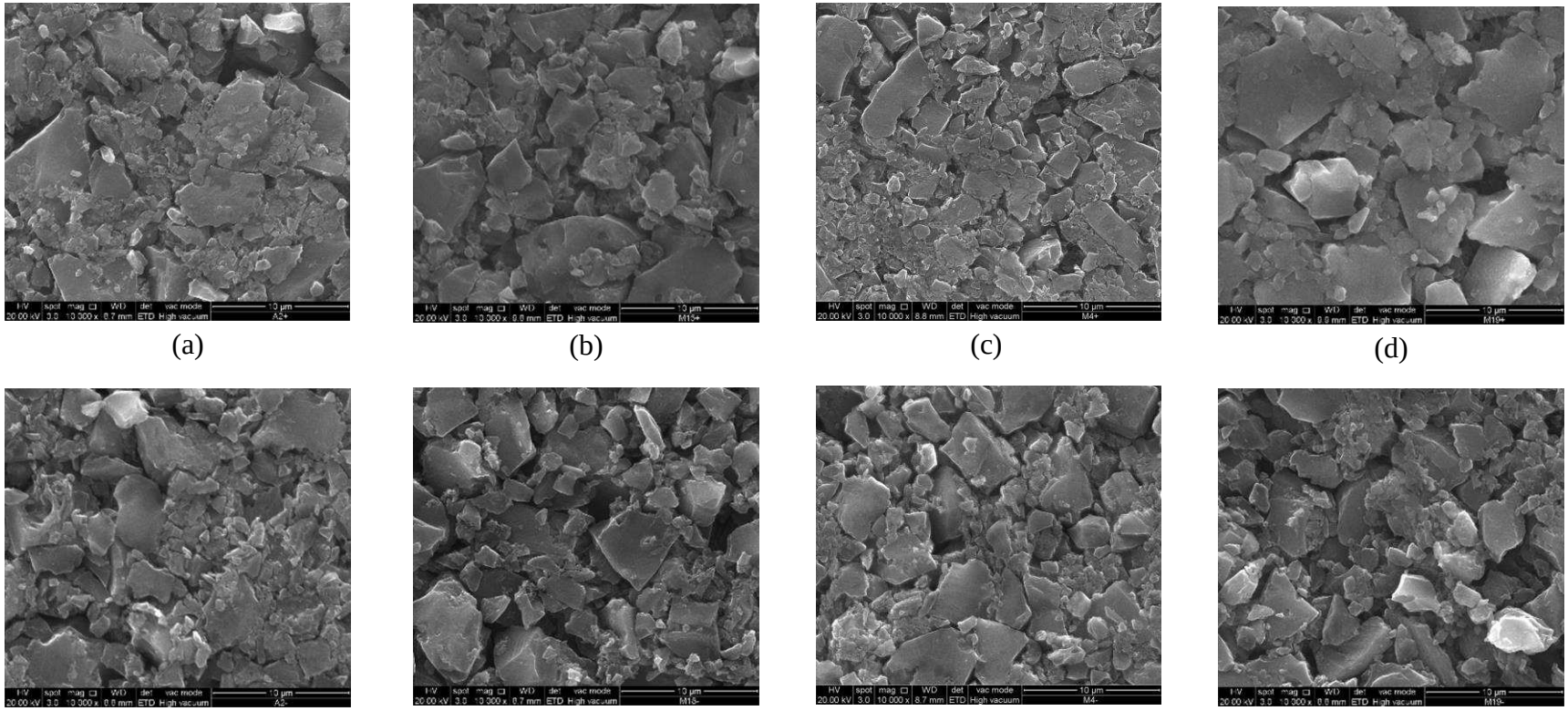

(a) (b) (c) (d)

(e) (f) (g) (h)

Fig. 5.17 Results from FESEM analysis at magnification of 10,000x: positive electrodes of (a) fresh sample, (b) storage test 85℃ (c) 0.6A, 85℃, (d) 2.7V, 85℃; negative electrodes of (e) fresh sample, (f) storage test 85℃, (g) 0.6A, 85℃, (h) 2.7V, 85℃.

Table 5.2 presents the relative atomic mass of all elements detected on the aged samples obtained from EDX analysis. The EDX analysis detected a small presence of aluminium oxide layer on aged electrodes which was not observed in fresh cells. It can be noticed that the amount of aluminium was higher in positive aged electrodes than in the negative aged electrodes. The highest aluminium content was detected at the positive electrode in SC from 2.7V, 85℃ test. The presence of aluminium oxide layer was assumed from the aluminium current collector and casing surfaces which contained a thin layer of oxide.

Table 5.2 Relative atomic mass of carbon, oxygen, fluorine and aluminium in (a) positive electrodes and (b) negative electrodes of aged SCs after the accelerated ageing tests.

(a)

Test Conditions	**Relative Atomic Mass (%)**			
	C	**O**	**F**	**Al**
Fresh Cell	83.99	2.26	13.75	-
Storage Test at 85℃	81.47	4.81	13.55	0.17
0.6A, 85℃	83.66	2.92	13.32	0.10
2.7V, 85℃	80.00	6.55	12.84	0.61
0.6A, 20℃	83.46	1.84	14.70	-
2.7V, 20℃	84.47	4.34	11.19	-

Table 5.2 Relative atomic mass of carbon, oxygen, fluorine and aluminium in (a) positive electrodes and (b) negative electrodes of aged SCs after the accelerated ageing tests. (continued)

(b)

Test Conditions	Relative Atomic Mass (%)			
	C	O	F	Al
Fresh Cell	84.70	2.55	12.75	-
Storage Test at 85℃	83.27	1.68	15.00	0.05
0.6A, 85℃	83.00	2.06	14.88	0.07
2.7V, 85℃	85.66	3.17	11.17	-
0.6A, 20℃	83.61	2.62	13.71	0.06
2.7V, 20℃	85.47	2.46	12.01	0.06

5.6 Comparison and Discussion

The loss of capacitance and the increase in ESR in aged SCs in all test conditions are compared in Fig. 5.18. The calculation of capacitance and ESR are according to Eq. (4.2) and Eq. (4.3), respectively, using the results in constant current test. It was found that the end-of-life (EOL) criteria for both capacitance and ESR were not reached at the same time.

The strong effect of both voltage and temperature in the constant voltage (2.7V, 85℃) test was clearly seen that the EOL criteria was reached the earliest at this condition. A drastic 20% loss in capacitance was monitored as soon as 480H, whereas a 100% increase of ESR was only seen after 900H. Similar effect was also observed in the cycling (0.6A, 85℃) test; the capacitance EOL criteria was met after 1,200H, as noted by the sharp yet steady drop throughout the

duration of the experiment. The ESR EOL criteria is projected to reach after 2,100H if the graph continues to rise steadily. In the storage test at 85℃, only the ESR was affected, in which the 100% increase of ESR was measured at 1,000H. Interestingly, the capacitance value did not show a marked degradation even after 2,500H in test, apparent by a gentle change in its value over the period of ageing.

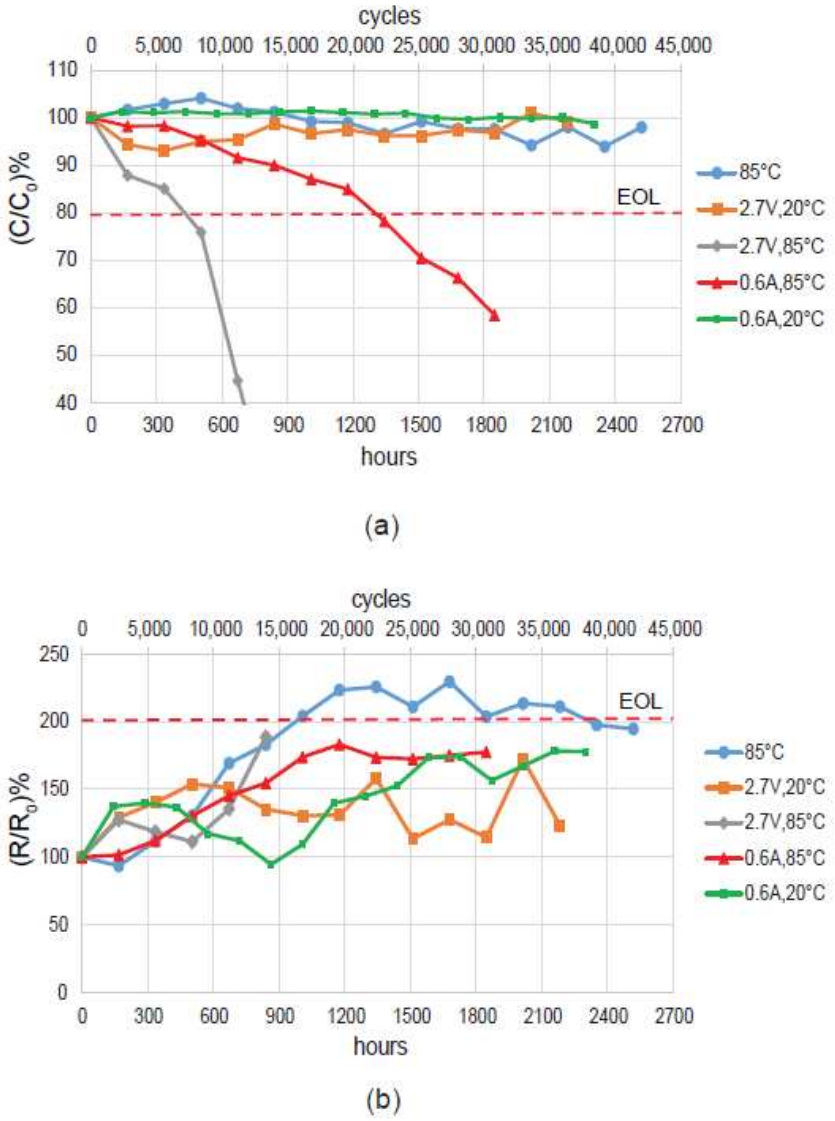

Fig. 5.18 Comparison between the evolutions of normalised parameters in all test conditions: (a) capacitance normalised to initial value, (b) resistance normalised to initial value.

Meanwhile, constant voltage (2.7V, 20℃) test did not show any remarkable change in capacitance after 2,100H (Fig. 5.18a). However, a fluctuation in the ESR was detected between 100% and 150% mark, although the ESR EOL criteria was not yet met after the test was stopped. Contrary to expectations, the cycling (0.6A, 20℃) test did not seem to affect the capacitance in which case, the capacitance value levelled off even after 38,000 cycles of charge and discharge. Nevertheless, the test condition had an effect on ESR, evident by an upward trend of the graph.

It is interesting to note that in all five conditions tested in this work, the SC reached its EOL, either in terms of capacitance and/or ESR, only in: (1) 2.7V, 85℃ test, (2) 0.6A, 85℃ test, and (3) storage at 85℃ test. This finding agrees with previous observations from the periodic characterisation test, hence, conforming the strong effect of these conditions on SC ageing. Note that, in the periodic characterisation test, the impedance spectra and the cyclic voltammograms were greatly affected in the said test conditions.

A possible explanation for these results may be the lack of adequate test time for both constant voltage (2.7V, 20℃) test and cycling (0.6A, 20℃) test to show any considerable effect on SC ageing. Furthermore, in both conditions, the temperature change in SC during test was merely to a small degree to have any significant influence on the cell properties. Moreover, in view of 500,000 to 1,000,000 cycles that are commonly required for commercial products to demonstrate a loss in capacitance or an increase in ESR, the demonstrated 38,400 cycles in the cycling test merely covered 4-8% of the aimed cycle life. A more aggressive charge-discharge regime is therefore recommended to observe a quicker degradation since the present current profile is proven to be rather

gentle on SC in which only 2℃ raise in the cell core temperature was recorded during the entire test duration. Meanwhile, the internal heating caused by constant voltage (2.7V, 20℃) test also did not cause enough warming to degrade the cell quickly. Nevertheless, cycling and constant voltage had indeed caused warming of the cell in the form of Joule losses, consistent to (Dandeville et al., 2011). Therefore, in the condition where the applied voltage or the cycling current used is relatively low, the ageing behaviour at a given temperature is mainly governed by the Arrhenius law (Uno and Tanaka, 2012), like for the case in cycling (0.6A, 85℃) test and constant voltage (2.7V, 85℃).

Nevertheless, the effect of cycling, constant voltage and temperature on SC impedance can be summarised take into three forms: (1) a shift of the impedance spectrum along real axis, (2) a continual growth of high frequency semicircle, and (3) a change in the slope of the imaginary part at low frequency. The shift of the impedance spectrum along the real axis is related to the increase of ohmic resistance over time. The ohmic resistance has typically been ascribed to the sum of resistance contributions from electrolyte, separator, current collector and electrode material and thickness (Masarapu et al., 2009). Therefore, the movement of the real part of the impedance along the real axis shows that the ageing process in SC increases the resistance of its internal components.

From the accelerated ageing test results, a semicircle has consistently appeared in all test where high temperature stress is present. The appearance of semicircle at SC impedance data is associated with an increase in contact resistance between the electrode and current collector (Kötz et al., 2010) and an increase in distributed resistance in the electrode (Ruch, Cericola, Foelske-Schmitz, et al., 2010). The appearance of semicircle has been reported to be

consistent to the formation of aluminium oxide and the delamination of electrode from the current collector (Kötz et al., 2010). The crystallisation of AN electrolyte also gives rise to the formation of semicircle in the complex plane at high frequency (Iwama et al., 2012). In fact, all of the causes of the development of semicircle in SC impedance data were found in the post-mortem analysis of the aged cells stressed at high temperature.

The delamination of the electrode due to high temperature stress showed that high temperature affects the bonding of the electrode to the current collector. Polymeric binder, which was added during the making of the electrode to promote adhesion of the carbon-mixture to the current collector in order to reduce the contact resistance between the elements in the electrode (Burke, 2000), so that the cell resistance is small, may have decomposed at high temperature and consequently reducing adhesion (Kurzweil et al., 2015).

Moreover, it had been monitored that the semicircle grew in diameter as a function of time; this phenomena showed that the contact resistance had progressively increased with ageing. That is, the contact between active material and the current collector deteriorates as SC ages. In addition, (Zhang, 2010) and (Gaberscek et al., 2008) have demonstrated the effect of poor interphase contacts on the size of the semicircle. Furthermore, the semicircle appeared when the SCs were still in test; this observation, in fact, proves that the appearance of the semicircle is a progressive effect of ageing stress on SCs, and it is not the after-effect of the ‘can opening’ as stated in (Kötz et al., 2010).

In addition to that, the reduced slope of the impedance imaginary part at low frequencies, together with the tilting of the impedance line from its original

response, was observed in test conditions involving cycling and constant voltage applications. The decreased slope and the tilting from the ideal capacitor response (an ideal capacitor will have an impedance spectrum with an angle of 90°), revealed that the phenomenon may arise from a decrease of a constant phase exponent (Bohlen et al., 2007a; Briat et al., 2010; El Brouji, Briat, Vinassa, Bertrand, et al., 2009). The constant phase exponent has been associated to inhomogeneity in the electrode, surface roughness and non-uniformity of the double layer thickness (Bohlen et al., 2007a), porosity and effective surface area (Briat et al., 2010), pore size dispersion (El Brouji, Briat, Vinassa, Bertrand, et al., 2009). The decrease of constant phase exponent and deviation from the capacitive behaviour suggest that there was a modification of the electrode structure—perhaps related to a change in pore size distribution as had been observed in (Song and Bazant, 2013; Song et al., 2000).

Since the deviation was only observed in tests involving cycling and constant voltage, this finding shows that cycling and constant voltage induce mechanical stress on the electrode in which these ageing factors cause obstruction of the pores (El Brouji, Briat, Vinassa, Bertrand, et al., 2009; Briat et al., 2010; Oukaour, Tala-Ighil, et al., 2013), thereby modifying the electrode structure. Briat et al. (2010) reported that a large amount of ions that flows during charging/discharging can affect the integrity of the porous electrode (Briat et al., 2010). This phenomena, therefore, leads to decohesion of carbon particles and consequently gives rise to the ESR. At the same time, the porous behaviour of electrodes is affected. Indeed, the decohesion of carbon particles had been observed in the post-mortem analysis.

Concerning the narrowing of cyclic voltammograms on aged SCs during the CV test, the changes to the CV waveshape show that the capacitance reduces as SC ages since the charge Q is the area between the CV curves and capacitance decreases as Q decreases. The change to the CV waveshape has been associated to the modification of chemical composition in the electrode surface in (El Brouji, Briat, Vinassa, Henry, et al., 2009). Additionally, this narrowing has also been related to the saturation of active surface area of the electrode material by the stored ions which contributes to a fading of capacitive current (Ratajczak et al., 2014). Moreover, during the constant voltage at high temperature (2.7V, 85℃) test, the 30mV/s CV scan rate had become too fast for the aged SC. A probable reason for this may be due to the electrochemical reactions in aged SC had slowed down.

From the electrochemical point of view, notable ageing mechanisms in SC can be deduced based on the two important ageing processes that had been observed during the tests and they are: (1) the emergence of high frequency semicircle, and (2) the tilting of the low frequency part of the impedance spectrum. The first ageing mechanism is proposed to be, according to point 1, the loss of contact within electrodes and also between electrodes to the current collector, hence increasing the contact resistance in aged SCs. Since this ageing mechanism was only observed in the condition where SC was exposed to high temperature, this observation reveals that this ageing mechanism is a product of long-term exposure to high temperature. Hence, when temperature is high, it affects the contact resistance in SCs.

The second ageing mechanism is the modification of electrodes pores, deduced from the observed tilting of the low frequency part on aged SCs as it

generally relates to the reduction of the slope, hence, the decrease of constant phase exponent. This ageing mechanism was only observed in conditions where SC was exposed to cycling or constant voltage application; on that note, this observation permits an interpretation that that this type of ageing mechanism is a distinctive result for applications involving repeated cycling or long-term constant voltage on SCs.

Moreover, through comparing the observations in electrochemical measurements (EIS and CV) with SC electrical performance, it was found that ESR increased in aged SCs that had semicircle in their impedance responses. This finding revealed the strong effect of contact resistance in the increase of ESR in SCs. In the same way, it was also found that the tilting of low frequency part also increased the ESR. It was interesting that SC suffered from capacitance loss only when both ageing mechanisms took place in SCs, i.e. when SCs experienced both an increase in contact resistance and a modification to the electrode pores and surface. If SC only shows one ageing mechanism, either the increase in contact resistance or the electrode pores modification, the increase in ESR is expected.

From the post-mortem results, the main cause of ageing in all aged SCs was identified to be due to electrolyte decomposition. The AN-based electrolyte, used in all SCs, decomposed at high temperature, leaving decomposition products which then caused deposition of unwanted substance on electrode surface. The deposition of these unwanted substances on electrode surface blocked the pores; thereupon, reducing the capacitance. The effect of blocked pores, due to these unwanted substances, to the loss of capacitance have been reported in (Azaïs et al., 2007; Jänes et al., 2012; Omar et al., 2014). In addition,

both (Azaïs et al., 2007) and (Zhu et al., 2008) reported a decrease of the electrode specific surface areas in aged SCs.

Moreover, the post-mortem results revealed a modification to the electrodes surface morphology and a formation of large crystals at aged positive electrodes, in particular. This may also be the effect from clogging of electrolyte degradation products at the pores. Besides, (El Brouji, Briat, Vinassa, Bertrand, et al., 2009) have stated that the ions mobility reduces as a consequence of the diminution of pores diameters. This modification increases the ESR and reduces the capacitance in aged SCs. Furthermore, the finding in this thesis is consistent to the results reported in the literature, whereby, ageing in SCs was indeed more profound at the positive electrode than at the negative electrode in SCs based on AN electrolyte, thus, agreeing to the ageing of SC is certainly dominated by the ageing of a single electrode as it has been stated in (Ruch, Cericola, Foelske, et al., 2010).

During the accelerated ageing test, the build-up of pressure in the SC cell due to chemical reactions of AN-electrolyte with the ageing factor caused the X-groove of the casing to open up to allow the accumulation of gas inside the cell to escape, thus, preventing any explosion. This 'can opening' act, however, did not only allow the escape of gas but also caused electrolyte to leak out of the SC. Although the analysis of the content of the gas was not conducted in this thesis, (Ruch, Cericola, Foelske-Schmitz, et al., 2010) and (El Brouji, Briat, Vinassa, Henry, et al., 2009) reported that the main gaseous decomposition product in $TEABF_4$/AN is CO_2. By the same token, (Azaïs et al., 2007) relate the emission of CO_2 to the binder decomposition. Nevertheless, consistent to (Zhu et al., 2008), the decomposition of electrolyte did indeed affect SC performance

in two ways: first, the active material was irreversibly consumed, which was also supported by the observed tilting in the impedance spectrum in EIS measurement, changes in the electrode surface morphology and the loss of weight of aged SC; and second, it was due to gassing and blockage pores that gave rise to the internal pressure within the cell. Moreover, Zhu et al. (2008) describe that this whole process is akin to the formation of the solid-electrolyte interphase (SEI) in lithium ion batteries.

In addition, the aluminium oxide layer found on aged SCs, whereby a high content was detected on positive electrodes, in particular, further verifies that the increase of contact resistance was also due to the accumulation of aluminium oxide layer on the electrode. Again, this finding is in line with (Kötz et al., 2010) where it is reported that the aluminium oxide gives rise to a semicircle, which in fact, is also observed in this thesis. The aluminium oxide was formed from the passivation of the current collector due to the accumulation of humidity and oxygen in the cell.

The results gathered from this study show that the isolation of ageing factors and studying the impact of each ageing factor individually have indeed enabled the identification of the ageing mechanism for each ageing factor in SCs. Each ageing factor affects SC ageing differently depending on the level of stress the SC is exposed to. Based on the results gathered here, temperature is the dominant ageing factor. Whereas, cycling and constant voltage have minimal effects on SC when they are applied separately. In spite of that, they can aggravate ageing when they are applied along with high temperature. This finding shows that cycling and constant voltage, which represent operational stresses on SC, play a secondary role in SCs ageing.

This view again is related to the amount of generated heat from these two ageing factors. Although both cycling and constant voltage induced heat generation within SC, they did not produce enough warming to cause ageing like those observed in high temperature test. Nevertheless, the effect of cycling and constant voltage on SC was still apparent though not as profound as the effect of high temperature. Cycling and constant voltage cause mechanical stress on SC, whereby after a long exposure to these ageing factors, they will cause structural changes to SC porous electrodes. In order to observe a quicker ageing a higher current, which can induce heat generation in SC close to the SC operational temperature limit, should be used.

5.7 Summary

This chapter reports the effect of constant voltage and cycling and the influence of high temperature in SCs ageing. The effect of each ageing factor was studied individually unlike the common method where many factors were studied at the same time. Based on the isolation of ageing factor and studying its effect individually, specific ageing process and ageing mechanism for each ageing factor were identified without the interference from other factors. Not only the results of this method aid in the identification of the cause of failure in SCs, the results also show the dominant ageing factor in SCs ageing. In addition, solutions can now be targeted individually based on which ageing mechanism is observed.

Each ageing factor has a distinctive impedance signature on SC performance; this brings up to two most notable ageing processes in SCs. These

ageing processes lead to the identification of two ageing mechanims in SCs. First, is the loss of contact within electrodes which gives rise to the contact resistance. Second, is the changes to SC porous electrodes. Each ageing factor has a distinct ageing mechanism: the increase of contact resistance is always consistent to the effect from a long-term exposure to high temperature and the changes to the SC porous electrodes is an effect from mechanical stress caused by a long-term cycling or contant voltage application.

It is also found that the increase in contact resistance in SC causes an increase in ESR, likewise, the modification of the electrode structure also gives rise to the ESR. This observation is true if only either one of these ageing mechanisms takes place in SCs. However, when SCs experience both of the ageing mechanims, only then, the capacitance is reduced. Besides, it is also found that the end-of-life criteria for ESR and for capacitance are not reached at the same time. Moreover, it depends on which ageing mechanism is dominating, based on the applied ageing factor.

Furthermore, the effect of ageing is more glaring on the positively charged electrode. Aluminium oxide layer has been detected on the electrode surface of aged SCs which are exposed to high temperature. Positive electrodes, in particular, contain a higher relative atomic mass percentage of aluminium than negative electrodes. The aluminium oxide is believed to have increased the contact resistance in aged SCs, besides other effects from decohesion of the carbon particles from the electrodes and the crystallisation of AN electrolyte. To recapitulate from the findings, the aim of this study has been achieved with the identification of SC ageing mechanisms in relation to the ageing factor.

CHAPTER 6

MODELLING SUPERCAPACITOR AND ITS AGEING BEHAVIOUR

"There are no facts, only interpretations."

—Friedrich Nietzche

6 Introduction

In the previous chapter, the main ageing mechanism has been identified by isolation of ageing factors that contribute to loss of SC performance. Accelerated ageing test has been used to increase the rate of ageing so that the ageing process can be monitored in a practical timescale for laboratory environment. The collected data can be used in the development of generic model for general evaluations of SC performance or in a more detailed modelling work that includes SCs ageing for a more comprehensive performance evaluation.

In this chapter, an electrical equivalent circuit (EEC) is proposed to model the effect of ageing factors on SC performance. The data collected in

Chapter 5 is used to build a baseline model. Then, from the observation that new processes occur in aged SCs, the baseline model is modified and updated to produce an ageing model. Therefore, the proposed EEC is divided into 2 parts: the baseline model and the ageing model. Moreover since it is found that the ageing process is specific to the ageing factor applied in the test, this requires a separation of the ageing model by ageing factor. Through continuous monitoring during the long-term test, the parameters that contribute to the observed anomaly in the impedance spectrum are identified and parameterised to uncover the process of ageing in SCs.

6.1 Supercapacitor Modelling

Ageing influences SC performance and it can be discerned through an analysis of the impedance spectrum that appears anomalous from the original response. In order to validate the comprehension of the ageing effects, it is appropriate to interpret the ageing data in Chapter 5 by means of electrical equivalent circuits (EECs). The method was done by fitting an EEC to the impedance spectrum.

Each impedance spectrum obtained by EIS was fitted to EECs using complex least-squares (CNLS) to obtain accurate values for the circuit components. This process was carried out on a commercial software Nova 1.10.3. As many circuit combinations can result in a similar impedance response, caution had been taken by analysing the fit of each circuit combination using chi-square, x^2 as an indicator of goodness of fit of the simulated response to the actual data. Estimated error produced by each component in the circuit was also

used to evaluate the significance of this component to the EEC and the overall response.

6.1.1 Baseline model

The impedance data in the form of a Nyquist plot, from a fresh SC is used to build a baseline model. The baseline model, hence, acts as a reference for any observed anomaly that may take place during the accelerated ageing test. The Nyquist plot of the fresh SC is shown in Fig. 6.1. The impedance measurement was carried out in a frequency range between 10kHz and 100mHz with 10mV AC amplitude signal.

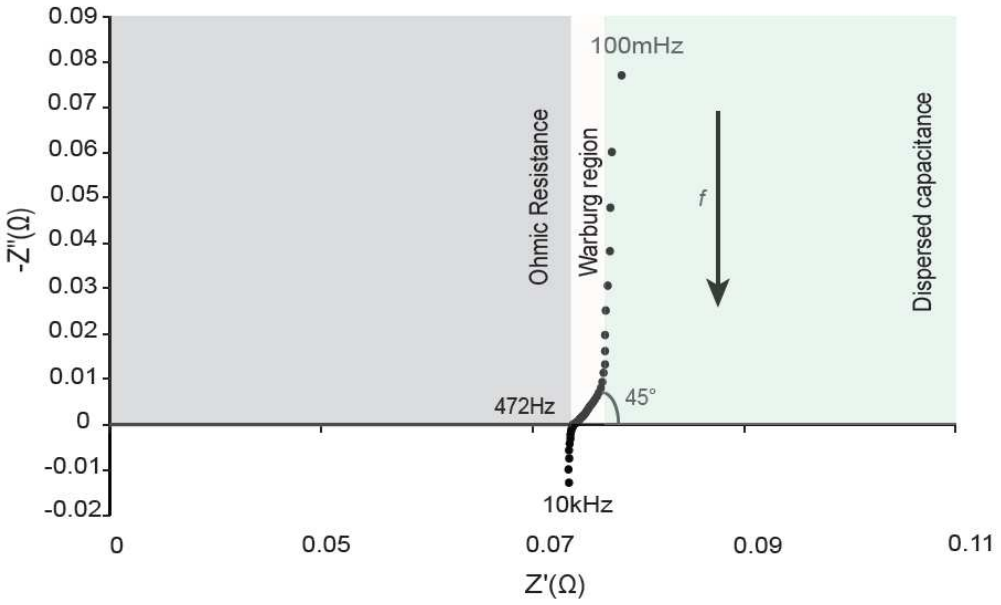

Fig. 6.1 Kinetic steps of a fresh cell as interpreted by electrochemical impedance spectroscopy at 0V DC bias, 10mV AC amplitude and frequency range 10kHz to 100mHz.

The modelling of the impedance spectrum in Fig. 6.1 is done through sectioning the impedance spectrum based on the kinetic steps, and accordingly,

three regions are identified: (i) ohmic resistance, (ii) Warburg region, (iii) dispersed capacitance. Noteworthy, since the inductive line at frequency range between 10kHz and 472Hz is small (of the order of nanohenries), the contribution is ignored in the development of the EEC. Nevertheless, the inductive line has been attributed to external artefacts such as external wiring and measurement system, and also due to the wound technology of the SC cylindrical cell (Lajnef et al., 2004).

A. Ohmic resistance

The intercept of high frequency impedance with real axis at 472Hz is the ohmic resistance and is represented by a series resistance, R_Ω (see Fig. 6.2). The ohmic resistance is the sum of cell internal resistance from various cell components including resistance from current collector, electrolyte, separator and electrode material and thickness (Masarapu et al., 2009; Stoller and Ruoff, 2010). As shown in Fig. 6.2, the Nyquist plot is shifted by an amount of R_Ω. This R_Ω also gives the value of the equivalent series resistance (ESR) by the relation given in Eq. (5.2) (Miller, 2006; Li and Chen, 2008).

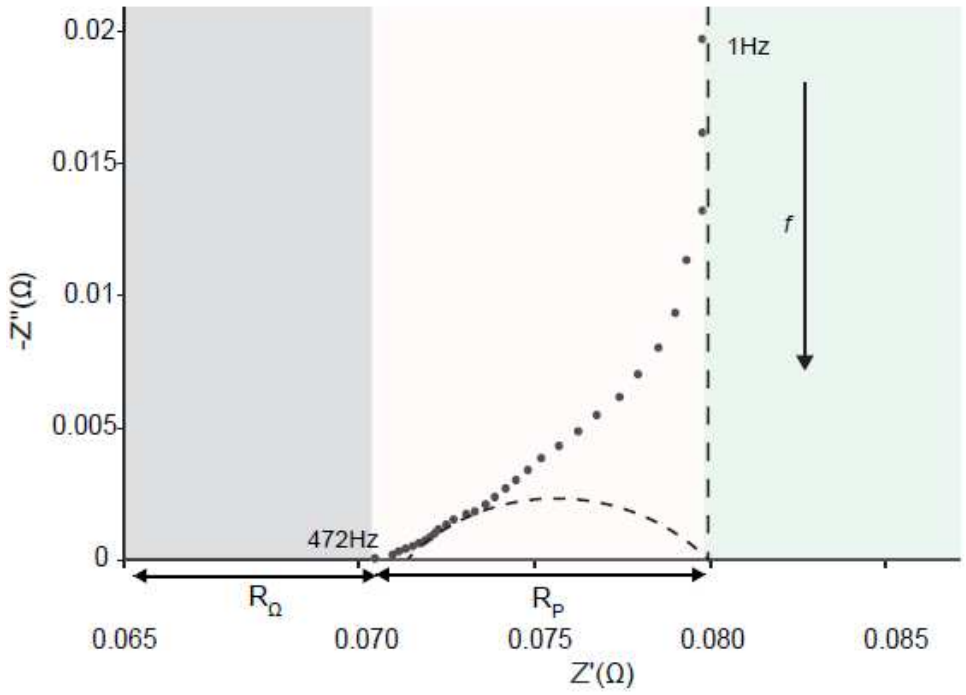

Fig. 6.2 Determination of ohmic resistance R_Ω and contact resistance R_P from the enlarged impedance spectrum (dotted line: experimental data, dashed line: drawn line used to determine R_P).

B. Warburg region

At medium frequency range where a 45° line reclines, is the Warburg region. The Warburg region is an indicative of a distributed resistance/capacitance in porous electrode (Kötz and Carlen, 2000) and it corresponds to a diffusion phenomenon. The 45° line is actually part of an arc of a semicircle but is depressed below the Z' axis. The semicircle can be generated with a parallel combination of resistor and capacitor. However, since the semicircle is depressed below the Z' axis, it is not plausible to simply use a capacitor to model this region.

As it has been shown in (García et al., 2010; Dzieliński et al., 2011; Quintana et al., 2006), this region is better characterised by a fractional-order

integrator. Furthermore, the Warburg region in Fig. 6.2 is not that of a true semicircle because it is depressed below the real axis, therefore, a CPE is considered to replace capacitor in the EEC. The impedance of CPE is given in Eq. (3.17).

The angle of depression of the semicircle can be accounted by the exponent n of the CPE term. When n is close to 1, the CPE behaves like a capacitor, although the phase angle is not 90°. Therefore, a resistor in parallel with a CPE having n equals to 1 will produce a semicircle that equals to that of a resistor in parallel to a capacitor. As n decreases, the semicircle is pushed below the Z' axis, as illustrated in Fig. 6.3. Thereafter, the circuit in Fig. 6.3a is employed to model this region.

The resistor R_P in Fig. 6.3a is the contact resistance which can be determined from the diameter of the semicircle. However in this case, only the arc of the semicircle is visible; therefore, R_P is determined by the diameter of the arc from the interception of the low frequencies vertical line to the abscissa axis, as illustrated in Fig. 6.2.

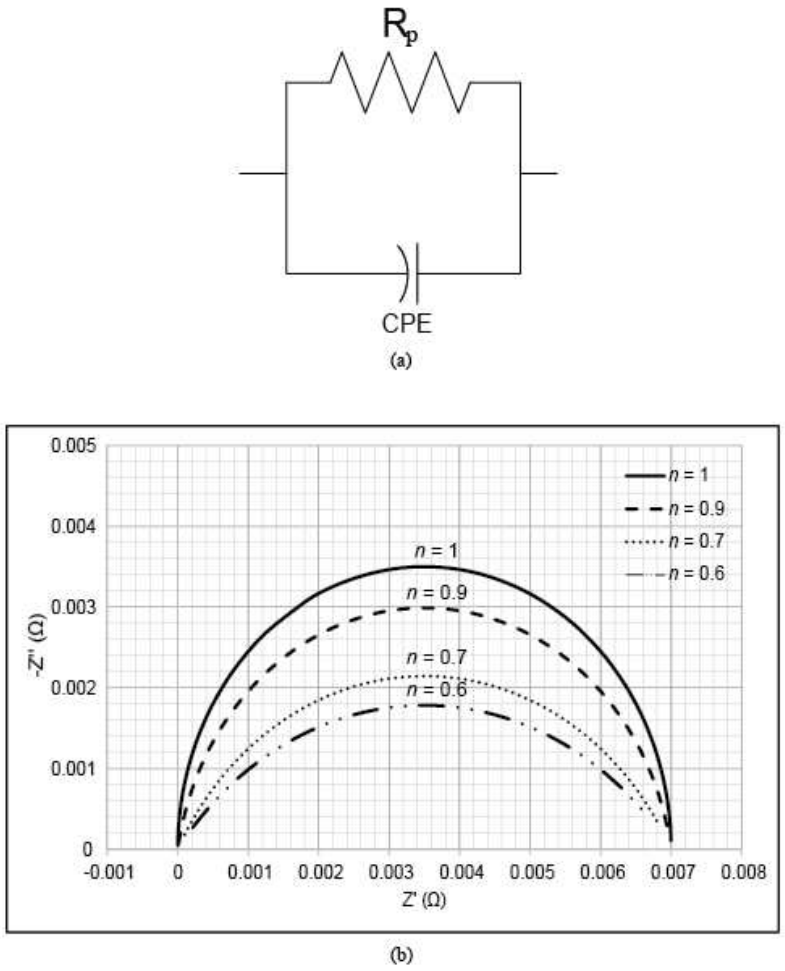

Fig. 6.3 CPE fractional exponent n, reflects the angle of the semicircle: (a) ZARC element consists of a resistor in parallel with a CPE used to model the Warburg region and (b) Nyquist plot of the ZARC element with various values of n.

Fig. 6.4 shows that the simulated response from the circuit model fits well to the experimental response at high frequencies. For comparative purposes, a simulated response from a resistor connected in parallel with a capacitor (R-C) is also included. As it can be seen, the parallel resistor and capacitor circuit overestimates the Warburg region. The fitting of the parallel R-C at this region can be improved by using a series connection of parallel resistors-capacitors such as in (Buller et al., 2002) or by using a ladder network

such as in (Fletcher et al., 2014). Nevertheless, it has been shown here that the parallel resistor-CPE (R-CPE) circuit yields a satisfactory fit and thus extricating from the need to use a circuit element consisting of a distributed resistors and capacitors which will only add to the complexity of the model.

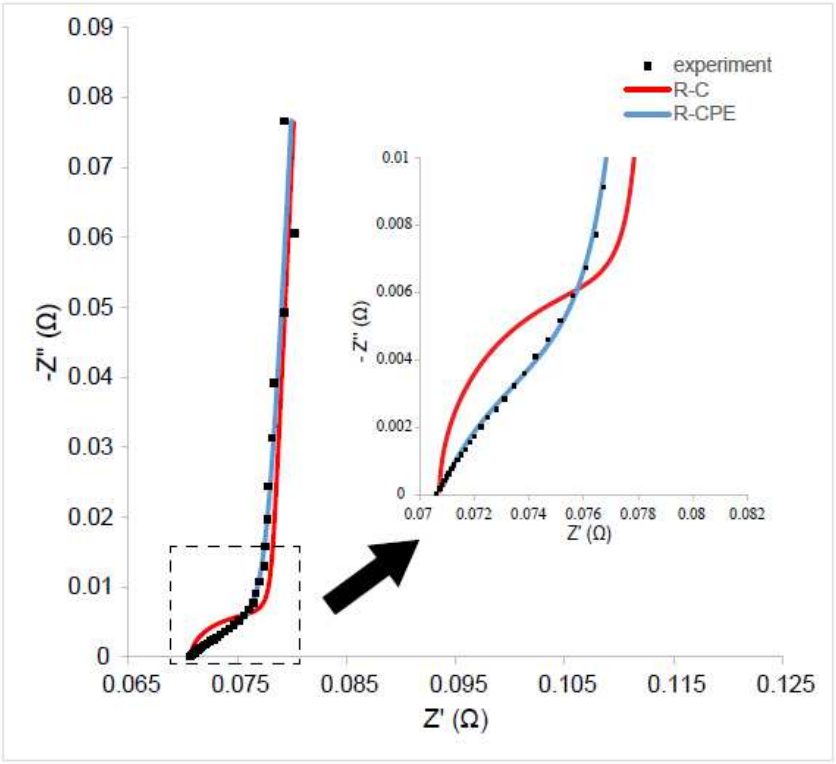

Fig. 6.4 Different fits of the Warburg region at high frequencies (inset) from a parallel combination of R-C (red line) and R-CPE (blue line). R-C overestimate the experiment data (dotted line) whereas R-CPE gives a satisfactory fit.

In this respect, if one needs to determine the effective capacitance from the parallel combination of R-CPE, the following relations can be derived based on the distributed time constant for the case of normal distributions [11] through a

[11] The distribution of the resistance and capacitance in SC porous electrode takes form of a normal distribution where the distributed time-constant behaviour can be expressed as a summation of impedances (Hirschorn et al., 2010).

surface layer (Hirschorn et al., 2010) illustrated in Fig. 6.5, i.e. the time constant in the normal distribution is given by,

$$\tau^n = \left(R_p C_{eff}\right)^n \tag{6.1}$$

and the semicircle can be described mathematically by the following impedance form (Raistrick et al., 2005),

$$Z_{arc} = \frac{R_p}{1+(j\omega\tau)^n} \tag{6.2}$$

where R_p is the low frequency intercept at real axis and $0 \leq n \leq 1$.

Since, the semicircle can be reproduced with a parallel combination of resistance R_p and CPE (Orazem et al., 2002) and therefore yields,

$$Z_{RCPE} = \frac{R_P}{1+ Y_0 R_P (j\omega)^n} \tag{6.3}$$

Comparing Eq. (6.2) with Eq. (6.3), the effective capacitance can thus be determined as such,

$$\tau^n = Y_0 R_P \tag{6.4}$$

$$\left(R_P C_{eff}\right)^n = Y_0 R_P \tag{6.5}$$

which is equivalent to

$$C_{eff} = \frac{(R_P Y_0)^{1/n}}{R_P} = \left(Y_0 {R_P}^{(1-n)}\right)^{1/n} \tag{6.6}$$

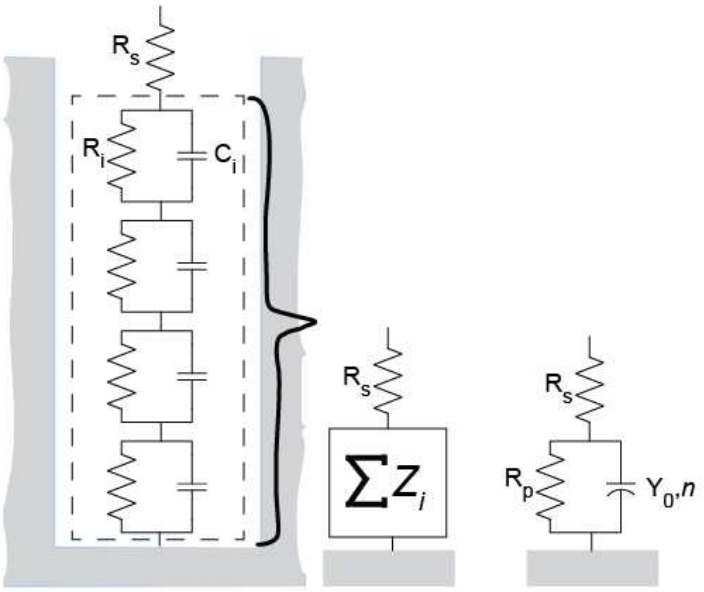

Fig. 6.5 Schematic representation of a normal distribution of time constants of distributed resistors and capacitors inside a pore (also known as 'in-a pore dispersion'[12]). The parallel combination of resistors and capacitors can be expressed as a CPE. Adapted from (Hirschorn et al., 2010).

C. Dispersed capacitance

The third region marked in Fig. 6.1 exhibits a frequency dispersion characteristic. The low frequency line departs from the behaviour of an ideal capacitor which should draw a vertical straight line in the complex plane. The capacitance graph in Fig. 6.6 shows that the capacitance of a SC is frequency-dependent with the highest capacitance is achieved at low frequencies. This observation prevents the use of a conventional capacitor to model this region. Instead, what is needed is a model that can describe the capacitive dispersion

[12] Song, H.-K., Hwang, H.-Y., Lee, K.-H. and Dao, L.H. (2000) 'The effect of pore size distribution on the frequency dispersion of porous electrodes', Electrochimica Acta, Vol. 45 No.14, pp.2241–2257., DOI:10.1016/S0013-4686(99)00436-3

effect. Nonetheless, the simulated response of a resistor and a capacitor connected in series is drawn in Fig. 6.7 for comparison purposes. Even if a series capacitor is added to the parallel connection of a resistor and a CPE (refer Fig. 6.7b), the circuit combination still produces a poor fit at low frequency region.

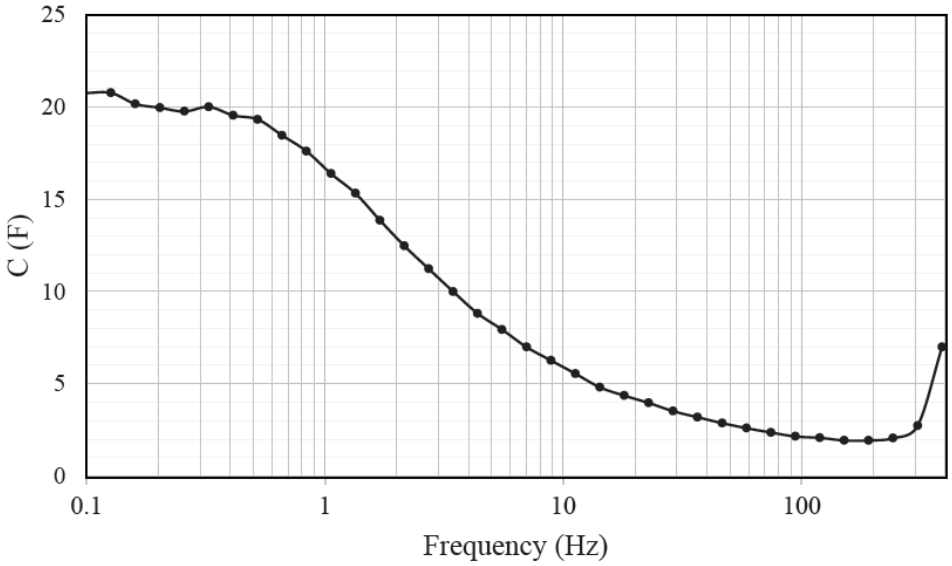

Fig. 6.6 Capacitance of a fresh SC shows a clear dependency on frequency. At low frequencies, the capacitance increases.

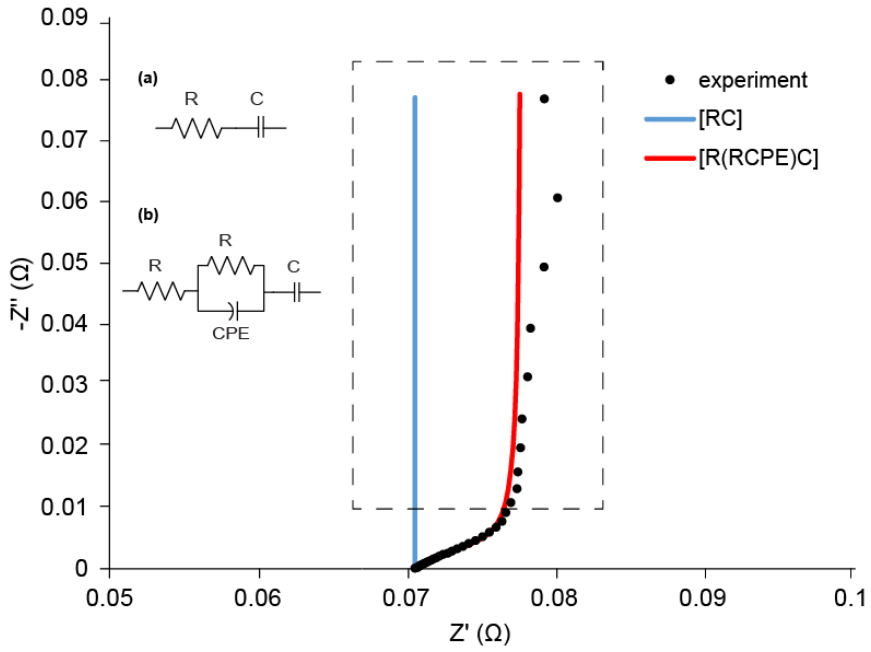

Fig. 6.7 Impedance response from experiment (dotted line) is compared against different combinations of equivalent circuits used for the simulation of the impedance response. The blue line is the simulated response from circuit (a) and the red line is the simulated response from circuit (b). Both circuits show a poor fit.

The frequency-dependent behaviour in SCs shows a 'distributed characteristic' or 'frequency dispersion' of electrical properties (Song et al., 1999). The frequency dispersion occurs due to many reasons; one of them being that the pore lengths are longer than the penetration depth of the AC signal, thus, contributing to a 'in-a-pore dispersion' (see Fig. 6.8) (Song et al., 2000). The frequency dispersion due to the 'in-a-pore dispersion' can be seen when the penetration depth of the AC signal is low, usually at high frequency; for the case of SCs, this is seen at the Warburg region. Besides the effect of 'in-a-pore dispersion', the frequency-dispersed behaviour is also caused by the geometric heterogeneity of the porous electrodes like roughness or distribution of pore

sizes (Song et al., 1999). Song et al. (2000) showed that the frequency dispersion at low frequency (high penetrability of AC signal) in highly porous electrode and no Faradic reactions electrochemical systems is due to the effect of pore size distributions (PSD) (see Fig. 6.9) (Song et al., 2000). The PSD, which causes the vertical line at low frequency to deviate from the 90° angle, is in fact a result from "…a vector sum of the in-a-pore dispersions for each pore…"[13] of the porous electrode. Likewise, particle geometry and size distribution also affect the impedance at low frequency in battery electrodes (Song and Bazant, 2013).

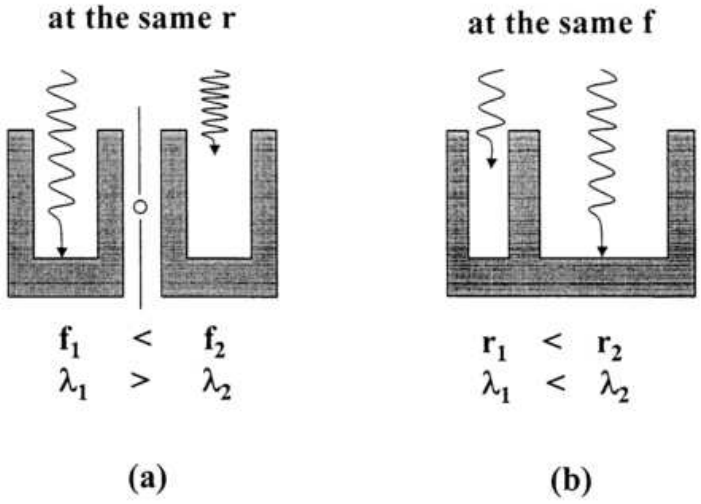

Fig. 6.8 Two types of frequency dispersions in porous materials. (a) In-a-pore dispersions where the penetration depth in a pore, λ, decreases with frequency of the AC signal and (b) by-PSD dispersion where different penetrations depth at the same frequency occurs in pores with different dimensions (Song et al., 2000).

[13] Song, H.-K., Hwang, H.-Y., Lee, K.-H. and Dao, L.H. (2000) 'The effect of pore size distribution on the frequency dispersion of porous electrodes', Electrochimica Acta, Vol. 45 No.14, pp.2241–2257., DOI:10.1016/S0013-4686(99)00436-3

In addition, surface roughness also contributes to the inclined line (Pajkossy, 2005). The rougher the surface, the farther the line is driven away from the ideal capacitive behaviour. Therefore, the capacitance dispersion is an indicator for that there is something which exerts resistance to the charge movement (Pajkossy, 2005). This is certainly true since the size of the pore determines the penetration depth of the AC signal (Fig. 6.8). As the penetrability of the AC signal increases with decreasing frequencies in a pore with large radius, the impedance line approaches the ideal capacitive behaviour—the AC signal can effectively charge the entire surface of the pore (Song et al., 2000; Song and Bazant, 2013). However, this is not the case for SCs. As it has been discussed in Chapter 2, the surface area of SC porous electrodes is never homogenous nor smooth and that the surface area is made up of pores of irregular sizes ranging from macro-. meso- and miro-pores. Therefore, an inclined line almost approaching a vertical line is always observed.

CPE and fractional differential equation have been used to describe the frequency dispersion of capacitance in (Song et al., 2000; García et al., 2010; Kötz and Carlen, 2000; Quintana et al., 2006; Dzieliński et al., 2011). Moreover, Jović and Jović (2003) showed that the fractional exponent of CPE has an influence on the differential capacitance, depicted in Fig. 6.9 (Jović and Jović, 2003). In that regard, the influence of CPE fractional exponent on the low frequency line is also simulated in Fig. 6.10. As it can be seen, the inclination of the low frequency region is better explained with the CPE fractional exponent, in which a conventional capacitor does not make possible. Therefore, the capacitive dispersion at low frequency is more reasonably modelled with a CPE,

instead of a capacitor. On that note, the series capacitor in circuit (b) of Fig. 6.7 is replaced with a CPE.

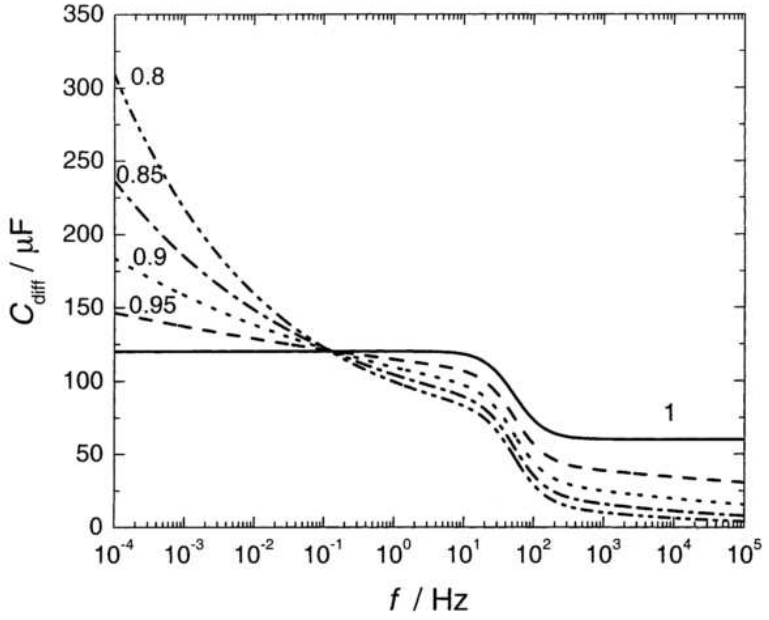

Fig. 6.9 The influence of CPE fractional exponent on the differential capacitance (Jović and Jović, 2003).

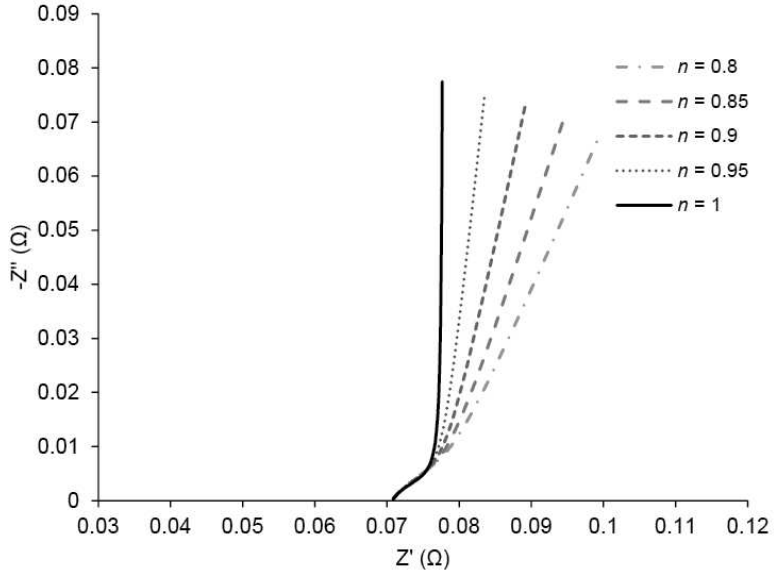

Fig. 6.10 The influence of CPE fractional exponent on the inclination of low frequency line. The CPE behaves like a capacitor when $n = 1$ and is depicted by a vertical line in the complex plane.

D. The proposed baseline model

The model used to describe SC is therefore presented in Fig. 6.11. Complex nonlinear least squares (CNLS) is performed on the EEC model using Nova 1.10.3 by simultaneously fitting the data to find the circuit parameters. A start value for each circuit component is given to the Nova 1.10.3. The start value can be roughly estimated based on the response at the complex plane. Then, the application will iteratively modify and refine these values until a satisfactory fit is achieved.

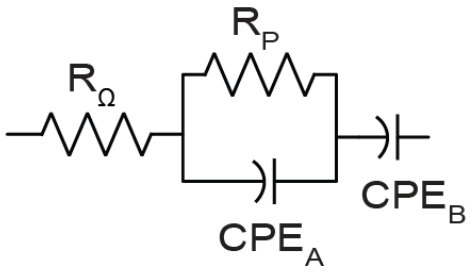

Fig. 6.11 The baseline model in the form of electrical equivalent circuit.

Nova 1.10.3 reports estimated error of each component which represents the margin of confidence of the calculated value of the component (Autolab, n.d.). Therefore, the effect from adding each circuit component in the model to describe the experimental data can be analysed by comparing the experimental data with simulated data and analysing the error estimated for each inclusion of circuit component.

In addition, chi-square value, x^2, which is a measure of the goodness of fit, is also used to analyse if the fitting is good. In this way, it prevents extra terms or unnecessary components from being added to the EEC model to describe the impedance data to obtain a small chi-square value. For instance, in

this work a chi-square value between 10^{-1} and 10^{-4} is often observed, although in some reported work the chi-square value can be as low as 10^{-6}, such as in (Dhirde et al., 2010). This is because, even though the model will look correct in form, the extra component will make the fitting more flexible than it should and hence, CNLS will attempt to describe the variation in the data, which may be due to measurement error, to a certain electrochemical process.

The same modelling process is also performed on SCs from two other manufacturers in order to verify that the proposed model is universal and applicable to all cylindrical type SCs. The fitted parameters are summarised in Table 6.1 and the results from each fitting are presented in Fig. 6.12 to Fig. 6.14. The impedance of the baseline model in Fig. 6.11 can be expressed by:

$$Z = R_{\Omega} + \frac{R_P}{1+R_P \cdot Y_A(j\omega)^{nA}} + \frac{1}{Y_B(j\omega)^{nB}} \tag{6.7}$$

Table 6.1 Circuit parameter values of the proposed baseline model for supercapacitors from three manufacturers. x^2 is the chi-square and the value in bracket is the estimated error expressed in % of each circuit parameter.

Elements		Fitted value		
		Maxwell Technologies BCAP0025 A (2.7V/25F)	Cornell Dubilier EDLHW226DRER B (2.3V/22F)	Vina Technologies VEC2R5256QG C (2.5V/60F)
$\mathbf{R_\Omega(\Omega)}$		0.070729 (0.167%)	0.043488 (0.404%)	0.037334 (0.667%)
$\mathbf{R_p(\Omega)}$		0.0071778 (6.306%)	0.017155 (4.939%)	0.02199 (15.379%)
$\mathbf{CPE_A}$	Y_A(mho)	13.315 (12.751%)	12.678 (8.386%)	24.813 (9.497%)
	n_A	0.70942 (5.130%)	0.64218 (4.189%)	0.48131 (6.956%)
$\mathbf{CPE_B}$	Y_B(mho)	20.659 (0.423%)	27.452 (0.750%)	56.283 (2.434%)
	n_B	0.98113 (0.443%)	0.9881 (0.323%)	0.998 (0.786%)
$\mathbf{x^2}$		4.0958×10^{-4}	4.615×10^{-3}	6.9684×10^{-3}

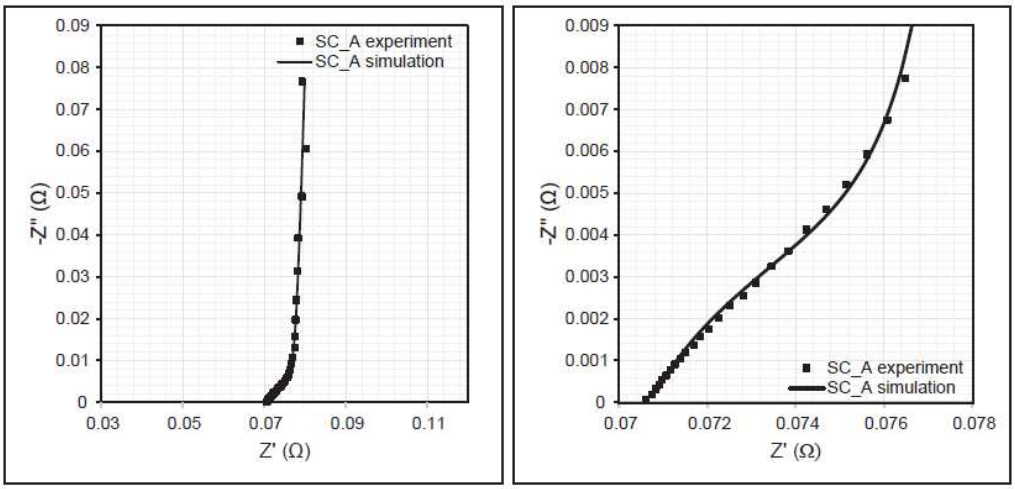

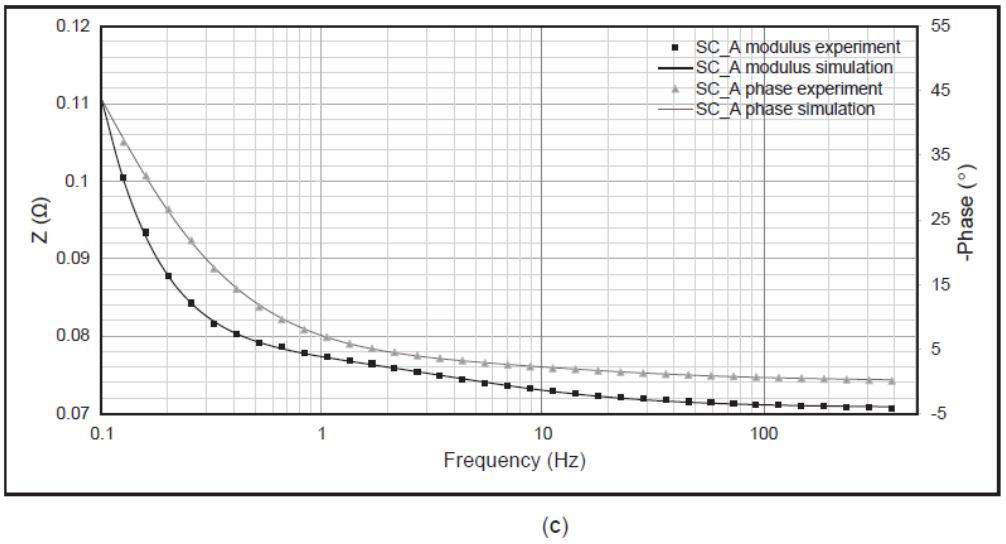

Fig. 6.12 Results from the fitting of supercapacitor A (2.7V/25F): (a) Nyquist plot, (b) enlargement segment of (a), and (c) bode plot. The dotted lines are from experiment and the solid lines are from simulation.

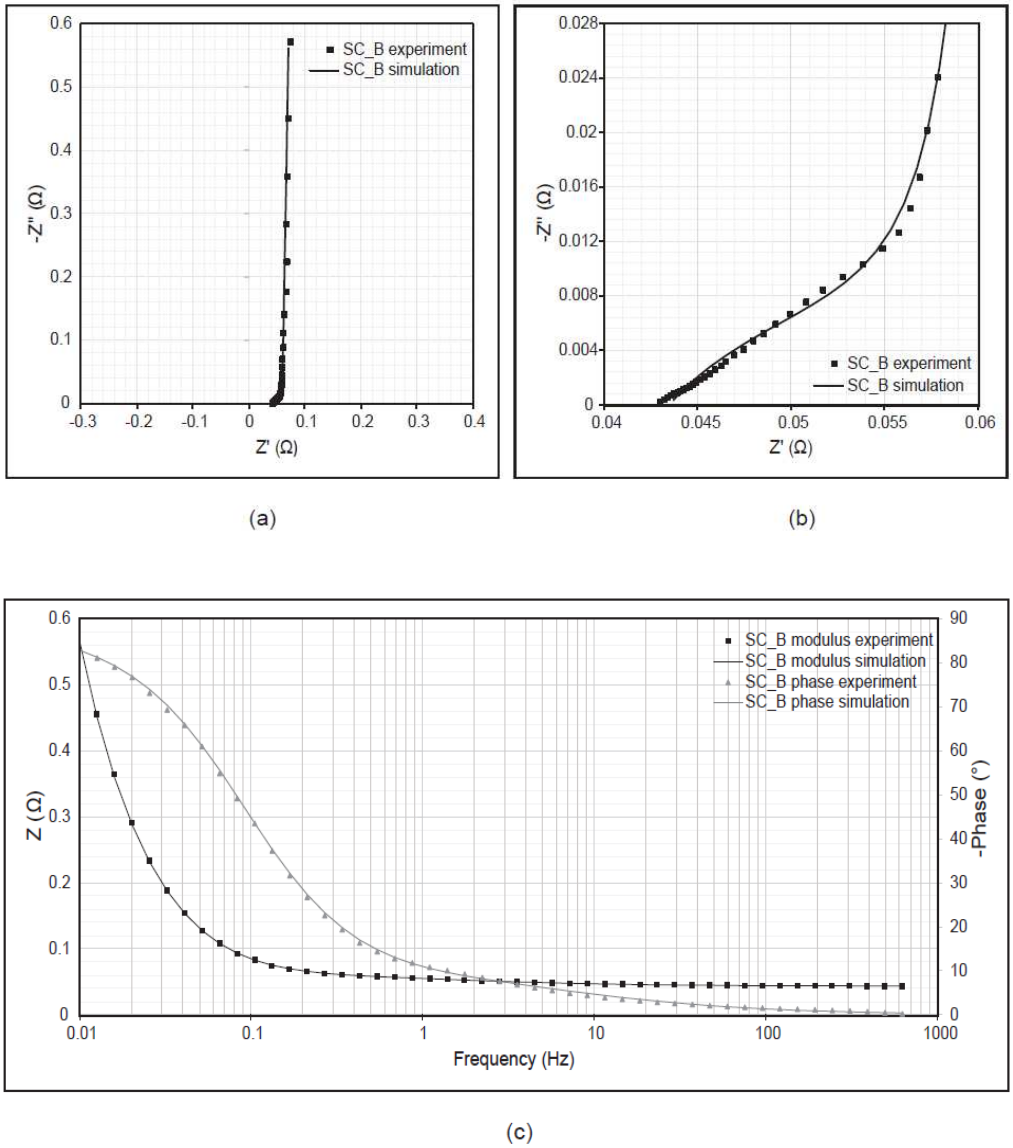

Fig. 6.13 Results from the fitting of supercapacitor B (2.3V/22F): (a) Nyquist plot, (b) enlargement segment of (a), and (c) bode plot. The dotted lines are from experiment and the solid lines are from simulation.

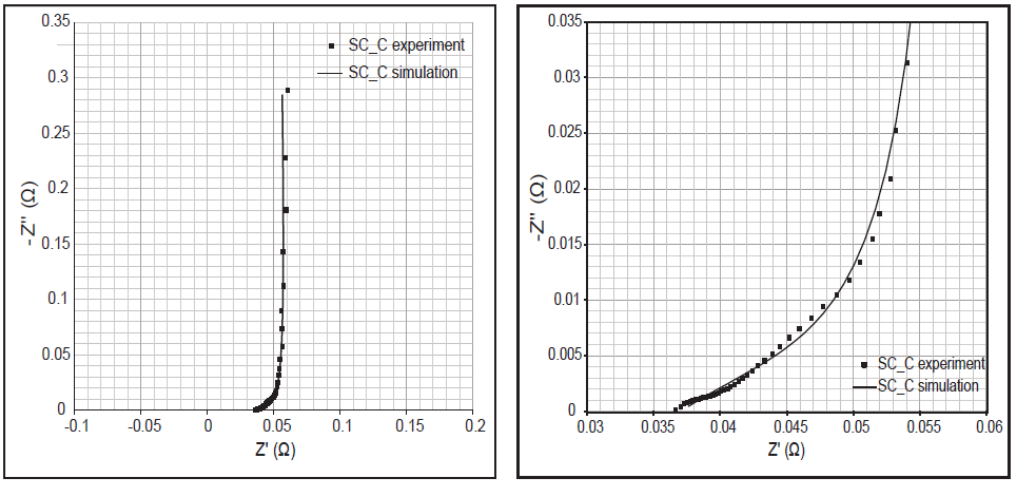

(a)

(b)

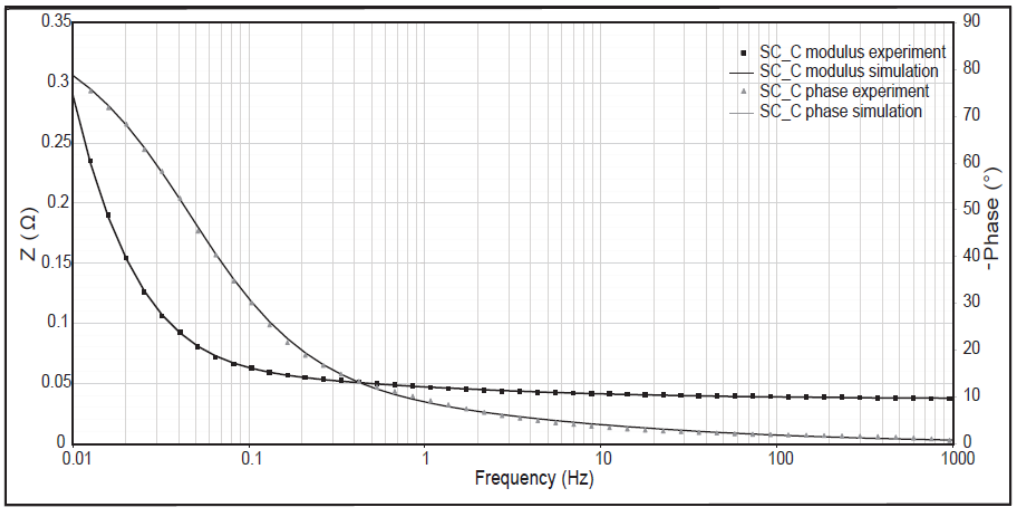

(c)

Fig. 6.14 Results from the fitting of supercapacitor C (2.5V/60F): (a) Nyquist plot, (b) enlargement segment of (a), and (c) bode plot. The dotted lines are from experiment and the solid lines are from simulation.

6.1.2 Ageing models

In Chapter 5, it was demonstrated that the deterioration of active materials due to ageing causes changes in SC electrical behaviour and the effect of this deterioration is also perceptible in SC response at the complex plane. From the

data gathered in Chapter 5, ageing models are developed to illuminate the ageing characteristic and to assess the impact of ageing on the SCs dynamic behaviour.

The ageing model is built by fitting an EEC to the impedance response. Therefore, the observable ageing mechanisms can be reflected on the model and also aids in elucidating electrochemical processes that take place during ageing. Moreover, the ageing model will enable the relation between the ageing process in SC and its electrical behaviour to be understood.

It is found that the ageing process is specific to the applied ageing factor, thus requiring a separation of the ageing model according to ageing factors. For that reason, two ageing models are proposed based on the test condition and ageing factors tested in this thesis. Similar to the modelling process carried out to obtain the baseline model in subsection 6.1.1, CNLS is applied during the fitting of the ageing models to obtain accurate values for the circuit components. The process is done using NOVA 1.10.3.

6.1.2.1 Ageing due to storage at high temperature and current cycling at high temperature

The response of aged SCs from storage test at high temperature (Fig. 6.15a) and cycling test at high temperature (Fig. 6.15b) have both veered from the initial spectrum (Fig. 6.1). The kinetic steps of electrochemical processes labelled on the impedance spectrum shows the presence of new electrochemical processes in aged SCs. The baseline model will no longer be suitable for the new response. Therefore, the baseline model is revisited to include this response. This process leads to the development of ageing model to reflect the ageing state of SC.

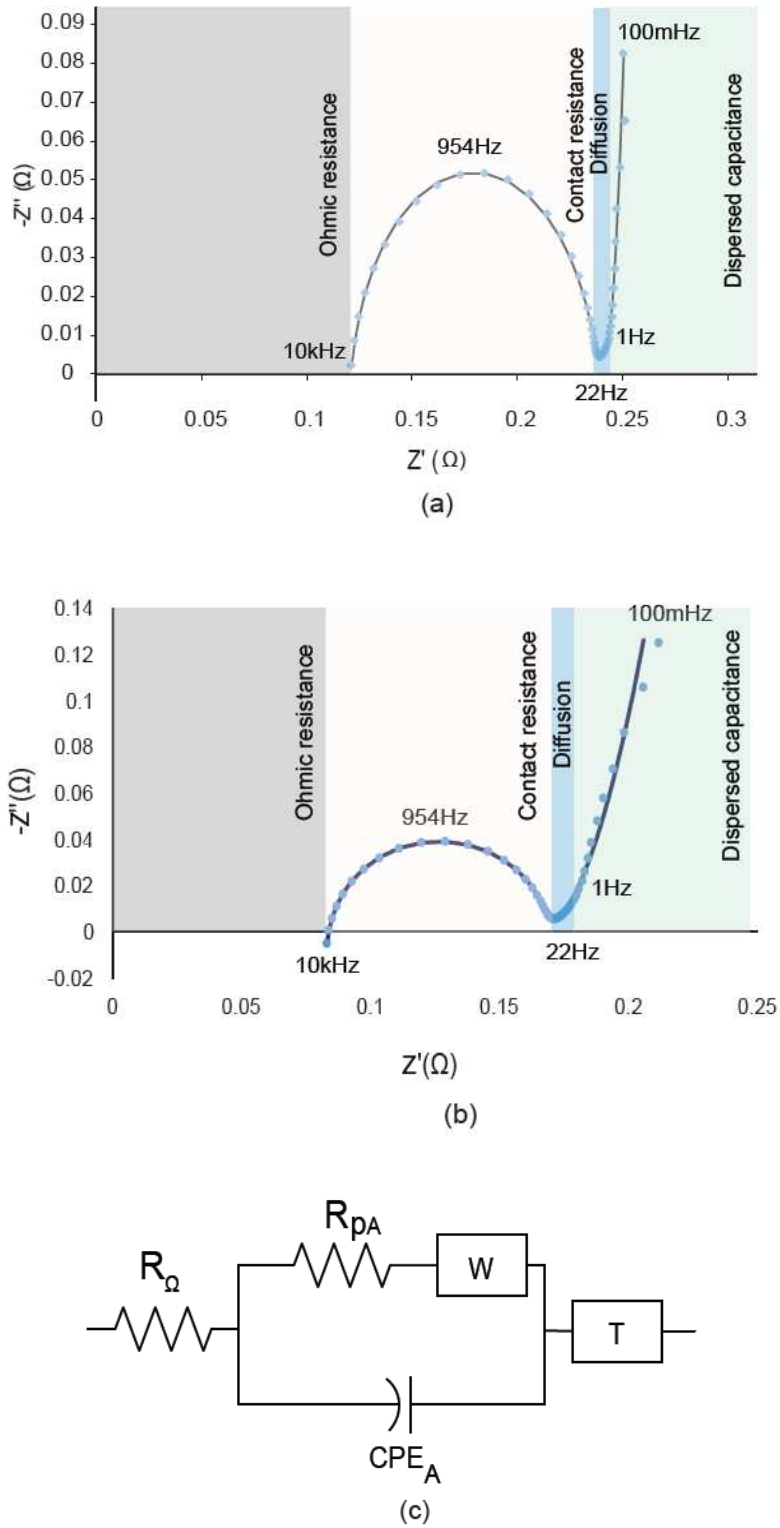

Fig. 6.15 Impedance spectrum of aged SCs (a) after 1,392H in storage test at 85℃, (b) after 26,400 cycles in cycling test 0.6A, 85℃, and (c) is the electrical equivalent circuit used to simulate the impedance spectrum. (Dotted line: experimental data; solid line: simulation from the circuit).

Since the responses from both test conditions are almost identical, only Fig. 6.15b will be discussed to avoid repetition. The high frequency intercept (10kHz) corresponds to the value of the ohmic resistance, R_{Ω}. This resistance is usually related to the resistance from current collector, electrolyte and separator. The second electrochemical process is the contact resistance between electrode and current collector, marked by a semicircle with its centre below the real axis at frequencies between 10kHz and 22Hz. The semicircle can be drawn with a ZARC element which consists of a parallel connection resistor R_{PA} and a CPE. The third process which occurs between frequency 22Hz and 1Hz shows a transition from the semicircle to a more capacitive region as frequency decreases and this response is pertaining to the diffusion effect. The 45° line at the kink of the low frequency part has a form of semi-infinite diffusion and follows the impedance of a Warburg element, W. The impedance of the Warburg element is given in Eq. (3.19). Warburg impedance is sometimes written as,

$$Z_W = = \frac{\sigma(1-j)}{\sqrt{\omega}}\ (\Omega);\ \sigma\ (\Omega \cdot s^{-1/2}\ )\ \text{is the Warburg coefficient} \qquad (6.8)$$

and σ relates to Y_0 in Eq. (3.19) by

$$\sigma = \frac{1}{\sqrt{2} \cdot Y_0}\ (\Omega \cdot s^{-1/2}\ ) \qquad (6.9)$$

As frequency decreases, the Warburg behaviour becomes more capacitive but not quite of the ideal capacitance response. This non-vertical line of the low frequency part shows what is known as an ‘asynchronous charging’ which causes open circuit voltage decay, capacitance loss at high frequency and voltammetric distortions (Fletcher et al., 2014). Moreover, after the accelerated ageing test has stopped, the inclination of the non-vertical line at low frequency

increases; this observation shows that the PSD has become wider (Song et al., 1999) or the heterogeneity in the particle size have increased (Song and Bazant, 2013) in aged SCs. Nonetheless, the transition from the semi-infinite diffusion to a capacitive behaviour cannot be modelled properly with a capacitor nor a CPE; therefore, a bounded diffusion element T is chosen instead. This behaviour suggests that the diffusion layer is restricted, possibly due to the aluminium oxide layer that forms on the electrode surface on the aged SC. Eq. (3.20) and Eq. (3.21) give the impedance of the T element.

6.1.2.2 Ageing due to constant voltage at high temperature

While the effect of storage and cycling at high temperature can be represented by a single ageing model, constant voltage at high temperature requires a slightly different ageing model. This is pertaining to the two semicircles that emerge on the impedance spectrum of the aged SC, shown in Fig. 6.16. The first semicircle emerges between frequency 10kHz and 295Hz. The second semicircle lies in frequency between 295Hz and 0.8Hz. Each semicircle can be represented by a parallel connection of a resistor and a CPE.

The first semicircle is related to an increase of contact resistance between electrode and current collector. However, the appearance of the second semicircle is unexpected and cannot be assigned directly to any electrochemical process, although if observed carefully, it shows a response of a charge transfer reaction. Presently, the explanation for this phenomenon has not yet been found; therefore, the discovered behaviour is open to interpretation. Nonetheless, it is possible that this condition is likely to occur due to electrolyte reactions with

oxygenated-containing groups on the electrode surface (Wang et al., 2012; Ratajczak et al., 2014).

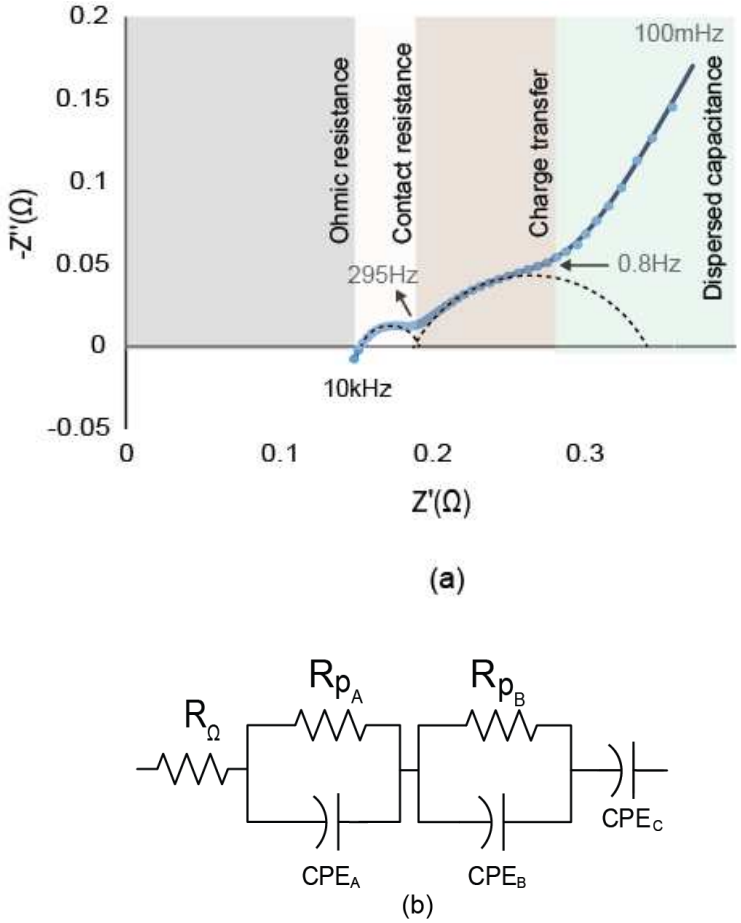

Fig. 6.16 Impedance spectrum of aged SC after 648H in constant voltage test 2.7V, 85℃: (a) experimental (dotted line) and simulated (solid line), (b) the equivalent circuit used to simulate the impedance spectrum.

A similar response has been reported in (Ruch, Cericola, Foelske-Schmitz, et al., 2010) for SCs aged at evelated voltages. The response is also similar as the one appeared in (Gaberscek et al., 2008) in the study of interphase contacts in lithium ion electrodes. Perhaps, the second semicircle is specific effect from voltage stress. Meanwhile at low frequencies, diffusion leads to the end of the second semicircle to rise from the real axis and this behaviour is

represented by a series CPE in the proposed EEC. The values of the circuit parameters are summarised in Table 6.2 along with the chi-square, x^2 .

Table 6.2 Circuit parameters of the ageing models.

Elements		**Fitted Value**	
		Ageing model Fig. 6.15b	Ageing model Fig. 6.16b
$\boldsymbol{R_{\Omega}}$ (Ω)		0.08123	0.11986
$\boldsymbol{R_{pA}}$ (Ω)		0.086212	0.073344
$\boldsymbol{CPE_A}$	Y_A (mho)	0.002469	0.038095
	n_A	0.95938	0.56049
$\boldsymbol{R_{pB}}$ (Ω)		-	0.090441
$\boldsymbol{CPE_B}$	Y_B (mho)	-	1.1517
	n_B	-	0.68711
W	Y_W (mho)	24.557	-
T	Y_T (mho)	53.961	-
	B	0.32732	-
$\boldsymbol{CPE_C}$	Y_C (mho)	-	7.2564
	n_C	-	0.67614
$\boldsymbol{x^2}$		1.8525×10^{-3}	3.0875×10^{-4}

6.2 Model Validation

6.2.1 Baseline model

The use of a CPE component in the model, however, leads to a more difficult implementation in circuit simulation software due to the fractional-order term. It is tempting to approximate the CPE to the double layer capacitance by Eq. (6.6) since in practice the CPE exponent n is very close to 1 for SCs. The easy way to do would be by simply replacing the CPE with a capacitor. However, this will defy the purpose of adding the CPE in the first place, that is to represent the distributed time constant seen in SC response.

In the time domain, an open circuit voltage decay is observed following the removal of the current source, evident in Fig. 6.17. The open circuit voltage decay is a result from the charge redistribution phenomenon in SC (Fletcher et al., 2014). The ion distribution after charging and discharging process does not take place with the same time constant—it is influenced by the pore sizes in which a fast diffusion process happen at the macro-pores due to their smaller time constant, thus are charged quickly, while the rest of the pore structures experience a much slower diffusion process due to their longer time constant (Kaus et al., 2010).

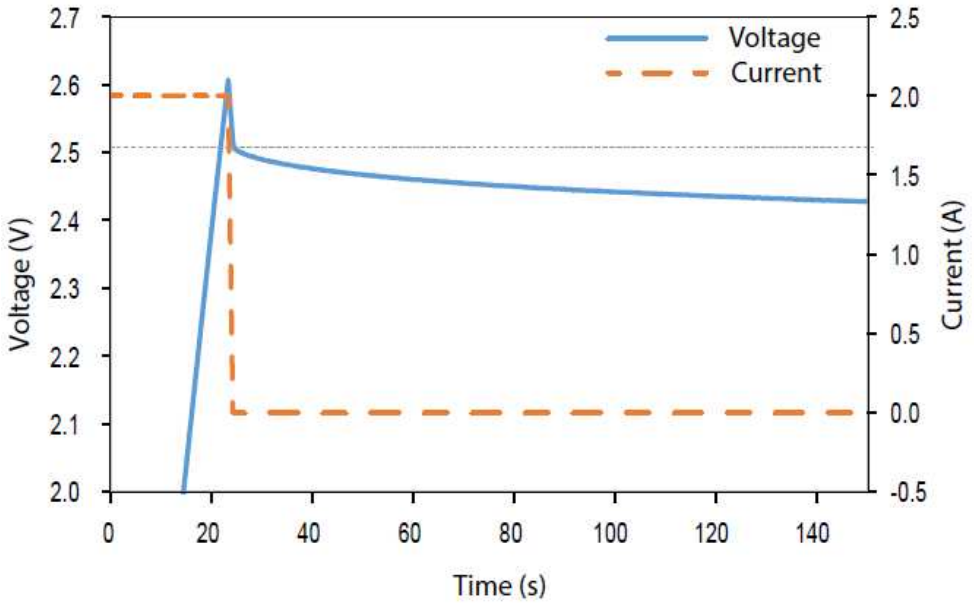

Fig. 6.17 A supercapacitor is charged to its rated voltage (solid line) with a 2A current source (dashed line) and then is left open circuit for the rest of the experimental duration. An open circuit voltage decay is observed with an immediate drop at the beginning of the open circuit period before a much slower decay takes place.

In order to investigate whether the baseline model would be a better choice to simulate the distribution of time constants in SC dynamic behaviour than the lumped model, the time domain response of the baseline model is compared with the time domain response of three RC circuits. Each of the RC circuits has a different number of RC branches to resemble the time constants in SC transient behaviour. The RC circuits are drawn in Fig. 6.18. The circuit parameters (Table 6.3) are obtained using CNLS fitting to the experimental impedance response.

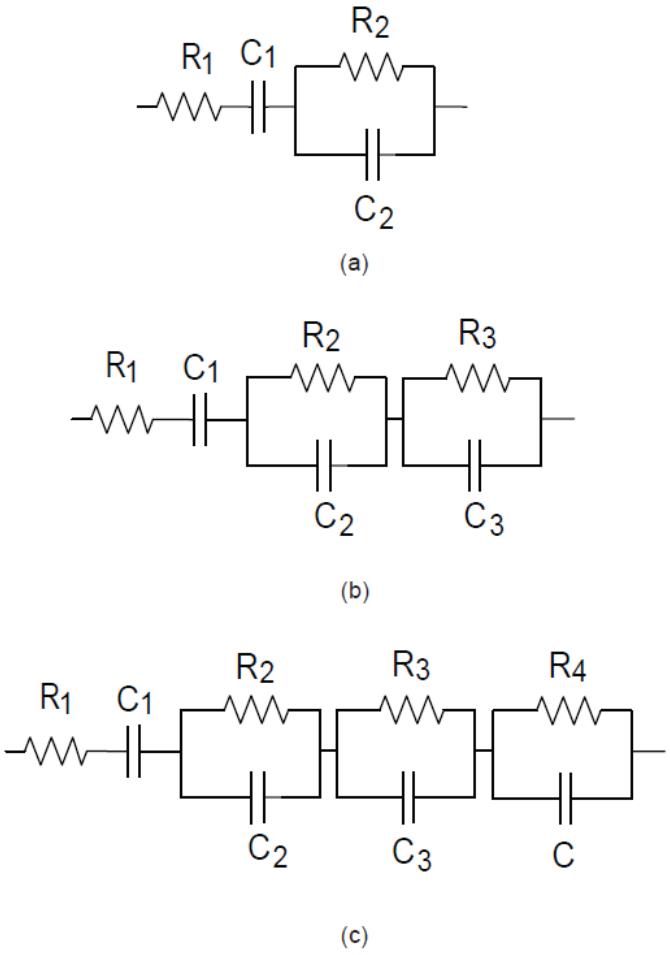

Fig. 6.18 RC circuits used in simulation: (a) 1-branch RC circuit, (b) 2-branch RC circuit and (c) 3-branch RC circuit. Each branch represents the distribution of time constants in SC dynamic behaviour.

Table 6.3 Circuit parameters of the RC circuits in Fig. 6.18.

Elements	Fitted Values		
	1-branch RC	2-branch RC	3-branch RC
R_1 (Ω)	0.071458	0.07103	0.070902
C_1 (F)	20.54	20.697	21.387
R_2 (Ω)	0.0063366	0.0030345	0.0019224
C_2 (F)	6.6026	3.6378	3.012
R_3 (Ω)	-	0.0043364	0.0041807
C_3 (F)	-	24.258	271.17
R_4 (Ω)	-	-	0.0044341
C_4 (F)	-	-	12.109
x^2	3.7115×10^{-3}	1.2676×10^{-3}	3.3117×10^{-4}

Each circuit is modelled in SIMULINK using the transfer function method to obtain the relation of the output voltage to a current input. Since the RC circuits in Fig. 6.18 are linear, the ordinary different equation ODE of a linear system is given by,

$$a_n\mathcal{D}^n y(t) + a_{n-1}\mathcal{D}^{n-1}y(t) + \cdots + a_0 y(t) = b_m\mathcal{D}^m u(t) + b_{m-1}\mathcal{D}^{m-1}u(t) + \cdots + b_0 u(t) \quad (6.10)$$

where $y(t)$ is the output, $u(t)$ is the input.

Taking Laplace transform of Eq. (6.10) and the initial condition is given as zero, the transfer function of the circuits takes the form of,

$$Z(s) = \frac{V(s)}{I(s)} = \frac{b_0 s^m + b_{m-1}s^{m-1} + \cdots + b_0}{a_n s^n + a_{n-1}s^{n-1} + \cdots + a_0} \quad (6.11)$$

The circuit parameters according to the coefficients of its transfer function is tabulated in Table 6.4.

Table 6.4 RC circuits parameters and the transfer function coefficients.

	Circuit coefficients		
	1-branch RC	2-branch RC	3-branch RC
	$Z(s)=\frac{As^2+Bs+1}{Cs^2+Ds}$	$Z(s)=\frac{As^3+Bs^2+Cs+1}{Ds^3+Es^2+Fs}$	$Z(s)=\frac{As^4+Bs^3+Cs^2+Ds+1}{Es^4+Fs^3+Gs^2+Hs}$
A	$R_1R_2C_1C_2$	$R_1R_2R_3C_1C_2C_3$	$R_1R_2R_3R_4C_1C_2C_3C_4$
B	$R_1C_1+R_2C_2$ $+R_2C_1$	$R_1R_2C_1C_2$ $+R_1R_3C_1C_3$ $+R_2R_3C_2C_3$ $+R_2R_3C_1C_3$ $+R_2R_3C_1C_2$	$R_1R_2R_4C_1C_2C_4$ $+R_1R_3R_4C_1C_3C_4$ $+R_2R_3R_4C_2C_3C_4$ $+R_2R_3R_4C_1C_3C_4$ $+R_2R_3R_4C_1C_2C_4$ $+R_1R_2R_3C_1C_2C_3$ $+R_2R_3R_4C_1C_2C_3$
C	$R_2C_1C_2$	$R_1C_1+R_2C_2$ $+R_2C_1+R_3C_3$ $+R_3C_1$	$R_1R_4C_1C_4+R_2R_4C_2C_4+$ $R_2R_4C_1C_4+R_3R_4C_3C_4+$ $R_3R_4C_1C_4+R_2R_4C_1C_2+$ $R_3R_4C_1C_3+R_1R_2C_1C_2+$ $R_1R_3C_1C_3+R_2R_3C_2C_3+$ $R_2R_3C_1C_3+R_2R_3C_1C_2$

Table 6.4 RC circuits parameters and the transfer function coefficients. (continued)

	Circuit coefficients		
	1-branch RC	2-branch RC	3-branch RC
	$Z(s)=\frac{As^2+Bs+1}{Cs^2+Ds}$	$Z(s)=\frac{As^3+Bs^2+Cs+1}{Ds^3+Es^2+Fs}$	$Z(s)=\frac{As^4+Bs^3+Cs^2+Ds+1}{Es^4+Fs^3+Gs^2+Hs}$
D	C_1	$R_2R_3C_1C_2C_3$	$R_1C_1+R_2C_2+$ $R_2C_1+R_3C_3+$ $R_3C_1+R_4C_4+R_4C_1$
E	-	$R_2C_1C_2+R_3C_1C_3$	$R_2R_3R_4C_1C_2C_3C_4$
F	-	C_1	$R_2R_4C_1C_2C_4$ $+R_3R_4C_1C_3C_4$ $+R_2R_3C_1C_2C_3$
G	-	-	$R_2C_1C_2$ $+R_3C_1C_3$ $+R_4C_1C_4$
H	-	-	C_1

The introduction of CPE in the baseline model (Fig. 6.11) to take into account the redistribution of time constant in SC behaviour leads to a fractional-order (non-integer) model. A fractional-order dynamic system can be expressed by a fractional differential equation of the following form (Chen et al., 2009; Monje et al., 2010);

$$a_n \mathcal{D}^{\alpha_n} y(t) + a_{n-1} \mathcal{D}^{\alpha_{n-1}} y(t) + \cdots + a_0 \mathcal{D}^{\alpha_0} y(t) = b_m \mathcal{D}^{\beta_m} u(t) + b_{m-1} \mathcal{D}^{\beta_{m-1}} u(t) + \cdots + b_0 \mathcal{D}^{\beta_0} u(t) \quad (6.12)$$

where $\mathcal{D}^{\gamma} \equiv {}_0\mathcal{D}_t^{\gamma}$; $a_k (k = 0, \dots n), b_k (k = 0, \dots m)$ are constant; and $\alpha_k (k = 0, \dots n), \beta_k (k = 0, \dots m)$ are arbitrary real number or rational number.

Taking the Laplace transforms of both sides of the above equation with zero initial conditions, the fractional-order transfer function (FOTF) can be obtained as follows,

$$G(s) = \frac{Y(s)}{X(s)} = \frac{b_m s^{\beta m} + \cdots + b_1 s^{\beta 1} + b_0 s^{\beta 0}}{a_n s^{\alpha n} + \cdots + a_1 s^{\alpha 1} + a_0 s^{\alpha 0}} \quad (6.13)$$

The order vectors of numerator and denominator and the coefficient vectors of the above model can be summarised as follow (Chen et al., 2009):

$$n_b = [\beta_m, \beta_{m-1}, \dots, \beta_0], n_a = [\alpha_n, \alpha_{n-1}, \dots, \alpha_0]$$

$$b = [b_m, b_{m-1}, \dots, b_0], \quad a = [a_n, a_{n-1}, \dots, a_0] \quad (6.14)$$

Fig. 6.19 illustrates the baseline model in s-domain. The FOTF transfer function of the baseline model is derived as follows:

$$Z_{BS}(s) = \frac{V(s)}{I(s)} = \frac{As^{am} + Bs^{bm} + Cs^{cm} + 1}{Ds^{dn} + Es^{en}} \quad (6.15)$$

where,

$$A = R_p Y_A$$

$$B = R_\Omega Y_B + R_p Y_B$$

$$C = R_\Omega R_p Y_A Y_B$$

$$D = Y_B \tag{6.16}$$

$$E = R_p Y_A Y_B$$

$$a_m = n_A$$

$$b_m = n_B$$

$$c_m = n_A + n_B$$

$$d_n = n_B$$

$$e_n = n_A + n_B$$

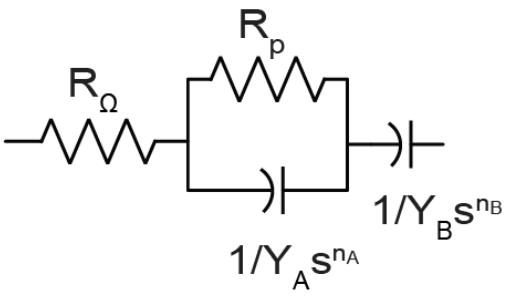

Fig. 6.19 The baseline model in s-domain.

Due to the fractional-order term of the baseline model, it cannot be simulated directly in MATLAB/SIMULINK. Therefore, FOMCON toolbox, developed by (Tepljakov et al., 2011), is employed to implement the fractional-order model in SIMULINK . The FOMCON toolbox is an extension to the MATLAB class FOTF which has been previously developed by (Chen et al.,

2009). Fractional-order model can then be entered in the form of Eq. (6.13). Therefore, the baseline model (Fig. 6.19) takes the form of,

$$Z_{BS}(s) = \frac{0.13975s^{1.69}+1.6121s^{0.981}+0.095494s^{0.709}+1}{1.9767s^{1.69}+20.7s^{0.981}} \quad (6.17)$$

and it can also be written in MATLAB in the following form,

$$n_b = [1.69, 0.981, 0.709, 0]; \; n_a = [1.69, 0.981];$$

$$b = [0.13975, 1.6121, 0.095494, 1]; \; a = [1.9767, 20.7]; \quad (6.18)$$

The stability of the baseline model has to satisfy the Matignon's stability theorem (Chen et al., 2009),

$$\left|\arg\left(eig\ (A)\right)\right| > q\frac{\pi}{2}, \quad (6.19)$$

where $0 < q < 1$ and $eig\ (A)$ is the eigenvalues of matrix A. The following condition can be tested using the `isstable` function.

```
>> Z = fotf(a,na,b,nb);

  [K , q, err, apol] = isstable(Z);
```

The stability function K shows whether a system is stable, with 1 for a stable system and 0 for unstable system (Chen et al., 2009). By default, the commensurate-order q is restricted to 0.01. The result obtained shows that K = 1, thus, the system appears stable with order q = 0.01. The result from the stability test is shown in Fig. 6.20. From the enlarged segment, there is no pole inside the shaded area, thus the baseline model is stable.

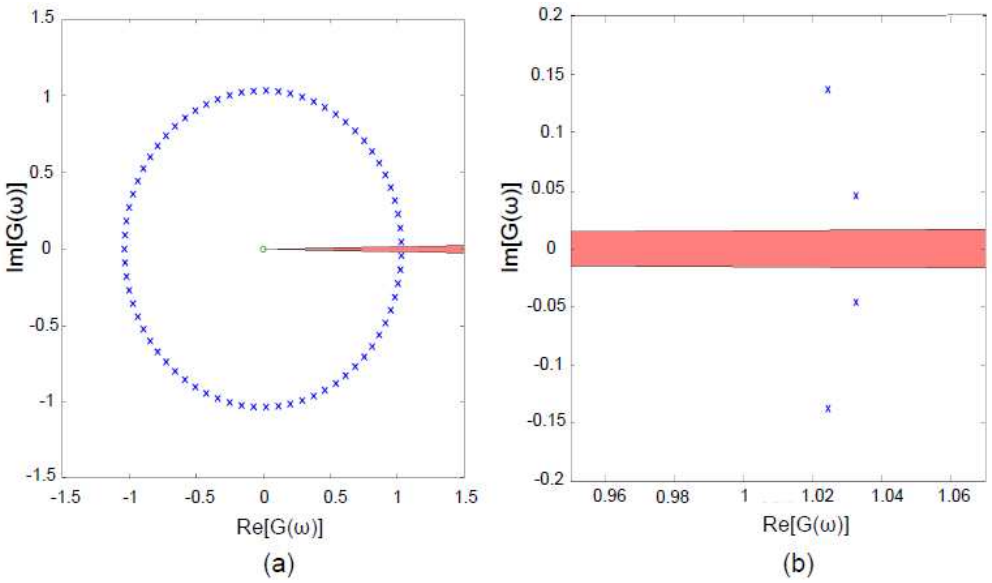

Fig. 6.20 Stability test of the baseline model: $\boldsymbol{b}$ = [0.13975, 1.6121, 0.095494, 1]; $\boldsymbol{n_b}$ = [1.69, 0.981, 0.709, 0]; $\boldsymbol{a}$ = [1.9767, 20.7]; $\boldsymbol{n_a}$ = [1.69, 0.981]; with order $\boldsymbol{q}$ = 0.01 and **K** = 1. Figure on right is the enlarged segment. No pole inside the shaded region.

The baseline model (Fig. 6.19) is simulated in SIMULINK with an input current made up of 2A charge and discharge pulses. The fractional transfer function blockset provided in FOMCON SIMULINK library is used. Since the model is stiff, the solver used for this simulation is `ode15s` in variable-step to ensure fast simulation and accuracy. For comparative purposes, the circuits in Fig. 6.18 are also simulated. Fig. 6.21 shows the results from the comparison.

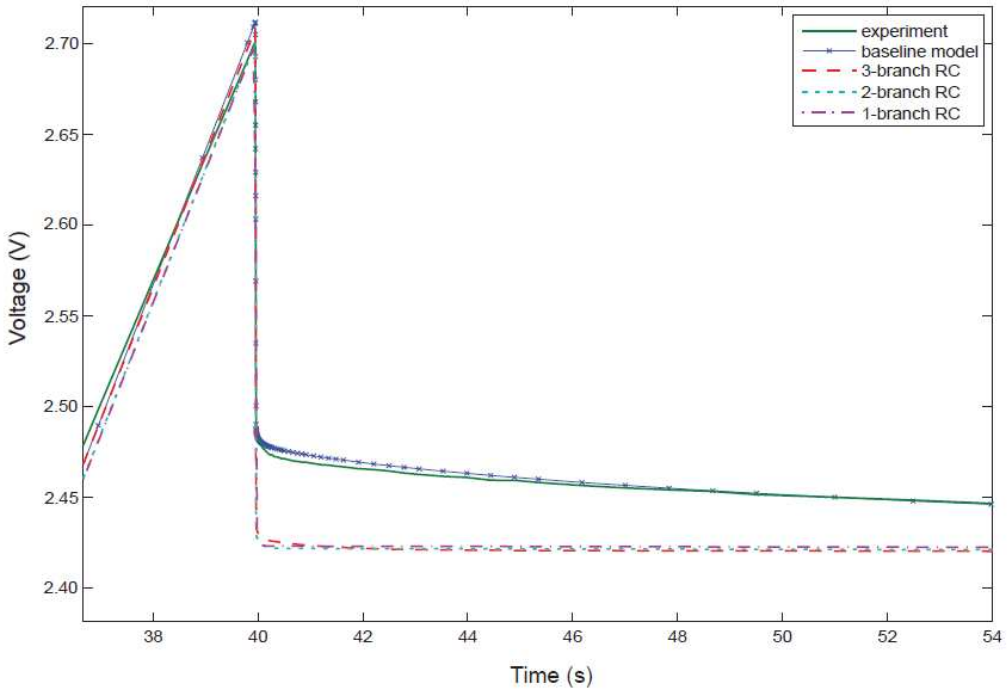

Fig. 6.21 Simulated voltage from a 2A input current with a focus on the voltage behaviour after the introduction of the open circuit period at 40s.

Fig. 6.21 shows the voltage responses of the RC circuits and the baseline model, against the experimental result. The experimental result is obtained through a 2A charge current. As soon as the rated voltage (2.7V) is met, the current source is removed and the SC is left open circuit for the rest of the time. It is shown that the RC circuits and the baseline model are able to simulate the voltage response from the beginning of charging until the rated voltage is reached. However, upon the introduction of the open circuit period, the RC circuits overestimate the voltage drop. Furthermore, all RC circuits fail to address the open circuit voltage decay, and instead they draw a practically straight response during the open circuit period. Meanwhile, the simulated response from the baseline model follows very closely to the experimental result, particularly at the open circuit voltage decay.

Supposedly, by increasing the number of branches of the RC circuit, the accuracy of the simulation will be improved. However in this case, even though the number of RC branches has been increased to three branches, it still does not produce a satisfactory fit. Referring to a circuit representation that is similar to those tested in this thesis, (Buller et al., 2002) reported on using 10 RC circuits. Unfortunately, increasing the number of branches has a downside—more parameters will need to be identified and this will only add to the complexity of the model.

The ability of the baseline model to simulate the open circuit voltage decay with such accuracy is due to the fractional-order term of the CPE. Again, the baseline model requires only four parameters to be identified whereas the 3-branch RC requires 8, and still, the baseline model surpasses the RC circuit in terms of accuracy. CPE is indeed a distributed element as it is shown in Fig. 6.5 and its response is identical to the transmission line (Fletcher et al., 2014).

The cause of the voltage decay in SC transient response at long time constant is related to the non-vertical tail at low frequencies. This response is well represented by the series CPE in the baseline model. The CPE fractional exponent reflects the slope of the low frequency line (refer Fig. 6.10) and since the low frequency line is the main cause for the open circuit voltage decay in SCs, as it has also been noted by (Fletcher et al., 2014), adjusting the value of the fractional exponent, therefore, will influence the decay, as shown in Fig. 6.22. When the exponent n = 1, no voltage decay is observed upon the current turn-off. As n gets smaller, the decay is larger and the slope decreases.

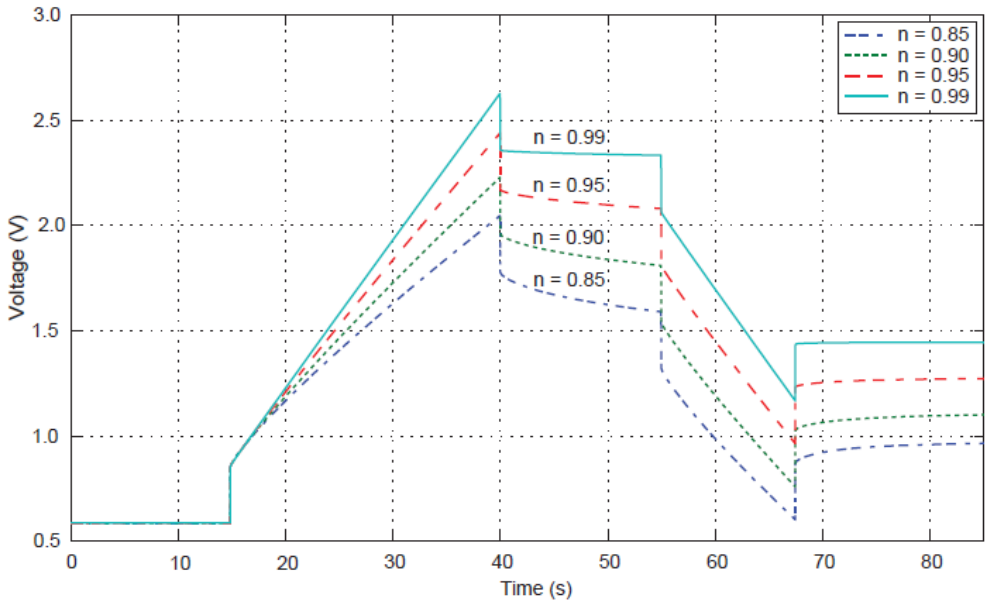

Fig. 6.22 The influence of the exponent, n of the series CPE on the voltage decay.

The lesser parameter required from the baseline model than the lumped model is the key. Furthermore, Martin et al. (2008b) observed that circuits built out of discrete components need 7 parameters to obtain the accuracy close to the fractional circuits. Therefore, the proposed baseline model is able to minimise the number of parameters to be identified without compromising the accuracy. Moreover, the baseline model is more meaningful than the RC circuits as each component of the baseline model can directly be linked to the physical structures of SCs and at the same time provides some insight on the electrochemical processes involved in the SC overall response.

Accordingly, Fig. 6.23 presents the overall voltage response of the baseline model against the experimental result. Root mean square error (RMSE) is calculated to measure differences between the simulated values by the model and the actual voltage. RMSE between the measured data and the simulated data can be calculated as,

$$RMSE = \sqrt{\frac{\sum(\hat{y}_i - y_i)^2}{N}} \tag{6.20}$$

where N is the total number of simulated data points, $\hat{y}_i$ and y_i are the simulated and measured values, respectively.

It can be seen from Fig. 6.23 that the baseline model gives a satisfactory simulation result over a large duration with the RMSE according to Eq. (6.20), is 0.0319. The RMSE is small compared with the SC voltage range used in the experiment, thus indicating that the model's ability to represent the real device.

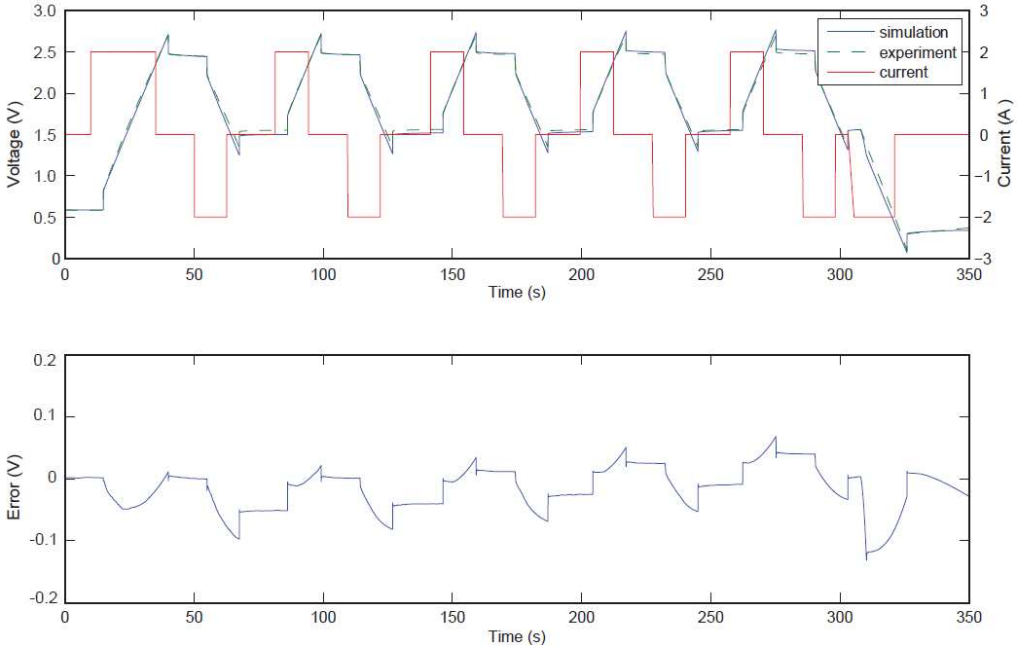

Fig. 6.23 Validation test with 2A current profile: simulation of the baseline model (solid blue line) and experimental data (dashed line) (top) and the error from the simulation (bottom). The model gives a fairly good result particularly during current switch-off period following charging and discharging with RMSE = 0.0319.

6.2.2 Ageing model

This section discusses the performance of the ageing model in Fig. 6.15. For ease of exposition, Fig. 6.24 illustrates the ageing model and the impedance of each component. The circuit is made up of a serial combination of a resistor, a bounded diffusion element T and a complex impedance Z_{ARC}. The Z_{ARC} consists of a parallel combination of a CPE and a series resistor and a Warburg element W.

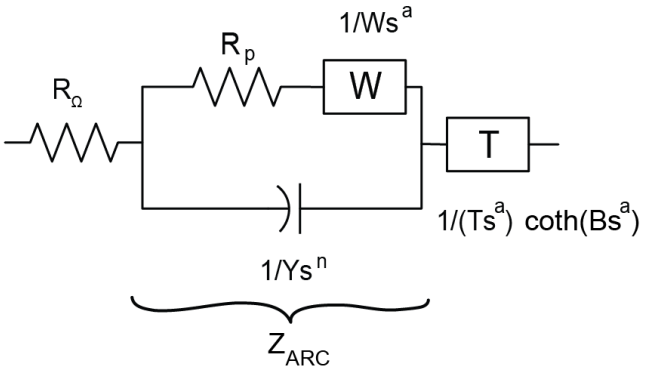

Fig. 6.24 The ageing model and its components.

The s-domain expression of the $Z_{ARC}(s)$ is

$$Z_{ARC}(s) = \frac{R_p W s^a + 1}{W s^a + (R_p Y W) s^{a+n} + Y s^n} \quad (6.21)$$

The impedance of the ageing model, $Z_{AG}(s)$ is thus,

$$Z_{AG}(s) = R_\Omega + \frac{R_p W s^a + 1}{W s^a + (R_p Y W) s^{a+n} + Y s^n} + \frac{1}{T s^a} \coth(B s^a) \quad (6.22)$$

where a is 0.5 and n is determined from CNLS fitting.

However, the coth function in Eq. (6.22) makes it difficult to simulate in a circuit simulation software, thus, the coth function needs to be approximated to form a rational model. According to (Nicolas Bertrand et al., 2010), Padé

approximant gives a better approximation than the Taylor series because of its rational function. Following (Riu et al., 2004), the coth function for low frequencies is approximated as follows,

$$\coth(x) = \frac{\cosh(x)}{\sinh(x)} \underset{x\to 0}{\cong} \frac{1+x^2/2}{x} \tag{6.23}$$

From the development of $\sqrt{1+x^2}$, Eq. (6.23) becomes:

$$\coth(x) \underset{x\to 0}{\cong} \frac{\sqrt{1+x^2}}{x} \tag{6.24}$$

Substituting Eq. (6.24) to Z_T in Eq. (3.20), the impedance of the T-element is then equal to:

$$Z_T(s) = \left\{\frac{1}{Ts^a}\right\}\coth(Bs^a) = \frac{\sqrt{1+(Bs^a)^2}}{TBs^{2a}}; a = 0.5 \tag{6.25}$$

Therefore, the approximated impedance of Eq. (6.22) now becomes,

$$Z_{AG}(s) = R_\Omega + \frac{R_pWs^a+1}{Ws^a+(R_pYW)s^{a+n}+Ys^n} + \frac{\sqrt{1+(Bs^a)^2}}{TBs^{2a}} \tag{6.26}$$

Expanding and arranging Eq. (6.26) yields the FOTF transfer function of $Z_{AG}(s)$ in the form of,

$$Z_{AG}(s) = \frac{V(s)}{I(s)} \tag{6.27}$$

$$= \frac{As^{am} + Bs^{bm} + Cs^{cm} + Ds^{dm} + Es^{em} + Fs^{fm} + Gs^{gm} + Hs^{hm} + Is^{im} + Js^{jm} + Ks^{km} + Ls^{lm}}{Ms^{mn} + Ns^{nn} + Os^{on}}$$

where the coefficients of the transfer function and the circuit parameters are given in Table 6.5.

Table 6.5 The relation of the transfer function coefficients to the circuit parameters.

Transfer function coefficients and the circuit parameters	
$A = \sqrt{T^2 {R_\Omega}^2 B^2 W^2 + 2T^2 B^2 W^2 R_\Omega R_p + T^2 B^2 W^2 {R_p}^2}$	$a_m = 3a$
$B = TBYWR_\Omega R_p$	$b_m = 3a + n$
$C = TBYR_\Omega + R_p Y\mathrm{BW}$	$c_m = 2a + n$
$D = TB + BW$	$d_m = 2a$
$E = W$	$e_m = a$
$F = \sqrt{2R_p YW^2}$	$f_m = \frac{2a + n}{2}$
$G = \sqrt{2R_p B^2 YW^2}$	$g_m = \frac{4a + n}{2}$
$H = \sqrt{2YW}$	$h_m = \frac{a + n}{2}$
$I = \sqrt{2B^2 YW}$	$i_m = \frac{3a + n}{2}$
$J = \sqrt{2R_p B^2 Y^2 W}$	$j_m = \frac{3a + 2n}{2}$
$K = Y$	$k_m = n$
$L = BY + R_p YW$	$l_m = a + n$
$M = BTW$	$m_n = 3a$
$N = R_p BYTW$	$n_n = 3a + n$
$O = BYT$	$o_n = 2a + n$

From Table 6.2 and Eq. (6.27) the transfer function $Z_{AG}(s)$ of the aged SC can be derived as in Eq. (6.28),

$$Z_{AG}(s) = \frac{V(s)}{I(s)} \tag{6.28}$$

$$= \frac{0.0074995s^{2.4594} + 0.0052533^{1.9594} + 0.001663s^{1.7094} + 72.626s^{1.5} + 0.16585s^{1.4797} + 0.0060353s^{1.4594} + 0.11398s^{1.2297} + 25.7005s + 0.50668s^{0.97969} + 0.002469s^{0.95938} + 0.34823s^{0.72969} + 24.557s^{0.5}}{0.092324s^{2.4594} + 0.043609s^{1.9594} + 433.7384s^{1.5}}$$

To simulate the ageing model in MATLAB, FOMCON toolbox is used and it allows for Eq. (6.28) to be written in the form of Eq. (6.14) and thus becomes,

n_b= [2.4594, 1.9594, 1.7094, 1.5, 1.4797, 1.4594, 1.2297, 1, 0.97969, 0.95938, 0.72969, 0.5];

n_a = [2.4594, 1.9594, 1.5]; (6.29)

b = [0.0074995, 0.0052533, 0.001663, 72.626, 0.16585, 0.0060353, 0.11398, 25.7005, 0.50668, 0.002469, 0.34823, 24.557];

a = [0.092324, 0.043609, 433.7384];

The stability assessment of the ageing model is carried out using the `isstable` function in MATLAB, and the result is presented in Fig. 6.25. As it can be seen, all poles are located in the stable area and no poles fall in the shaded area. Therefore, the stability function K for the model is 1, indicating that ageing model is stable with q = 0.05.

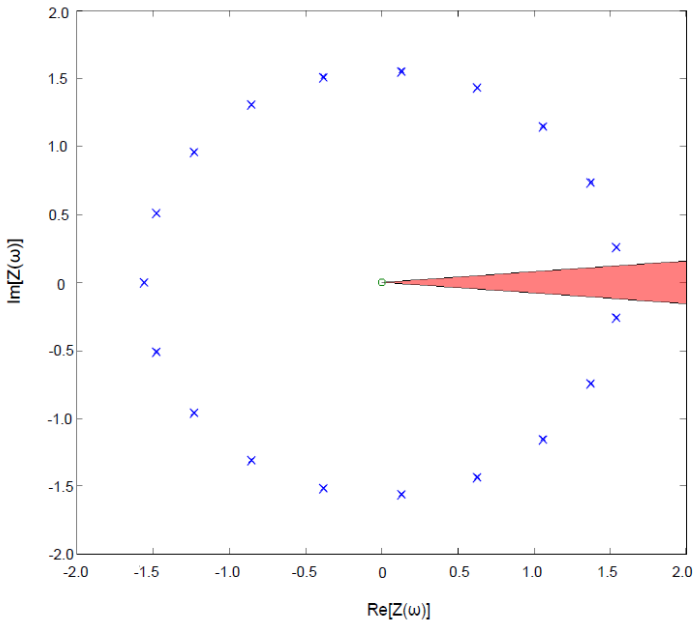

Fig. 6.25 Stability test of the ageing model using the parameters in Eq. (6.29); with order $\boldsymbol{q}$ = 0.05 and **K** = 1.

To validate the ageing model in the frequency domain, a frequency range from 100mHz to 10kHz is applied to excite the model. Fig. 6.26 shows the simulated Bode diagram of the ageing model against the data from experiment. It can be seen that the ageing model fits the Bode diagram in all frequencies at interest.

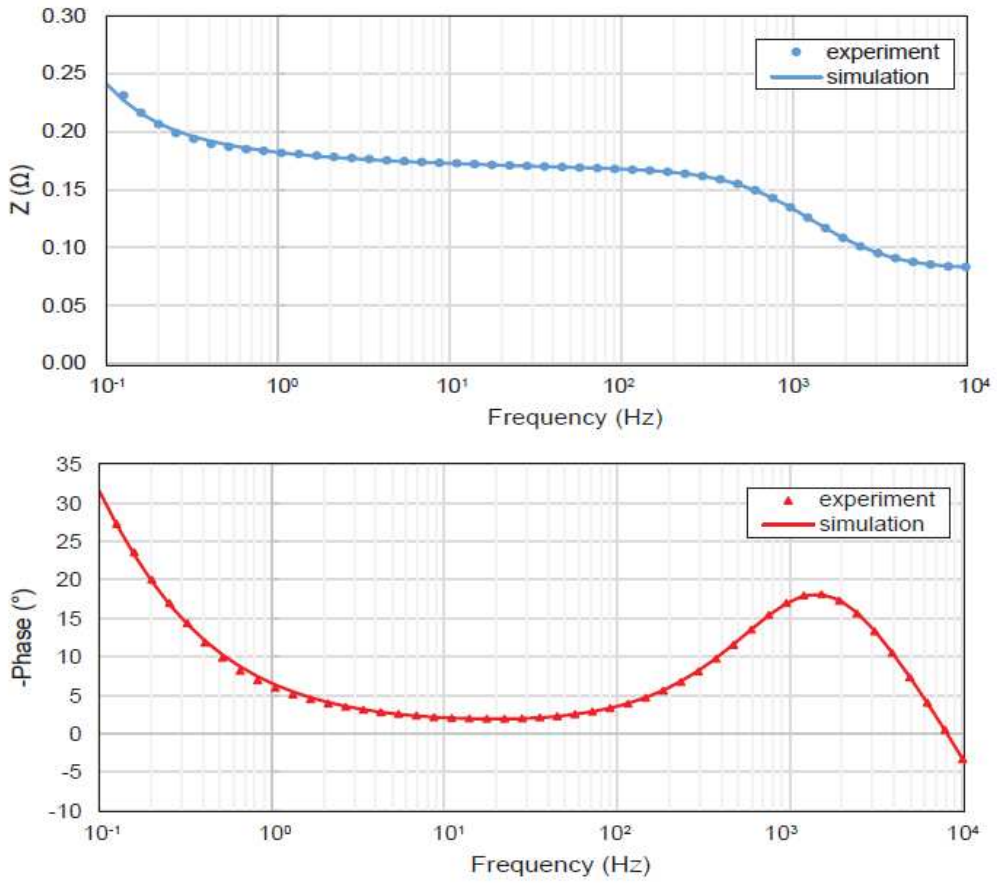

Fig. 6.26 Comparison of the frequency response between the experimental data (dotted lines) and the data from simulation (solid lines) of the ageing model. The result shows a perfect fit.

The simulation of the ageing model in the time domain is performed with the fractional transfer function blockset provided in FOMCON SIMULINK library. The ageing model (Fig. 6.24) is simulated and the voltage response from an input current made up of 2A charge and discharge pulses is recorded. Since the model is stiff, the solver `ode15s` in variable-step is used for fast simulation and accuracy. The voltage response is simulated according to the following relation,

$$V(t) = V_0 + ESR \cdot I + IZ \tag{6.30}$$

where V_0 is the initial voltage, Z is the impedance of the ageing model and $ESR = R_\Omega + R_p$.

Fig. 6.27 shows the simulated voltage response of the ageing model from the 2A current pulses input. It can be seen that the ageing model gives a satisfactory result over a large duration, although there is a small difference between the simulated values and the real one at the end of the simulation when the current source is completely removed. Nevertheless, the RMSE between the measured data and the simulated data is 0.054 and still, it is small when it is compared with the SC voltage range used in the experiment. Therefore, the result indicates that the model's ability to represent the aged SC.

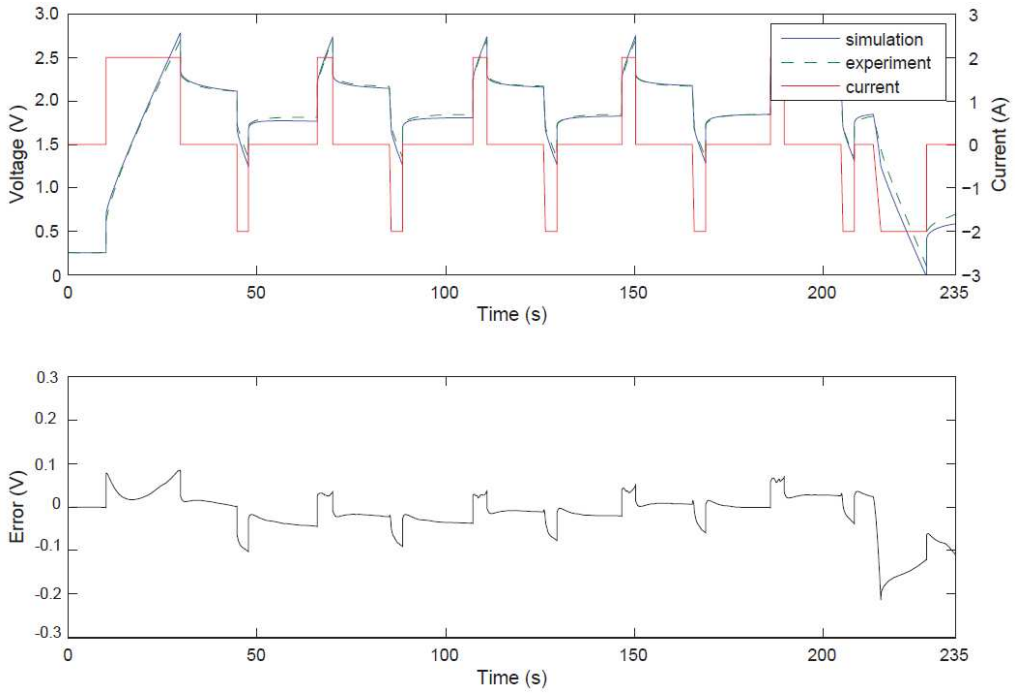

Fig. 6.27 Validation test of the ageing model with a 2A current profile: voltage simulated from the ageing model (solid blue line) and experimental data (dashed line) (top) and the error from the simulation (bottom). The model gives a fairly good result during most of the simulation period with RMSE = 0.054, although there is small differences between the measured data and the simulated data at the end i.e. when the current source is completely turned off.

6.3 Parameterisation of the Ageing Behaviour

While the baseline model has been validated to represent SC well, it is only applicable when SC is in a good SOH. Moreover from the EIS measurement in Chapter 5, aged SC develops anomalous behaviour at the impedance response, indicating changes in its health status and this observation requires an update to the baseline model to include its ageing state.

The semicircle and the diffusion effect in aged SCs lead to the addition of new circuit components to the baseline model. These components are the Warburg element W and the bounded diffusion element T, and they are added to consider the transition from the effect caused by contact resistance (i.e. the semicircle) to a capacitive region, but, is restricted due to the diffusion effect at low frequencies. The addition of these new components produces an ageing model.

The change of state from the baseline model to a complex ageing model occurs after SC is stressed for 672H in the storage test or 9,600 cycles in the cycling test at high temperature with the current profile in Fig. 5.2. This transition is illustrated in Fig. 6.28. Likewise, this observation is also recorded from the other two SC cells from the same manufacturer tested under the same condition. However, it should be noted that the time for the semicircle formation, hence the transition from the baseline model to the ageing model is specific to the SCs and the test condition considered in this thesis. Depending on the cell size, chemistry and technology and also the stress level, this observation can happen at different times than that observed here.

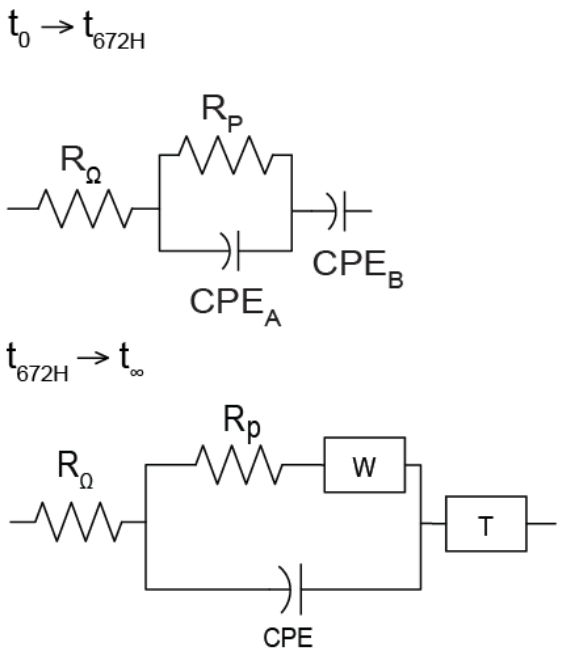

Fig. 6.28 Transition from the baseline model to the ageing model.

Based on the findings in Chapter 5, we can see that for most of the SC life, its dynamic behaviour can be represented by the ageing model. Therefore, a description of the ageing behaviour built upon the evolution of the parameters in the ageing model can be used to predict SC health status. By analysing these trends, we can anticipate the changes that the SC will experience in time.

It has been identified that the semicircle which appears on the impedance response of aged SCs is the dominant ageing mechanism in SC in the storage test. The semicircle formation, pertaining to the contact resistance between electrode and current collector, is in fact the main cause for the increase in ESR in SCs. The next step is to identify the parameters relevant to the observed ageing mechanism. The model parameters R_P, CPE, W have been monitored to be impacted by ageing. Meanwhile, parameter R_Ω shows a large scattering over time and T, which is the magnitude of the T element, does not show any significant change during the entire test duration, indicating that these

parameters are less sensitive to ageing (refer to Fig. 6.29). Therefore, model parameters R_Ω and T are not considered in the parameterisation. Similarly, CPE exponent n and the parameter B of the T element are also omitted from the parameterisation.

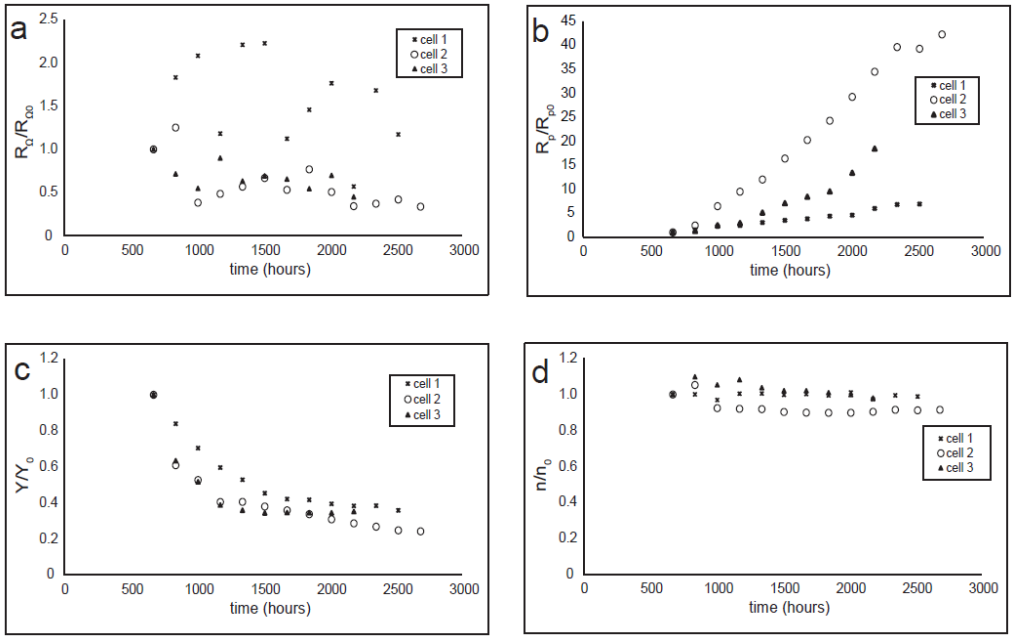

Fig. 6.29 Parameters of the ageing model normalised to initial values for 3 SC cells stored at 85℃. Cell 1, cell 2 and cell 3 are from the same manufacturer and are identical. The parameters are obtained from fitting the ageing model to the impedance response of discharged SCs measured at 20℃ using EIS at every stage of the SC life.

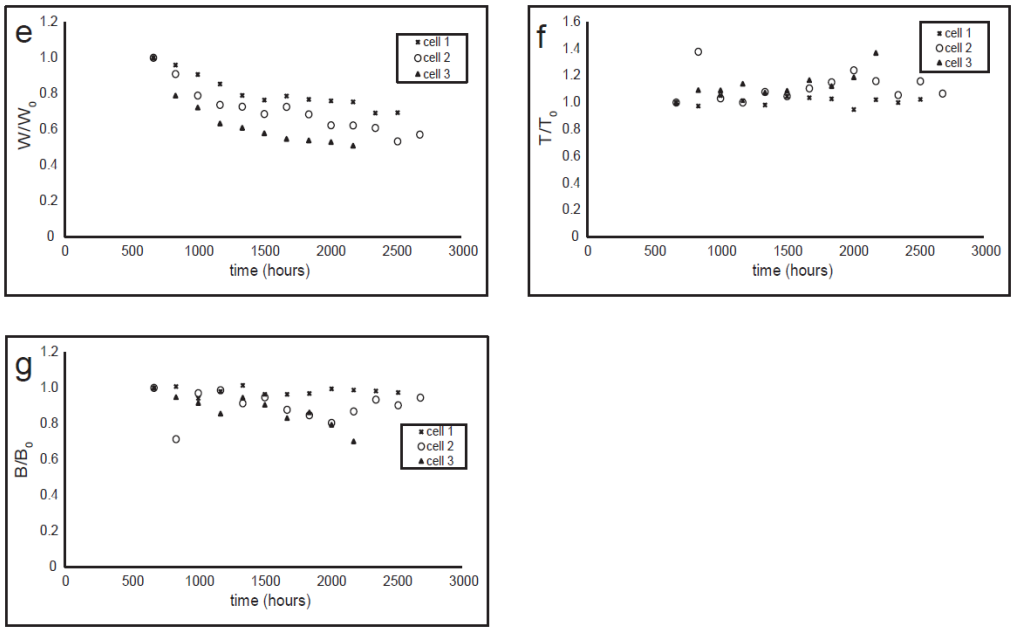

Fig. 6.29 Parameters of the ageing model normalised to initial values for 3 SC cells stored at 85℃. Cell 1, cell 2 and cell 3 are from the same manufacturer and are identical. The parameters are obtained from fitting the ageing model to the impedance response of discharged SCs measured at 20℃ using EIS at every stage of the SC life. (continued)

An empirical approach is employed to describe parameters R_P, CPE and W. Each model parameter can generally be described by a polynomial expression and the order of the polynomial depends on the distribution of the parameters across the x −axis. The evolution of a model parameter a with time compared with its initial value a_0 can be described empirically by the following equation:

$$a(t) = a_0(t_0)(p_0 + \sum_{k=1}^{n} p_k t^k) \tag{6.31}$$

where the coefficients $p_k(k = 1, \dots n)$ are determined using linear least squares and t is time in hours.

All fittings are done using Curve Fitting Toolbox in MATLAB. Fitting with polynomial curve can be very flexible, especially when a higher-order polynomial is used. Therefore, to avoid from over-fitting the data, the quality of each fitting is assessed by examining goodness of fit statistics and the confidence bounds for each fitted coefficient. The goodness of fit statistics includes the sum of squares due to error (SSE), R-square, adjusted R-square and root mean squared error (RMSE). The confidence levels for the bounds are set at 95%.

Fig. 6.30 shows fitting results using Eq. (6.31) on model parameters from three SC cells. The normalised R_p increases over time as SC ages and its evolution follows a linear polynomial, meanwhile the magnitude Y of the CPE, normalised to its initial value, decreases following a cubic function of time. The increase in R_p and the decrease of the CPE magnitude Y as ageing proceeds, indicates the increased of the distributed resistance in the pores of the SC electrode over time. It is also interesting to note that the magnitude of the Warburg element denoted by W, decreases as the SC ages, thus, increasing the Warburg impedance (according to Eq. (3.19)). Warburg element represents the diffusion process at the electrode/electrolyte interface, and with the increase in the impedance of this element, it shows that the diffusion length increases during the transition from the semicircle at high frequencies to the capacitive region at low frequencies as ageing manifests. The evolution of the normalised Warburg magnitude W during storage at 85℃ can be described by a quadratic function of time.

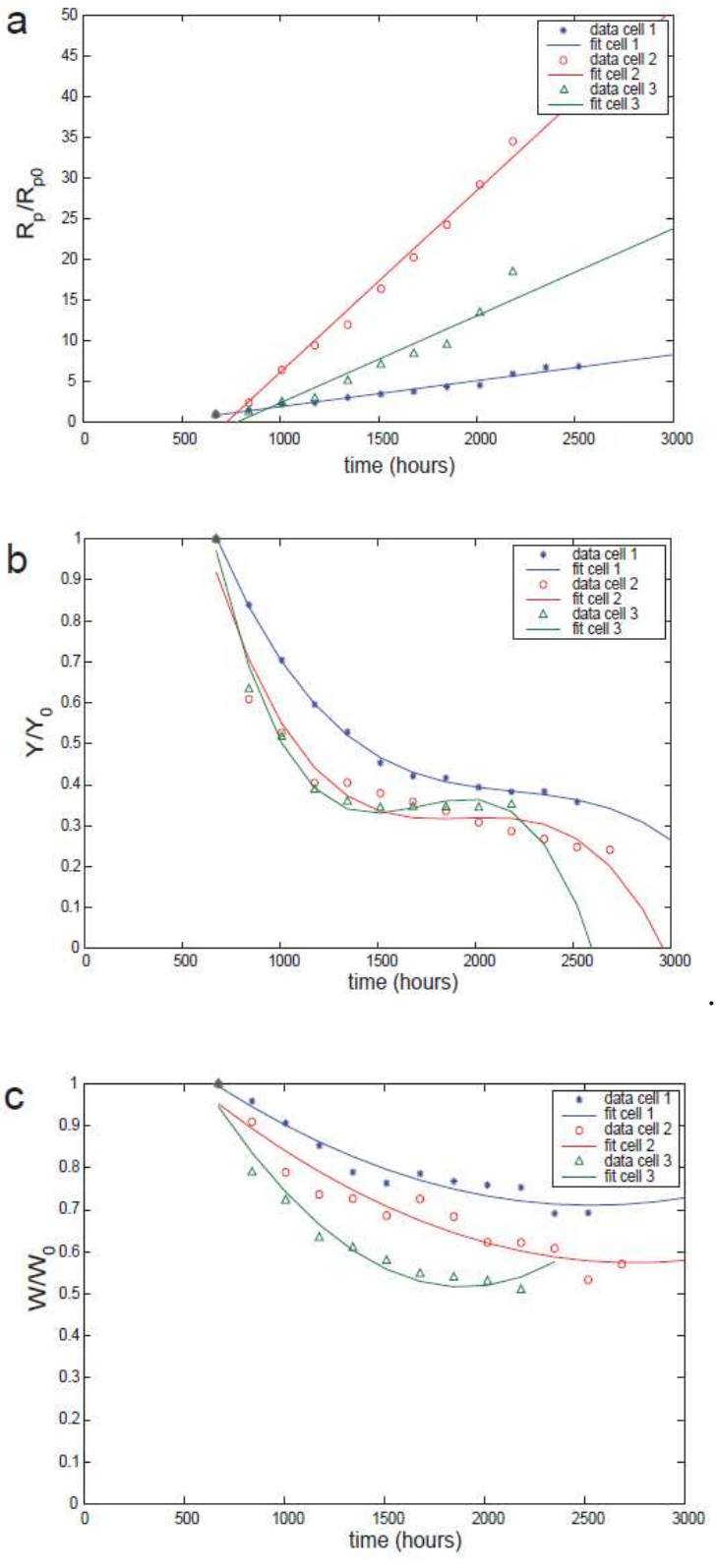

Fig. 6.30 Fitting results for 3 SC cells for parameters (a) R_p, (b) the CPE parameter Y and (c) Warburg W. All parameters are normalised to initial values. The dots are from measured data and the lines are from fittings.

The results of the fittings shows that each model parameter is impacted differently by the test condition, noted from the three different equations used to describe their evolutions. Nevertheless, the evolution of each model parameter is consistent with the other two SC cells, where similar equations can be used to fit these parameters. This confirms that the same behaviour can be expected in other SC cells, as long as their physical and chemical characteristics are similar with the one tested in this thesis. The results of the fittings for all parameters are summarised in Table 6.6. The goodness of fit statistics are also presented.

Table 6.6 Fitting parameters of the ageing model using polynomial equations in Eq. (6.31) for: (a) cell 1, (b) cell 2, and (c) cell 3. The confidence levels for the bounds are set at 95%.

(a)

Cell 1 Fitted parameters						
		Coefficients	SSE	R^2	Adjusted R^2	RMSE
$\frac{R_P}{R_{P0}}$	p_1	0.003187	1.013	0.9759	0.9735	0.3182
	p_0	-1.233				
$\frac{Y}{Y_0}$	p_3	-1.54E-10	5.33E-04	0.9989	0.9984	0.008164
	p_2	1.02E-06				
	p_1	-2.29E-03				
	p_0	2.127				
$\frac{W}{W_0}$	p_2	8.15E-08	0.005899	0.9453	0.9331	0.0256
	p_1	-0.00041				
	p_0	1.235				

Table 6.6 Fitting parameters of the ageing model using polynomial equations for: (a) cell 1, (b) cell 2, and (c) cell 3. The confidence levels for the bounds are set at 95%. (continued)

(b)

Cell 2 Fitted parameters						
		Coefficients	SSE	R^2	Adjusted R^2	RMSE
$\frac{R_P}{R_{P0}}$	p_1	0.02229	29.34	0.9886	0.9876	1.633
	p_0	-16.12				
$\frac{Y}{Y_0}$	p_3	-3.1E-10	0.02713	0.9469	0.9292	0.0549
	p_2	1.79E-06				
	p_1	-0.00344				
	p_0	2.52				
$\frac{W}{W_0}$	p_2	0.0375	0.01598	0.9235	0.9082	0.03997
	p_1	-0.1227				
	p_0	0.6743				

Table 6.6 Fitting parameters of the ageing model using polynomial equations for: (a) cell 1, (b) cell 2, and (c) cell 3. The confidence levels for the bounds are set at 95%. (continued)

(c)

Cell 3 Fitted parameters						
		Coefficients	SSE	R^2	Adjusted R^2	RMSE
$\frac{R_P}{R_{P0}}$	p_1	0.01068	24.94	0.9142	0.9035	1.766
	p_0	-8.263				
	p_3	-6.44E-10	0.005536	0.9863	0.9795	0.03038
$\frac{Y}{Y_0}$	p_2	3.32E-06				
	p_1	-0.0056				
	p_0	3.428				
	p_2	2.87E-07	0.008795	0.9583	0.9464	0.3545
$\frac{W}{W_0}$	p_1	-0.00109				
	p_0	1.547				

6.4 Summary

This chapter reports on the development of SC model which is based on the SC dynamic response in the frequency domain. The impedance response is fitted with an EEC to interpret and evaluate the electrochemical process which contributes to the dynamic response in SCs. Due to the unique physical characteristic of the SC, electrochemical components are used in the circuit to better represent its nature. The model is thus referred as the baseline model.

During the ageing of the SCs, it is found that the model built upon the response from a fresh SC will no longer be suitable for the ageing SC. This is due to the fact that chemical reactions inside the cell cause changes in the impedance spectra signifying the emergence of new electrochemical processes on aged SCs. Therefore, to represent the changes of the SOH of aged SCs, the model is modified with the inclusion of new components to take into account the new observed electrochemical processes. This model is named the ageing model.

Since electrochemical components are used in the models, the models take the form of fractional-order models. The voltage responses of both models are validated to follow the experimental response. It is shown that the model is better than the discrete model—it requires lesser parameters and is able to simulate the open circuit voltage decay accurately and more importantly it is directly relatable to the underlying process in SCs.

Then, the chapter proceeds with the parameterisation of the ageing model. The parameters of the ageing model relevant to the previously observed

ageing mechanism are identified. For this case, contact resistance is found to be the cause for the increase in ESR in SCs that are stored at high temperature. The evolutions of these parameters are extrapolated to derive equations for describing the ageing process using empirical method. The parameterisation of the model parameters, not only describes how these parameters change with time, it will also help in anticipating future changes in its behaviour. Moreover, since each model parameter is related to the electrochemical processes involved in the SC overall response, the parameterisation of these parameters provide insights how these processes react in time. This chapter, therefore, highlights that the SCs change state when aged and hence proposing the ageing model to elucidate the change.

CHAPTER 7

CONCLUSIONS

"By perseverance the snail reached the ark."

—Charles H. Spurgeon

7 Introduction

The work of this thesis is concerned on the ageing of SCs and its effect on their declining performance after a number of years of usage. Therefore, much of the work in this thesis was motivated by the prioritisation of the ageing mechanism in SCs for effective product improvement and reliability prediction. The principle effect of each ageing factor on the declining performance of SCs was investigated by means of electric circuit modelling to elucidate the dynamic interactions between them so that the ageing process can be more understood.

7.1 General conclusions and discussion

The research confirms that each ageing factor did reveal distinct effects on SCs through the separation of the ageing factors; this was shown in Chapter 5 of the thesis. Changes in the impedance spectra when the SCs experience ageing showed that modifications to the SCs properties had occurred. Moreover, each ageing factor exhibited a distinct change in the impedance spectra whereby each of these changes can be attributed to a change in the electrochemical process in SCs. Using the EIS as a diagnostic tool, these processes were separated and identified to explicate the ageing process in SCs.

Those ageing factors tested in this thesis were: high temperature, current cycling and constant voltage. The thesis identified two notable ageing process in SCs, they were: (1) the emergence of high frequency semicircle which is a result of loss of contact within the SC internal, and (2) the tilting of the low frequency part of the impedance spectrum of aged SCs. The thesis found that each of these ageing processes was ageing factor-dependent. Besides the above ageing process, SCs in all conditions showed an increase of the real impedance. All of these ageing processes were, in fact, consistent to the findings in several literatures for big cell SCs (e.g. (El Brouji, Vinassa, et al., 2009; Kötz et al., 2010; N Bertrand et al., 2010; El Brouji, Briat, Vinassa, Bertrand, et al., 2009; Bohlen et al., 2007a; El Brouji, Briat, Vinassa, Henry, et al., 2009; Alcicek et al., 2007)). All the literatures mentioned used SCs ranging between 350F and 2,600F in organic electrolyte.

From the two observed ageing processes, the thesis concludes that the main ageing mechanisms in SCs, respective to the ageing process above, are: (1)

the loss of contact within electrode, which gives rise to the contact resistance, and (2) the changes to the SC porous electrode. Based on the results from the accelerated ageing test (Chapter 5), the thesis identifies that high temperature affects the contact within SCs electrodes and also between electrodes and the current collector interface because of an accumulation of heat and pressure inside the cell. The contact loss can be linked to: (1) the increase in contact resistance between the electrode and the current collector, (2) the formation of aluminium oxide and the delamination of electrode from the current collector, (3) the crystallisation of AN electrolyte and (4) the decomposition of binder. Cycling and constant voltage, on the other hand, affect the electrode structure. The tilting at the low frequency indicates a reducing slope of the line. This behaviour suggests that there is a modification to the electrode structure pertaining to a change in the pore size distribution—cycling and constant voltage may have increased the heterogeneity in pore sizes. Another important finding is that, the increase in ESR in aged SCs is caused by either one of these two ageing mechanisms and that the loss of capacitance only takes place when SCs experience both of the ageing mechanisms. From this finding, it is possible that SC can be tailored to meet applications requirements by addressing areas that SC is susceptible to fail in the circumstances of the application. The finding, therefore, fulfils the first objective of the research.

The thesis contributes to existing knowledge in SC ageing by taking it one step further through the modelling of the ageing process in SCs by means of electrical equivalent circuit (EEC). This was done to understand the underlying mechanism that governs the observed ageing process. In Chapter 6, the thesis found that the changes of the SC properties due to ageing require a new outlook

on the EEC model. This is pertaining to the changes in the SC properties relating to new electrochemical processes. This finding indicates that for a model to be useful for the entire SC lifetime, the model must be able to accommodate the observed changes. The implication of this finding signifies that a SC model is useful only for the state at which the model is developed. Due to this situation, the thesis proposes two models: the baseline model and the ageing model. The baseline model represents the SC before it starts to degrade and the ageing model represents the situation when SCs began to experience ageing.

In view of the frequency dispersion in SCs, due to the use of highly porous electrodes, electrochemical components were used in the development of the baseline model and the ageing model to model this behaviour, in addition to discrete electrical components. CPE was used in the development of the baseline model. Whereas, the ageing model consists of a Warburg element and a bounded diffusion element T to model diffusion, in addition to the components from the baseline model (see Fig. 6.28). Following the transition from the baseline model to the ageing model and the evolution of the parameters related to the main ageing mechanisms of the SCs at high temperature, the aged SCs when they are exposed to high temperature will experience the following: (1) an increase of distributed resistance in the pores of the SC electrode (in-a-pore dispersion), (2) an increase of diffusion impedance which indicates that charge has to diffuse farther, but at low frequency, the diffusion length becomes limited due to the formation of a thin layer on the SC electrode (possibly from the passivation of the current collector based on the detected aluminium on aged SCs, refer to Chapter 5 page 211). SCs stressed under cycling at high temperature also experienced similar ageing, but with a reduced slope of the low

frequency line—an indication that the pore size distribution became wider overtime. Therefore, the third and the fourth objectives of the thesis with regard to finding the link between the ageing mechanism and the EEC are met.

The transition from the baseline model to the ageing model occurred at the same time for all SCs tested in this thesis, i.e. after 672H being stored at high temperature of 85℃. This was actually when the high frequency semicircle was first detected. Therefore, the start of its appearance in the impedance spectrum is something to be observed carefully as it marks the beginning of the changes in the SC state. Noteworthy that the thesis observes that the formation of the semicircle is the most fundamental source of the increase in ESR in SCs. As the emergence of the semicircle shows that the ageing process has become more pronounced, in which we can expect to see an increase in the ESR, thus, the key to effective failure prediction is to detect when the semicircle starts to form. In spite of that, it should be kept in mind that the time for the semicircle starts to appear can differ in SCs; its appearance is influenced by the SOH of the SCs, also including many factors like the stress level and cell design. Furthermore, manufacturing dispersion and batch variations could also lead to different times, even though the SCs are essentially similar. With this finding, the second objective of the thesis is achieved with the identification of the process which precipitates the failure of SCs.

Besides the use of the models to elucidate the ageing process in SCs, the proposed models (i.e. the baseline model and the ageing model) have been used to simulate the SC electrical response. The use of electrochemical components like CPE, Warburg element and bounded diffusion element T, in modelling SC dynamic behaviour, have provided several benefits including (refer to Chapter

6): (1) it provides a better approximation of SC dynamic response as the elements cover a wider frequency range than the conventional circuit elements, (2) the components are electrochemical process-related elements, thus, the relation of the component to a electrochemical process can be made directly, and (3) minimises the number of circuit components, hence, the parameters to be identified in the models are reduced. The thesis proves that the use of these electrochemical components in the proposed models, in which the models take the form of fractional-order models, can simulate the SC electrical response more accurately than the lumped model, in particularly, at the open circuit voltage decay (Fig. 6.21). It is demonstrated in this thesis that the development of the models in simulation software like MATLAB/SIMULINK can be done easily with the use of a special toolbox for fractional-order models—although a pre-treatment may be required, such as changing the model to a rational model, before simulating it in MATLAB/SIMULINK. Moreover, the simulations from the proposed models show that the baseline model and the ageing model are not only able to elucidate the ageing process in SCs, but they can also be used to simulate SC electrical response satisfactorily (refer to Fig. 6.23 and Fig.6.27). This work meets the second objective of the thesis with regard to modelling SC electrical performance using EEC.

These findings, thus, meet the main aim of this thesis, which is to seek an approach that can link the different areas in the SC reliability improvement field. With the capability of the models to expound the physicochemical process in SCs and also to be able to give information on the electrical performance of SCs, these models will benefit those in the field.

7.2 Findings with regard to the research questions

This section presents explicit findings with regard to the research questions the thesis was set to answer. Some of the findings have been reported before, thus, reference to the papers are provided.

7.2.1 Research question 3

Supercapacitors are sensitive to the ageing process and can only meet the requirements on life expectancy if certain boundary conditions are met. Can this failure be investigated and characterised? (explored in Chapter 5)

The durability of a SC depends on the characteristics of the electrolyte system. The chemical reactions in SCs are driven by either temperature or voltage. In organic electrolyte, the decomposition voltage can be as high as 3.5V, while the aqueous electrolyte is about 1.2V (Section 2.1.4.2). Besides, AN organic electrolyte has a boiling temperature of 81.6℃ (Gualous et al., 2012). The chemical reactions in SCs generally follow the Arrhenius law. Therefore, if the SC is exposed to temperature or voltage higher than its maximum capability, the chemical reaction rates will increase according to the Arrhenius law, thus, reducing its life (Section 2.3.2).

In chapter 5, it was found that after a prolong exposure to high temperature, under cycling and constant voltage, SCs showed: (1) capacitance loss, and/or (2) an increase in ESR. This finding matched those observed in (Kötz et al., 2010), (Chaari et al., 2011), and (Gualous et al., 2012). Besides the parametric loss, SCs experienced chemical and physical changes due to

chemical reactions mostly from the decomposition of electrolyte. SCs too experienced electrode-based ageing. SCs exposed to high temperature showed mostly electrolyte-based ageing, in which electrolyte loss (also reported in (Kötz et al., 2010)) and package swelling (Kularatna et al., 2010; Kurzweil and Chwistek, 2008) due to the increase of the internal pressure, were observed. Continuous current cycling and constant voltage mostly contributed to electrode-based ageing in SCs, whereby, aged SCs showed microstructural changes (Zhu et al., 2008) and the formation of large crystals, reduced adhesion of the carbon electrode to the current collector and an increase in the heterogeneity in the pore size which affected the pore size distribution (also reported in (El Brouji, Vinassa, et al., 2009; Ruch, Cericola, Foelske-Schmitz, et al., 2010)). Aside from the above findings, ageing was more pronounced at the positive electrode than at the negative electrode, consistent with (Bittner et al., 2012). Other components in the SCs were also affected by ageing. It was observed that SCs aged by constant voltage at high temperature showed oxidation of the separator (consistent with (Oukaour, Tala-Ighil, et al., 2013)) and passivation of aluminium current collector (Bittner et al., 2012; Kurzweil and Chwistek, 2008). Note that, all the above observations were found in the post-mortem analysis (Section 5.5, page 207).

The thesis noted the strong contribution of high temperature on the SC ageing. It was observed that the SCs experienced ageing more dramatic at high temperature than those at cycling and constant voltage alone. During cycling and constant voltage alone, the heat generation in the SC cell was small, thus, ageing was slower compared with those aged under high temperature. In spite of that, cycling and constant voltage have certainly caused mechanical stress on the SCs

through changes of the electrode structure. Noteworthy that when the build-up of pressure reaches the cell limit, it will cause the top of the SC to crack to allow the escape of gaseous products from the decomposition of electrolyte; fortunately, the design of the casing has prevented it from being explosive. The current study found that temperature is indeed the dominant ageing factor in the ageing of SCs and cycling and constant voltage which represent the operational stress on SC, have a secondary effect of SC ageing. Primarily, the degradation process of the SCs observed in this thesis was mainly caused by the decomposition of electrolyte.

The research demonstrates that the changes in the SC properties can be characterised using electrochemical measurements (EIS and CV) and time domain characterisation (CC test). Electrochemical measurements and time domain characterisation were carried out at the beginning of the accelerated ageing test and then periodically at each defined stage of SCs lifetime. The periodic characterisation made sure that every facet of SC life was captured. During the ageing process, the changes in SC properties appeared as anomalies in the impedance spectrum. The changes at the impedance spectrum, hence, the changes in the SC properties were characterised by following the parametric change of the SC impedance. This non-invasive monitoring via measurements at SC terminals gave a live view of the process happening inside the SCs during operation. By conducting two types of characterisations, electrochemical measurement and time domain characterisation, the thesis is able to find the link of how the changes in the SC properties have an effect on its declining electrical performance—in which the thesis identifies that contact loss is the fundamental

source for the increase of ESR and capacitance is affected when SC experiences contact loss and changes in the electrode structure (Section 5.6, page 212).

7.2.2 Research question 4

What type of model that is able to capture and replicate this degradation mechanism? (explored in Chapter 6)

This question established how the entire research was conducted. During the beginning of the research, the thesis had placed a few requirements for the model (Chapter 1, section 1.2.2, page 15). The most important criteria the model has to fill is the ability of the model to represent the physicochemical process in SCs. To enable the thesis to propose such model, the thesis researched for the right tool that can extract information on the electrochemical reactions inside SCs which usually were difficult to obtain by common methods which use DC measurements.

During the search, it was discovered from literature (Section 2.3.3 and Section 2.2) that EIS can aid in the construction of the model and at the same time can separate contributions of each electrochemical process to the overall response and represents them in an electrical equivalent circuit made up of discrete and electrochemical components (to address the distributed response in electrochemical systems). Since the model is built based on the impedance response of the SC, this feature enables the simulation the current-voltage characteristics of the SCs for the electrical performance evaluation.

With the focus of the thesis lies in the dynamic and the ageing behaviours of the SCs, the EIS measurements were applied at frequencies which covered

time constants of these dynamic effects (refer to Fig. 2.24); so that, the equivalent circuit model can simulate the current-voltage characteristic. At frequencies 10kHz to 100mHz, the proposed baseline model, which comprised of resistors and electrochemical element CPEs, demonstrated satisfactory performance in the frequency domain and in the time domain simulations. In the frequency domain (Section 6.1.1), the baseline model modelled the frequency dispersion characteristic at the Warburg region (medium frequency) and dispersed capacitance region (low frequency) satisfactorily with the goodness-of-fit of 4.0958×10^{-4}. The universality of the baseline model on other SCs was also tested with the goodness-of-fit of the baseline model falling between 10^{-3} and 10^{-4} (Table 6.1, page 241).

In the time domain, the performance of the proposed baseline model surpassed that of the lumped models (Fig. 6.21, page 262), in particular, during the open circuit voltage decay—the baseline model followed closely the experimental data even at the cessation of the charging process. In addition, the error produced from the simulation of the baseline model to the experimental data (Fig. 6.23, page 265) was small with RMSE of only 0.0319 compared with the SC voltage range. In comparison to the lumped model, the baseline model required fewer parameters. This finding, thus, in agreement to (Martín et al., 2008b)—baseline model, which takes the form of a fractional-order model, minimises the number of parameters to be identified without compromising the simulation accuracy. Furthermore, the baseline model can directly be linked to the SC physicochemical process, for instance, the CPE used in the baseline model shows in-a-pore-dispersion (at medium frequency) and pore size distribution (at low frequency) and the resistor is related to the ohmic resistance

due to the contribution from separator, current collector, electrolyte and electrode material.

From the success of the baseline model to simulate accurately the SC current-voltage characteristic, an ageing model was built using the same approach as in the construction of the baseline model. The ageing mechanism observed in Chapter 5 was modelled by fitting the impedance spectrum to the EEC, thus, producing the ageing model (Section 6.1.2.1). The ageing model for SC aged under high temperature stress consists of electrochemical components such as the Warburg element to represent the semi-infinite diffusion at medium frequency and bounded diffusion element T to represent the tilted low frequency line, in addition to the components from the baseline model. From the ageing model, it was found that the distributed resistance in the pores of the SC electrode increases during ageing. In addition to that, it was also found that there is an increase of the diffusion impedance in aged SC.

The ageing model performed well in the frequency domain (Fig. 6.26), with the chi-square values of the model between 10^{-3} and 10^{-4}. In the time domain, the ageing model produced a satisfactory result (Fig. 6.27), with the RMSE between the simulated data to the experimental data at 0.054, which was small when comparing to the SC voltage range used in the experiment. The simulation of the ageing model, thus, revealing the impact of ageing mechanism on SC electrical performance. Hence, the findings show that if the ageing model of a SC is known, the SC electrical performance, particularly the current-voltage characteristic, can be predicted.

7.3 Contribution of the thesis

The thesis contributes to the current literature in the following aspect:

- Proposes an ageing model for the ageing condition in SCs and proves that the ageing model is able to elucidate the ageing process in SCs and at the same time simulate the current-voltage characteristic of aged SCs, hence, is useful to predict the SC transient behaviour over the studied conditions.
- Identifies a clear distinction of the ageing mechanisms in SCs with respect to the studied ageing factors. The thesis concludes that the main ageing mechanism in SCs are:
    - The loss of contact within electrode which is due to a prolonged exposure to high temperature.
    - The structural change at the electrodes is a consequence of cycling or constant voltage stress.
- Identifies that the contact loss in aged SCs is the fundamental source for the increase in ESR. The capacitance is lost when there is a contact loss and modification at the electrode structure.
- Proves that the proposed models are able to model the SC frequency and time domain behaviours with satisfactory accuracy. The RMSE of the baseline model and the ageing model are 0.0319 and 0.054, respectively.

As a whole, the implications of this research are: (1) SCs can be tailored for a specific application (2) a targeted solution can be devised based upon the application under which they are operated, (3) aids in the identification of the cause of failure, which could lead to saving the resources invested during the

post-failure analysis and (4) shows replicability of SC testing; SCs regardless of their sizes, essentially experience similar ageing.

7.4 Recommendations

The thesis has shown the effectiveness of the ageing model to study the ageing process in SCs. Along the way, this research has stumbled upon many questions in need of further investigation in order to use the ageing model in SC prognostic and health monitoring, particularly. The ageing model could be further developed in a number of ways and those are:

Extending the ageing model for wider temperature range

The appearance of the semicircle at the SC impedance indicating the start of ageing has become pronounced in SCs stressed under high temperature, in which the beginning of its appearance at the impedance spectrum should be observed closely. Therefore, this thesis recommends the SCs ageing behaviour should be investigated under various temperature conditions to establish the relationship between temperature and the formation of semicircle, so that, the transition from the baseline model to the ageing model can be predicted. The contribution of various temperature on the evolution of the ageing model parameters will also be known, therefore, the model can be used in a wider temperature spectrum and in more detailed modelling such as in SC prognostic and health monitoring.

Extending the ageing model for various voltages

It has been pointed out in the literature (Section 2.3.2) that the chemical reactions in SC follow the Arrhenius law in which for each 100mV above nominal voltage

(2.7V in this case), the chemical reaction rate doubles. The thesis investigated the ageing process only at 2.7V. In order to establish how voltage influences the ageing process, for instance, the dependency of the tilting at the low frequency with voltage, the thesis recommends the accelerated ageing tests to be conducted at various voltage above 2.7V to quantify the ageing rate so that these data can be collected, hence, will be a fruitful source of information for a much detailed modelling.

Extending the ageing model for various current level to quantify ageing rate

The current profile used in this thesis only generated a small amount of heat inside the SC cell (Section 5.6), which in turn produced a slow ageing. As it has been shown that temperature is the main contributor to the ageing in SCs, the thesis recommends a more aggressive current profile that can raise the core temperature of the SC close to the maximum operating temperature. This can also be achieved with a larger current if the current profile like the one used in this thesis is used. It is also recommended for the test to be conducted at various current values, so that, we can compute the stress rate of each current to the ageing process in SCs, especially, pertaining to the change of the electrode structure after several charge-discharge cycles.

Other area to be investigated

The thesis observes that the ageing at constant voltage at high temperature has caused two semicircles to appear at SC impedance data. The first semicircle was assigned to the effect of contact resistance; however, the thesis is unable to come up with a definite answer for the appearance of the second semicircle, although, it appears similar to the ageing effect in battery during power cycling (Eddahech

et al., 2011). The thesis assumes it is a charge transfer response which may have been initiated by a redox reaction due to the non-entirely inert carbon materials of the electrode. Therefore, it is suggested that a deeper investigation on the second semicircle to be done and the correlation of this behaviour to the SC electrical performance will be investigated in future studies.

REFERENCES

Alcicek, G., Gualous, H., Venet, P., Gallay, R. and Miraoui, A. (2007) 'Experimental study of temperature effect on ultracapacitor ageing', in 2007 European Conference on Power Electronics and Applications. IEEE, Aalborg, pp.1–7., DOI:10.1109/EPE.2007.4417619

Araujo, R.E., de Castro, R., Pinto, C., Melo, P. and Freitas, D. (2014) 'Combined Sizing and Energy Management in EVs With Batteries and Supercapacitors', IEEE Transactions on Vehicular Technology, Vol. 63 No.7, pp.3062–3076., DOI:10.1109/TVT.2014.2318275

Autolab AUTOLAB NOVA Impedance Spectroscopy Tutorial. Metrohm Autolab B.V.

Ayadi, M., Briat, O., Eddahech, A., German, R., Coquery, G. and Vinassa, J.M. (2013) 'Thermal cycling impacts on supercapacitor performances during calendar ageing', Microelectronics Reliability, Vol. 53 No.9-11, pp.1628–1631., DOI:10.1016/j.microrel.2013.07.079

Azaïs, P., Duclaux, L., Florian, P., Massiot, D., Lillo-Rodenas, M.-A., Linares-Solano, A., Peres, J.-P., Jehoulet, C. and Béguin, F. (2007) 'Causes of supercapacitors ageing in organic electrolyte', Journal of Power Sources, Vol. 171 No.2, pp.1046–1053., DOI:10.1016/j.jpowsour.2007.07.001

Ban, S., Zhang, J., Zhang, L., Tsay, K., Song, D. and Zou, X. (2013) 'Charging and discharging electrochemical supercapacitors in the presence of both parallel leakage process and electrochemical decomposition of solvent', Electrochimica Acta, Vol. 90 No.2013, pp.542–549., DOI:10.1016/j.electacta.2012.12.056

Barsali, S., Ceraolo, M., Marracci, M. and Tellini, B. (2010) 'Frequency dependent parameter model of supercapacitor', Measurement, Vol. 43 No.10, pp.1683–1689., DOI:10.1016/j.measurement.2010.09.016

Barsoukov, E. (2005) '4.5.1 Special Aspects of Impedance Modeling of Power Sources', in Barsoukov, E. and Macdonald, J. R. (Eds.), Impedance Spectroscopy: Theory, Experiment, and Applications. John Wiley & Sons, Inc, New Jersey, USA, pp.430–443, ISBN:978-0-471-64749-2.

Béguin, F. and Frąckowiak, E. (2013) Supercapacitors: Materials, Systems, and Applications. Béguin, F. and Frąckowiak, E. (Eds.),. Wiley-VCH Verlag GmbH & Co. KGaA, Weinheim, Germany. , ISBN:9783527646661., DOI:10.1002/9783527646661

Belhachemi, F., Rael, S. and Davat, B. (2000) 'A physical based model of power electric double-layer supercapacitors', in Conference Record of the 2000 IEEE Industry Applications Conference. Thirty-Fifth IAS Annual Meeting and World Conference on Industrial Applications of Electrical Energy (Cat. No.00CH37129). IEEE, Rome, Italy, pp.3069–3076, ISBN:0-7803-6401-5., DOI:10.1109/IAS.2000.882604

Bertrand, N., Briat, O., El Brouji, H. and Vinassa, J.-M. (2010) 'Impact of the ageing of supercapacitors in power cycling on the behaviour of hybrid electric vehicles applications', in 2010 IEEE Vehicle Power and Propulsion Conference. IEEE, Lille, France, pp.1–5, ISBN:978-1-4244-8220-7., DOI:10.1109/VPPC.2010.5729183

Bertrand, N., Sabatier, J., Briat, O. and Vinassa, J. (2010) 'Embedded Fractional Nonlinear Supercapacitor Model and Its Parametric Estimation Method', IEEE Transactions on Industrial Electronics, Vol. 57 No.12, pp.3991–4000., DOI:10.1109/TIE.2010.2076307

Bisquert, J. (2002) 'Theory of the Impedance of Electron Diffusion and Recombination in a Thin Layer', The Journal of Physical Chemistry B, Vol. 106 No.2, pp.325–333., DOI:10.1021/jp011941g

Bisquert, J., Garcia-Belmonte, G., Fabregat-Santiago, F. and Bueno, P.R. (1999) 'Theoretical models for ac impedance of finite diffusion layers exhibiting low frequency dispersion', Journal of Electroanalytical Chemistry, Vol. 475 No.2, pp.152–163., DOI:10.1016/S0022-0728(99)00346-0

Biswas, K., Sen, S. and Dutta, P.K. (2006) 'Realization of a constant phase element and its performance study in a differentiator circuit.pdf', IEEE Transactions on Circuits and Systems II: Express Briefs, Vol. 53 No.9, pp.802–806., DOI:10.1109/TCSII.2006.879102

Bittner, A.M., Zhu, M., Yang, Y., Waibel, H.F., Konuma, M., Starke, U. and Weber, C.J. (2012) 'Ageing of electrochemical double layer capacitors', Journal of Power Sources, Vol. 203 No.1 April 2012, pp.262–273., DOI:10.1016/j.jpowsour.2011.10.083

Bohlen, O., Kowal, J. and Sauer, D.U. (2007a) 'Ageing behaviour of electrochemical double layer capacitors Part I. Experimental Study and ageing model', Journal of Power Sources, Vol. 172 No.1, pp.468–475., DOI:10.1016/j.jpowsour.2007.07.021

Bohlen, O., Kowal, J. and Sauer, D.U. (2007b) 'Ageing behaviour of electrochemical double layer capacitors Part II. Lifetime simulation model for dynamic applications', Journal of Power Sources, Vol. 173 No.1, pp.626–632., DOI:10.1016/j.jpowsour.2007.07.059

Briat, O., Lajnef, W., Vinassa, J.-M. and Woirgard, E. (2006) 'Power cycling tests for accelerated ageing of ultracapacitors', Microelectronics Reliability, Vol. 46 No.9-11, pp.1445–1450., DOI:10.1016/j.microrel.2006.07.008

Briat, O., Vinassa, J.-M., Bertrand, N., El Brouji, H., Delétage, J.-Y. and Woirgard, E. (2010) 'Contribution of calendar ageing modes in the performances degradation of supercapacitors during power cycling', Microelectronics Reliability, Vol. 50 No.9-11, pp.1796–1803., DOI:10.1016/j.microrel.2010.07.118

El Brouji, H., Briat, O., Vinassa, J.-M., Bertrand, N. and Woirgard, E. (2008) 'Comparison between changes of ultracapacitors model parameters during calendar life and power cycling ageing tests', Microelectronics Reliability, Vol. 48 No.8-9, pp.1473–1478., DOI:10.1016/j.microrel.2008.07.022

El Brouji, H., Briat, O., Vinassa, J.-M., Bertrand, N. and Woirgard, E. (2009) 'Impact of Calendar Life and Cycling Ageing on Supercapacitor Performance', IEEE Transactions on Vehicular Technology, Vol. 58 No.8, pp.3917–3929., DOI:10.1109/TVT.2009.2028431

El Brouji, H., Briat, O., Vinassa, J.-M., Henry, H. and Woirgard, E. (2009) 'Analysis of the dynamic behavior changes of supercapacitors during calendar life test under several voltages and temperatures conditions', Microelectronics Reliability, Vol. 49 No.9-11, pp.1391–1397., DOI:10.1016/j.microrel.2009.06.033

El Brouji, H., Vinassa, J.-M., Briat, O., Bertrand, N., Deletage, J.-Y. and Woirgard, E. (2009) 'Ageing assessment of supercapacitors during calendar life and power cycling tests', in IEEE Energy Conversion Congress and Exposition 2009. IEEE, San Jose, CA, pp.1791–1798, ISBN:9781424428939., DOI:10.1109/ECCE.2009.5316293

Brown, S., Pyke, D. and Steenhof, P. (2010) 'Electric vehicles: The role and importance of standards in an emerging market', Energy Policy, Vol. 38 No.7, pp.3797–3806., DOI:10.1016/j.enpol.2010.02.059

BSI (2010) BS EN 62576 Electric double-layer capacitors for use in hybrid electric vehicles — Test methods for electrical characteristics. , ISBN:978 0 580 63350 8.

Buller, S., Karden, E., Kok, D. and De Doncker, R.W. (2002) 'Modeling the dynamic behavior of supercapacitors using impedance spectroscopy', IEEE Transactions on Industry Applications, Vol. 38 No.6, pp.1622–1626., DOI:10.1109/TIA.2002.804762

Burke, A. (2007) 'R&D considerations for the performance and application of electrochemical capacitors', Electrochimica Acta, Vol. 53 No.3, pp.1083–1091., DOI:10.1016/j.electacta.2007.01.011

Burke, A. (2010) 'Ultracapacitor technologies and application in hybrid and electric vehicles', International Journal of Energy Research, Vol. 34 No.2, pp.133–151., DOI:10.1002/er.1654

Burke, A. (2000) 'Ultracapacitors: why, how, and where is the technology', Journal of Power Sources, Vol. 91 No.1, pp.37–50., DOI:10.1016/S0378-7753(00)00485-7

Burke, A. and Miller, M. (2010) 'Testing of electrochemical capacitors: Capacitance, resistance, energy density, and power capability', Electrochimica Acta, Vol. 55 No.25, pp.7538–7548., DOI:10.1016/j.electacta.2010.04.074

Burke, A.F. (2007) 'Batteries and Ultracapacitors for Electric, Hybrid, and Fuel Cell Vehicles', Proceedings of the IEEE, Vol. 95 No.4, pp.806–820., DOI:10.1109/JPROC.2007.892490

Calvo, E.G., Lufrano, F., Staiti, P., Brigandì, A., Arenillas, A. and Menéndez, J.A. (2013) 'Optimizing the electrochemical performance of aqueous symmetric supercapacitors based on an activated carbon xerogel', Journal of Power Sources, Vol. 241, pp.776–782., DOI:10.1016/j.jpowsour.2013.03.065

Cap-XX (2008) Cap-XX [Internet], http://www.cap-xx.com/, (Accessed 27 June 2014).

CAP-XX (2013) CAP-XX Announces the Availability of 16V, 230F Supercapacitor Modules and 1400F Prismatic Supercapacitors [Internet], http://goo.gl/edHRKm, (Accessed 27 June 2014).

Carter, R., Cruden, A. and Hall, P.J. (2012) 'Optimizing for Efficiency or Battery Life in a Battery/Supercapacitor Electric Vehicle', IEEE Transactions on Vehicular Technology, Vol. 61 No.4, pp.1526–1533., DOI:10.1109/TVT.2012.2188551

Cazorla-Amorós, D., Lozano-Castelló, D., Morallón, E., Bleda-Martínez, M.J., Linares-Solano, A. and Shiraishi, S. (2010) 'Measuring cycle efficiency and capacitance of chemically activated carbons in propylene carbonate', Carbon, Vol. 48 No.5, pp.1451–1456., DOI:10.1016/j.carbon.2009.12.039

Cericola, D., Kötz, R. and Wokaun, A. (2011) 'Effect of electrode mass ratio on aging of activated carbon based supercapacitors utilizing organic electrolytes', Journal of Power Sources, Vol. 196 No.6, pp.3114–3118., DOI:10.1016/j.jpowsour.2010.11.157

Chaari, R., Briat, O., Delétage, J.Y., Woirgard, E. and Vinassa, J.-M. (2011) 'How supercapacitors reach end of life criteria during calendar life and power cycling tests', Microelectronics Reliability, Vol. 51 No.9-11, pp.1976–1979., DOI:10.1016/j.microrel.2011.07.014

Chen, Y., Petras, I. and Xue, D. (2009) 'Fractional order control - A tutorial', in 2009 American Control Conference. IEEE, MO, USA, pp.1397–1411, ISBN:978-1-4244-4523-3., DOI:10.1109/ACC.2009.5160719

Choi, H.S., Im, J.H., Kim, T., Park, J.H. and Park, C.R. (2012) 'Advanced energy storage device: a hybrid BatCap system consisting of battery–supercapacitor hybrid electrodes based on Li4Ti5O12–activated-carbon hybrid nanotubes', Journal of Materials Chemistry, Vol. 22 No.33, p.16986., DOI:10.1039/c2jm32841k

Conte, F.V. (2010) HCV D3100.4 Abuse Test Plan for Li Batteries and SC.

Conway, B.E. (1999) Electrochemical Supercapacitors: Scientific Fundamentals and Technological Applications. 1999th ed. Kluwer Academic/Plenum Publishers, New York. , ISBN:0306457369.

d'Entremont, A. and Pilon, L. (2014) 'First-principles thermal modeling of electric double layer capacitors under constant-current cycling', Journal of Power Sources, Vol. 246 No.15 January 2014, pp.887–898., DOI:10.1016/j.jpowsour.2013.08.024

Dandeville, Y., Guillemet, P., Scudeller, Y., Crosnier, O., Athouel, L. and Brousse, T. (2011) 'Measuring time-dependent heat profiles of aqueous electrochemical capacitors under cycling', Thermochimica Acta, Vol. 526 No.1-2, pp.1–8., DOI:10.1016/j.tca.2011.07.027

Devillers, N., Jemei, S., Péra, M.-C., Bienaimé, D. and Gustin, F. (2014) 'Review of characterization methods for supercapacitor modelling', Journal of Power Sources, Vol. 246, pp.596–608., DOI:10.1016/j.jpowsour.2013.07.116

Dhirde, A.M., Dale, N. V, Salehfar, H., Mann, M.D. and Han, T. (2010) 'Equivalent Electric Circuit Modeling and Performance Analysis of a PEM Fuel Cell Stack Using Impedance Spectroscopy', IEEE Transactions on Energy Conversion, Vol. 25 No.3, pp.778–786., DOI:10.1109/TEC.2010.2049267

Diab, Y., Venet, P., Gualous, H. and Rojat, G. (2009) 'Self-Discharge Characterization and Modeling of Electrochemical Capacitor Used for Power Electronics Applications', IEEE Transactions on Power Electronics, Vol. 24 No.2, pp.510–517., DOI:10.1109/TPEL.2008.2007116

Dominguez-Benetton, X., Sevda, S., Vanbroekhoven, K. and Pant, D. (2012) 'The accurate use of impedance analysis for the study of microbial electrochemical systems.', Chemical Society reviews, Vol. 41 No.21, pp.7228–46., DOI:10.1039/c2cs35026b

Dougal, R.A., Gao, L. and Liu, S. (2004) 'Ultracapacitor model with automatic order selection and capacity scaling for dynamic system simulation', Journal of Power Sources, Vol. 126 No.1-2, pp.250–257., DOI:10.1016/j.jpowsour.2003.08.031

Du, L. (2009) 'Study on supercapacitor equivalent circuit model for power electronics applications', in 2009 2nd International Conference on Power

Electronics and Intelligent Transportation System (PEITS). IEEE, Shenzhen, pp.51–54, ISBN:978-1-4244-4544-8., DOI:10.1109/PEITS.2009.5406744

Dzieliński, A., Sarwas, G. and Sierociuk, D. (2011) 'Comparison and validation of integer and fractional order ultracapacitor models', Advances in Difference Equations, Vol. 2011 No.11, p.11., DOI:10.1186/1687-1847-2011-11

Dzieliński, A., Sarwas, G. and Sierociuk, D. (2010) 'Time domain validation of ultracapacitor fractional order model', in 2010 49th IEEE Conference on Decision and Control (CDC). IEEE, Atlanta, GA, pp.3730–3735, ISBN:9781424477463., DOI:10.1109/CDC.2010.5717093

EATON (2013) Cooper Bussmann PowerStor Supercapacitors KR series [Internet], http://goo.gl/kUVbkp, (Accessed 27 June 2014).

Ecker, M., Gerschler, J.B., Vogel, J., Käbitz, S., Hust, F., Dechent, P. and Sauer, D.U. (2012) 'Development of a lifetime prediction model for lithium-ion batteries based on extended accelerated aging test data', Journal of Power Sources, Vol. 215, pp.248–257., DOI:10.1016/j.jpowsour.2012.05.012

Eddahech, A., Ayadi, M., Briat, O. and Vinassa, J.-M. (2013) 'Multilevel neural-network model for supercapacitor module in automotive applications', in 4th International Conference on Power Engineering, Energy and Electrical Drives. IEEE, Istanbul, Turkey, pp.1460–1465, ISBN:978-1-4673-6392-1., DOI:10.1109/PowerEng.2013.6635830

Eddahech, A., Briat, O., Henry, H., Delétage, J.-Y., Woirgard, E. and Vinassa, J.-M. (2011) 'Ageing monitoring of lithium-ion cell during power cycling tests', Microelectronics Reliability, Vol. 51 No.9-11, pp.1968–1971., DOI:10.1016/j.microrel.2011.07.013

Embrandiri, M., Isa, D. and Arehli, R. (2011) 'An Electric Vehicle Conversion using Batteries and Ultracapacitors', Journal of Asian Electric Vehicles, Vol. 9 No.2, pp.1521–1527., DOI:10.4130/jaev.9.1521

EUCAR Traction Battery Working Group (2003) Specification for Test Procedures for Supercapacitors in Electric Vehicle Application. , ISBN:2000000088.

Faranda, R. (2010) 'A new parameters identification procedure for simplified double layer capacitor two-branch model', Electric Power Systems Research, Vol. 80 No.4, pp.363–371., DOI:10.1016/j.epsr.2009.10.024

Faranda, R., Gallina, M. and Son, D.T. (2007) 'A new simplified model of Double-Layer Capacitors', in International Conference on Clean Electrical Power. IEEE, Capri, pp.706–710, ISBN:1-4244-0631-5., DOI:10.1109/ICCEP.2007.384288

Farma, R., Deraman, M., Awitdrus, Talib, I.A., Omar, R., Manjunatha, J.G., Ishak, M.M., Basri, N.H. and Dolah, B.N.M. (2013) 'Physical and Electrochemical Properties of Supercapacitor Electrodes Derived from Carbon Nanotube and Biomass Carbon', International Journal of Electrochemical Science, Vol. 8 No.2013, pp.257–273.

Fletcher, S., Black, V.J. and Kirkpatrick, I. (2014) 'A universal equivalent circuit for carbon-based supercapacitors', Journal of Solid State Electrochemistry, Vol. 18 No.5, pp.1377–1387., DOI:10.1007/s10008-013-2328-4

Frackowiak, E., Abbas, Q. and Béguin, F. (2013) 'Carbon/carbon supercapacitors', Journal of Energy Chemistry, Vol. 22 No.2, pp.226–240., DOI:10.1016/S2095-4956(13)60028-5

FreedomCAR (2004) FreedomCAR Ultracapacitor Test Manual. Report DOE/NE-ID-11173. Idaho National Engineering Laboratory.

Funaki, T. (2010) 'Evaluating Energy Storage Efficiency by Modeling the Voltage and Temperature Dependency in EDLC Electrical Characteristics', IEEE Transactions on Power Electronics, Vol. 25 No.5, pp.1231–1239., DOI:10.1109/TPEL.2009.2038473

Gaberscek, M., Moskon, J., Erjavec, B., Dominko, R. and Jamnik, J. (2008) 'The Importance of Interphase Contacts in Li Ion Electrodes: The Meaning of the High-Frequency Impedance Arc', Electrochemical and Solid-State Letters, Vol. 11 No.10, p.A170., DOI:10.1149/1.2964220

Gamry (2010) Application Note Rev. 1.0 9/3/2010 - Basics of Electrochemical Impedance Spectroscopy.

García, T., Roncero-sánchez, P., Parreño, A. and Feliu, V. (2010) 'Ultracapacitor-based Storage : Modelling , Power Conversion and Energy Considerations', in IEEE International Symposium on Industrial Electronics (ISIE). Bari, pp.2493–2498, ISBN:9781424463923., DOI:10.1109/ISIE.2010.5637966

Gonzalez, F. (2014) Supercapacitors market to achieve 30 % CAGR over the next decade [Internet], http://www.idtechex.com/research/articles/supercapacitors-market-to-achieve-30-cagr-over-the-next-decade-00006502.asp, (Accessed 23 June 2014).

Gonzalez, F. and Harrop, P. (2014) Batteries & Supercapacitors in Consumer Electronics 2013-2023 : Forecasts , Opportunities , Innovation [Internet], http://www.idtechex.com/research/reports/batteries-and-supercapacitors-in-consumer-electronics-2013-2023-forecasts-opportunities-innovation-000336.asp, (Accessed 22 June 2014).

Gualous, H., Bouquain, A., Berthon, A. and Kauffmann, J.M. (2003) 'Experimental study of supercapacitor serial resistance and capacitance

variations with temperature', Journal of Power Sources, Vol. 123 No.1, pp.86–93., DOI:10.1016/S0378-7753(03)00527-5

Gualous, H., Camara, M.B., Boudrat, B., Gallay, R. and Dakyo, B. (2013) 'Supercapacitor characterization for electric vehicle applications', in 2013 Fourth International Conference on Power Engineering, Energy and Electrical Drives (POWERENG). Istanbul, pp.13–17, ISBN:9781467363921., DOI:10.1109/PowerEng.2013.6635854

Gualous, H., Gallay, R., Alcicek, G., Tala-Ighil, B., Oukaour, A., Boudart, B. and Makany, P. (2010) 'Supercapacitor ageing at constant temperature and constant voltage and thermal shock', Microelectronics Reliability, Vol. 50 No.9-11, pp.1783–1788., DOI:10.1016/j.microrel.2010.07.144

Gualous, H., Gallay, R., Al Sakka, M., Oukaour, A., Tala-Ighil, B. and Boudart, B. (2012) 'Calendar and cycling ageing of activated carbon supercapacitor for automotive application', Microelectronics Reliability, Vol. 52 No.9-10, pp.2477–2481., DOI:10.1016/j.microrel.2012.06.099

Gualous, H., Louahlia-Gualous, H., Gallay, R. and Miraoui, A. (2007) 'Supercapacitor Thermal Characterization in Transient State', in Conference Record of the 2007 IEEE Industry Applications Conference, 2007. 42nd IAS Annual Meeting. IEEE, New Orleans, LA, USA, pp.722–729, ISBN:978-1-4244-1259-4., DOI:10.1109/IAS.2007.114

Gualous, H., Louahlia-Gualous, H., Gallay, R. and Miraoui, A. (2009) 'Supercapacitor Thermal Modeling and Characterization in Transient State for Industrial Applications', IEEE Transactions on Industry Applications, Vol. 45 No.3, pp.1035–1044., DOI:10.1109/TIA.2009.2018879

Hafsaoui, J. and Sellier, F. (2010) 'Electrochemical model and its parameters identification tool for the follow up of batteries ageing', World Electric Vehicle Journal, Vol. 4, pp.386–395.

Hahn, M., Barbieri, O., Campana, F.P., Kötz, R. and Gallay, R. (2006) 'Carbon based double layer capacitors with aprotic electrolyte solutions: the possible role of intercalation/insertion processes', Applied Physics A, Vol. 82 No.4, pp.633–638., DOI:10.1007/s00339-005-3403-1

Hahn, M., Kötz, R., Gallay, R. and Siggel, A. (2006) 'Pressure evolution in propylene carbonate based electrochemical double layer capacitors', Electrochimica Acta, Vol. 52 No.4, pp.1709–1712., DOI:10.1016/j.electacta.2006.01.080

Hahn, M., Wursig, A., Gallay, R., Novák, P. and Kötz, R. (2005) 'Gas evolution in activated carbon/propylene carbonate based double-layer capacitors', Electrochemistry Communications, Vol. 7 No.9, pp.925–930., DOI:10.1016/j.elecom.2005.06.015

Hammar, A., Venet, P., Lallemand, R., Coquery, G. and Rojat, G. (2010) 'Study of Accelerated Aging of Supercapacitors for Transport Applications', IEEE Transactions on Industrial Electronics, Vol. 57 No.12, pp.3972–3979., DOI:10.1109/TIE.2010.2048832

Harrop, P., Gonzalez, F., Armstrong, J. and Greaves, K. (2013) Supercapacitor / Ultracapacitor Strategies and Emerging Applications 2013-2025 [Internet], http://www.idtechex.com/research/reports/supercapacitor-ultracapacitor-strategies-and-emerging-applications-2013-2025-000337.asp, (Accessed 22 June 2014).

Harrop, P., Zhitomirsky, V. and Gonzalez, F. (2014) Electrochemical Double Layer Capacitors: Supercapacitors 2014-2024 [Internet], http://www.idtechex.com/research/reports/electrochemical-double-layer-capacitors-supercapacitors-2014-2024-000378.asp?viewopt=showall, (Accessed 22 June 2014).

Hijazi, A., Kreczanik, P., Bideaux, E., Venet, P., Clerc, G. and Di Loreto, M. (2012) 'Thermal Network Model of Supercapacitors Stack', IEEE Transactions on Industrial Electronics, Vol. 59 No.2, pp.979–987., DOI:10.1109/TIE.2011.2158769

Hirschorn, B., Orazem, M.E., Tribollet, B., Vivier, V., Frateur, I. and Musiani, M. (2010) 'Determination of effective capacitance and film thickness from constant-phase-element parameters', Electrochimica Acta, Vol. 55 No.21, pp.6218–6227., DOI:10.1016/j.electacta.2009.10.065

Hossain, R. and Adamiak, K. (2013) 'Dynamic properties of the electric double layer in electrolytes', Journal of Electrostatics, Vol. 71 No.5, pp.829–838., DOI:10.1016/j.elstat.2013.06.006

Hu, X., Tseng, K.J. and Srinivasan, M. (2011) 'Optimization of Battery Energy Storage System with Super-Capacitor for Renewable Energy Applications', in 8th International Conference on Power Electronics - ECCE Asia. Jeju, Korea, pp.1552–1557, ISBN:9781612849577., DOI:10.1109/ICPE.2011.5944515

IEC (2006a) IEC 62391-1 Fixed electric double-layer capacitors for use in electronic equipment-Part 1: Generic Specification.

IEC (2006b) IEC 62391-2 Fixed electric double-layer capacitors for use in electronic equipment-Part 2: Sectional specification — Electric double-layer capacitors for power application.

Ike, I.S., Sigalas, I., Iyuke, S. and Ozoemena, K.I. (2015) 'An overview of mathematical modeling of supercapacitor', Journal of Power Sources, Vol. 273 No.2015, pp.264–277., DOI:10.1016/j.jpowsour.2014.09.071

Ilinois capacitor (2012) Supercapacitor technical guide [Internet], http://www.illinoiscapacitor.com/tech-center/papers.aspx, (Accessed 27 June 2012).

Ionica-Bousquet, C.M., Casteel Jr., W.J., Pearlstein, R.M., GirishKumar, G., Pez, G.P., Gómez-Romero, P., Palacín, M.R. and Muñoz-Rojas, D. (2010) 'Polyfluorinated boron cluster – [B12F11H]2− – based electrolytes for supercapacitors: Overcharge protection', Electrochemistry Communications, Vol. 12 No.5, pp.636–639., DOI:10.1016/j.elecom.2010.02.018

Islam, S., Hossain, B., Hossain, N., Alam, S. and Chowdhury, E.H. (2010) 'Modeling of a Double-Layer Capacitor with Individual Branch Response', in Proceedings of the World Congress on Engineering and Computer Science 2010 Vol II WCECS 2010. Newswood Limited, San Francisco, USA, pp.863–867.

Itagaki, M., Suzuki, S., Shitanda, I., Watanabe, K. and Nakazawa, H. (2007) 'Impedance analysis on electric double layer capacitor with transmission line model', Journal of Power Sources, Vol. 164 No.1, pp.415–424., DOI:10.1016/j.jpowsour.2006.09.077

Iwama, E., Taberna, P.L., Azais, P., Brégeon, L. and Simon, P. (2012) 'Characterization of commercial supercapacitors for low temperature applications', Journal of Power Sources, Vol. 219, pp.235–239., DOI:10.1016/j.jpowsour.2012.07.029

Jacques, C. (2013) Market for Supercapacitors to Grow 128% to $836 Million in 2018 [Internet], http://www2.luxresearchinc.com/news-and-events/press-releases/201.html, (Accessed 22 June 2014).

Jänes, A., Eskusson, J., Kanarbik, R., Saar, A. and Lust, E. (2012) 'Surface Analysis of Supercapacitor Electrodes After Long-Lasting Constant Current Tests in Organic Electrolyte', Journal of The Electrochemical Society, Vol. 159 No.8, pp.A1141–A1147., DOI:10.1149/2.008208jes

Jang, Y., Jo, J., Choi, Y.-M., Kim, I., Lee, S.-H., Kim, D. and Yoon, S.M. (2013) 'Activated carbon nanocomposite electrodes for high performance supercapacitors', Electrochimica Acta, Vol. 102, pp.240–245., DOI:10.1016/j.electacta.2013.04.020

Jossen, A. (2006) 'Fundamentals of battery dynamics', Journal of Power Sources, Vol. 154 No.2, pp.530–538., DOI:10.1016/j.jpowsour.2005.10.041

Jović, V.D. and Jović, B.M. (2003) 'EIS and differential capacitance measurements onto single crystal faces in different solutions Part I : Ag (111) in 0 . 01 M NaCl', Journal of Electroanalytical Chemistry, Vol. 541, pp.1–11., DOI:http://dx.doi.org/10.1016/S0022-0728(02)01310-4

Karangia, R., Jadeja, M., Upadhyay, C. and Chandwani, H. (2013) 'Battery-Supercapacitor Hybrid Energy Storage System Used in Electric Vehicle', in International Conference on Energy Efficient Technologies for Sustainability (ICEETS). Nagercoil, pp.688–691, ISBN:9781467361507., DOI:10.1109/ICEETS.2013.6533468

Kaus, M., Kowal, J. and Sauer, D.U. (2010) 'Modelling the effects of charge redistribution during self-discharge of supercapacitors', Electrochimica Acta, Vol. 55 No.25, pp.7516–7523., DOI:10.1016/j.electacta.2010.01.002

Kötz, R. and Carlen, M. (2000) 'Principles and applications of electrochemical capacitors', Electrochimica Acta, Vol. 45 No.15-16, pp.2483–2498., DOI:10.1016/S0013-4686(00)00354-6

Kötz, R., Hahn, M. and Gallay, R. (2006) 'Temperature behavior and impedance fundamentals of supercapacitors', Journal of Power Sources, Vol. 154 No.2, pp.550–555., DOI:10.1016/j.jpowsour.2005.10.048

Kötz, R., Hahn, M., Ruch, P. and Gallay, R. (2008) 'Comparison of pressure evolution in supercapacitor devices using different aprotic solvents', Electrochemistry Communications, Vol. 10 No.3, pp.359–362., DOI:10.1016/j.elecom.2007.12.016

Kötz, R., Ruch, P.W. and Cericola, D. (2010) 'Aging and failure mode of electrochemical double layer capacitors during accelerated constant load tests', Journal of Power Sources, Vol. 195 No.3, pp.923–928., DOI:10.1016/j.jpowsour.2009.08.045

Kötz, R., Sauter, J.-C., Ruch, P., Dietrich, P., Büchi, F.N., Magne, P.A. and Varenne, P. (2007) 'Voltage balancing: Long-term experience with the 250V supercapacitor module of the hybrid fuel cell vehicle HY-LIGHT', Journal of Power Sources, Vol. 174 No.1, pp.264–271., DOI:10.1016/j.jpowsour.2007.08.078

Kowal, J., Avaroglu, E., Chamekh, F., Šenfelds, A., Thien, T., Wijaya, D. and Sauer, D.U. (2011) 'Detailed analysis of the self-discharge of supercapacitors', Journal of Power Sources, Vol. 196 No.1, pp.573–579., DOI:10.1016/j.jpowsour.2009.12.028

Kularatna, N., Fernando, J. and Pandey, A. (2010) 'Surge Endurance Capability Testing of Supercapacitor', in IECON 2010 - 36th Annual Conference on IEEE Industrial Electronics Society. IEEE, Glendale, Az, pp.1858–1863, ISBN:9781424452262., DOI:10.1109/IECON.2010.5675392

Kulsangcharoen, P., Klumpner, C., Rashed, M. and Asher, G. (2010) 'Characterization of Energy Storage Devices for Constant Power Applications', in 36th Annual Conference on IEEE Industrial Electronics Society IECON 2010. IEEE, Glendale, Az, pp.1805–1810, ISBN:9781424452262., DOI:10.1109/IECON.2010.5675401

Kurzweil, P. and Chwistek, M. (2006) 'Capacitance Determination and Abusive Aging Studies of Supercapacitors Based on Acetonitrile and Ionic Liquids', in The 16th International Seminar on Double Layer Capacitors. Deerfield Beach, Florida, pp.1–15.

Kurzweil, P. and Chwistek, M. (2008) 'Electrochemical stability of organic electrolytes in supercapacitors: Spectroscopy and gas analysis of decomposition products', Journal of Power Sources, Vol. 176 No.2, pp.555–567., DOI:10.1016/j.jpowsour.2007.08.070

Kurzweil, P., Frenzel, B. and Gallay, R. (2005) 'Capacitance Characterization Methods and Ageing Behaviour of Supercapacitors', in The 15th International seminar on double layer capacitors. Deerfield Beach, pp.5–7.

Kurzweil, P., Frenzel, B. and Hildebrand, A. (2015) 'Voltage-Dependent Capacitance, Aging Effects, and Failure Indicators of Double-Layer Capacitors during Lifetime Testing', ChemElectroChem, Vol. 2 No.1, pp.160–170., DOI:10.1002/celc.201402300

Lajnef, W., Vinassa, J.-M., Briat, O., Azzopardi, S. and Woirgard, E. (2007) 'Characterization methods and modelling of ultracapacitors for use as peak power sources', Journal of Power Sources, Vol. 168 No.2, pp.553–560., DOI:10.1016/j.jpowsour.2007.02.049

Lajnef, W., Vinassa, J.-M., Briat, O., Azzopardi, S. and Zardini, C. (2004) 'Study of ultracapacitors dynamic behaviour using impedance frequency analysis on a specific test bench', in 2004 IEEE International Symposium on Industrial Electronics (Volume:2). IEEE, pp.839–844 vol. 2, ISBN:0-7803-8304-4., DOI:10.1109/ISIE.2004.1571922

Lajnef, W., Vinassa, J.-M., Briat, O., El Brouji, H. and Woirgard, E. (2007) 'Monitoring fading rate of ultracapacitors using online characterization during power cycling', Microelectronics Reliability, Vol. 47 No.9-11, pp.1751–1755., DOI:10.1016/j.microrel.2007.08.005

Lasia, A. (1999) 'Electrochemical Impedance Spectroscopy and its Applications', in Conway, B. E., Bockris, J., and White, R. E. (Eds.), Modern Aspects of Electrochemistry. Kluwer Academic/Plenum Publishers, pp.143–248, ISBN:978-0-306-46916-9., DOI:10.1007/0-306-46916-2_2

De Levie, R. (1963) 'On porous electrodes in electrolyte solutions: I. Capacitance effects', Electrochimica Acta, Vol. 8 No.10, pp.751–780., DOI:10.1016/0013-4686(63)80042-0

Li, X. and Crow, M.L. (2009) 'Ultracapacitor Frequency Analysis and its Equivalent Circuit Modeling', in 2009 North American Power Symposium (NAPS). IEEE, Starkville, MS, USA, pp.1–6., DOI:10.1109/NAPS.2009.5484034

Li, X. and Wei, B. (2013) 'Supercapacitors based on nanostructured carbon', Nano Energy, Vol. 2 No.2, pp.159–173., DOI:10.1016/j.nanoen.2012.09.008

Li, Z. and Chen, J. (2008) 'An impedance-based approach to predict the state-of-charge for carbon-based supercapacitors', Microelectronic Engineering, Vol. 85 No.7, pp.1549–1554., DOI:10.1016/j.mee.2008.02.016

Lin, C., Ritter, J.A., Popov, B.N. and White, R.E. (1999) 'A mathematical model of an electrochemical capacitor with double layer and faradaic process', Journal of Electrochemical Society, Vol. 146 No.9, pp.3168–3175., DOI:10.1149/1.1392450

Liu, P., Verbrugge, M. and Soukiazian, S. (2006) 'Influence of temperature and electrolyte on the performance of activated-carbon supercapacitors', Journal of Power Sources, Vol. 156 No.2, pp.712–718., DOI:10.1016/j.jpowsour.2005.05.055

Lungoci, C.M. and Oltean, I.D. (2010) 'Comparative Analysis for the Supercapacitors Packaging Characteristics', in 2010 IEEE 16th International Symposium for Design and Technology in Electronic Packaging (SIITME). IEEE, Pitesti, Romania, pp.93–98, ISBN:9781424481248., DOI:10.1109/SIITME.2010.5653578

Mahon, P.J., Paul, G.L., Keshishian, S.M. and Vassallo, A.M. (2000) 'Measurement and modelling of the high-power performance of carbon-based supercapacitors', Journal of Power Sources, Vol. 91 No.1, pp.68–76., DOI:10.1016/S0378-7753(00)00488-2

Martín, R., Quintana, J.J., Ramos, A. and de la Nuez, I. (2008a) 'Modeling Electrochemical Double Layer Capacitor , from Classical to Fractional Impedance', in IEEE Electrotechnical Conference. IEEE, Ajoccio, pp.61–66., DOI:10.1109/MELCON.2008.4618411

Martín, R., Quintana, J.J., Ramos, A. and de la Nuez, I. (2008b) 'Modeling of Electrochemical Double Layer Capacitors by Means of Fractional Impedance', Journal of Computational and Nonlinear Dynamics, Vol. 3 No.2, p.021303., DOI:10.1115/1.2833909

Masarapu, C., Zeng, H.F., Hung, K.H. and Wei, B. (2009) 'Effect of temperature on the capacitance of carbon nanotube supercapacitors.', ACS nano, Vol. 3 No.8, pp.2199–206., DOI:10.1021/nn900500n

Mathew, S., Das, D., Rossenberger, R. and Pecht, M. (2008) 'Failure mechanisms based prognostics', 2008 International Conference on Prognostics and Health Management, pp.1–6., DOI:10.1109/PHM.2008.4711438

Maxwell (2014a) 48 Volt Modules - General Purpose Modules [Internet], http://goo.gl/YqDoi5, (Accessed 27 June 2014).

Maxwell (2014b) HC Series - Board Mounted Cells [Internet], http://goo.gl/w2rmo, (Accessed 27 June 2014).

Maxwell (2014c) K2 2.85V/3400F Cell - High Capacity Cells [Internet], http://www.maxwell.com/products/ultracapacitors/products/k285-series, (Accessed 27 June 2014).

Maxwell (2014d) Maxwell Datasheet HC Series Ultracapacitors Doc. No. 1013793.9 [Internet], http://www.maxwell.com/products/ultracapacitors/hc-series/documents, (Accessed 18 November 2014).

Maxwell (2009a) *Maxwell Technologies ' Test Procedures for Capacitance ,* ESR , Leakage Current and Self-Discharge Characterizations of Ultracapacitors. San Diego, CA.

Maxwell (2009b) Product Guide - Maxwell Technologies BOOSTCAP Ultracapacitors - Doc. No. 1014627.1. San Diego, CA.

Merrett, G. V, Weddell, A.S., Lewis, A.P., Harris, N.R. and White, N.M. (2008) 'An Empirical Energy Model for Supercapacitor Powered Wireless Sensor Nodes', in Proceedings of 17th International Conference on Computer *Communications and Networks, 2008. ICCCN '08*. IEEE, St. Thomas, US Virgin Islands, pp.1–6, ISBN:9781424423903., DOI:10.1109/ICCCN.2008.ECP.34

Metrohm (2012) Metrohm Autolab Instruments for Electrochemical Impedance Spectroscopy Presentation Slides.

Michel, H. (2006) 'Temperature and dynamics problems of ultracapacitors in stationary and mobile applications', Journal of Power Sources, Vol. 154 No.2, pp.556–560., DOI:10.1016/j.jpowsour.2005.10.084

Miller, J.M. (2011) 'Chapter 1 Types of ultracapacitors', in Ultracapacitor Applications (IET Power and Energy Series). Institution of Engineering and Technology, p.363, ISBN:1849190712.

Miller, J.R. (2006) 'Electrochemical capacitor thermal management issues at high-rate cycling', Electrochimica Acta, Vol. 52 No.4, pp.1703–1708., DOI:10.1016/j.electacta.2006.02.056

Miller, J.R. and Burke, A.F. (1994) Electric Vehicle Capacitor Test Procedures Manual. Report DOE/ID-10491. Idaho National Engineering Laboratory.

Miller, J.R. and Simon, P. (2008) 'Fundamentals of electrochemical capacitor design and operation', The Electrochemical Society Interface, Vol. c, pp.31–32.

Mitkowski, W. and Skruch, P. (2013) 'Fractional-order models of the supercapacitors in the form of RC ladder networks', Bulletin of the Polish

Academy of Sciences: Technical Sciences, Vol. 61 No.3, pp.581–587., DOI:10.2478/bpasts-2013-0059

Monje, C.A., Chen, Y., Vinagre, B.M., Xue, D. and Feliu-Batlle, V. (2010) 'Fundamentals of Fractional-order Systems', in Monje, C. A., Chen, Y., Vinagre, B. M., Xue, D., and Feliu-Batlle, V. (Eds.), Fractional-order Systems and Controls: Fundamentals and Applications. Springer-Verlag London, New York, pp.9–35, ISBN:978-1-84996-334-3.

Morita, M., Arizono, R., Yoshimoto, N. and Egashira, M. (2014) 'On the electrochemical activation of alkali-treated soft carbon for advanced electrochemical capacitors', Journal of Applied Electrochemistry, Vol. 44 No.4, pp.447–453., DOI:10.1007/s10800-013-0634-2

Moss, P.., Zheng, J.P., Au, G., Cygan, P.J. and Plichta, E.J. (2007) 'Transmission Line Model for Describing Power Performance of Electrochemical Capacitors P.L. Moss and J.P. Zheng', Journal of the Electrochemical Society, Vol. 154 No.11, pp.A1020–A1025., DOI:10.1149/1.2778126

Musolino, V., Piegari, L. and Tironi, E. (2013) 'New Full-Frequency-Range Supercapacitor Model With Easy Identification Procedure', IEEE Transactions on Industrial Electronics, Vol. 60 No.1, pp.112–120., DOI:10.1109/TIE.2012.2187412

NEC Tokin (2013) Super Capacitors Vol.13 [Internet], http://www.nec-tokin.com/english/product/dl_capacitor.html, (Accessed 18 November 2014).

Nelms, R.M., Cahela, D.R. and Tatarchuk, B.J. (2003) 'Modeling Double-Layer Capacitor Behavior Using Ladder Circuits', IEEE Transactions On Aerospace And Electronic Systems, Vol. 39 No.2, p.430., DOI:10.1109/TAES.2003.1207255

NESSCAP (2014) Datasheet - 2.7V / 3F Cell [Internet], http://www.nesscap.com/ultracapacitor/EDLC/Supercapacitor/Small_cell_supercapacitor_family/Lead_wired_capacitor.jsp, (Accessed 18 November 2014).

Niu, R. and Yang, H. (2011) 'Modeling and Identification of Electric Double-Layer Supercapacitors', in 2011 IEEE International Conference on Robotics and Automation (ICRA). IEEE, Shanghai, pp.1–4, ISBN:9781612843803., DOI:10.1109/ICRA.2011.5980586

Nozu, R., Iizuka, M., Nakanishi, M. and Kotani, M. (2009) 'Investigation of the life process of the electric double layer capacitor during float charging', Journal of Power Sources, Vol. 186 No.2, pp.570–579., DOI:10.1016/j.jpowsour.2008.10.025

Omar, N., Gualous, H., Salminen, J., Mulder, G., Samba, A., Firouz, Y., Monem, M.A., Bossche, P. and Mierlo, J. (2014) 'Electrical double-layer capacitors:

evaluation of ageing phenomena during cycle life testing', Journal of Applied Electrochemistry, Vol. 44 No.4, pp.509–522., DOI:10.1007/s10800-013-0640-4

Orazem, M.E., Shukla, P. and Membrino, M.A. (2002) 'Extension of the measurement model approach for deconvolution of underlying distributions for impedance measurements', Electrochimica Acta, Vol. 47 No.13-14, pp.2027–2034., DOI:10.1016/S0013-4686(02)00065-8

Orazem, M.E. and Tribollet, B. (2008) Electrochemical Impedance Spectroscopy. John Wiley & Sons, Inc, New Jersey, USA. , ISBN:0470041404.

Oukaour, A., Pouliquen, M., Tala-Ighil, B., Gualous, H., Pigeon, E., Gehan, O. and Boudart, B. (2013) 'Supercapacitors aging diagnosis using least square algorithm', Microelectronics Reliability, Vol. 53 No.9-11, pp.1638–1642., DOI:10.1016/j.microrel.2013.07.032

Oukaour, A., Tala-Ighil, B., AlSakka, M., Gualous, H., Gallay, R. and Boudart, B. (2013) 'Calendar ageing and health diagnosis of supercapacitor', Electric Power Systems Research, Vol. 95, pp.330–338., DOI:10.1016/j.epsr.2012.09.005

Pajkossy, T. (2005) 'Impedance spectroscopy at interfaces of metals and aqueous solutions — Surface roughness, CPE and related issues', Solid State Ionics, Vol. 176 No.25-28, pp.1997–2003., DOI:10.1016/j.ssi.2004.06.023

Panasonic (2014) Electric Double Layer Capacitors (Gold Capacitor)/ HW Radial lead Type [Internet], http://industrial.panasonic.com/www-cgi/jvcr21pz.cgi?E+PZ+3+ABC0008+4++WW, (Accessed 18 November 2014).

Pandolfo, A.G. and Hollenkamp, A.F. (2006) 'Carbon properties and their role in supercapacitors☆', Journal of Power Sources, Vol. 157 No.1, pp.11–27., DOI:10.1016/j.jpowsour.2006.02.065

Pascot, C., Dandeville, Y., Scudeller, Y., Guillemet, P. and Brousse, T. (2010) 'Calorimetric measurement of the heat generated by a Double-Layer Capacitor cell under cycling', Thermochimica Acta, Vol. 510 No.1-2, pp.53–60., DOI:10.1016/j.tca.2010.06.022

Paul, K., Christian, M., Pascal, V., Guy, C., Gerard, R. and Younes, Z. (2009) 'Constant power cycling for accelerated ageing of supercapacitors', in 13th European Conference on Power Electronics and Applications, 2009. *EPE '09.* IEEE, Barcelona, pp.1–10.

Quintana, J.J., Ramos, A. and Nuez, I. (2006) 'Identification of the fractional impedance of ultracapacitors', in Oustaloup, A. (Ed.), Proceedings of the 2nd IFAC Workshop on Fractional Differentiation and Its Applications.

International Federation of Automatic Control (IFAC), Porto, Portugal, pp.432–436., DOI:10.3182/20060719-3-PT-4902.00073

Rafik, F., Gualous, H., Gallay, R., Crausaz, A. and Berthon, A. (2007) 'Frequency, thermal and voltage supercapacitor characterization and modeling', Journal of Power Sources, Vol. 165 No.2, pp.928–934., DOI:10.1016/j.jpowsour.2006.12.021

Raistrick, I.D., Franceschetti, D.R. and Macdonald, J.R. (2005) 'Theory', in Barsoukov, E. and Macdonald, J. R. (Eds.), Impedance Spectroscopy: Theory, Experiment, and Applications. John Wiley & Sons, Inc, New Jersey, USA, pp.27–128, ISBN:978-0-471-64749-2.

Ran, L., Junfeng, W. and Gechen, L. (2010) 'Prediction of State of Charge of Lithium-ion Rechargeable Battery with Electrochemical Impedance Spectroscopy Theory', in 2010 the 5th IEEE Conference on Industrial Electronics and Applications (ICIEA). IEEE, Taichung, pp.684–688, ISBN:9781424450466., DOI:10.1109/ICIEA.2010.5516984

Ratajczak, P., Jurewicz, K. and Béguin, F. (2014) 'Factors contributing to ageing of high voltage carbon/carbon supercapacitors in salt aqueous electrolyte', Journal of Applied Electrochemistry, Vol. 44 No.4, pp.475–480., DOI:10.1007/s10800-013-0644-0

Riu, D., Retière, N. and Linzen, D. (2004) 'Half-order modelling of supercapacitors', in Conference Record of the 2004 IEEE Industry Applications Conference, 2004. 39th IAS Annual Meeting. IEEE, pp.2550–2554, ISBN:0-7803-8486-5., DOI:10.1109/IAS.2004.1348833

Rizoug, N., Bartholomeus, P. and Le Moigne, P. (2010) 'Modeling and Characterizing Supercapacitors Using an Online Method', IEEE Transactions on Industrial Electronics, Vol. 57 No.12, pp.3980–3990., DOI:10.1109/TIE.2010.2042418

Rizoug, N., Bartholomeus, P. and Le Moigne, P. (2012) 'Study of the Ageing Process of a Supercapacitor Module Using Direct Method of Characterization', IEEE Transactions on Energy Conversion, Vol. 27 No.2, pp.220–228., DOI:10.1109/TEC.2012.2186814

Ruch, P.W., Cericola, D., Foelske, A., Kötz, R. and Wokaun, A. (2010) 'A comparison of the aging of electrochemical double layer capacitors with acetonitrile and propylene carbonate-based electrolytes at elevated voltages', Electrochimica Acta, Vol. 55 No.7, pp.2352–2357., DOI:10.1016/j.electacta.2009.11.098

Ruch, P.W., Cericola, D., Foelske-Schmitz, A., Kötz, R. and Wokaun, A. (2010) 'Aging of electrochemical double layer capacitors with acetonitrile-based electrolyte at elevated voltages', Electrochimica Acta, Vol. 55 No.15, pp.4412–4420., DOI:10.1016/j.electacta.2010.02.064

Ruiz, V., Blanco, C., Granda, M., Menéndez, R. and Santamaría, R. (2008) 'Effect of the thermal treatment of carbon-based electrodes on the electrochemical performance of supercapacitors', Journal of Electroanalytical Chemistry, Vol. 618 No.1-2, pp.17–23., DOI:10.1016/j.jelechem.2008.02.016

Ruiz, V., Blanco, C., Granda, M. and Santamaría, R. (2008) 'Enhanced life-cycle supercapacitors by thermal treatment of mesophase-derived activated carbons', Electrochimica Acta, Vol. 54 No.2, pp.305–310., DOI:10.1016/j.electacta.2008.07.079

Sakka, M.A., Gualous, H., Van Mierlo, J. and Culcu, H. (2009) 'Thermal modeling and heat management of supercapacitor modules for vehicle applications', Journal of Power Sources, Vol. 194 No.2, pp.581–587., DOI:10.1016/j.jpowsour.2009.06.038

Schiffer, J., Linzen, D. and Sauer, D.U. (2006) 'Heat generation in double layer capacitors', Journal of Power Sources, Vol. 160 No.1, pp.765–772., DOI:10.1016/j.jpowsour.2005.12.070

Sharma, P. and Bhatti, T.S. (2010) 'A review on electrochemical double-layer capacitors', Energy Conversion and Management, Vol. 51 No.12, pp.2901–2912., DOI:10.1016/j.enconman.2010.06.031

Simon, P. and Gogotsi, Y. (2008) 'Materials for electrochemical capacitors.', Nature materials, Vol. 7 No.11, pp.845–54., DOI:10.1038/nmat2297

Song, H.-K., Hwang, H.-Y., Lee, K.-H. and Dao, L.H. (2000) 'The effect of pore size distribution on the frequency dispersion of porous electrodes', Electrochimica Acta, Vol. 45 No.14, pp.2241–2257., DOI:10.1016/S0013-4686(99)00436-3

Song, H.-K., Jung, Y.-H., Lee, K.-H. and Dao, L.H. (1999) 'Electrochemical impedance spectroscopy of porous electrodes: the effect of pore size distribution', Electrochimica Acta, Vol. 44 No.20, pp.3513–3519., DOI:10.1016/S0013-4686(99)00121-8

Song, J. and Bazant, M.Z. (2013) 'Effects of Nanoparticle Geometry and Size Distribution on Diffusion Impedance of Battery Electrodes', Journal of the Electrochemical Society, Vol. 160 No.1, pp.A15–A24., DOI:10.1149/2.023301jes

Soualhi, A., Sari, A., Razik, H., Venet, P., Clerc, G., German, R., Briat, O. and Vinassa, J.M. (2013) 'Supercapacitors Ageing Prediction by Neural Networks', in 39th Annual Conference of the IEEE Industrial Electronics Society, IECON 2013. IEEE, Vienna, pp.6812–6818, ISBN:9781479902248., DOI:10.1109/IECON.2013.6700260

Srinivasan, V. and Weidner, J.W. (1999) 'Mathematical Modeling of Electrochemical Capacitors', Journal of The Electrochemical Society, Vol. 146 No.5, p.1650., DOI:10.1149/1.1391821

Stoller, M.D. and Ruoff, R.S. (2010) 'Best practice methods for determining an electrode material's performance for ultracapacitors', Energy & Environmental Science, Vol. 3 No.9, pp.1294–1301., DOI:10.1039/c0ee00074d

Sun, L., Wang, C., Zhou, Y., Zhang, X. and Qiu, J. (2013) 'KOH-activated depleted fullerene soot for electrochemical double-layer capacitors', Journal of Applied Electrochemistry, Vol. 44 No.2, pp.309–316., DOI:10.1007/s10800-013-0636-0

Sun, W., Zheng, R. and Chen, X. (2010) 'Symmetric redox supercapacitor based on micro-fabrication with three-dimensional polypyrrole electrodes', Journal of Power Sources, Vol. 195 No.20, pp.7120–7125., DOI:10.1016/j.jpowsour.2010.05.012

Tecate (2011) Datasheet - TPL Powerburst Ultracapacitors [Internet], http://www.tecategroup.com/ultracapacitors-supercapacitors/powerburst.php, (Accessed 2 July 2012).

Tepljakov, A. (2013) FOMCON Toolbox for MATLAB, v.0.41 beta [Internet], http://fomcon.net/, (Accessed 14 May 2014).

Tepljakov, A., Petlenkov, E. and Belikov, J. (2011) 'FOMCON : a MATLAB Toolbox for Fractional-order System Identification and Control', International Journal of Microelectronics and Computer Science, Vol. 2 No.2, pp.51–62.

Tironi, E. and Musolino, V. (2009) 'Supercapacitor characterization in power electronic applications: Proposal of a new model', in 2009 International Conference on Clean Electrical Power. IEEE, Capri, pp.376–382, ISBN:978-1-4244-2543-3., DOI:10.1109/ICCEP.2009.5212028

Torregrossa, D., Bahramipanah, M., Cherkaoui, R. and Paolone, M. (2013) 'Experimental Evidences of Redistribution Phenomenon in Supercapacitors and Consequent Improvement of their Dynamic Model', in 2013 IEEE Grenoble PowerTech (POWERTECH). IEEE, Grenoble, France, pp.1–7., DOI:10.1109/PTC.2013.6652413

Umemura, T., Mizutani, Y., Okamoto, T., Taguchi, T., Nkajima, K. and Tanaka, K. (2003) 'Life Expectancy and Degradation behavior of Electric double layer Capacitor Part I', in Proceedings of the 7th International Conference on Properties and Applications of Dielectric Materials, 2003. (Volume 3). IEEE, pp.944–948., DOI:10.1109/ICPADM.2003.1218577

Uno, M. and Tanaka, K. (2011) 'Accelerated Ageing Testing and Cycle Life Prediction of Supercapacitors for Alternative Battery Applications', in 2011

IEEE 33rd International Telecommunications Energy Conference (INTELEC). IEEE, Amsterdam, pp.1–6, ISBN:9781457712500., DOI:10.1109/INTLEC.2011.6099720

Uno, M. and Tanaka, K. (2012) 'Accelerated Charge – Discharge Cycling Test and Cycle Life Prediction Model for Supercapacitors in Alternative Battery Applications', IEEE Transactions on Industrial Electronics, Vol. 59 No.12, pp.4704–4712., DOI:10.1109/TIE.2011.2182018

Vetter, J., Novák, P., Wagner, M.R., Veit, C., Möller, K.-C., Besenhard, J.O., Winter, M., Wohlfahrt-Mehrens, M., Vogler, C. and Hammouche, A. (2005) 'Ageing mechanisms in lithium-ion batteries', Journal of Power Sources, Vol. 147 No.1-2, pp.269–281., DOI:10.1016/j.jpowsour.2005.01.006

Vinatech (2014) Vinatech Product Catalogue [Internet], http://www.supercapacitorvina.com/winko.php?code=catalog_eng, (Accessed 18 November 2014).

Vishay (2014) Vishay BCcomponents Energy Storage Double Layer Aluminum Capacitors 196DLC [Internet], http://www.vishay.com/capacitors/double-layer/, (Accessed 18 November 2014).

Vishay (2012) Vishay Roederstein Aluminum Capacitors Radial Style [Internet], http://www.vishay.com/capacitors/list/product-25008/, (Accessed 27 June 2014).

Vlad, A., Singh, N., Rolland, J., Melinte, S., Ajayan, P.M. and Gohy, J.-F. (2014) 'Hybrid supercapacitor-battery materials for fast electrochemical charge storage.', Scientific Reports, Vol. 4, p.4315., DOI:10.1038/srep04315

Volfkovich, Y.M., Bograchev, D.A., Mikhalin, A.A. and Bagotsky, V.S. (2013) 'Supercapacitor carbon electrodes with high capacitance', Journal of Solid State Electrochemistry, Vol. 18 No.5, pp.1351–1363., DOI:10.1007/s10008-013-2271-4

Walden, G., Stepan, J. and Mikolajczak, C. (2011) 'Safety Considerations when Designing Portable Electronics with Electric Double-Layer Capacitors (Supercapacitors)', in 2011 IEEE Symposium on Product Compliance Engineering (PSES). IEEE, San Diego, CA, pp.1–5, ISBN:9781612846866., DOI:10.1109/PSES.2011.6088259

Wang, G., Zhang, L. and Zhang, J. (2012) 'A review of electrode materials for electrochemical supercapacitors', Chemical Society reviews, Vol. 41 No.2, pp.797–828., DOI:10.1039/c1cs15060j

Wang, H., Forse, A.C., Griffin, J.M., Trease, N.M., Trognko, L., Taberna, P.-L., Simon, P. and Grey, C.P. (2013) 'In situ NMR spectroscopy of supercapacitors: insight into the charge storage mechanism.', Journal of the American Chemical Society, Vol. 135 No.50, pp.18968–80., DOI:10.1021/ja410287s

Wang, H. and Pilon, L. (2013) 'Mesoscale modeling of electric double layer capacitors with three-dimensional ordered structures', Journal of Power Sources, Vol. 221 No.2013, pp.252–260., DOI:10.1016/j.jpowsour.2012.08.002

Wang, H. and Pilon, L. (2012) 'Physical interpretation of cyclic voltammetry for measuring electric double layer capacitances', Electrochimica Acta, Vol. 64, pp.130–139., DOI:10.1016/j.electacta.2011.12.118

Wang, Y., Carletta, J.E., Hartley, T.T. and Veillette, R.J. (2008) 'An ultracapacitor model derived using time-dependent current profiles', in 51st Midwest Symposium on Circuits and Systems, 2008. MWSCAS 2008. IEEE, Knoxville, TN, pp.726–729, ISBN:978-1-4244-2166-4., DOI:10.1109/MWSCAS.2008.4616902

Wei, T., Wang, S. and Gao, X. (2009) 'Deterioration diagnosis of ultracapacitor for power electronics applications', in 2009 International Conference on Sustainable Power Generation and Supply. IEEE, Nanjing, pp.1–6, ISBN:978-1-4244-4934-7., DOI:10.1109/SUPERGEN.2009.5348060

Winter, M. and Brodd, R.J. (2004) 'What are batteries, fuel cells, and supercapacitors?', Chemical reviews, Vol. 104 No.10, pp.4245–69., DOI:10.1021/cr020730k

Wu, C.H., Hung, Y.H. and Hong, C.W. (2012) 'On-line supercapacitor dynamic models for energy conversion and management', Energy Conversion and Management, Vol. 53 No.1, pp.337–345., DOI:10.1016/j.enconman.2011.01.018

Xing, Y., Miao, Q., Tsui, K.-L. and Pecht, M. (2011) 'Prognostics and health monitoring for lithium-ion battery', in 2011 IEEE International Conference on Intelligence and Security Informatics. IEEE, Beijing, China, pp.242–247, ISBN:978-1-4577-0082-8., DOI:10.1109/ISI.2011.5984090

Xue, D., Chen, Y. and Atherton, D.P. (2007) Linear Feedback Control: Analysis and Design with MATLAB. 1st ed. Society for Industrial and Applied Mathematics, Philadelphia, USA. , ISBN:9780898716382.

Yuan, X., Wang, H., Sun, J.C. and Zhang, J. (2007) 'AC impedance technique in PEM fuel cell diagnosis—A review', International Journal of Hydrogen Energy, Vol. 32 No.17, pp.4365–4380., DOI:10.1016/j.ijhydene.2007.05.036

Zhang, S. (2010) Carbon Nanotube Based Composites for Electricity Storage in Supercapacitors. The University of Nottingham.

Zhang, Y., Feng, H., Wu, X., Wang, L., Zhang, A., Xia, T., Dong, H., Li, X. and Zhang, L. (2009) 'Progress of electrochemical capacitor electrode materials: A review', International Journal of Hydrogen Energy, Vol. 34 No.11, pp.4889–4899., DOI:10.1016/j.ijhydene.2009.04.005

Zhang, Y. and Yang, H. (2011) 'Modeling and characterization of supercapacitors for wireless sensor network applications', Journal of Power Sources, Vol. 196 No.8, pp.4128–4135., DOI:10.1016/j.jpowsour.2010.11.152

Zhou, S., Li, X., Wang, Z., Guo, H. and Peng, W. (2007) 'Effect of activated carbon and electrolyte on properties of supercapacitor', Transactions of Nonferrous Metals Society of China, Vol. 17 No.6, pp.1328–1333., DOI:10.1016/S1003-6326(07)60271-4

Zhu, C., Lu, R., Song, L., Wu, G. and Wang, Q. (2007) 'An Equivalent Circuit Model for Tractive Super-Capacitor', in 2007 IEEE Vehicle Power and Propulsion Conference. IEEE, Arlington, TX, pp.567–573, ISBN:978-0-7803-9760-6., DOI:10.1109/VPPC.2007.4544187

Zhu, M., Weber, C.J., Yang, Y., Konuma, M., Starke, U., Kern, K. and Bittner, A.M. (2008) 'Chemical and electrochemical ageing of carbon materials used in supercapacitor electrodes', Carbon, Vol. 46 No.14, pp.1829–1840., DOI:10.1016/j.carbon.2008.07.025

Zubieta, L. and Bonert, R. (2000) 'Characterization of Double-Layer Capacitors for Power Electronics Applications', IEEE Transactions on Industry Applications, Vol. 36 No.1, pp.199–205., DOI:10.1109/28.821816

APPENDIX A:

Source code charge and discharge circuit

```
/* Charge and Discharge Circuit

       created January 2013
       by Nafisah Naim
*/

int enA = 10;
int in2 = 9;
int in1 = 8;

int enB = 11;
int in3 = 12;
int in4 = 13;
int flag = 0; // charge = 1, discharge = 0
int i = 1;    //cycle counter
int y = 0;    //cycle

void setup()
{
  pinMode(enB, OUTPUT);   // sets the pin as output
  pinMode(in3, OUTPUT);   // sets the pin as output
  pinMode(in4, OUTPUT);   // sets the pin as output

  Serial.begin(9600);
  while(!Serial)
  {
    ;
  }

  Serial.println("test");  //serial monitor print
}

void loop()
{
  int n = 10;
  int s0 = 0;
  int s1 = 0;

  for (int x = 0; x < n; x++)
  {
    s0 += analogRead(1);
    delay(10);
    s1 += analogRead(2);
    delay(10);
  }

  s0 = s0/n;
  s1 = s1/n;
```

```
  float voltage0 = s0 * (5.0/ 1023.0);
  float voltage1 = s1 * (5.0/1023.0);

  int sensorValue = s0-s1;
  float voltage = voltage0-voltage1;

  Serial.print("sensor = ");  //display sensor value
  Serial.print(sensorValue);
  Serial.print(" V = ");      //voltage
  Serial.print(voltage);
  Serial.print(" flag = ");  // flag 1 discharge, flag 0 charge
  Serial.println(flag);

    if(voltage >= 0 && voltage <= 2.7 && flag == 0)      //charge if
voltage >= 0 && <= 2.7
  {
     digitalWrite(in3, HIGH);
    digitalWrite(in4, LOW);
    for(sensorValue = 0; sensorValue < 1024; sensorValue++)
    {
      analogWrite(enB, sensorValue);
    }
   }

   if(voltage > 2.7)     //activate discharge
  {
    flag = 1;
    y++;
   }

 if(flag == 1)           //discharging command
 {

    digitalWrite(in3,LOW);
    digitalWrite(in4,HIGH);

    for(sensorValue = 0; sensorValue <1024; sensorValue++)
    {
      analogWrite(enB, sensorValue);

     }
 }

 if(flag == 0)           //charging command
 {

    digitalWrite(in3,HIGH);
    digitalWrite(in4,LOW);

    for(sensorValue = 0; sensorValue <1024; sensorValue++)
    {
      analogWrite(enB, sensorValue);
    }
 }

 if(voltage <= -0.01)   //activate charging
  { flag = 0;}

  Serial.print(" Cycle = ");
  Serial.println(y);

  delay(1000);}
```

APPENDIX B:

Datasheet and Schematics of Iteaduino Leonardo

APPENDIX C:

Datasheet and Schematics of MotoMama